frontiers | Research Topics

Advances in the research of diabetic nephropathy

Edited by
Katsumi Iizuka, Mohamed Abu-Farha, Jehad Ahmed Abubaker, Fahd Al Mulla and Daisuke Yabe

Published in
Frontiers in Endocrinology

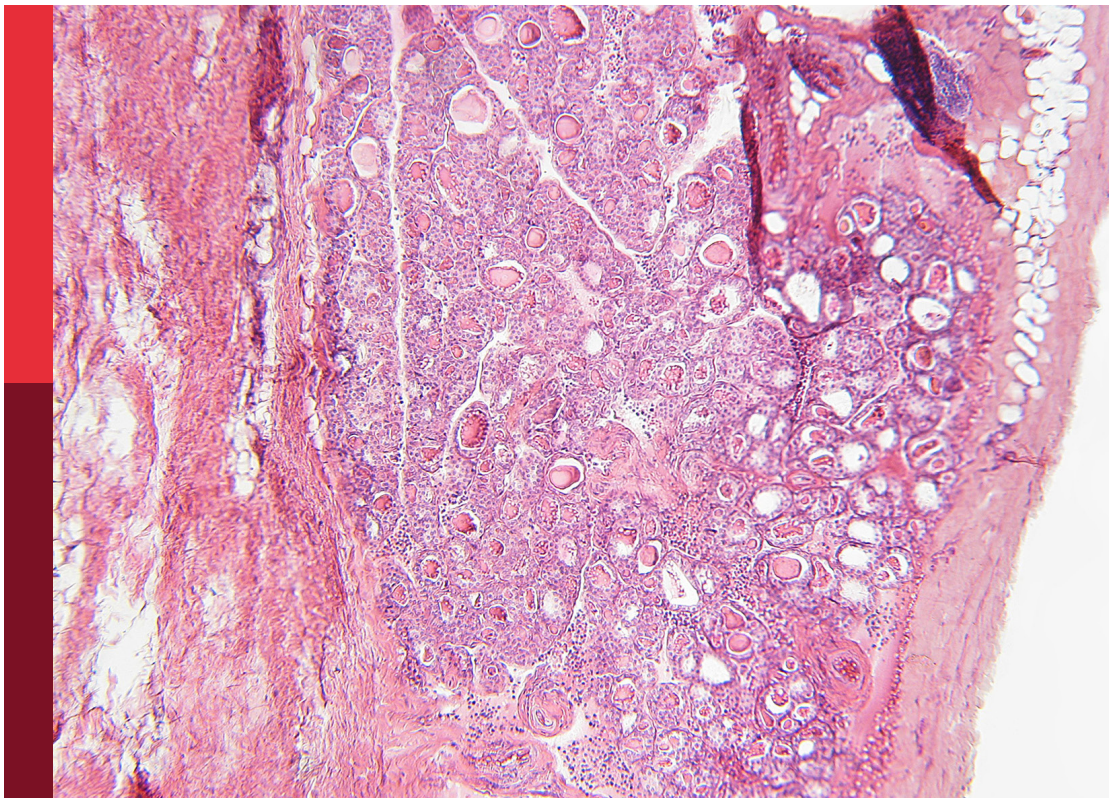

ISSN 1664-8714
ISBN 978-2-83251-378-1
DOI 10.3389/978-2-83251-378-1

About Frontiers

Frontiers is more than just an open access publisher of scholarly articles: it is a pioneering approach to the world of academia, radically improving the way scholarly research is managed. The grand vision of Frontiers is a world where all people have an equal opportunity to seek, share and generate knowledge. Frontiers provides immediate and permanent online open access to all its publications, but this alone is not enough to realize our grand goals.

Frontiers journal series

The Frontiers journal series is a multi-tier and interdisciplinary set of open-access, online journals, promising a paradigm shift from the current review, selection and dissemination processes in academic publishing. All Frontiers journals are driven by researchers for researchers; therefore, they constitute a service to the scholarly community. At the same time, the *Frontiers journal series* operates on a revolutionary invention, the tiered publishing system, initially addressing specific communities of scholars, and gradually climbing up to broader public understanding, thus serving the interests of the lay society, too.

Dedication to quality

Each Frontiers article is a landmark of the highest quality, thanks to genuinely collaborative interactions between authors and review editors, who include some of the world's best academicians. Research must be certified by peers before entering a stream of knowledge that may eventually reach the public - and shape society; therefore, Frontiers only applies the most rigorous and unbiased reviews. Frontiers revolutionizes research publishing by freely delivering the most outstanding research, evaluated with no bias from both the academic and social point of view. By applying the most advanced information technologies, Frontiers is catapulting scholarly publishing into a new generation.

What are Frontiers Research Topics?

Frontiers Research Topics are very popular trademarks of the *Frontiers journals series*: they are collections of at least ten articles, all centered on a particular subject. With their unique mix of varied contributions from Original Research to Review Articles, Frontiers Research Topics unify the most influential researchers, the latest key findings and historical advances in a hot research area.

Find out more on how to host your own Frontiers Research Topic or contribute to one as an author by contacting the Frontiers editorial office: frontiersin.org/about/contact

Advances in the research of diabetic nephropathy

Topic editors

Katsumi Iizuka — Fujita Health University, Japan
Mohamed Abu-Farha — Dasman Diabetes Institute, Kuwait
Jehad Ahmed Abubaker — Dasman Diabetes Institute, Kuwait
Fahd Al Mulla — Dasman Diabetes Institute, Kuwait
Daisuke Yabe — Gifu University, Japan

Citation

Iizuka, K., Abu-Farha, M., Abubaker, J. A., Al Mulla, F., Yabe, D., eds. (2023). *Advances in the research of diabetic nephropathy*. Lausanne: Frontiers Media SA. doi: 10.3389/978-2-83251-378-1

The authors declare that the research was conducted in the absence of any commercial or financial relationships that could be construed as a potential conflict of interest.

Table of contents

frontiers | Frontiers in Endocrinology

TYPE Editorial
PUBLISHED 05 January 2023
DOI 10.3389/fendo.2022.1116188

OPEN ACCESS

EDITED AND REVIEWED BY
Jared Rutter,
The University of Utah, United States

*CORRESPONDENCE
Mohamed Abu-Farha
mohamed.abufarha@dasmaninstitute.org
Jehad Abubaker
jehad.abubakr@dasmaninstitute.org

SPECIALTY SECTION
This article was submitted to Diabetes: Molecular Mechanisms, a section of the journal Frontiers in Endocrinology

RECEIVED 05 December 2022
ACCEPTED 19 December 2022
PUBLISHED 05 January 2023

CITATION
Abu-Farha M, Iizuka K, Yabe D, Al-Mulla F and Abubaker J (2023) Editorial: Advances in the research of diabetic nephropathy. *Front. Endocrinol.* 13:1116188. doi: 10.3389/fendo.2022.1116188

Editorial: Advances in the research of diabetic nephropathy

Mohamed Abu-Farha[1*], Katsumi Iizuka[2], Daisuke Yabe[3], Fahd Al-Mulla[4] and Jehad Abubaker[1*]

[1]Biochemistry and Molecular Biology Department, Dasman Diabetes Institute, Dasman, Kuwait, [2]Department of Clinical Nutrition, Graduate School of Medicine, Fujita Health University, Toyoake, Japan, [3]Department of Diabetes and Endocrinology, Gifu University Graduate School of Medicine, Gifu, Japan, [4]Dasman Diabetes Institute, Dasman, Kuwait

KEYWORDS

diabetic nephropathy, lipidomic, cystatin C (Cys C), N-cadherin expression, EGFR

Editorial on the Research Topic
Advances in the research of diabetic nephropathy

The increased prevalence of diabetes is associated with an increased incidence of diabetic nephropathy, which is estimated to affect approximately 40% of patients with diabetes. Diabetic Nephropathy, or Diabetic Kidney Disease (DKD), refers to the deterioration of kidney function in patients affected by type 1 and type 2 diabetes. To date, diabetic kidney disease is the leading cause of kidney failure and the single highest cause of diabetic mortality. Nevertheless, research has yet to reveal a definitive mechanism for the association between hyperglycemia and damage to the kidneys.

Through this Research Topic, the heterogeneity of diabetic nephropathy etiology and the underlying molecular mechanisms was explored. To this end, genetic and epigenetic factors associated with nephropathy were considered, as well as the role of oxidative stress and ferroptosis. Also pertinent to this topic was how the oxidative-stress pathway can be modulated to prevent or reverse diabetic nephropathy. Additionally, a special focus was given to early biomarkers that can lead to a better understanding and early detection of the disease.

In this special issue, several articles focused on the use of early diagnostic markers for diabetic nephropathy. To use lipidomics to compare the kidney cortex of normal and diabetic rats, Hou et al. showed a unique signature of lipid molecules associated with DKD kidney. They used targeted lipidomic approach spanning 437 lipid species and 25 lipid classes to study changes in the kidney cortex in normal and DKD rat model. The main characteristics of DKD lipidome are changes in side chain composition and unsaturated bonds. Neutral lipids exhibiting a higher degree of unsaturation and side chains of linoleic acid were the most lipids associated with DKD. Additionally, Glyceride lipids, lysophospholipids, and sphingolipids showed a significant increase in the DKD

kidney cortex. Taken together, the authors documented lipid changes associated with increased kidney damage, which can be used to better understand the pathophysiology and early detection of kidney damage in people with diabetes.

In another study, Wang et al. explored, in a retrospective cohort, the association of the trajectory of serum Cystatin C level with diabetic kidney disease development [2]. It was shown that the Cystatin C level was higher in people with diabetes. Additionally, once the people with diabetes were divided into low, middle, and high increasing Cystatin C levels, people in the middle and high increasing Cystatin C classes had higher incidence of diabetic kidney disease.

Furthermore, Wei et al. and Ali et al. showed that increased serum VEGF-B level and N-Cadherin levels were associated with diabetic kidney disease [3; 4]. Wei et al. showed that the circulating level of VEGF-B was associated with renal impairment. The diabetic population was divided based on eGFR, showing that serum VEGF-B level was an independent risk factor of eGFR<90 mL/min/1.73m2. Ali et al. measured the plasma level of N-Cadherin in a group of healthy controls and in people with T2D with and without DKD. It was shown that the plasma level of N-Cadherin was significantly higher in the DKD compared to the diabetic patients without DKD, and with the non-diabetic control group [4].

Additionally, a few articles also focused on the pathophysiology of DKD. Zhang et al. utilized RNA-Seq to identify novel genes involved in developing diabetic kidney diseases. They measured mRNA gene expression from glomeruli isolated from db/db and db/m mice with albuminuria. Gene expression analysis showed that genes upstream of glycolysis, such as *Hk1* and *Pfkp*, were upregulated, while genes downstream of glycolysis, such as Pkm and *Ldhaw*, were downregulated [5]. *PFKP* was shown to play a protective role against podocytes damage through the production of fructose-1,6-bisphosphate. Exogenous fructose-1 and 6-bisphosphate administration was also associated with improved kidney injury caused by high glucose cytoskeletal remodeling in podocytes [5]. Taken together, the authors demonstrated the potential for targeting *PFKP* for the treatment of DKD.

To elucidate the role of long non-coding RNA in DKD, Yang et al. focused on a previously identified lncRNA that high-throughput RNA-seq identified. The authors showed that the RNA component of mitochondrial RNAase P (Rmrp) lncRNA was highly expressed in the kidneys of db/db DKD mice and glomerular mesangial cells. They showed that Rmrp was controlled at the transcriptional level by transcription factor Sp-1. Rmrp up-regulated JunD expression through sponge miR-1a-3p, which may contribute to mesangial cell proliferation and fibrosis in DKD.

Increased reactive oxygen species and lipid peroxidation has been linked to an iron-dependant cell death called ferroptosis. Feng et al. linked ferroptosis and renal damage in diabetic mice to an increased HIF-1α/HO-1 pathway activity. Two studies investigated the role of autophagy in the development of kidney damage. Tang et al. investigated the role of melatonin in the clearance of damaged mitochondria in the kidney. The authors first showed that diabetic mice with DKD had abnormal mitophagy accompanied by increased oxidative stress and inflammation. Melatonin alleviated kidney damage by promoting AMPK phosphorylation and the translocation of mitophagy associated proteins PINK1 and Parkin to the mitochondria [8]. Wang et al. investigated the impact of hyperglycemia during a 6 h hyperglycemic clamp where blood glucose was increased from normal blood glucose of 5.37 ± 0.52 mmol/L to 11.67 ± 1.21 mmol/L, 16.67 ± 2.11 mmol/L, 24.73 ± 3.43 mmol/L. The authors showed that acute hyperglycemia resulted in renal tubular injury *via* mitophagy AMPK/mTOR pathway inhibition. They also showed that this damage could be inhibited by AMPK activation or mTOR inhibition.

Author contributions

MA-F drafted the editorial. All authors contributed to editing the manuscript. All authors contributed to the article and approved the submitted version.

Conflict of interest

The authors declare that the research was conducted in the absence of any commercial or financial relationships that could be construed as a potential conflict of interest.

Publisher's note

frontiers in Endocrinology

ORIGINAL RESEARCH
published: 19 June 2020
doi: 10.3389/fendo.2020.00359

Comprehensive Lipidome Profiling of the Kidney in Early-Stage Diabetic Nephropathy

Biyu Hou[1], Ping He[1], Peng Ma[1], Xinyu Yang[1], Chunyang Xu[2], Sin Man Lam[3], Guanghou Shui[3], Xiuying Yang[1], Li Zhang[1], Guifen Qiang[1] and Guanhua Du[1]**

[1] State Key Laboratory of Bioactive Substance and Function of Natural Medicines, Institute of Materia Medica, Peking Union Medical College, Beijing Key Laboratory of Drug Target, Screening Research, Chinese Academy of Medical Sciences, Beijing, China, [2] Beijing Obstetrics and Gynecology Hospital, Capital Medical University, Beijing, China, [3] Institute of Genetics and Developmental Biology, Chinese Academy of Sciences, Beijing, China

Metabolic changes associated with diabetes are reported to lead to the onset of early-stage diabetic nephropathy (DN). Furthermore, lipotoxicity is implicated in renal dysfunction. Most studies of DN have focused on a single or limited number of lipids, and the lipidome of the kidney during early-stage DN remains to be elucidated. In the present study, we aimed to comprehensively identify lipid abnormalities during early-stage DN; to this end, we established an early-stage DN rat model by feeding a high-sucrose and high-fat diet combined with administration of low-dose streptozotocin. Using a high-coverage, targeted lipidomic approach, we established the lipid profile, comprising 437 lipid species and 25 lipid classes, of the kidney cortex in normal rats and the DN rat model. Our findings additionally confirmed that the DN rat model had been successfully established. We observed distinct lipidomic signatures in the DN kidney, with characteristic alterations in side chain composition and degree of unsaturation. Glyceride lipids, especially cholesteryl esters, showed a significant increase in the DN kidney cortex. The levels of most phospholipids exhibited a decline, except those of phospholipids with side chain of 36:1. Furthermore, the levels of lyso-phospholipids and sphingolipids, including ceramide and its derivatives, were dramatically elevated in the present DN rat model. Our findings, which provide a comprehensive lipidome of the kidney cortex in rats with DN, are expected to be useful for the identification of pathologically relevant lipid species in DN. Furthermore, the results represent novel insights into the mechanistic basis of DN.

Keywords: diabetic nephropathy, lipidomics, glomerular filtration barrier, lipotoxicity, sphingolipids

OPEN ACCESS

Edited by:
Sandra Merscher, University of Miami, United States

Reviewed by:
Ilse Sofia Daehn, Icahn School of Medicine at Mount Sinai, United States
Mario Ollero, INSERM U955 Institut Mondor de Recherche Biomédicale (IMRB), France

****Correspondence:***
Guifen Qiang
qianggf@imm.ac.cn
Guanhua Du
dugh@imm.ac.cn

Specialty section:
This article was submitted to Diabetes: Molecular Mechanisms, a section of the journal Frontiers in Endocrinology

Received: *05 January 2020*
Accepted: *07 May 2020*
Published: *19 June 2020*

Citation:
Hou B, He P, Ma P, Yang X, Xu C, Lam SM, Shui G, Yang X, Zhang L, Qiang G and Du G (2020) Comprehensive Lipidome Profiling of the Kidney in Early-Stage Diabetic Nephropathy. Front. Endocrinol. 11:359. doi: 10.3389/fendo.2020.00359

INTRODUCTION

Diabetes mellitus (DM) is a metabolic disorder characterized by hyperglycemia and is accompanied by an increased risk of macrovascular and microvascular complications (1). As one of the most common microvascular complications of diabetes, diabetic nephropathy (DN) is characterized by altered glomerular filtration and proteinuria, resulting in end-stage renal disease (ESRD), which makes timely diagnosis and prevention critical (2). Although hyperglycemia and hypertension are known to drive the onset and progression of DN, intensive glycemic control has only modest effects and fails to stop DN progression to ESRD and death (3, 4). Therefore, elucidation of the

mechanisms underlying DN and the development of effective therapeutic strategies are essential for the prevention of renal dysfunction (5).

Abnormal lipid metabolism is associated with prediabetes, type 1, and type 2 DM (T2DM). Metabolic changes induced by diabetes lead to glomerular hypertrophy, glomerulosclerosis, tubulointerstitial inflammation, and fibrosis. Renal lipotoxicity has been implicated in renal dysfunction as well as several pathological hallmarks of DN patients (4, 6, 7). As important biomolecules, lipids have many essential biological functions, which can be identified and quantified by lipidomics (1). In studies over the last few decades, lipidomic analyses have been performed to investigate biomarkers indicative of DN progression. Zhu et al. performed normal-phase liquid chromatography coupled with time-of-flight mass spectrometry (NPLC-TOF/MS) to analyze plasma phospholipids in T2DM and DN patients, and we identified two new biomarkers that distinguish healthy individuals, T2DM, and DN patients (8). Zhao et al. used gas chromatography (GC)/TOF/MS in tandem to analyze the effect of the Chaihuang–Yishen formula on the lipidome in progressive DN induced by uninephrectomy combined with streptozotocin (STZ) injection (9). Most previous studies have focused on a single or a limited number of lipids and lack analysis of the side chains. Sas et al. found the negative correlation with levels of ceramides (Cer) C16:0 and C24:1 in plasma and kidney tissue in diabetic mice (6). Zhao et al. focused on several kinds of phospholipids and sphingomyelins in progressive DN (9), whereas Kumari performed an integrated lipidomic analysis of urinary exosomes in DN patients to identify glycerol lipids that may be involved in phospholipid and sphingolipid metabolism (10). Chen et al. reported that perturbations in fatty acid and triglyceride (TG) metabolism are strongly correlated with phospholipids in patients with advanced chronic kidney disease (11). However, a comprehensive lipidomic analysis of early-stage DN has not been reported to date, and the physiological and molecular mechanisms associated with DN development remain to be identified.

In this study, we established an early-stage DN rat model by feeding rats a high-sucrose and high-fat diet (HFD) combined with STZ injection. We found that diabetic rats exhibited early-stage DN symptoms with microalbuminuria, injured renal function, basement membrane thickening, and glomerular hypertrophy. Further, using a high-coverage and targeted lipidomic approach, we identified a comprehensive lipidome of the kidney cortex, comprising 437 lipid species and 25 lipid classes. We additionally sought to identify pathologically relevant lipid species via comparison of the kidney lipidome between normal and diabetic rats. The findings offer new insights into the mechanistic basis of DN and may be useful for the development of potential novel therapeutic strategies against this disease.

MATERIALS AND METHODS

Reagents and Internal Standards

STZ was purchased from Sigma Chemical Co, USA. Chloroform and methanol were purchased from Merck (Merck Pte. Ltd., China). d5-Triacylglycerol (TAG)(16:0)3, d5-TAG(14:0)3, d5-TAG(18:0)3, d5-diacylglycerol (DAG)(1,3-16:0), d5-DAG(1,3-18:1), and cholesteryl-2,2,3,4,4,6-d6 octadecanoate cholesterol-26,26,26,27,27,27-d6 were obtained from Avanti Polar Lipids (Alabaster, AL, USA). Phosphatidylinositol (PI)-d31(16:0/18:1) was obtained from Echelon Biosciences, Inc. (Salt Lake City, UT). Phosphatidylcholine (PC)-d31(16:0/18:1), phosphatidylethanolamine (PE)-d31(16:0/18:1), phosphatidylserine (PS)-d31(16:0/18:1), phosphatidic acid (PA)-d31(16:0/18:1), PA(17:0/17:0), phosphatidylglycerol (PG)-d31(16:0/18:1), lyso-bisphosphatidic acid (LBPA)-(14:0/14:0), lyso-PC(LPC)-17:0, lyso-PE(LPE)-17:1, lyso-PS(LPS)-17:1, Cer-d18:1/17:0, glucosylceramide (GluCer)-d18:1/8:0, and galactosylceramide (GalCer)-d18:1/8:0, d31-16:0, and d8-20:4 were obtained from Avanti Polar Lipids (Alabaster, AL).

Animal Experiments

Animals

All animal experiments were approved by the Animal Care Committee of the Institute of Materia Medica, Chinese Academy of Medical Sciences. Male Sprague–Dawley (SD) rats (130–150 g) were provided by Beijing HFK Bioscience Co. Ltd. (Beijing, China) and housed in a temperature-controlled and humidity-controlled specific-pathogen free (SPF) barrier system, with a 12-h light/12-h dark cycle.

Establishment of Diabetic Nephropathy Rat Model

The DN rat model was induced as previously described (2). Briefly, after feeding with a high-sucrose and HFD for 4 weeks (standard diet supplemented with 10% sucrose, 10% lard stearin, 2% cholesterin, and 0.5% cholic acid), rats were intraperitoneally injected with 30 mg/kg of STZ dissolved in 0.1 M of citrate buffer (pH 4.4). Three days after injection, rats with fasting blood glucose (FBG) levels between 10 and 20 mM were identified as diabetic rats and selected for continued feeding of HFD (10% lard stearin, 2% cholesterin, and 0.5% cholic acid) for another 8 weeks (DN group). An age-matched control group (NC group) was injected with citrate buffer and fed a normal diet throughout the duration of the experiment. Each group contained six rats. FBG levels were measured using an ACCU-CHEK® active glucometer (Roche). Serum fructosamine, blood TGs, and total cholesterol (TCHO) were detected with an automatic analyzer (TOSHIBA Acute TBA-40FR, TOSHIBA, Tokyo, Japan) at the end of the experimental period.

Renal Function Analysis

At the eighth week, we performed 24-h urine collection from rats housed in metabolism cages with free access to water and food. The kidney coefficient was calculated as the ratio of kidney weight to body weight. Twenty-four-hour urinary albumin was assessed by ELISA assay (CUSABIO, Wuhan, China). Urinary creatinine (CR) levels were determined using a commercial assay kit (Jiancheng Biotech Co., Ltd., Nanjing, China). CR clearance (Ccr) was calculated using the formula: Ccr (μl/min) = (Ucr/Pcr) × urine

volume (μl/min), as previously described (2, 12). After completion of the experiments, rats were humanely sacrificed, and blood samples were collected. Serum CR, blood urea nitrogen (BUN), and serum *N*-acyl-β-glucosidase (NAG) activity was assessed in accordance with the manufacturer's instructions.

Renal Histopathology Analysis

Rats were humanely sacrificed, and their left kidneys were fixed in 10% (w/v) neutral formaldehyde, dehydrated with a graded series of alcohol, and embedded in paraffin wax. Paraffin sections (4 μm thick) of kidney were subjected to hematoxylin–eosin (HE), periodic acid-Schiff (PAS), and periodic acid-silver methenamine (PASM) staining following the standard staining protocols. The sections were imaged with a microscope (Nikon Eclipse Ti-U, Nikon Corporation, Tokyo, Japan).

Dewaxed sections were blocked with 5% bovine serum albumin (BSA) after antigen retrieval. Sections were then incubated with primary antibody against CD68 (1:100; CST, USA) followed by incubation with horseradish peroxidase (HRP)-conjugated goat anti-rabbit IgG (Dako, Wuhan, China). CD68 expression was visualized by diaminobenzidine (DAB) (Dako, Wuhan, China) staining. The sections were then imaged with a microscope (Nikon Eclipse Ti-U, Nikon Corporation, Tokyo, Japan).

Kidney Cortex Lipidome Analysis

Sample Preparation and Lipid Extraction

Prior to tissue collection, kidneys were perfused to exclude the possible interference from the blood. Frozen kidney cortex tissue was deactivated with a 900-μl mixture of chloroform:methanol (1:2) containing 10% deionized H_2O. Finely cut pieces were homogenized and incubated for 1 h at 4°C. Next, 300 μl of chloroform and 400 μl of deionized H_2O were added to the sample. The mixture was vortexed vigorously for 1 min and centrifuged for 5 min at 12,000 rpm, at 4°C. The organic phase in the lower layer was transferred to a new tube, and 500 μl of chloroform was added for another extraction step. The combined extracts were dried using a SpeedVac (Geneva, UK) and stored at −80°C for further analysis.

Quantitative Lipidomic Analysis

A comprehensive lipidomic platform based on an Exion ultra-performance liquid chromatography (UPLC) coupled with Sciex QTRAP 6500 Plus was used. UPLC-MS/MS analyses were conducted in electrospray ionization (ESI) mode, with conditions as follows: curtain gas = 20, ion spray voltage = 5,500 V, temperature = 400°C, ion source gas 1 = 35, and ion source gas 2 = 35. Briefly, polar lipids were separated using a Phenomenex Luna 3 μm of silica column (inner diameter 150 × 2.0 mm) with two mobile phases: mobile phase A (chloroform:methanol:ammonium hydroxide, 89.5:10:0.5) and mobile phase B (chloroform:methanol:ammonium hydroxide:water, 55:39:0.5:5.5). Gradient separation was conducted as follows: the gradient was maintained with 95% A for 5 min and then linearly reduced to 60% in 7 min and held for 4 min, after which it declined to 30% and was then held for 15 min; finally, the original gradient was applied and maintained for 5 min. PC-d31(16:0/18:1), PEd31(16:0/18:1), PS-d31(16:0/18:1), PI-d31(16:0/18:1), PA-d31(16:0/18:1), PA(17:0/17:0), PG-d31(16:0/18:1), LBPA-(14:0/14:0), LPC-17:0, LPE-17:1, LPS-17:1, Cer-d18:1/17:0, GluCer-d18:1/8:0, and GalCer-d18:1/8:0, d31-16:0, and d8-20:4 were used as internal standards to spike individual lipids. Separation of TAGs and DAGs was carried out with modified reversed-phase HPLC/ESI/MS/MS, as described previously, with a Phenomenex Kinetex 2.6 μm of C18 column (4.6 × 100 mm) (13). Isocratic elution was used to separate lipids with a mobile phase of chloroform:methanol:0.1 M ammonium acetate (100:100:4), at a flow rate of 160 μl/min for 20 min. d5-TAG(16:0)3, d5-TAG(14:0)3, and d5-TAG(18:0)3 were used to spike individual TAG. d5-DAG(1,3-16:0) and d5-DAG(1,3-18:1) were used to spike individual DAG based on Neutral miss MS/MS technology. Free cholesterol (Cho), free fatty acids (FFAs), sterols, and their esters were analyzed by HPLC–MS–atmospheric pressure chemical ionization (APCI) mode with a Phenomenex Kinetex column of 2.6 μm of C18 (4.6 × 100 mm).

Statistical Analysis

Data are presented as means ± standard error of the mean (SEM). Differences between NC and DN groups were determined by statistical analysis using the unpaired two-tailed Student's *t*-test. Principal component analysis (PCA) was implemented using MetaboAnalyst (http://www.metaboanalyst.ca/). Data were auto-scaled before analysis. A value of $P < 0.05$ was considered to indicate statistically significant results.

RESULTS

Confirmation of the Rat Model of Early-Stage Diabetic Nephropathy

Eight weeks of HFD feeding combined with low-dose STZ injection resulted in the induction of elevated blood glucose and fructosamine levels in the DN group of rats (**Figures 1A,B**). Furthermore, serum lipid levels were significantly increased, as evidenced by elevated TG and TCHO (**Figures 1C,D**). As shown in **Figures 1E–G**, the kidneys in the DN group exhibited hypertrophy (ratio of kidney weight to body weight). Significantly increased CR and BUN indicated damaged glomerular filtration function. The 24-h urinary albumin levels in DN rats increased to 14.21 μg/ml, and the Ccr rate declined to 999.26 μl/min (**Figures 1H,I**). In addition, elevated NAG suggested compromised tubular function in diabetic rats (**Figure 1J**). Further, we observed increased glomerular size in DN rats and mesangial expansion with increased red staining areas in diabetic glomeruli stained with PAS (**Figure 1K**). PASM staining revealed that basement membranes in DN rats were thickened in comparison with those of the NC group (**Figure 1L**); this phenomenon is indicative of early-stage DN. These findings confirm the successful induction of early-stage DN in the rat model.

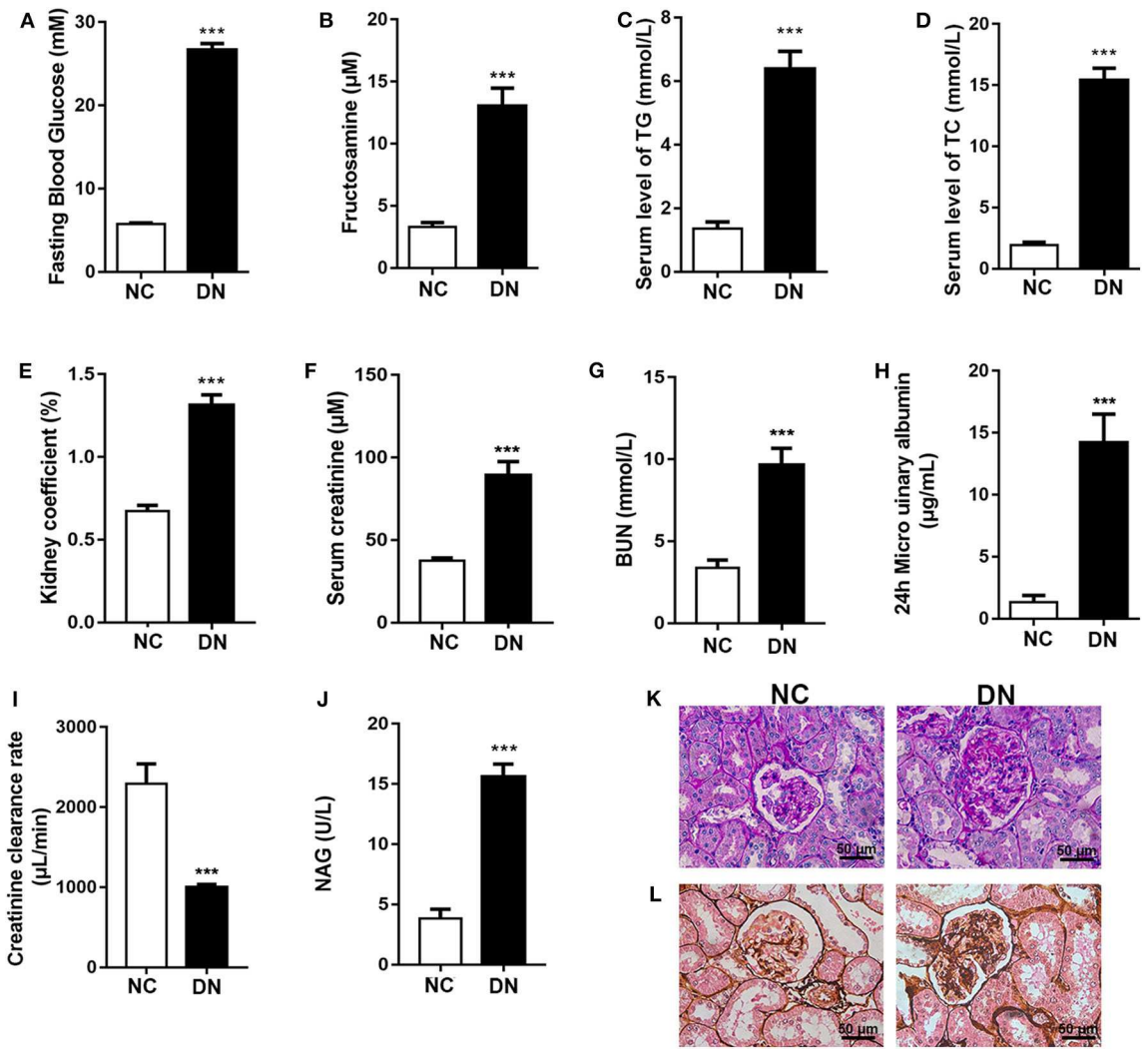

FIGURE 1 | Confirmation of the early-stage diabetic nephropathy (DN) rat model. After diabetic nephropathy was induced by feeding high-fat diet (HFD) combined with injection of low-dose streptozotocin (STZ) for 8 weeks, **(A)** fasting blood glucose; **(B)** fructosamine; serum level of **(C)** TG and **(D)** TCHO; **(E)** kidney coefficient; serum level of **(F)** creatinine and **(G)** BUN; **(H)** 24-h microurinary albumin; **(I)** creatinine clearance; and **(J)** *N*-acyl-β-glucosidase (NAG) activity were determined. **(K)** Periodic acid-Schiff (PAS) staining and **(L)** periodic acid-silver methenamine (PASM) staining were conducted to examine renal structural changes. Data are presented as means ± SEM, $n = 6$ per group; $^{***}P < 0.001$.

General Lipid Composition of the Kidney Cortex in Early-Stage Diabetic Nephropathy

High-coverage, targeted lipidomic analysis of the kidney cortex revealed 437 lipid species and 25 classes (see **Supplementary Material**). PCA of the whole lipidome showed clear differences between the data for the NC group and the DN group, suggesting a contrasting lipidome signature between normal and DN (**Figure 2A**). Detailed changes in lipid class are shown in **Figure 2B**, with a distinguishing pattern observed for glycerides and phospholipids as well as sphingolipids. Glycerides, including TAG, DAG, FFAs, Cho, and cholesteryl esters (CE), were significantly increased in the kidneys of the DN group. Interestingly, the levels of some phospholipids, such as PSs, were decreased; and those of lyso-phospholipids, such as LBPAs, were increased in the DN group. Volcano plot analysis with false discovery rate (FDR) < 0.05 and fold change (FC) > 1.5 was performed using Student's *t*-test after quality control. Of the 149 species that were differentially expressed, 114 species from 11 classes were significantly elevated; most of these belonged to TAG, CE, and LBPA classes. Among the lipid species that exhibited a significant decrease in levels, phospholipids, including PE, were predominant (**Figure 2C**). Heatmap analysis of overall lipid species in terms of chain length and unsaturated bonds showed a similar alteration pattern with the total quantities of lipid classes. However, some specific lipid species, such as DAG with 38C or DAG with four unsaturated bonds, and PS 34C or PS with one to two unsaturated bonds, showed different alterations as compared with TAG, CE, and LBPA (**Figures 2D,E**).

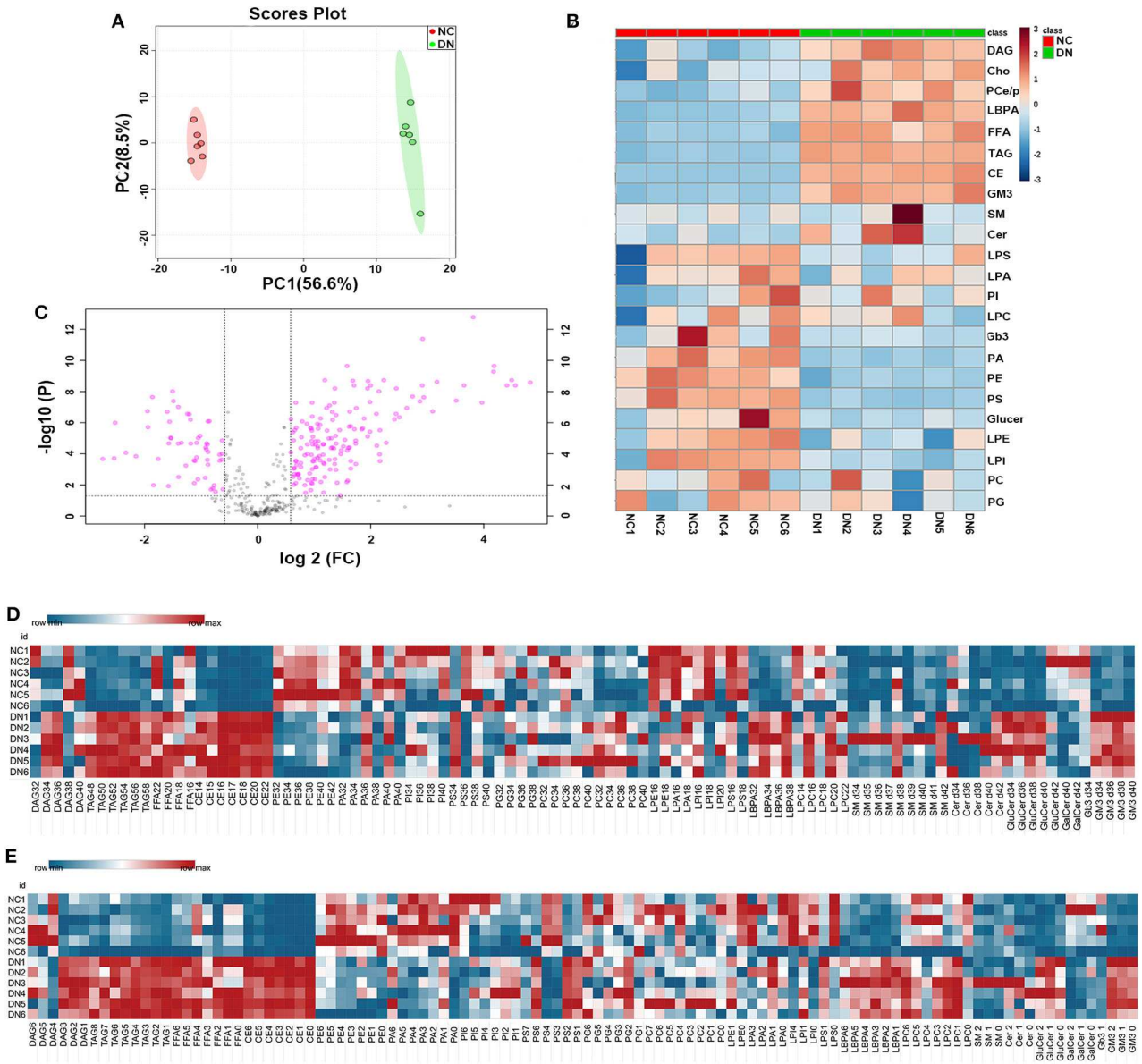

FIGURE 2 | General analysis of lipidomic profiles in the kidney cortex of diabetic nephropathy (DN) and normal rats. **(A)** Principal component analysis (PCA) of whole lipidome of the two groups. **(B)** Volcano plot of all lipid species detected in the two groups. Data are shown as ratios of DN/NC, false discovery rate (FDR) < 0.05, and fold change > 1.5 is highlighted. Heatmap analysis of **(C)** main lipid class, **(D)** overall enrichment of chain length for lipid species, and **(E)** overall quantification of unsaturated bonds for lipid species; $n = 6$ per group.

Homogeneous Increases in Glyceride and Sterol Lipids in Early-Stage Diabetic Nephropathy

Analysis of the changes in total carbon and unsaturated bonds of glycerides showed that the most drastic alterations, representing a 2.9- to 3.3-fold increase, were observed in TAG with 50–52C in DN rats. However, the content was lower than that of DAG and FFA (**Figure 3A**). Interestingly, DAG with 38C was the only glyceride species in DN kidneys to exhibit a decrease, with a 30% reduction observed in comparison with that in normal rats. TAG and FFA with two unsaturated bonds showed the most marked increase, whereas DAG with four unsaturated bonds showed a significant decrease (**Figure 3B**). Because TAG was the most altered glyceride lipid class, we analyzed the concentration and relative differences in its side chains (**Figure 3C**). The horizontal axis of the bubble plot indicates the FC of TAG (DN/NC), whereas the vertical axis indicates the concentration of TAG lipid species in the DN kidney cortex. Each dot represents a TAG species and was assigned a color on the basis of the number of unsaturation bonds in its side chain. The size of each dot represents the $-\log_2$ (P-value) obtained by comparing the NC

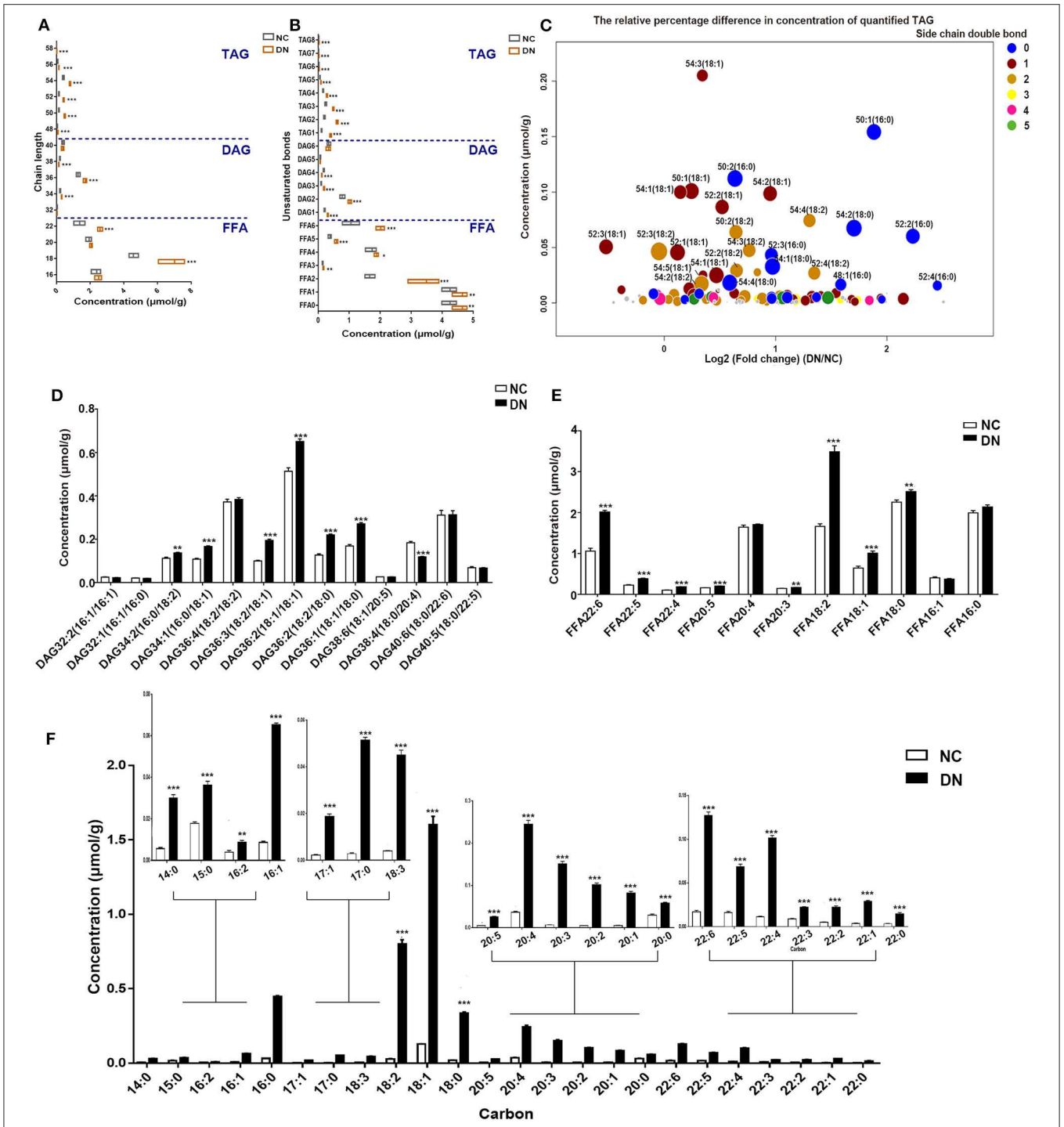

FIGURE 3 | Differences in glycerides, fatty acids, and sterol lipids between normal and diabetic nephropathy (DN) rats. **(A)** Changes in the numbers of total carbons were analyzed for free fatty acid (FFA), diacylglycerol (DAG), and triacylglycerol (TAG) total concentrations. **(B)** Analysis of the changes in the number of unsaturated bonds in FFA, DAG, and TAG lipid species. **(C)** Bubble map showing the differences in TAG species content between the two groups, with the sizes of circles representing the level of significance calculated by –log 2 (*P*), colored by the number of unsaturated side chains. The content of DAG species **(D)**, FFA species **(E)**, and CE species **(F)** was analyzed. Data are presented as means ± SEM, $n = 6$ per group; $^{*}P < 0.05$, $^{**}P < 0.01$, $^{***}P < 0.001$.

and DN groups. As shown in **Figure 3C**, the majority of dots were distributed to the right side of the plot with $\log_2$ (FC) larger than 0, indicating that most TAG species were increased in the kidney cortex of DN. TAG with side chains containing one to two unsaturated bonds (blue dots and orange dots) were the major components of the overall TAG class. TAG with unsaturated

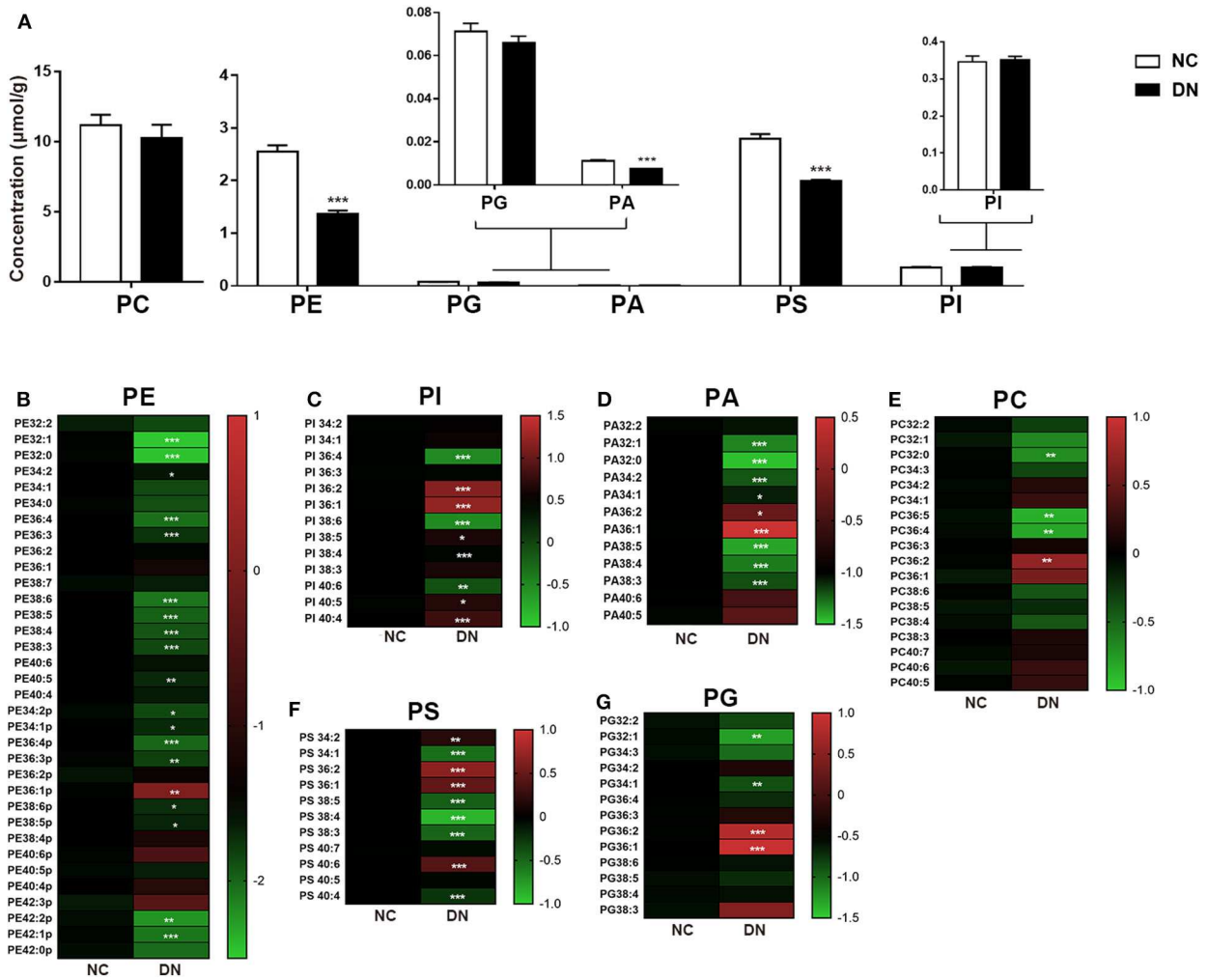

FIGURE 4 | Phospholipid remodeling in the kidney cortex of diabetic nephropathy (DN) and normal rats. **(A)** Total content of each phospholipid class. Ratio heat plot analysis of **(B)** phosphatidylethanolamine (PE), **(C)** phosphatidylinositol (PI), **(D)** phosphatidic acid (PA), **(E)** phosphatidylcholine (PC), **(F)** phosphatidylserine (PS), and **(G)** phosphatidylglycerol (PG) lipid species. The color bars represent the ratio of DN/NC in each lipid species, with the relative abundance of the normal group fixed as a value of 1. Only statistically significant changes are shown. Data are presented as means ± SEM, $n = 6$ per group; $^{*}P < 0.05$, $^{**}P < 0.01$, $^{***}P < 0.001$.

side chains including 18:0 and 16:0, especially TAG 50:1(16:0), TAG 52:2(16:0), and TAG 52:4(16:0), showed the most marked alterations. Both DAG and FFA with 18C were significantly increased in DN kidneys (**Figures 3D,E**). In the CE class, each CE species was significantly elevated, particularly CE with 18C side chains, including 18:2, 18:1, and 18:0, with a 12- to 28-fold increase relative to normal rats (**Figure 3F**). Collectively, neutral lipid content; increased unsaturation for TAG, DAG, and fatty acids; and a homogeneous increase in CE were observed in the cortex of early-stage DN kidneys.

Remodeling of Phospholipids in Early-Stage Diabetic Nephropathy

As shown in **Figure 4A**, the comprehensive alterations in the relative abundance of phospholipids were analyzed. The total class content of PE, PA, and PS exhibited uniform reduction. Ratio heat plots were generated using the normalized intensity of the DN group compared with that of the NC group, in which the relative abundance within the NC group was assigned a fixed value of 1 (**Figures 4B–H**). Lipids with side chains of 36:1 and 36:2, including PE, PA, PI, PS, and PC, showed a heterogeneous increase in DN kidneys. Although no gross perturbations in PG or PI content were observed, those of PG 32:1 and PG 34:1 decreased significantly. Furthermore, PI with more than four double bonds showed a significant decrease in the DN kidney cortex. Taken together, the results show that remodeling of the kidney cortex during early-stage DN was characterized by a reduction in phospholipids, except in those with side chains of 36:1 or 36:2.

Diverse Alterations in Lyso-Phospholipids During Early-Stage Diabetic Nephropathy

LBPA plays a crucial role in macrophage biology and function (14). Here, we observed a drastic alteration in LBPA in DN rats. As shown in **Figure 5A**, most LBPA molecules contained

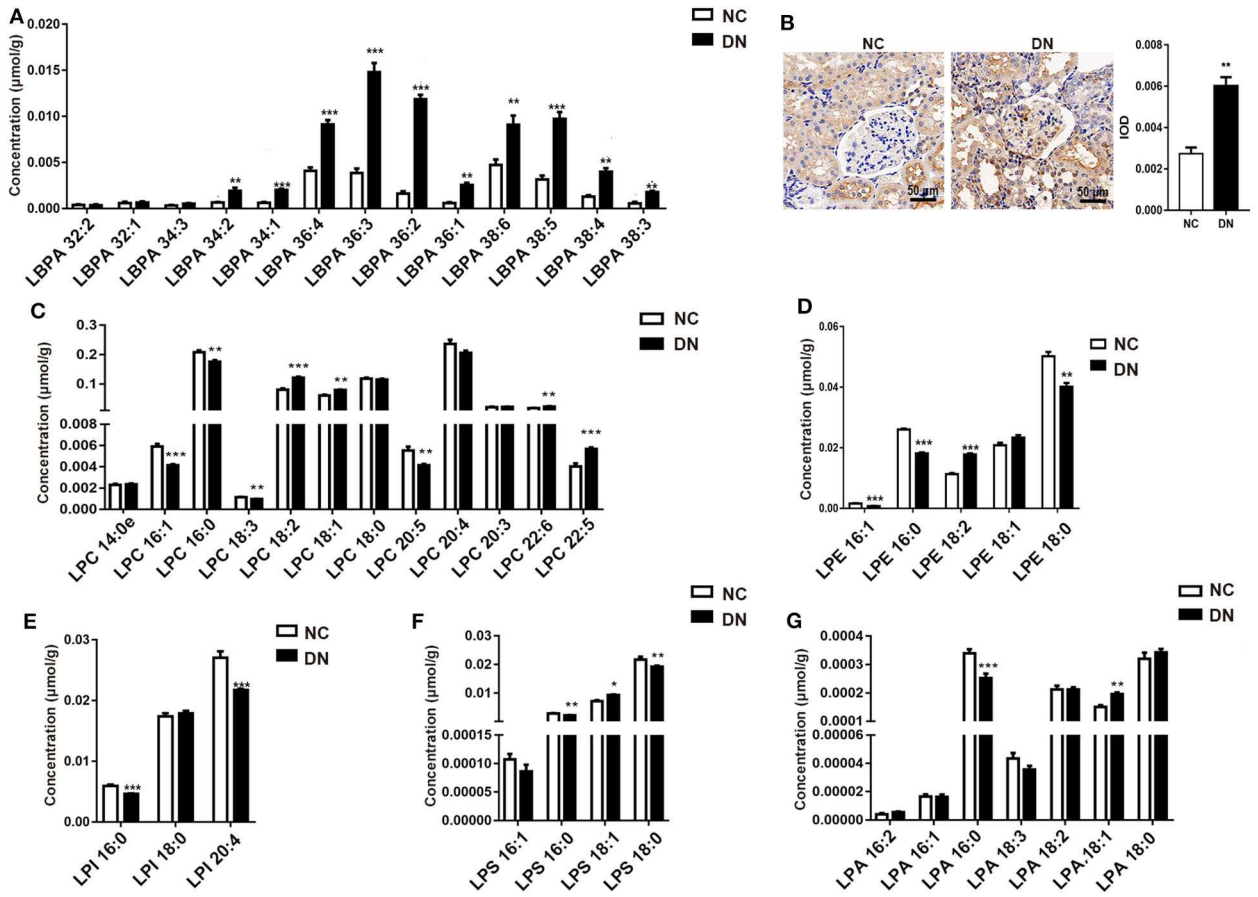

FIGURE 5 | Diabetic nephropathy differentially affected the abundance of lyso-phospholipids. After diabetic nephropathy (DN) was induced by feeding high-fat diet (HFD) in combination with injection of low-dose streptozotocin (STZ) for 8 weeks, **(A)** the content of specific species of lyso-bisphosphatidic acid (LBPA) within the kidney cortex was analyzed; $n = 6$ per group. **(B)** Immunohistochemical staining of CD68, at 400× magnification, and quantitative analysis of positivity in kidney glomeruli are shown. Five glomeruli were assessed for each slide; $n = 3$ per group. Content of specific species of **(C)** lyso-phosphatidylcholine (LPC), **(D)** lyso-phosphatidylethanolamine (LPE), **(E)** (LPI), **(F)** LPS, and **(G)** LPA in the kidney cortex was analyzed; $n = 6$ per group. Data are presented as means ± SEM; $^{*}P < 0.05$, $^{**}P < 0.01$, $^{***}P < 0.001$.

long-chains (C34, C36, and C38). Unsaturated acyl-chains, especially LBPA (36:2), increased by 2- to 4-fold in the DN group, with a 7.3-fold increase observed relative to the normal group. The significant increase in LBPA indicated the activation of macrophages in kidneys in the DN group, which was confirmed by the detection of detection of higher levels of the macrophage marker CD68 in DN glomeruli (**Figure 5B**). We examined other lyso-phospholipids, including LPC, LPE, LPI (lyso-phosphatidylinositols), LPS, and LPA (lyso-phosphatidic acids). Among them, the levels of LPC with side chains of LPC(16:1), LPC(18:2), LPC(22:5), and LPC(22:6) significantly increased, whereas LPC with side chains of LPC(16:0), LPC(18:3), and LPC(20:5) decreased in the DN kidney cortex (**Figure 5C**). Interestingly, unsaturated LPEs, including LPE(16:0) and LPE(18:0), were reduced in the DN group, whereas LPE(18:2) showed an increase of 50% in comparison with the normal group (**Figure 5D**). All LPI species decreased in the DN group (**Figure 5E**). The composition of LPS showed the same pattern as that of LPE, in that LPS containing unsaturated fatty acid chains, such as LPS(16:0) and LPS (18:0), was reduced, whereas LPS(18:1) was significantly increased (**Figure 5F**). As shown in **Figure 5G**, LPA(16:0) decreased by 25%, whereas LPA(18:1) increased by 30% in the DN kidney cortex. Collectively, LBPA exhibited a homogeneous increase, whereas other lyso-phospholipids showed variable changes. The precise pathological relationships between these various lipid species during DN require further investigation.

Comprehensive Changes in Sphingolipids During Early-Stage Diabetic Nephropathy

Sphingolipids, which are enriched in the kidney cortex, play important roles in the regulation of cellular function (5). In the current study, we analyzed several classes of sphingolipids and their species. As shown in **Figure 6A**, most sphingolipids were increased in DN rats without alteration of total sphingomyelin. Globotriaosylceramide (Gb3) showed a decreasing tendency in DN, although the decrease was not significant (**Figure 6B**). Although the total Cer significantly

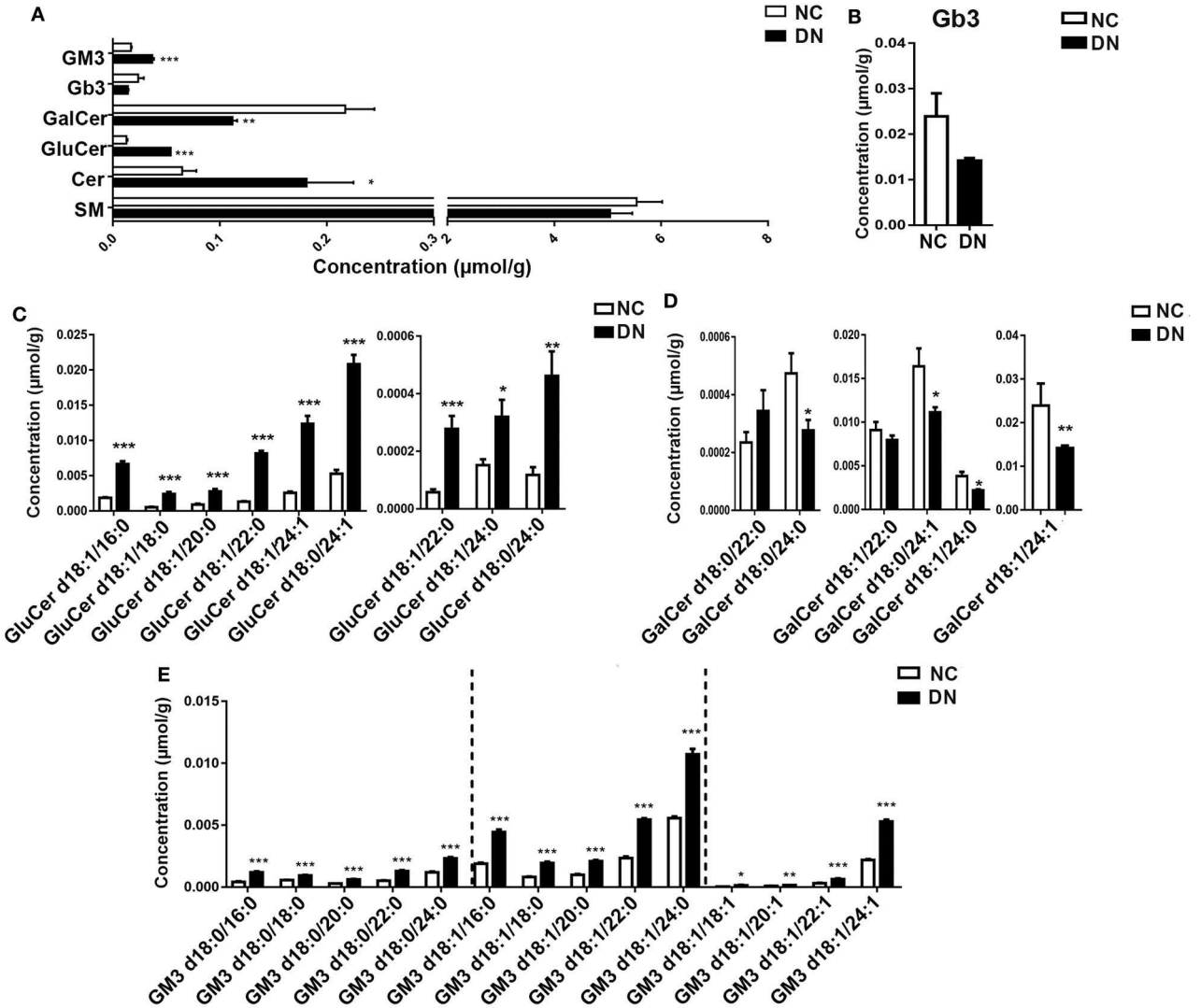

FIGURE 6 | Sphingolipids were significantly altered in the diabetic kidney cortex. Total content of sphingolipid classes **(A)** and specific species of Gb3 **(B)**, glucosylceramide (GluCer) **(C)**, galactosylceramide (GalCer) **(D)**, and monosialo-dihexosyl gangliosides (GM3) **(E)** were analyzed. Data are presented as means ± SEM, $n = 6$ per group; $^{*}P < 0.05$, $^{**}P < 0.01$, $^{***}P < 0.001$.

increased, the changes in ceramide derivatives were not consistent. GluCer markedly decreased, whereas GalCer and monosialo-dihexosyl gangliosides (GM3) increased significantly. We then examined the alteration of species in detail. Results showed that all species of GluCer greatly increased, especially GluCer d18:1/22:0, which increased by 6.25-fold in the DN kidney cortex (**Figure 6C**). Interestingly, in the DN group, most GalCer species decreased by 20–40% compared with those in the normal group, except for GalCer d18:0/22:0 (**Figure 6D**). GM3, the most abundant ganglioside, is characterized by the presence of sialic acid groups linked to the ceramide skeleton structure. As shown in **Figure 6E**, compared with those in the NC group, all GM3 species were significantly increased in DN rats; in particular, the most abundant species of GM3, which contained one unsaturated bond, was intensely elevated. Specific GM3 species were identified in three classes on the basis of their number of unsaturated bonds; among these, GM3 with a side chain of 24 carbons was predominant. Moreover, differences in GM3 between the NC and DN groups were positively correlated with chain length, except in GM3 d18:1/18:1, which was decreased by 4.66-fold in the DN kidney cortex. Collectively, marked alterations were observed in sphingolipids in the early-stage DN model, as evidenced by a homogenous increase in GM3 and diverse changes in GluCer and GalCer. Such changes may serve as potential biomarkers; however, further studies are required to verify this.

DISCUSSION

Abnormal lipid accumulation induces detrimental changes to renal lipid metabolism that promotes insulin resistance, oxidative

stress, and endoplasmic reticulum (ER) stress. These changes ultimately result in deterioration of renal structure and function (15). The most detrimental effect of abnormal lipid accumulation is damage to the glomerular filtration barrier (GFB) as a result of degradation of the glycocalyx, which induces podocyte death and mesangial cell instability (16). These injuries lead to increased GFB permeability, which is a hallmark of, and central event in, DN progression. Lipotoxicity promotes the development of early-stage DN prior to epithelial–mesenchymal transition (EMT) (17). Therefore, comprehensive lipidome analysis is crucial to the identification of potential biomarkers of DN and elucidation of the mechanistic basis of DN. Herein, we applied a high-coverage, targeted lipidomic approach to analyze the lipidome of the kidney cortex in early-stage DN rats, and we identified a lipid profile comprising 437 lipid species from 25 classes. Glycerolipids, sterol lipids, phospholipids, and sphingolipids were additionally identified in this study.

Neutral lipids are closely associated with DN progression. In this study, neutral lipids, such as TAG, DAG, FFA, Cho, and CE, were found to be major components of the kidney lipidome. The observed increase in blood lipids was accompanied by a homogeneous increase in glyceride lipids in the DN kidney cortex. Podocytes are the main site of excess lipid accumulation in DN (7); however, these cells are particularly sensitive to lipid accumulation and undergo induction of insulin resistance or cell death readily as a result of this phenomenon (18). In this study, a significant increase in FFA chain length and degree of unsaturation was observed in the DN kidney cortex. Elevated FFAs not only induced aggravated dyslipidemia and diabetes by increasing plasma TAG but also induced podocyte injury and exacerbated proteinuria by stimulating aberrant micropinocytosis by podocytes (19). Further, fatty acid metabolites, DAG, and ceramides were also elevated. Excessive accumulation of FFA in non-adipose organs results in toxicity and death of tubular epithelial cells in the diabetic kidney (20). A notable finding in this study was that highly unsaturated TAG species markedly accumulated in the cortex of DN kidneys, indicative of susceptibility to lipid peroxidation. Downregulation of fatty acid β-oxidation pathways as well as TAG hydrolase, including PPAR-α, carnitine palmitoyltransferase 1 (CPT1), acyl-CoA oxidase (ACO), and L-FABP, has been strongly linked to glomerular hyperfiltration and inflammation as evidenced by studies of biopsies from DM patients (7). Such TAG species might therefore be potentially relevant to inflammatory processes in DN progression. In a previous study, CE with 23C containing two to four unsaturated bonds was positively related to diabetes (21), and CE with 20C was positively related to T2DM development in women with previous gestational DM (22). Interestingly, in this study, CE with 20C containing two to four unsaturated bonds dramatically increased by 15- to 23-fold in the kidney cortex of early-stage DN model rats. Further, an increase in the side chains of linoleic acid (18:2) was observed in TAG, DAG, FFA, and CE, indicating that linoleic acid plays an important role in DN progression. Wang et al. confirmed that linoleic acid served as a potential indicator of the occurrence and development of DN (23). Furthermore, we observed a dramatic increase in CE containing linoleic acid (18:2) in the DN kidney cortex, with a 28.3-fold increase relative to normal rats. However, further investigation is necessary to establish whether linoleic acid or glycerides can serve as positive indicators for DN progression.

Although phospholipids constitute the minority of the kidney cortex lipidome, they carry out many crucial biological functions such as the maintenance of cellular membrane stability and regulation of cell signaling (24). In this study, significantly altered phospholipid metabolism was characterized by remodeling of polyunsaturated PI as well as PE. In a previous study, phospholipidomic analysis of human plasma demonstrated that PI C18:0/22:6 could be used to discriminate healthy individuals from T2DM or DN patients (8). Consistent with this previous finding, we observed significantly decreased PI 40:6 as well as PI 38:6 in the early-stage DN rat model in this study. Amadori-glycated PE formation triggers lipid peroxidation and may serve as a pathogenic factor during DN (25, 26). However, using matrix-assisted laser desorption ionization imaging mass spectrometry (MALDI IMS), Grove et al. found that Amadori-PEs played only a minor role in DN pathogenesis (24). Here, we observed a homogeneous decline in PE with or without plasmalogen bonds. Decreased PE in the DN cortex has also been observed in progressive DN induced by uninephrectomy with a single intraperitoneal injection of STZ (9). These observations indicate that PE plays an important role in the maintenance of renal function. Although the total amount of PC barely changed, there was a significant decrease in total PE within the DN kidney cortex. Hence, the ratio of PC/PE increased drastically, which has been reported to contribute to ER stress (27). The conversion of PE to PC is catalyzed by phosphatidylethanolamine *N*-methyltransferase (Pemt). Glomerular hypertrophy and albuminuria have been shown to be significantly attenuated in Pemt-deficient mice as a result of a decrease in the ratio of PC/PE and alleviation of ER stress (28). Interestingly, although most phospholipids declined, a specific side chain, 36:1, was increased in almost every phospholipid, including PE, PI, PA, PG PC, and PS. In addition, PC(36:1) has been reported to be independently associated with increased risk for T2DM (29). However, the 36:1 side chain of phospholipids has been rarely reported. The potential for this side chain to serve as a specific biomarker for DN, that is, to distinguish DM from DN, requires further study.

LBPA, also known as bis(monoacylglycerol)phosphate, is crucial for macrophage biology and activity because of its unique role in lysosomal function and storage (14). In this study, elevated LBPA levels were observed in the DN kidney cortex; most of the increased LBPA contained long-chain unsaturated fatty acids, indicating intrinsic regulation of macrophages in DN. The upregulation of CD68 protein levels is consistent with enhanced macrophage infiltration into diabetic glomeruli. Previous studies have revealed that LPA and LPC participate in the pathogenesis of chronic kidney disease through receptor-dependent promotion of proliferation, inflammation, and fibrosis within the kidney (30, 31). Although saturated LPC is usually associated with pro-inflammatory conditions, polyunsaturated LPC is considered to prevent the inflammatory response. In this study, we observed significant accumulation of LPC(18:1), LPC(18:2), LPC(22:5),

LPC(22:6), and LPA(18:1) in the kidneys of DN rats. These results are partially consistent with Saulnier-Blache's observation of the urinary lipidome in T2DM patients, in which LPC(18:0) and LPC(18:1) were significantly elevated, along with macroalbuminuria and mildly reduced estimated glomerular filtration rate (eGFR) (32). Although LPA and LPC are known to promote renal inflammation and tubulo-interstitial fibrosis, some species of LPA and LPC, such as LPC(16:0) and LPC(16:1), are rarely reported in the normal kidney but significantly decreased in the kidneys of DN rats. However, the mechanisms by which these lyso-phospholipids influence the progression of DN are unknown.

It has been reported that sphingolipid accumulation contributes to the development of diabetic kidney disease (33). Consistent with this report, we observed that most sphingolipids were dramatically elevated in the kidney cortex of early-stage DN rats. In the current study, we examined ceramides and their derivatives, including GluCer, GalCer, SM, GM3, and Gb3. Consistent with the results of Liu et al. in a type 1 diabetic rat model (33), most ceramides were greatly increased in the present DN rat model. However, in a type 2 db/db mouse model of DN, ceramides were decreased in the kidney cortex and increased in the plasma (6). One possible explanation for this discrepancy related to DN stage; in the type 2 DN rat model used in this study, kidney cortex tissue was obtained shortly after onset, during the early stages of DN. Sas et al. examined the renal cortex of diabetic mice 24 weeks after the onset of severe renal fibrosis (6). Partial confirmation of this hypothesis was provided by the work of Geoffroy, who demonstrated that the activity and expression of neutral ceramidase was elevated in the diabetic glomeruli 4 days after induction of diabetes but decreased after 28 days (34).

GluCer, which is one of the simplest subclasses of glycosphingolipids (GSLs), is generated from ceramide UDP-Glc:ceramide glucosyltransferase (35). Increasing evidence has been reported for the key role of GSLs in insulin resistance (36). In a previous study, GluCer was found to be increased in early-stage DN (9 weeks) and to increase further with advanced DN (17 weeks), with elevated GSLs mediating renal mesangial hypertrophy (37). However, this previous study did not distinguish individual species of GSLs. Applying advanced lipidomics, we distinguished between the individual species of GSLs on the basis of fatty acyl groups and, unexpectedly, found that the levels of most GalCer species decreased in the DN kidney cortex. Ceramides with the α-anomeric linkage of a galactose sugar are lipid antigens, such as α-GalCer, which strongly activates natural killer (NK) T-cells (38) and inhibits the development of T-cell-mediated autoimmune type 1 diabetes (30, 31). Furthermore, Uchida et al. reported that administration of α-GalCer caused damage to renal vascular endothelial cells as well as tubular epithelial cells and ultimately led to acute kidney injury (39). However, few reports have demonstrated a relationship between GalCer and the progression of DN. Because inflammation is key to the onset and progression of DN, further investigation is required to determine how decreased GalCer in DN disrupts the balance of inflammatory mediators and the mechanisms underlying the resulting toxic effects against glomerular endothelial cells.

GM3, the most abundant ganglioside and predominant lipid in the kidney, is involved in a variety of cellular functions including signal transduction, proliferation, differentiation, and apoptosis (40, 41). Interestingly, our results showed that GM3, especially GM3 containing one unsaturated bond, increased 2- to 4-fold in the DN kidney cortex. In contrast, Kwak et al. observed a decrease in GM3 in STZ-induced diabetic rat glomeruli and the consequent loss of a charge-selective filtration barrier in the renal glomeruli (42). Other studies have shown that GM3 compromises cell regeneration of the GFB through VEGF and AKT pathways (43, 44). Further, GM3 is an important component of lipid rafts (45), which are key to renal SGLT2 and Na/K/Cl co-transporters (46). Therefore, increased GM3 may in turn increase tubular reabsorption and efferent arterial hydrostatic pressure by upregulating Na^+-glucose co-transporter activity, resulting in the decreased glomerular filtration. Furthermore, podocyte function depends on the integrity of lipid rafts, which are largely composed of sphingolipids, including gangliosides (47). In the current study, not all GM3s showed a marked increase; only GM3 containing the oleic acid (18:1) side chain, including GM3 d18:1/24:0, GM3 d18:1/22:0, and GM3 d18:1/24:1, was elevated. Although GM3 has been reported to exert deleterious effects on renal function and structure, few studies have sought to identify the species that are related to the progression of DN. The results from the present lipidomic analysis of GM3 in the kidneys of our DN rat model may offer new insights into the mechanistic basis of DN.

In conclusion, the comparison of the lipidome of the kidney cortex of normal and diabetic rats revealed a distinguishing signature for the DN kidney lipidome, which is characterized by changes in side chain composition and unsaturated bonds. Neutral lipids comprised the majority of the DN kidney lipidome, with most exhibiting a higher degree of unsaturation and side chains of linoleic acid, which may serve as potential markers for DN. Substantial changes were observed in the least abundant lipid classes, especially phospholipids and sphingolipids such as ceramide and GM3. These may exert deleterious effects on the GFB during early-stage DN. The present results provide a detailed overview of the lipidome of the kidney cortex in DN; additionally, the findings offer new insights into the mechanistic basis of DN and reveal pathologically relevant lipid species. However, further investigation is required to identify specific biomarkers for the timely diagnosis of DN.

DATA AVAILABILITY STATEMENT

The datasets generated for this study are available on request to the corresponding author.

ETHICS STATEMENT

The animal study was reviewed and approved by Animal care committee of Institute of Materia Medica, Chinese Academy of Medical Sciences.

AUTHOR CONTRIBUTIONS

BH: conceptualization. PH, PM, and XinY: investigation. SL and GS: methodology. XiuY, LZ, GQ, and GD: supervision. CX: visualization. BH: Writing-original draft. GQ: writing-review and editing. All authors contributed to the article and approved the submitted version.

FUNDING

This project was funded by the National Natural Science Foundation of China (81770847), the Drug Innovation Major Project (2018ZX09711001-003-005), the CAMS Innovation Fund for Medical Sciences (CIFMS) (2017-I2M-1-010 and 2016-I2M-3-007), and the National Key Research and Development Plan (2016YFC1000905).

SUPPLEMENTARY MATERIAL

The Supplementary Material for this article can be found online at: https://www.frontiersin.org/articles/10.3389/fendo.2020.00359/full#supplementary-material

REFERENCES

1. Lam SM, Shui G. Lipidomics as a principal tool for advancing biomedical research. *J Genet Genom.* (2013) 40:375–90. doi: 10.1016/j.jgg.2013.06.007
2. Hou B, Qiang G, Zhao Y, Yang X, Chen X, Yan Y, et al. Salvianolic acid a Protects against diabetic nephropathy through ameliorating glomerular endothelial dysfunction via inhibiting aGE-RAGE signaling. *Cell Physiol Biochem.* (2017) 44:2378–94. doi: 10.1159/000486154
3. Coca SG, Ismail-Beigi F, Haq N, Krumholz HM, Parikh CR. Role of intensive glucose control in development of renal end points in type 2 diabetes mellitus. *Int Med.* (2011) 2011:172. doi: 10.1001/archinternmed.2011.2230
4. de Boer IH, Rue TC, Hall YN, Heagerty PJ, Weiss NS, Himmelfarb J. Temporal trends in the prevalence of diabetic kidney disease in the united states. *JAMA.* (2011) 305:2532–9. doi: 10.1001/jama.2011.861
5. Falkevall A, Mehlem A, Palombo I, Heller Sahlgren B, Ebarasi L, He L, et al. Reducing vEGF-B signaling ameliorates renal lipotoxicity and protects against diabetic kidney disease. *Cell Metab.* (2017) 25:713–26. doi: 10.1016/j.cmet.2017.01.004
6. K.M.S. Viji Nair, Pradeep Kayampilly JB, Jharna Saha HZ. Targeted lipidomic and transcriptomic analysis identifies dysregulated renal ceramide metabolism in a mouse model of diabetic kidney disease. *J Proteomics Bioinform.* (2015) 14:002. doi: 10.4172/jpb.S14-002
7. Herman-Edelstein M, Scherzer P, Tobar A, Levi M, Gafter U. Altered renal lipid metabolism and renal lipid accumulation in human diabetic nephropathy. *J Lipid Res.* (2013) 55:561–72. doi: 10.1194/jlr.P040501
8. Zhu C, Liang QL, Hu P, Wang YM, Luo GA. Phospholipidomic identification of potential plasma biomarkers associated with type 2 diabetes mellitus and diabetic nephropathy. *Talanta.* (2011) 85:1711–20. doi: 10.1016/j.talanta.2011.05.036
9. Zhao T, Zhang H, Zhang X, Zhao T, Lan HY, Liang Q, et al. Metabolomic and lipidomic study of the protective effect of chaihuang-Yishen formula on rats with diabetic nephropathy. *J Ethnopharmacol.* (2015) 166:31–41. doi: 10.1016/j.jep.2015.02.019
10. Kumari S, Singh A. Urinary exosomal lipidomics reveals markers for diabetic nephropathy. *Curr Metab.* (2018) 6:131–9. doi: 10.2174/2213235X05666170607135244
11. Chen H, Chen L, Liu D, Chen DQ, Vaziri ND, Yu XY, et al. Combined clinical phenotype and lipidomic analysis reveals the impact of chronic kidney disease on lipid metabolism. *J Proteome Res.* (2017) 16:1566–78. doi: 10.1021/acs.jproteome.6b00956
12. Moreau D, Vacca F, Vossio S, Scott C, Colaco A, Paz Montoya J, et al. Drug-induced increase in lysobisphosphatidic acid reduces the cholesterol overload in niemann-Pick type c cells and mice. *EMBO Rep.* (2019) 20:e47055. doi: 10.15252/embr.201847055
13. Shui G, Guan XL, Low CP, Chua GH, Goh JS, Yang H, et al. Toward one step analysis of cellular lipidomes using liquid chromatography coupled with mass spectrometry: application to saccharomyces cerevisiae and schizosaccharomyces pombe lipidomics. *Molecular bioSystems.* (2010) 6:1008–17. doi: 10.1039/b913353d
14. Akgoc Z, Iosim S, Seyfried TN. Bis(monoacylglycero)phosphate as a macrophage enriched phospholipid. *Lipids.* (2015) 50:907–12. doi: 10.1007/s11745-015-4045-5
15. Izquierdo-Lahuerta A, Martínez-García C, Medina-Gómez G. Lipotoxicity as a trigger factor of renal disease. *J Nephrol.* (2016) 29:603–10. doi: 10.1007/s40620-016-0278-5
16. Rutledge JC, Ng KF, Aung HH, Wilson DW. Role of triglyceride-rich lipoproteins in diabetic nephropathy. *Nat Rev Nephrol.* (2010) 6:361–70. doi: 10.1038/nrneph.2010.59
17. Xu Y, Huang J, Xin W, Chen L, Zhao X, Lv Z, et al. Lipid accumulation is ahead of epithelial-to-mesenchymal transition and therapeutic intervention by acetyl-CoA carboxylase 2 silence in diabetic nephropathy. *Metabolism.* (2014) 63:716–26. doi: 10.1016/j.metabol.2014.02.010
18. Lennon R, Pons D, Sabin MA, Wei C, Shield JP, Coward RJ, et al. Saturated fatty acids induce insulin resistance in human podocytes: implications for diabetic nephropathy. *Nephrol Dialys Trans.* (2009) 24:3288–96. doi: 10.1093/ndt/gfp302
19. Chung J-J, Huber TB, Gödel M, Jarad G, Shaw AS. Albumin-associated free fatty acids induce macropinocytosis in podocytes. *J Clin Invest.* (2015) 125:9641. doi: 10.1172/JCI79641
20. Kim Y, Lim JH, Kim MY, Kim EN, Yoon HE, Shin SJ, et al. The adiponectin receptor agonist adipoRon ameliorates diabetic nephropathy in a model of type 2 diabetes. *J Am Soc Nephrol.* (2018) 29:1108. doi: 10.1681/ASN.2017060627
21. Zhao C, Mao J, Ai J, Shenwu M, Shi T, Zhang D, et al. Integrated lipidomics and transcriptomic analysis of peripheral blood reveals significantly enriched pathways in type 2 diabetes mellitus. *BMC Med Gen.* (2013) 6:S12. doi: 10.1186/1755-8794-6-S1-S12
22. Lappas M, Mundra PA, Wong G, Huynh K, Jinks D, Georgiou HM, et al. The prediction of type 2 diabetes in women with previous gestational diabetes mellitus using lipidomics. *Diabetologia.* (2015) 58:1436–42. doi: 10.1007/s00125-015-3587-7
23. Wang L, Du Y, Xu BJ, Deng X, Liu QH, Zhong QQ, et al. Metabolomics study of metabolic changes in renal cells in response to high-Glucose exposure based on liquid or gas chromatography coupled with mass spectrometry. *Front Pharmacol.* (2019) 10:928. doi: 10.3389/fphar.2019.00928
24. Grove KJ, Voziyan PA, Spraggins JM, Wang S, Paueksakon P, Harris RC, et al. Diabetic nephropathy induces alterations in the glomerular and tubule lipid profiles. *J Lipid Res.* (2014) 55:1375–85. doi: 10.1194/jlr.M049189
25. Levi V, Villamil Giraldo AM, Castello PR, Rossi JPFC, González Flecha FL. Effects of phosphatidylethanolamine glycation on lipid-protein interactions and membrane protein thermal stability. *Biochemical J.* (2008) 416:145–52. doi: 10.1042/BJ20080618
26. Ravandi A, Kuksis A, Shaikh NA. Glucosylated glycerophosphoethanolamines are the major lDL glycation products and increase lDL susceptibility to oxidation : evidence of their presence in atherosclerotic lesions. *Arterioscler Thromb Vasc Biol.* (2000) 20:467–77. doi: 10.1161/01.ATV.20.2.467
27. Fu S, Yang L, Li P, Hofmann O, Dicker L, Hide W, et al. Aberrant lipid metabolism disrupts calcium homeostasis causing liver endoplasmic reticulum stress in obesity. *Nature.* (2011) 473:528–31. doi: 10.1038/nature09968

28. Mayu W, Atsuko N, Kazutoshi M, Kentaro I, Takahiro T, Chigusa H, et al. Pemt deficiency ameliorates endoplasmic reticulum stress in diabetic nephropathy. *PLoS ONE.* (2014) 9:e92647. doi: 10.1371/journal.pone.0092647
29. Floegel A, Stefan N, Yu Z, Muhlenbruch K, Drogan D, Joost H-G, et al. Identification of serum metabolites associated with risk of type 2 diabetes using a targeted metabolomic approach. *Diabetes.* (2013) 62:639–48. doi: 10.2337/db12-0495
30. Chen Y-G, Choisy-Rossi C-M, Holl TM, Chapman HD, Besra GS, Porcelli SA, et al. Activated nKT cells inhibit autoimmune diabetes through tolerogenic recruitment of dendritic cells to pancreatic lymph nodes. *J Immunol.* (2005) 174:1196–204. doi: 10.4049/jimmunol.174.3.1196
31. Ghazarian L, Diana J, Beaudoin L, Larsson PG, Puri RK, van Rooijen N, et al. Protection against type 1 diabetes upon coxsackievirus b4 infection and iNKT-Cell stimulation: role of suppressive macrophages. *Diabetes.* (2013) 62:3785–96. doi: 10.2337/db12-0958
32. Saulnier-Blache JS, Feigerlova E, Halimi JM, Gourdy P, Roussel R, Guerci B, et al. Urinary lysophopholipids are increased in diabetic patients with nephropathy. *J Diab Compl.* (2017) 31:1103–8. doi: 10.1016/j.jdiacomp.2017.04.024
33. Liu G, Han F, Yang Y, Xie Y, Jiang H, Mao Y, et al. Evaluation of sphingolipid metabolism in renal cortex of rats with streptozotocin-induced diabetes and the effects of rapamycin. *Nephrol Dial Transpl.* (2011) 26:1493–502. doi: 10.1093/ndt/gfq633
34. Geoffroy K, Wiernsperger N, Lagarde M, El Bawab S. Bimodal effect of advanced glycation end products on mesangial cell proliferation is mediated by neutral ceramidase regulation and endogenous sphingolipids. *J Biol Chem.* (2004) 279:34343–52. doi: 10.1074/jbc.M403273200
35. Mather AR, Siskind LJ. Glycosphingolipids and kidney disease. *Adv Exp Med Biol.* (2011) 721:121–38. doi: 10.1007/978-1-4614-0650-1_8
36. Unger RH. Lipotoxic diseases. *Ann Rev Med.* (2002) 53:319–36. doi: 10.1146/annurev.med.53.082901.104057
37. Subathra M, Korrapati M, Howell LA, Arthur JM, Shayman JA, Schnellmann RG, et al. Kidney glycosphingolipids are elevated early in diabetic nephropathy and mediate hypertrophy of mesangial cells. *Am J Physiol Renal Physiol.* (2015) 309:F204–15. doi: 10.1152/ajprenal.00150.2015
38. Brossay L, Chioda M, Burdin N, Koezuka Y, Casorati G, Dellabona P, et al. CD1d-mediated recognition of an a-Galactosylceramide by natural killer t Cells is highly conserved through mammalian evolution. *J Exp Med.* (1988) 188:1521–8. doi: 10.1084/jem.188.8.1521
39. Uchida T, Nakashima H, Ito S, Ishikiriyama T, Nakashima M, Seki S, et al. Activated natural killer t cells in mice induce acute kidney injury with hematuria through possibly common mechanisms shared by human cD56(+) t cells. *Am J Physiol Renal Physiol.* (2018) 315:F618–27. doi: 10.1152/ajprenal.00160.2018
40. Uemura S, Feng F, Kume M, Yamada K, Kabayama K, Nishimura S, et al. Cell growth arrest by sialic acid clusters in ganglioside gM3 mimetic polymers. *Glycobiology.* (2007) 17:568–77. doi: 10.1093/glycob/cwm020
41. Alessandri G, Cornaglia-Ferraris P, Gullino PM. Angiogenic and angiostatic microenvironment in tumors–role of gangliosides. *Acta Oncol.* (1997) 36:383–7. doi: 10.3109/02841869709001284
42. Kwak DH, Rho YI, Kwon OD, Ahan SH, Song JH, Choo YK, et al. Decreases of ganglioside gM3 in streptozotocin-induced diabetic glomeruli of rats. *Life Sci.* (2003) 72:1997–2006. doi: 10.1016/S0024-3205(03)00090-0
43. Jin J, Sison K, Li C, Tian R, Wnuk M, Sung HK, et al. Soluble fLT1 binds lipid microdomains in podocytes to control cell morphology and glomerular barrier function. *Cell.* (2012) 151:384–99. doi: 10.1016/j.cell.2012.08.037
44. Shimamura H, Terada Y, Okado T, Tanaka H, Inoshita S, Sasaki S. The pI3-kinase-Akt pathway promotes mesangial cell survival and inhibits apoptosis *in vitro* via nF-kappa b and bad. *J Am Soc Nephrol.* (2003) 14:1427–34. doi: 10.1097/01.ASN.0000066140.99610.32
45. Chen Y, Qin J, Chen ZW. Fluorescence-topographic nSOM directly visualizes peak-valley polarities of gM1/GM3 rafts in cell membrane fluctuations. *J Lipid Res.* (2008) 49:2268–75. doi: 10.1194/jlr.D800031-JLR200
46. Welker P, Bohlick A, Mutig K, Salanova M, Kahl T, Schluter H, et al. Renal na+-K+-Cl- cotransporter activity and vasopressin-induced trafficking are lipid raft-dependent. *Am J Physiol Renal Physiol.* (2008) 295:F789–802. doi: 10.1152/ajprenal.90227.2008
47. Grove KJ, Voziyan PA, Spraggins JM, Wang S, Paueksakon P, Harris RC, et al. Diabetic nephropathy induces alterations in the glomerular and tubule lipid profiles. *J Lipid Res.* (2014) 55:1375–85. doi: 10.1194/jlr.M049189

Conflict of Interest: The authors declare that the research was conducted in the absence of any commercial or financial relationships that could be construed as a potential conflict of interest.

frontiers in Endocrinology

ORIGINAL RESEARCH
published: 16 December 2020
doi: 10.3389/fendo.2020.536213

Acute Hyperglycemia May Induce Renal Tubular Injury Through Mitophagy Inhibition

Jingyu Wang[1†], Xiaodan Yue[1,2†], Cheng Meng[1], Ziyan Wang[1], Xiaofang Jin[1], Xiao Cui[1], Juhong Yang[1], Chunyan Shan[1], Zhongai Gao[1], Yanhui Yang[1], Jing Li[1], Bai Chang[1] and Baocheng Chang[1*]*

[1] NHC Key Laboratory of Hormones and Development, Tianjin Key Laboratory of Metabolic Diseases, Chu Hsien-I Memorial Hospital & Tianjin Institute of Endocrinology, Tianjin Medical University, Tianjin, China, [2] Tianjin Medical University General Hospital Airport Site, Tianjin, China

Aim: Acute hyperglycemia is closely related to kidney injury. Oxidative stress activation and notable mitochondria damages were found under acute hyperglycemia treatment in our previous work. In the present study, we explored the dose-effect relationship and the pivotal role of mitophagy in acute hyperglycemia induced tubular injuries.

Methods: Forty non-diabetic SD rats were randomly divided and treated with different concentrations of hyperglycemia respectively during the 6-h clamp experiment. Renal morphological and functional alterations were detected. Rat renal tubular epithelial cells were treated with different concentrations of glucose for 6 h. Markers and the regulation pathway of mitophagy were analyzed.

Results: Significant tubular injuries but not glomeruli were observed under both light and electron microscope after acute hyperglycemia treatment, which manifested as enlargement of tubular epithelial cells, disarrangement of epithelial cell labyrinths and swelling of mitochondria. Urinary microalbumin, β2-MG, CysC, NAG, GAL, and NGAL were increased significantly with the increase of blood glucose ($P < 0.05$). ROS was activated, mitochondrial membrane potential and LC3-II/LC3-I ratio were decreased but P62 and BNIP3L/Nix were increased in hyperglycemia groups ($P < 0.05$), which were reversed by AMPK activation or mTOR inhibition.

Conclusion: Acute hyperglycemia causes obvious tubular morphological and functional injuries in a dose-dependent manner. Acute hyperglycemia could inhibit mitophagy through AMPK/mTOR pathway, which would aggravate mitochondria damage and renal tubular impairment.

Keywords: acute hyperglycemia, mitophagy, mitochondria, renal tubule, kidney injury

OPEN ACCESS

Edited by:
Mohamed Abu-Farha, Dasman Diabetes Institute, Kuwait

Reviewed by:
Matthew M. Robinson, Oregon State University, United States
Livia Lopez Noriega, Imperial College London, United Kingdom

***Correspondence:**
Baocheng Chang
changbc1970@126.com
Bai Chang
changbai1972@126.com

[†]These authors have contributed equally to this work

Specialty section:
This article was submitted to Diabetes: Molecular Mechanisms, a section of the journal Frontiers in Endocrinology

Received: *19 February 2020*
Accepted: *10 November 2020*
Published: *16 December 2020*

Citation:
Wang J, Yue X, Meng C, Wang Z, Jin X, Cui X, Yang J, Shan C, Gao Z, Yang Y, Li J, Chang B and Chang B (2020) Acute Hyperglycemia May Induce Renal Tubular Injury Through Mitophagy Inhibition. Front. Endocrinol. 11:536213. doi: 10.3389/fendo.2020.536213

INTRODUCTION

Diabetes mellitus (DM) is becoming a more threatening public health problem not only because of its high prevalence, but also owing to its high incidence and poor outcomes of vascular complications such as diabetic kidney disease (DKD). People have used to concentrate on the bad effects of chronic, longstanding hyperglycemia for a long period, but neglect the injuries resulting from acute hyperglycemia. In peoples' traditional view, acute hyperglycemia occurred in diabetic ketosis and hypertonic hyperglycemia state could induce a series of metabolic disorders; in addition, acute hyperglycemia could suppress the insulin secretion function of β-cells transiently which is called "acute hyperglycemic toxicity". We often encounter patients with diabetic ketosis accompanied by transient albuminuria, who are usually misdiagnosed as "diabetic kidney disease". Does it mean rapidly elevated blood glucose could also lead to "acute hyperglycemic renal toxicity"? Patients admitted in intensive care unit (ICU) with acute hyperglycemia usually have a high prevalence of acute kidney injury (AKI), and strict control of blood glucose could obviously improve this outcome (1). In order to investigate the specific effects of acute hyperglycemia, we used hyperglycemic clamp in non-diabetic conscious rats keeping blood glucose concentration around 16.7 mmol/L for 6 h, and detected obvious morphological and reabsorption functional injuries of renal tubular epithelial cells in our previous work (2).

The abnormal increase of reactive oxygen species (ROS) in renal tubular epithelial cells is the pivotal mechanism of renal tubular injury (3, 4). In our previous study, we found acute hyperglycemia could lead to obvious renal oxidative stress activation and notable mitochondria damages including mitochondria swelling and irrecognizable mitochondrial crista (2). ROS is mainly produced by mitochondria, and excess ROS accumulation can aggravate mitochondria damages and even cell apoptosis (5). Clearing away damaged mitochondria in time is crucial for cellular homeostasis. Cells clear away damaged organelles and other components through autophagy to keep a stable state. The insufficiency of mitophagy can lead to ROS accumulation in cells which will aggravate cell injury and involve in the occurrence and development of many renal diseases. Autophagy is up-regulated and plays a protective role in drug induced acute kidney injury or acute ischemic renal injury (6–9); while it is down-regulated in both type 1 and type 2 diabetic rats (10–13). But what role might mitophagy play in acute hyperglycemia induced kidney injury is still unknown. In this study, we explored the dose-injury relationship of acute hyperglycemia induced renal tubular injury and investigated the possible role of mitophagy and its regulation pathway in acute hyperglycemia induced renal tubular injury.

MATERIALS AND METHODS

Animals

Forty male Sprague-Dawley rats (body weight 250–280 g) supplied by Beijing HuaFuKang Bioscience Co., LTD were included in this study. All rats were maintained at 20–25°C and 50%–60% humidity on a 12-h–12-h light-dark cycle with free access to food and water. This study was permitted by the Tianjin Medical University Animal Committee, and all the animals were maintained according to the guidelines for the care and use of laboratory animals.

Surgical Preparation

All animals received surgical placement of catheters into the left internal jugular vein which were then externalized to the back of the neck under anesthesia (10% chloral hydrate, 0.3 ml/kg body weight) after 1 week of adaptation. All the rats regained their presurgical body weight and kept in a good health condition before the clamp, which were preformed 5 days after surgery.

Hyperglycemia Clamp Study and Sample Collection

Rats were randomly assigned to four groups, control group, hyperglycemia group A (HG-A, 11.1 mmol/L), hyperglycemia group B (HG-B, 16.7 mmol/L), and hyperglycemia group C (HG-C, 25.0 mmol/L), 10 in each group. Rats were kept in a postabsorptive state before the clamp, and stayed awake in the fixator during the clamp. A 6-h hyperglycemia-clamp procedure was performed as described in our previous study (2). 50% glucose solution was infused continuously through the catheters at the speed of 0.4–1.0, 0.6–1.2, or 1.8–2.5 ml/h, respectively, to keep blood glucose concentrations maintained around 11.1, 16.7, or 25.0 mmol/L in each hyperglycemia group after a bolus injection for about 3–5 min to raise blood glucose to the target level rapidly. Normal saline was infused in control group at the same speed as that in hyperglycemia group. Blood glucose level was determined from the tail vein every 5 min. Twenty-four–hour urine samples were collected in metabolic cages after clamp for the detection of urinary microalbumin (UMA), β2-microglobulin (β2-MG), N-acetyl-beta-D-glucosaminidase (NAG), galactosidase (GAL), neutrophil gelatinase-associated lipocalin (NGAL), and Cystatin C (CysC). Blood sample was collected from the femoral artery for serum creatinine (Scr), blood urea nitrogen (BUN) analysis, and creatinine clearance rate (Ccr) was calculated. Kidneys were isolated immediately upon the time rats were sacrificed. The left kidney was frozen for western blot and RT-PCR analysis, and the right one was kept for morphological observation.

Morphological Observation

The kidney tissue was fixed with 4% paraformaldehyde and embedded in paraffin. Tissue sections with 4-um thickness were prepared, dewaxed in xylene, rehydrated in decreasing concentrations of ethanol and stained with hematoxylin-eosin (HE) stain. After staining, tissue sections were dehydrated in increasing concentrations of ethanol and xylene and sealed with gum. The changes of glomerular and tubular morphology were observed using light microscope (OLYMPUS IX5O/BX5O).

Kidney tissue specimens (1 mm^3) were fixed in 2.5% glutaraldehyde and 1% osmium tetraoxide, dehydrated with gradient alcohol (50%, 70%, 90%, and 100%) and epoxypropane. Samples were then oriented longitudinally and

embedded in Epon 812. Ultrathin sections were cut into 50 μm ± using ultramicrotome and then dyed with uranyl acetate and lead citrate. Transmission electron microscope (HITACHI-7500) was used to observe glomerular and tubular morphology and autophagosome.

Renal Function Analysis

The Scr and BUN were tested using Hitachi 7600A-020 automatic biochemical analyzer, and Ccr which represented glomerular filtration function was calculated as described previously (14). Urinary UMA, β2-MG, NAG, and GAL were measured with Roche analyzer, and urinary NGAL and CysC were detected using enzyme linked immunosorbent assay (ELISA) Kits according to the manufacturers' protocol (Wuhan Huamei Bioengineering Co., Ltd).

Cell Culture and Treatments

Rat renal tubular epithelial cells (NRK-52E cells) purchased from Chinese Academy of Sciences Cell Library were cultured in Dulbecco's modified Eagle's medium (DMEM) containing 10% fetal bovine serum (Tianjin Bacchus Biotechnology Co., Ltd.) and 1% penicillin/streptomycin (Gibco) at 37°C and 5% CO_2, and the 3–5 passages of cells were used. Cells were exposed to different concentrations of glucose (5.5, 11.1, 16.7, or 25.0 mmol/L) for 6 h. 3-(4, 5-dimethylthiazol-2-yl) -2, 5-diphenyltetrazolium bromide (MTT) assay was used to assess cell viability. NRK-52E cells were treated with hyperglycemia (16.7 mmol/L) in the presence or absence of 5'-AMP- activated protein kinase (AMPK) activator 5-Aminoimidazole-4-carboxamide1-β-D-ribofuranoside (AICAR) (500umol/L, MedChem Express) or mammalian target of rapamycin complex (mTOR) inhibitor rapamycin (50nmol/L, MedChem Express) for 6 h in order to detect the role of AMPK or mTOR in acute hyperglycemia induced kidney injury. Total RNA and protein were extracted for further analysis. Studies were replicated three times.

ROS and Mitochondrial Membrane Potential Detection

Cells were incubated with H2-DCFDA (Cat. NO: KGAF018, KeyGEN BioTECH) for ROS detection. Media was aspirated from the cells grown in 24-well plates and the cells were washed twice with 500 μl PBS. 10μM H2-DCFDA was added to the monolayer of cells. The plate was incubated in the dark at 37°C for 30 min. After incubation, cells were washed with 500-μl PBS and then observed using fluorescence microscope (Olympus Corp., Tokyo, Japan).

Mitochondrial Membrane Potential Assay Kit (5,5',6,6'-tetrachloro-1,1',3,3'-tetraethylbenzimidazolcarbocyanine iodide, JC-1) (Beijing Solarbio Science & Technology Co., Ltd) was used for quantifying changes in mitochondrial membrane potential (MMP) in NRK-52E cells. JC-1 exhibits potential-driven accumulation in mitochondria, decreased red fluorescence and corresponding increased green fluorescence suggest depolarized mitochondria. Cells grown in 24-well plates were incubated with JC-1 dyeing working solution in the dark at 37°C for 20 min. After incubation, cells were washed with JC-1 dyeing buffer and examined using fluorescence microscope (Olympus Corp., Tokyo, Japan).

Western Blotting

Renal tissues and cells were homogenized in RIPA buffer containing Protease/Phosphatase Inhibitor Cocktail (Beijing Suo Lai Bao Technology Co., Ltd.) after washing with PBS, and total protein concentration was estimated using BCA Protein Assay Kit (Wuhan Doctorate Bioengineering Co., Ltd.). Protein samples (40-80μg) were submitted to SDS-PAGE and then transferred to nitrocellulose membranes. Membranes were blocked for 2 h in 5% non-fat milk and then incubated with primary antibodies against LC3 (1:1,000, Cell Signaling), SQSTM1/p62 (1:1,000, Abcam), BNIP3L/Nix (1:1,000, Cell Signaling), mTOR (1:1,000, Cell Signaling), Phospho-mTOR (1:1,000, Cell Signaling), AMPKα (1:1,000, Cell Signaling), Phospho-AMPKα (1:1,000, Cell Signaling), SGLT2 (1:1,000, Abcam), and β-actin (1:500, Sanjian Biotechnology) at 4°C overnight. After being washed with TBST, the membranes were incubated with peroxidase-conjugated secondary antibodies (1:5000, Ai Meijie Technology Co., Ltd, China). The reactive bands were detected using the ECL system (Advansta). Signal intensity was then assessed using automatic gel imaging system (SYNGENE). Studies were replicated 3 times.

RT-PCR Analysis

Total RNA was extracted from rat kidneys and cells using Trizol Reagent (Thermo Fisher, USA). The cDNA was synthesized using Reverse Transcription Kit (Thermo Fisher, USA) according to the following protocol: 25°C for 5min, 42°C for 60min, 70°C for 5 min. All primers were designed and synthesized by Beijing oak Biotech Corp. Primers are listed in **Table 1**. Then Quantitative real-time PCR was performed using the SYBR® Premix Ex TaqTM Kit (Dalian Bioengineering Co., Ltd.) with primers on Applied Biosystems (BIO-RAD, USA) according to the following protocol: 95°C for 1min, 94°C for 10s, 60°C for 15s, 72°C for 15s, 40 cycles. The mRNA expression levels were calculated according to the $2^{-\Delta\Delta CT}$ method (15). The β-actin mRNA expression was used as reference control. Studies were replicated 3 times.

Statistical Analysis

SPSS 20.0 was used to analyze the data. All values were tested for normality and homogeneity of variance. Normally distributed values were expressed as means ± SD. Independent t-test was

TABLE 1 | Primer sequences used in the RT-PCR analysis.

Genes	Primer sequences
LC3B	Forward, 5′-CGAACAAAGAGTGGAAGATGTC-3′
	Reverse, 5′-AGGCTTGGTTAGCATTGAGC-3′
P62	Forward, 5′-AGTCGGAGCGGGTTCTCTAT-3′
	Reverse, 5′-GTGACACACATTCCAGCGAT-3′
BNIP3L/Nix	Forward, 5′-GCACTTCAGCAATGGGAATG-3′
	Reverse, 5′-GCTCTGTTGGTATCTTGTGGTGT-3′
SGLT2	Forward, 5′-GGTCATTGCCGCGTATTTCC-3′
	Reverse, 5′-ATGTTGCTGGCGAACAGAGA-3′
AMPK	Forward, 5′-TTCTGTCTGCCGTGGACTACT-3′
	Reverse, 5′-CAGCCTTCCTGAGATGACCT-3′
mTOR	Forward, 5′-CCAGGAAATACCCTCTCCATC-3′
	Reverse, 5′-GAAGGTCACAAAGCCGTCTT-3′

used to compare differences between two groups. One-way analysis of variance was used to analyze the differences among multiple groups. Parameters that were not normally distributed were expressed as (P25, P75) and compared using Rank sum test. Values of $P < 0.05$ were considered statistically significant.

RESULTS

The Establishment of Acute Hyperglycemia Model

During the hyperglycemic clamp, as shown in **Figure 1**, the blood glucose level in each hyperglycemia group increased significantly compared with that in control group [11.67 ± 1.21 mmol/L, 16.67 ± 2.11 mmol/L, 24.73 ± 3.43 mmol/L vs. 5.37 ± 0.52 mmol/L, $P < 0.05$].

Renal Morphological Alterations Under Acute Hyperglycemic State

We detected the renal glomerular and tubular morphology alterations in rats using both optical microscope and transmission electron microscope under different concentrations of acute hyperglycemia treatment.

Under optical microscope, swelling of tubular epithelial cells and tubular stenosis in each hyperglycemic group were noticed, which became more severe with the increase of blood glucose. However, no obvious differences in glomeruli were detected compared with that in control group (**Figure 2A**).

Under transmission electron microscope, we detected obvious foot process fusion, glomerular basement membrane thickening and endothelial cell window enlargement in acute hyperglycemia groups (**Figure 2B**). Compared to glomerular cells, more serious damages were observed in tubular epithelial cells including the disarrangement of epithelial cell labyrinths, swelling of mitochondria, irrecognizable mitochondrial crista and even apoptotic manifestation of nucleus, which also became more obvious with the increase of blood glucose concentration (**Figure 2C**).

Alterations in Renal Function

No significant differences were found for the plasma level of SCr, BUN and CCr reflecting glomerular filtration function as well as the ratio of kidney-body weight reflecting the degree of kidney hypertrophy between each two groups ($P > 0.05$). However, 24-h UMA increased significantly in hyperglycemia groups compared with that in control group, which increased gradually with blood glucose increase (16.40 ± 0.85 μg/24 h, 32.00 ± 4.95 μg/24 h, 32.70 ± 4.67 μg/24 h vs. 10.25 ± 0.84 μg/24 h, $P < 0.05$) (**Figure 3A**).

Urinary β2-MG and CysC were used to assess the reabsorption function of renal tubules, while NAG, GAL and NGAL were used to evaluate injuries of tubular epithelial cells. All these indicators increased significantly in hyperglycemia groups compared with that in control group ($P < 0.05$). As shown in **Figure 3B**, urinary GAL and NGAL began to increase significantly since blood glucose reached 11.1 mmol/L ($P < 0.05$), and urinary NAG, β2-MG and CysC began to elevate significantly since blood glucose reached 16.7 mmol/L ($P < 0.01$ for NAG, CysC and $P < 0.05$ for β2-MG vs. Control).

Acute Hyperglycemia Could Induce Obvious Mitochondria Injuries and ROS Production

We observed obvious mitochondrial morphological changes after rats were treated with different concentrations of glucose, which shown as swelling of mitochondria, mitochondrial fragmentation, irregular arrangement and irrecognizable mitochondrial crista under transmission electron microscope (**Figure 4A**). We also investigated the MMP changes with JC-1 staining, and detected gradually decreased MMP with the increased glucose concentration, as evidenced by increased green fluorescence and decreased red fluorescence (**Figure 5F**). Mitochondria is the major site of ROS production. After 6-h

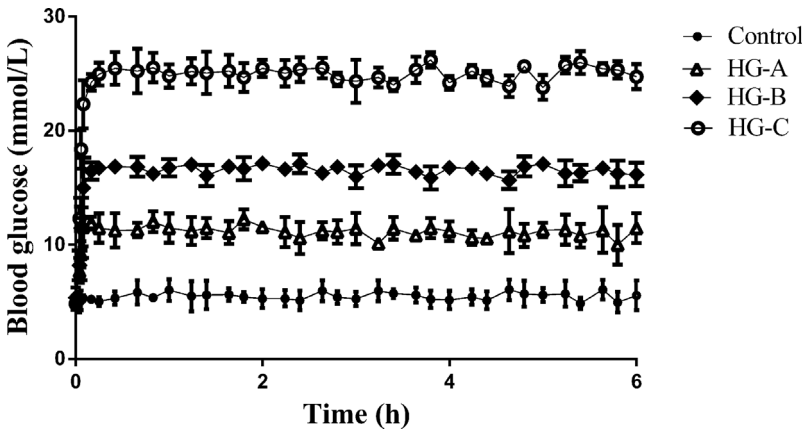

FIGURE 1 | Blood glucose level during hyperglycemic clamp in different groups. N = 10 in each group. Data were expressed as means ± SD in each group. Control, control group; HG-A, hyperglycemia group A; HG-B, hyperglycemia group B; HG-C, hyperglycemia group C.

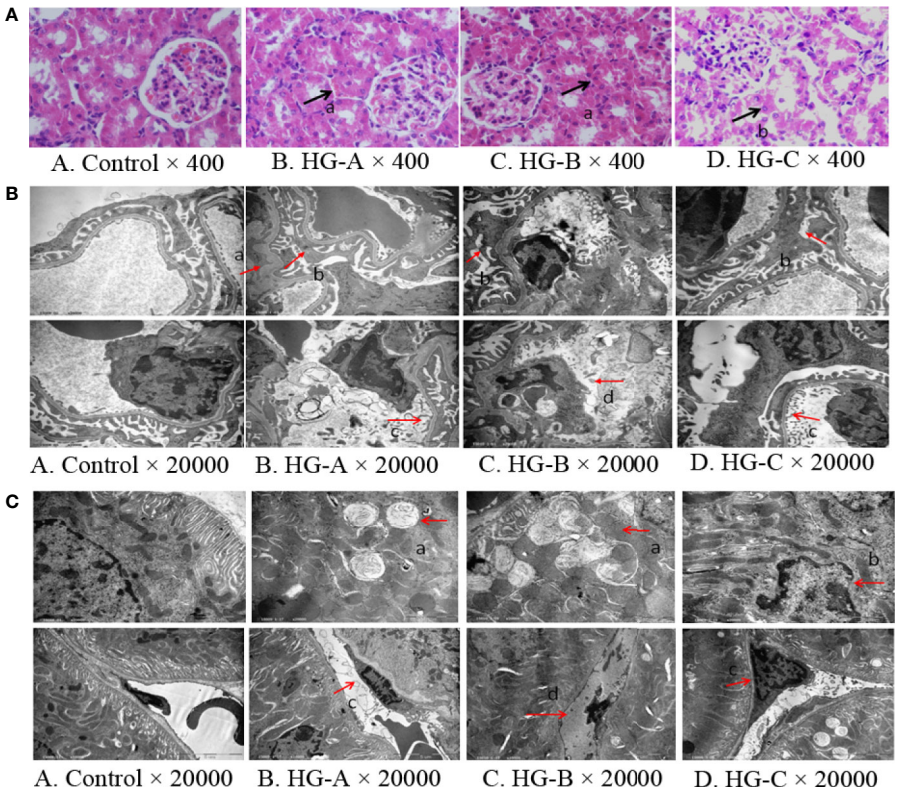

FIGURE 2 | Renal morphological alterations under acute hyperglycemic state. **(A)** Renal morphological alterations under optical microscope. Arrow "a" indicates swelling of tubular epithelial cells and tubular stenosis, arrow "b" indicates fragmentation of tubular epithelial cells. **(B)** Ultrastructural alterations of glomerulus. Arrow "a" indicates thickening of glomerular basement membrane; arrow "b" indicates fusion of foot process; arrow "c" indicates enlargement of glomerular endothelial cell window; and arrow "d" indicates apoptosis of endothelial cells. **(C)** Ultrastructural alterations of renal tubular epithelial cells. Disorder of tubular epithelial cell labyrinths, vesicles development (arrow a), apoptotic changes of nucleus (arrow b) were noticed in tubular epithelial cells and swelling or apoptosis of nucleus (arrows c and d) were indicated in renal tubular vascular endothelial cells in hyperglycemia groups. Control, control group; HG-A, hyperglycemia group A; HG-B, hyperglycemia group B; HG-C, hyperglycemia group C.

hyperglycemia treatment, ROS accumulated gradually in tubular epithelial cells with the glucose concentration increase (**Figure 5C**).

Acute Hyperglycemia May Induce Renal Tubular Injury Through Mitophagy Inhibition

Under transmission electron microscope, swelling of mitochondria and irrecognizable mitochondrial crista with abnormally accumulated autophagosome containing partial degraded mitochondria were detected in hyperglycemia groups, which were more serious with the increase of blood glucose concentration (**Figure 4A**). P62 reflecting the inhibition of autophagy, ratio of LC3-I to LC3-II reflecting the formation of autophagosome and BNIP3L/Nix mediating the recognition of damaged mitochondria during the process of mitophagy were studied in the present study. We detected the decrease of LC3-II/LC3-I ratio accompanied with the increase of P62 and BNIP3L/Nix in hyperglycemia groups ($P < 0.05$) (**Figures 4B, C**).

Renal tubular epithelial cells contain large amount of mitochondria, and are more sensitive to oxidative stress. From the results of both morphological and functional alterations mentioned above, we could conclude that renal tubular injuries were more severe than that of glomerulus under acute hyperglycemic state. We then treated renal tubular epithelial cells (NRK-52E cells) with different concentrations of glucose to study the effects of acute hyperglycemia on tubular epithelial cells.

As shown in **Figures 5A, B**, no obvious differences of cell viability were found in MTT assay among the four groups ($P > 0.05$). Consistent with the results *in vivo*, we also detected the gradually down-regulated LC3-II/LC3-I ratio accompanied with the gradually up-regulated P62 and BNIP3L/Nix in hyperglycemia groups ($P < 0.05$) (**Figures 5D, E**).

SGLT2/AMPK/mTOR Pathway Played a Key Role in Acute Hyperglycemia Induced Mitophagy Inhibition in Renal Tubular Epithelial Cells

SGLT2 mediates glucose uptake of tubular epithelial cells. The SGLT2 level was elevated after 6-h hyperglycemia treatment both *in vivo* and *in vitro* in this study ($P < 0.05$ for HG-C vs. Control).

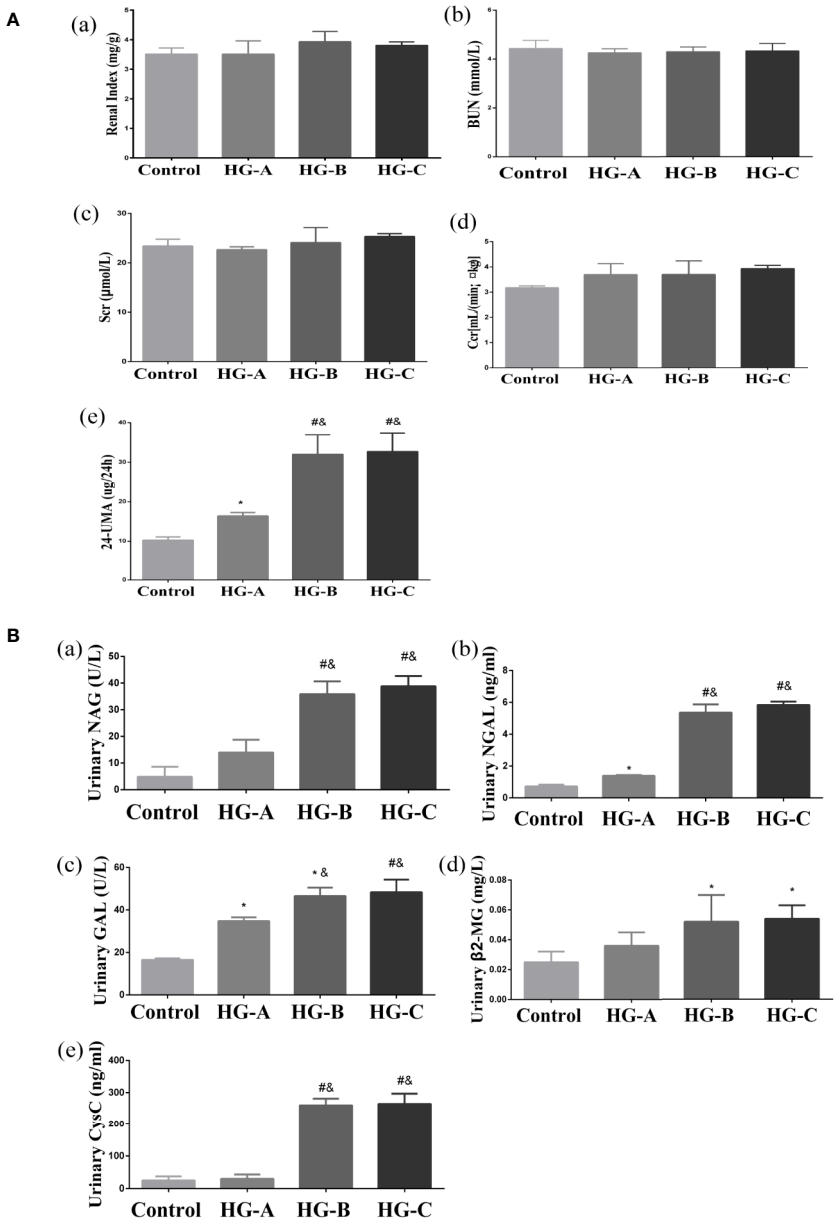

FIGURE 3 | Renal glomerular function, 24-h UMA and renal tubular function alterations. N = 10 in each group. **(A)** Renal glomerular function and 24-h UMA changes. **(B)** Renal tubular function alterations. Values were expressed as means ± SD in each group. $^{*}P < 0.05$ vs. Control; $^{\#}P < 0.001$ vs. Control; $^{\&}P < 0.05$ vs. HG-A. Control, control group; HG-A, hyperglycemia group A; HG-B, hyperglycemia group B; HG-C, hyperglycemia group C. BUN, blood urea nitrogen; Scr, serum creatinine; Ccr, creatinine clearance rate; 24-h UMA, 24-h urinary microalbumin; NAG, N-acetyl-β-D-glucosaminidase; NGAL, neutrophil gelatinase-associated lipocalin; GAL, β-D-galactosidase; β2-MG, β2-microglobulin; CysC, Cystatin C.

The ratio of p-AMPK/AMPK were decreased and p-mTOR/mTOR were increased by high glucose treatment ($P < 0.05$ for HG-B and C vs. Control) (**Figure 6**). In order to study the role of AMPK/mTOR in mitophagy inhibition, we further treated NRK-52E cells in hyperglycemic group (16.7 mmol/L) with AMPK activator AICAR or mTOR inhibitor rapamycin (RAPA), and detected decreased ROS production, improved MMP, increased LC3-II/LC3-I ratio and decreased P62 and BNIP3L/Nix compared with those in hyperglycemia group ($P < 0.05$) (**Figure 7**).

DISCUSSION

As the prevalence of diabetes is increasing rapidly, people are used to concentrate more on chronic hyperglycemia, the main

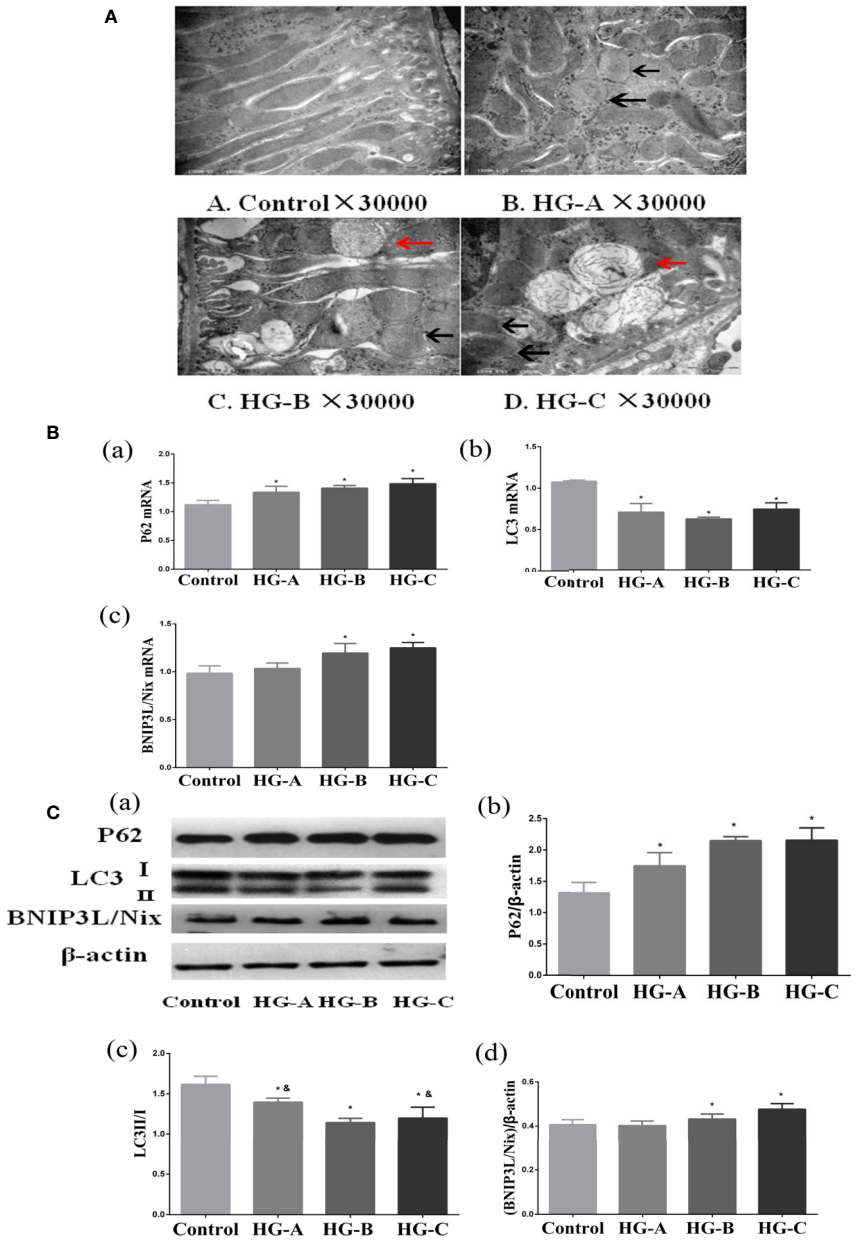

FIGURE 4 | Mitophagy was inhibited in the kidney under acute hyperglycemic state. N = 10 in each group. **(A)** Swelling of mitochondria, mitochondrial fragmentation, irregular arrangement and irrecognizable mitochondrial crista observed using transmission electron microscope (black arrow). Abnormal autophagosome accumulation under transmission electron microscope (red arrow). **(B, C)** Alterations of mitophagy related markers in different groups. Values are presented as means ± SD in each group. $^{*}P < 0.05$ vs. Control; $^{\&}P < 0.05$ vs. HG-B. Control, control group; HG-A, hyperglycemia group A; HG-B, hyperglycemia group B; HG-C, hyperglycemia group C.

clinical sign of diabetes, and its poor outcomes. But acute hyperglycemia, often occurs in diabetic patients with ketoacidosis and hyperosmolar states and non-diabetic patients with severe injuries, is usually neglected. Studies have revealed a strong relationship between acute hyperglycemia and kidney injuries. Albuminuria occurs commonly in new diagnosed diabetic patients especially those with diabetic ketosis, who are usually misdiagnosed as "diabetic kidney disease". For critically ill patients with or without pre-diagnosed diabetes, acute elevated blood glucose could increase the incidence of acute kidney injury, and strict control of blood glucose could improve this outcome (1, 16–18). Animal studies also proved that acute hyperglycemia induced by anesthetics or serious burns could lead to glomerular filtration function impairment and tubular dilatation (19, 20). Acute hyperglycemia is usually diagnosed as random blood glucose higher than 10.0 mmol/L or 11.1 mmol/L

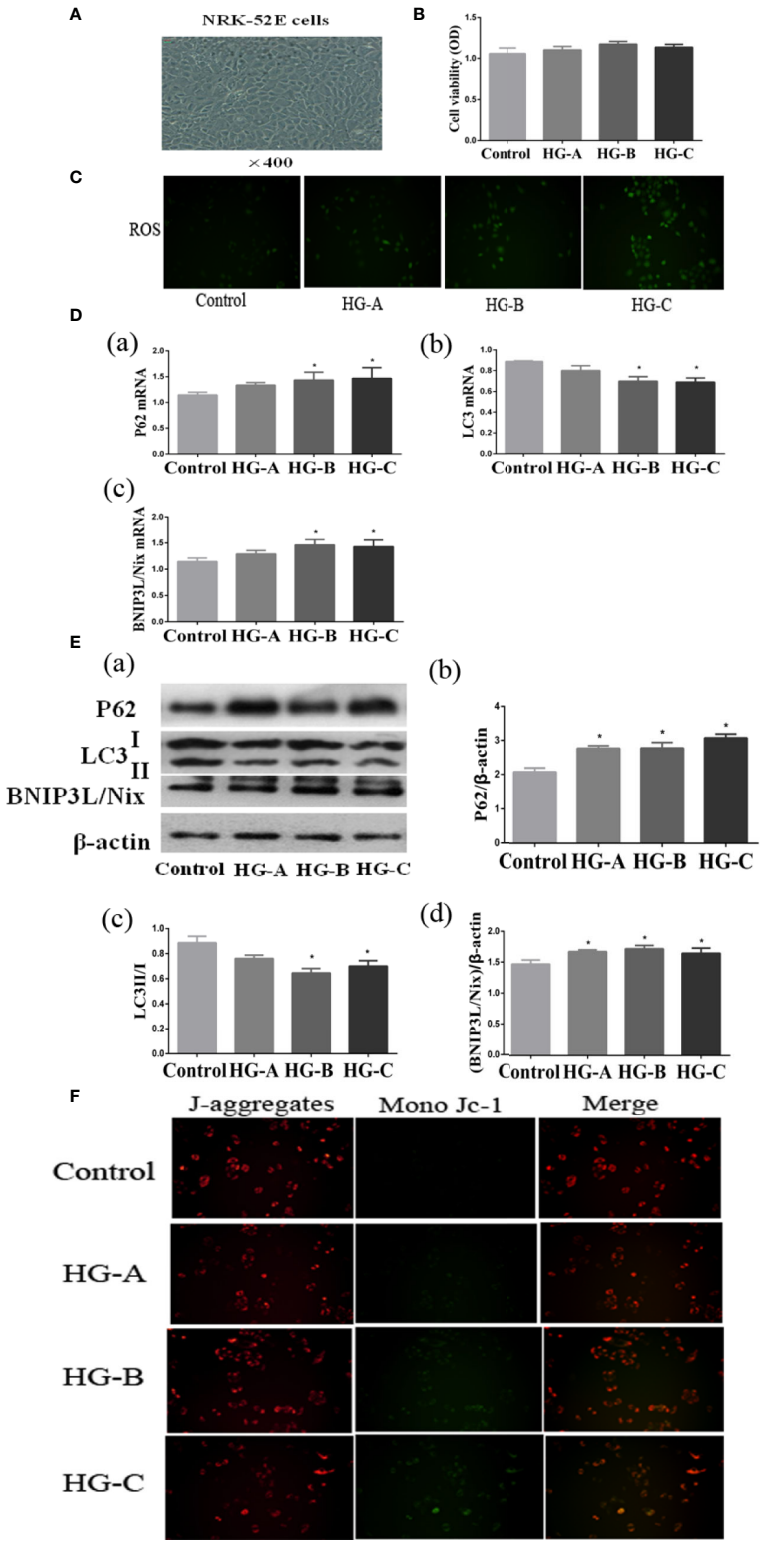

FIGURE 5 | Mitophagy was inhibited in NRK-52E cells under acute hyperglycemic state. **(A, B)** Morphology and viability of NRK-52E cells. **(C)** ROS detection in NRK-52E cells (200*). **(D, E)** Alterations of mitophagy related markers in NRK-52E cells in different groups. **(F)** Mitochondrial membrane potential changes in NRK-52E cells (200*). Values are presented as means ± SD in each group. *$P < 0.05$ vs. Control. Control, control group; HG-A, hyperglycemia group A; HG-B, hyperglycemia group B; HG-C, hyperglycemia group C.

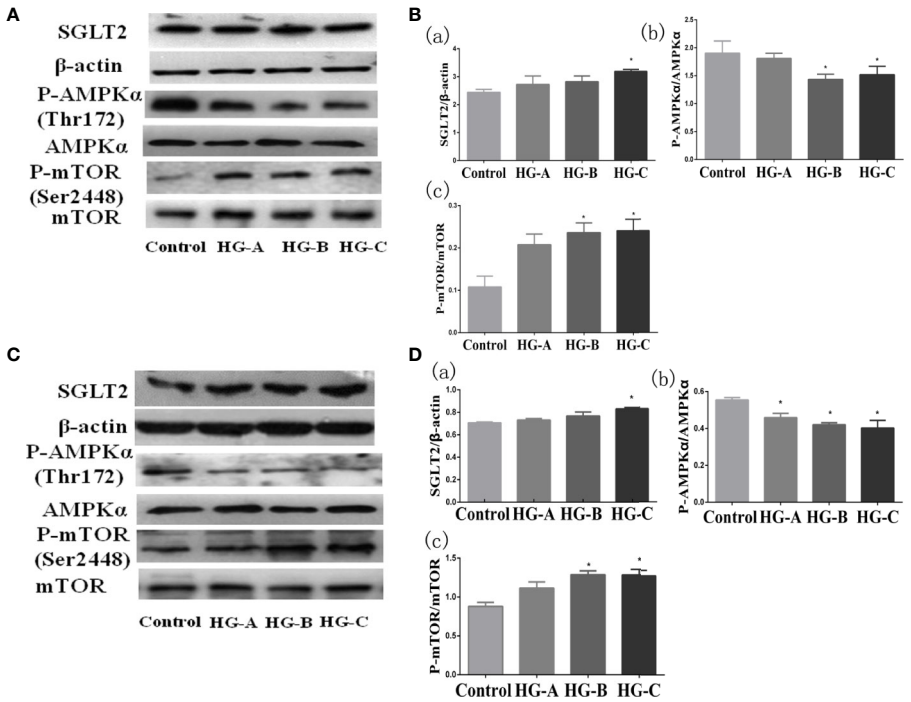

FIGURE 6 | SGLT2/AMPK/mTOR pathway changes under acute hyperglycemic state both *in vivo* **(A, B)** and *in vitro* **(C, D)**. Values are expressed as means ± SD in each group. *$P < 0.05$ vs. Control. Control, control group; HG-A, hyperglycemia group A; HG-B, hyperglycemia group B; HG-C, hyperglycemia group C. SGLT2, sodium glucose co-transporter 2; AMPK, 5'-AMP-activated protein kinase; mTOR, mammalian target of rapamycin complex.

on admission (21). In our previous study, we used hyperglycemic clamp to mimic the acute hyperglycemia state, and detected obvious glomerular and tubular injuries (2). In the present study, we further demonstrated that acute hyperglycemia could lead to renal glomerular and tubular injuries in a dose-dependent manner, and tubular injuries appeared more obvious. Hyperglycemic clamp was used in this study to increase the blood glucose of rats rapidly to a specific stable level. In this model, rats are kept fully conscious which can avoid the impacts of drugs, anesthetization or surgery on kidney. We also found that mitochondria in tubular epithelial cells were seriously injured and mitophagy was inhibited by acute hyperglycemia through AMPK/mTOR regulation.

Renal tubules manifested to be more seriously damaged under acute hyperglycemic treatment in the present study. Tubular morphological changes could be detected since blood glucose reached 11.1 mmol/L under both light and electron microscope, and became more obvious with blood glucose concentration increase. Urinary microalbumin (UMA), a traditional marker representing damages of glomerular filtration barrier and glomerular hyperfiltration, increased gradually in a dose-dependent manner since blood glucose reached 11.1 mmol/L. In recent years, UMA is believed to be primarily controlled by renal tubular epithelial cells, which represents tubular reabsorption dysfunction defined as "diabetic tubulopathy" (22–24). A good correlation was found between urinary albumin excretion and markers of tubular dysfunction. Tubular injury has been described to be a better predictor in the progression of renal disease for diabetes (25). Functions and its critical role of tubular epithelial cells are attracting more people's eyes in recent years, and indicators of tubular injuries with higher sensitivity and specificity are springing up rapidly. Combining multiple indicators could provide more details about the type, location, severity and even the underling pathophysiological process of tubular injuries.

Plasma low molecular weight proteins (LMWP) β2-MG and CysC are freely filtered through glomerular filtration membrane and almost reabsorbed by proximal tubular epithelial cells. The raise of urinary β2-MG and CysC reflect the impaired proximal tubular reabsorption (26). In the present study, urinary β2-MG and CysC elevated significantly with blood glucose increase since blood glucose concentration reached 11.1 mmol/L, which represented acute hyperglycemia could induce obvious tubular reabsorption dysfunction in a dose-dependent manner. While urinary NAG, GAL, and NGAL are substances directly from renal tubular cells, and excreted in urine as a result of tubular epithelial cell damages. All these indicators increased significantly in hyperglycemia groups compared with those in control group ($P < 0.05$). Urinary GAL and NGAL even began to increase significantly since blood glucose reached 11.1 mmol/L ($P < 0.05$). In this study, we could conclude that acute hyperglycemia could induce obvious morphological and functional damages of tubular epithelial cells in a dose-dependent manner.

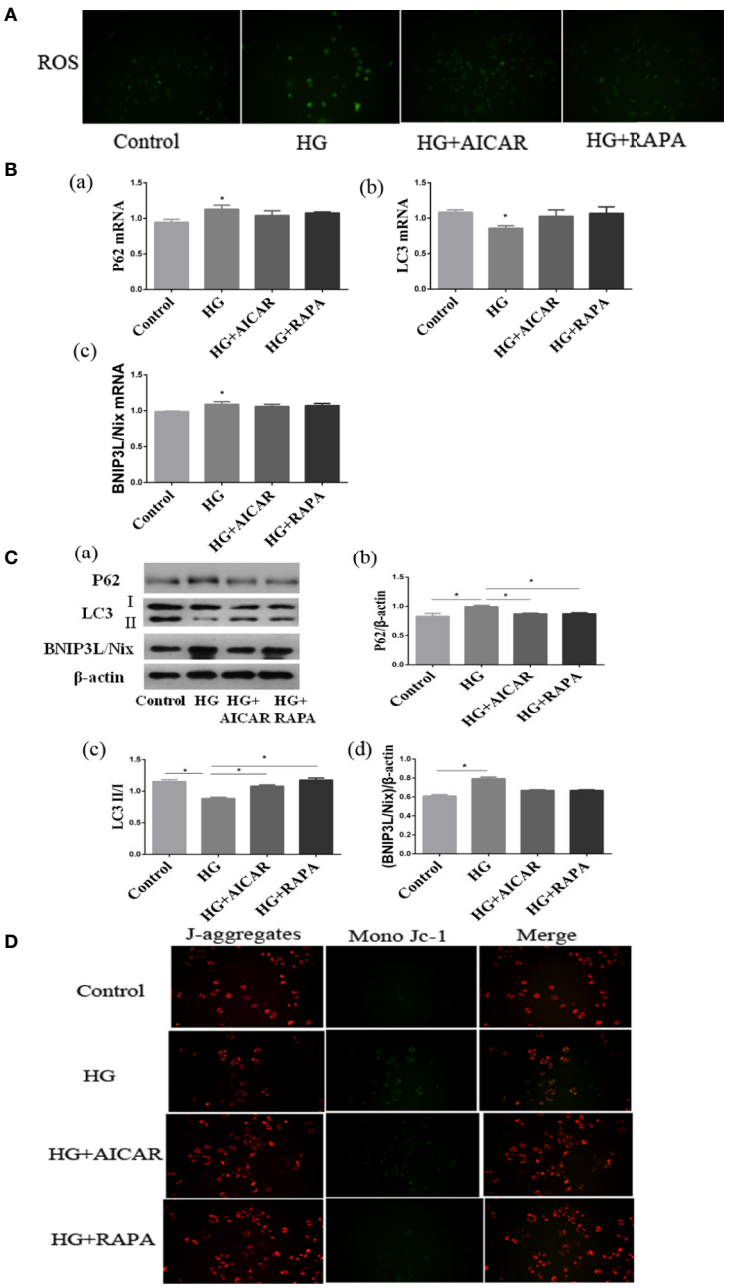

FIGURE 7 | Damages could be reversed by AMPK activation or mTOR inhibition. **(A)** ROS changes in NRK-52E cells (200*). **(B, C)** AMPK/mTOR signaling pathway of mitophagy in NRK-52E cells in acute hyperglycemia group (16.7 mmol/L). **(D)** Mitochondrial membrane potential changes in NRK-52E cells (200*). Values are expressed as means ± SD in each group. *$P < 0.05$ vs. Control. Control, control group; HG, hyperglycemia group. AMPK, 5'-AMP-activated protein kinase; mTOR, mammalian target of rapamycin complex. AICAR, 5-Aminoimidazole-4-carboxamide1-β-D-ribofuranoside; RAPA, rapamycin.

Renal tubule is responsible for the reabsorption, secretion, and excretion of many important molecules and is susceptible to various kinds of harmful factors such as ischemia, hypoxia, and oxidative stress because of its structural and functional characteristics. Proximal tubular epithelial cells are very vulnerable to high glucose damage, as they cannot decrease glucose transport to prevent excessive changes of intracellular glucose concentration when exposed to hyperglycemia (27). Blood supply of tubular epithelial cells could also be easily damaged according to its structural characteristics. Impaired microcirculation had been observed in healthy persons with acute elevated blood glucose (28, 29).

Tubular epithelial cells contain large amounts of mitochondria for their energy requirement, and an impairment of mitochondrial bioenergetics can result in renal functional decline. In our previous

study, mitochondria in tubular epithelial cells were seriously damaged, and oxidative stress was obviously activated after 6-h hyperglycemia treatment (2). Oxidative stress activation in the kidney is the direct consequence of hyperglycemia, and is thought to be the core mechanism of tubular epithelial cell injuries (3, 4). In the present study, ROS increased gradually after 6-h hyperglycemia treatment on renal tubular epithelial cells, which indicated that acute hyperglycemia could activate oxidative stress in a dose-dependent manner. Intermittent glucose excursion, compared with constant hyperglycemia, was proved to activate more oxidative stress (30). Patients with isolated postprandial hyperglycemia had markedly higher urine albumin excretion, which suggested that the magnitude of glycemic spike but not the baseline glucose concentration had bad effects on urinary albumin excretion, and oxidative stress activation and free radicals generation caused by acute increase of blood glucose levels maybe the underlying mechanism (31). Mitochondria are the major source and organelle target of ROS, and mitochondrial dysfunction will trigger excessive ROS accumulation. Obvious mitochondrial morphological injuries and MMP decrease were also detected after 6-h hyperglycemia treatment. So, we concluded that acute hyperglycemia could cause serious mitochondrial damage and oxidative stress activation. Under the condition of damaged mitochondria accumulate, excess ROS increase, which would further aggravate tubular epithelial cell injuries.

Autophagy is a lysosome degradation pathway that plays an important role in maintaining intracellular homeostasis and cell integrity through removing protein aggregates and damaged or excess organelles. Autophagy was up-regulated and provided a protected effect in acute kidney injuries induced by drugs or toxins (6–9). While in both type 1 and type 2 diabetic models, autophagy was usually inhibited in tubular epithelial cells participating in the pathogenesis of DKD (11, 32). But what role may autophagy play in acute hyperglycemic kidney injuries is still not clear. LC3 is the core of autophagy. The conversion of LC3-II to LC3-I is considered as the formation of autophagosome. P62, which anchored to the autophagosome interacting with LC3, is usually degraded by autolysosome. P62 accumulates when autophagy is attenuated. In the present study, we detected the accumulated p62 and decreased expression of LC3-II/LC3-I after 6-h hyperglycemia treatment both *in vivo* and *in vitro*, which suggested the inhibited autophagy under acute hyperglycemic treatment.

Excess oxidative stress activation could aggravate mitochondria damages and even cell apoptosis, and clearing away damaged mitochondria through mitophagy in time is crucial for cellular homeostasis. Mitophagy, firstly proposed by Lemasters in 2005 (33), was defined as selectively clearance of damaged or malfunctioning mitochondria. In the kidney, mitophagy mainly occurs in proximal tubules. Mitophagy is an important component of mitochondrial quality control, which is critical for cell survival. If damaged mitochondria number exceed the clearance capacity of mitophagy, ROS accumulates, which forms a vicious circle of mitochondria injury. The observed accumulation of damaged mitochondria indicates impairment in the mitophagy system.

In the present study, we further explored the pivotal role of mitophagy and its regulatory pathway in acute hyperglycemia induced renal tubular injuries both *in vivo* and *in vitro*. Mitophagy was inhibited in a dose-dependent manner in tubular epithelial cells both *in vivo* and *in vitro* after acute hyperglycemia treatment, which was in consistence with long term hyperglycemia treatment (12, 13). The accumulated BNIP3L/Nix was detected in renal tubular cells under acute hyperglycemia treatment in this study. Nix, also known as BNIP3L, is a BH3-only proapoptotic protein. BNIP3L/Nix locates on the mitochondrial outer membrane, and was found to be important for mitochondrial elimination during erythroid cell maturation. BNIP3L/Nix was reported to depolarize mitochondria (34). CCCP induced superoxide burst could be suppressed by the deletion of Nix (35).

Kidney plays an important role in maintaining the homeostasis of blood glucose. Approximately, 180-g glucose filters through glomerulus in a healthy person every day, and is almost all reabsorbed by renal tubules, among which nearly 90% is reabsorbed by renal proximal tubules through sodium glucose co-transporter 2 (SGLT2). In the present study, SGLT2 increased gradually in hyperglycemia groups which aggravated glucose reabsorption in renal tubular epithelial cells. P62 accumulation decreased in type 1 diabetic mice after *sglt2* knocking out, which suggested SGLT2 might be involved in the regulation of autophagy activity by regulating glucose reabsorption (36).

AMPK and mTOR play a central role in the regulation of autophagy initiation. AMPK is a metabolic master-switch that regulates and maintains cellular energy homeostasis. Loss of sensitivity of AMPK activation to cellular stress impairs metabolic regulation, increases oxidative stress and apoptosis, and reduces autophagic clearance. AMPK activation will then turn off mTOR signaling and resulting in autophagy induction (37).

Activating mTOR signaling pathway could aggravate podocytes damage and glomerular filtration rate decline in patients with DKD (38). Acute glucose challenge could suppress cardiac AMPK phosphorylation and mitochondria enzyme activities in non-diabetic rats (39). Acute hyperglycemia could enhance ischemic brain damage though mTOR pathway activation, which could be relieved by mTOR inhibitor rapamycin (40). ROS production can reduce AMPK activation, then form a vicious circle that contributes to mitochondrial damage and perhaps further enhance ROS production.

Our results also showed that acute hyperglycemia could improve the phosphorylation level of mTOR, but decrease phosphorylation level of AMPK both in renal tissues of healthy rats and NRK-52E cells. Restoration through AMPK activation or mTOR inhibition could improve mitophagy activity, decrease ROS production and improve MMP in NRK-52E cells, suggesting AMPK/mTOR pathway was directly involved in the regulation of mitophagy inhibited by acute hyperglycemia induced tubular injuries.

Our study still has some limitations. First, gene knockout or overexpression model should be used to further verify the possible regulation pathway of acute hyperglycemic tubular injury; second, the reversibility of acute hyperglycemic tubular injury should be discussed in the future study.

In conclusion, acute hyperglycemia could lead to obvious tubular morphological and functional injuries when the blood glucose level was greater than 11.1 mmol/L, and behaved in a dose-dependent

manner. Acute hyperglycemia could inhibit mitophagy through AMPK/mTOR pathway, which would aggravate damaged mitochondria accumulation and renal tubular injuries. The protective role of mitophagy improvement under acute hyperglycemic stress is in urgent need to be verified in the future.

DATA AVAILABILITY STATEMENT

All datasets generated for this study are included in the article/supplementary material.

AUTHOR CONTRIBUTIONS

JW, XY, BaiC, and BaoC conceptualized the study. XY, ZW, and XJ contributed to the methodology. XC and ZG were in charge of the data curation. JY and CS contributed to the project administration. YY and JL were in charge of the validation. JW, and BaoC acquired the funding. JW and XY wrote the original draft. BaiC and BaoC wrote, reviewed, and edited the manuscript. CM contributed to the methology and validation. All authors contributed to the article and approved the submitted version.

FUNDING

This work was supported by the National Key R&D Program of China (No. 2018YFC1314000), National Natural Science Foundation of China (No. 81603461, 81774043 and 81700631), Tianjin Natural Science Foundation (No. 17JCZDJC34700, 17ZXMFSY00140 and 18ZXZNSY00280), and the fund of the State Key Laboratory of Kidney Diseases in PLA General Hospital (KF-01-133).

REFERENCES

1. Schetz M, Vanhorebeek I, Wouters PJ, Wilmer A, Van den Berghe G. Tight blood glucose control is renoprotective in critically ill patients. *J Am Soc Nephrol* (2008) 19:571–8. doi: 10.1681/ASN.2006101091
2. Wang JY, Yang JH, Xu J, Jia JY, Zhang XR, Yue XD, et al. Renal tubular damage may contribute more to acute hyperglycemia induced kidney injury in non-diabetic conscious rats. *J Diabetes Its Complications* (2015) 29:621–8. doi: 10.1016/j.jdiacomp.2015.04.014
3. Chen Q, Su Y, Ju Y, Ma K, Li W, Li W. Astragalosides IV protected the renal tubular epithelial cells from free fatty acids-induced injury by reducing oxidative stress and apoptosis. *BioMed Pharmacother* (2018) 108:679–86. doi: 10.1016/j.biopha.2018.09.049
4. Han Y, Xu X, Tang C, Gao P, Chen X, Xiong X, et al. Reactive oxygen species promote tubular injury in diabetic nephropathy: The role of the mitochondrial ros-txnip-nlrp3 biological axis. *Redox Biol* (2018) 16:32–46. doi: 10.1016/j.redox.2018.02.013
5. Jiang H, Shao X, Jia S, Qu L, Weng C, Shen X, et al. The Mitochondria-Targeted Metabolic Tubular Injury in Diabetic Kidney Disease. *Cell Physiol Biochem* (2019) 52:156–71. doi: 10.33594/000000011
6. Takahashi A, Kimura T, Takabatake Y, Namba T, Kaimori J, Kitamura H, et al. Autophagy guards against cisplatin-induced acute kidney injury. *Am J Pathol* (2012) 180:517–25. doi: 10.1016/j.ajpath.2011.11.001
7. Guan X, Qian Y, Shen Y, Zhang L, Du Y, Dai H, et al. Autophagy protects renal tubular cells against ischemia/reperfusion injury in a time - dependent manner. *Cell Physiol Biochem* (2015) 36:285–98. doi: 10.1159/000374071
8. Mei S, Livingston M, Hao J, Li L, Mei C, Dong Z. Autophagy is activated to protect against endotoxic acute kidney injury. *Sci Rep* (2016) 6:22171. doi: 10.1038/srep22171
9. Kaushal GP, Shah SV. Autophagy in acute kidney injury. *Kidney Int* (2016) 89:779–91. doi: 10.1016/j.kint.2015.11.021
10. Wu WH, Zhang MP, Zhang F, Liu F, Hu ZX, Hu QD, et al. The role of programmed cell death in streptozotocin-induced early diabetic nephropathy. *J Endocrinol Invest* (2011) 34:e296–301. doi: 10.3275/7741
11. Kitada M, Ai T, Nagai T, Ito H, Kanasaki K, Koya D. Dietary Restriction Ameliorates Diabetic Nephropathy through Anti-Inflammatory Effects and Regulation of the Autophagy via Restoration of Sirt1 in Diabetic Wistar Fatty (fa/fa) Rats: A Model of Type 2 Diabetes. *J Diabetes Res* (2011) 2011:908185. doi: 10.1155/2011/908185
12. Zhan M, Usman IM, Sun L, Kanwar YS. Disruption of Renal Tubular Mitochondrial Quality Control by Myo-Inositol Oxygenase in Diabetic Kidney Disease. *J Am Soc Nephrol* (2014) 26:1304–21. doi: 10.1681/ASN.2014050457
13. Xiao L, Xu X, Zhang F, Wang M, Xu Y, Tang D, et al. The mitochondria-targeted antioxidant MitoQ ameliorated tubular injury mediated by mitophagy in diabetic kidney disease via Nrf2/PINK1. *Redox Biol* (2017) 11:297–311. doi: 10.1016/j.redox.2016.12.022
14. Coresh J, Toto RD, Kirk KA, Whelton PK, Massry S, Jones C. Creatinine clearance as a measure of GFR in screenees for the African- American Study of Kidney Disease and Hypertension pilot study. *Am J Kidney Dis* (1998) 32:32–42. doi: 10.1053/ajkd.1998.v32.pm9669421
15. Livak KJ, Schmittgen TD. Analysis of relative gene expression data using real-time quantitative PCR and the 2-ddCT method. *Methods* (2001) 25:402–8. doi: 10.1007/s11033-008-9430-1
16. Moriyama N, Ishihara M, Noguchi T, Nakanishi M, Arakawa T, Asaumi Y, et al. Admission hyperglycemia is an independent predictor of acute kidney injury in patients with acute myocardial infarction. *Circ J* (2014) 61:1475–80. doi: 10.1016/S0735-1097(13)60171-0
17. Giannini F, Latib A, Jabbour RJ, Ruparelia N, Aurelio A, Ancona MB, et al. Impact of post-procedural hyperglycemia on acute kidney injury after transcatheter aortic valve implantation. *Int J Cardiol* (2016) 221:892–7. doi: 10.1016/j.ijcard.2016.07.029
18. Gordillo R, Ahluwalia T, Woroniecki R. Hyperglycemia and acute kidney injury in critically ill children. *Int J Nephrol Renovasc Dis* (2016) 9:201–4. doi: 10.2147/IJNRD.S115096
19. Vanhorebeek I, Gunst J, Ellger B, Boussemaere M, Lerut E, Debaveye Y, et al. Hyperglycemic kidney damage in an animal model of prolonged critical illness. *Kidney Int* (2009) 76:512–20. doi: 10.1038/ki.2009.217
20. Efrati S, Berman S, Hamad RA, El Nakib R, Chanimov M, Siman-Tov Y, et al. Hyperglycemia, inflammation, RAS activation: three culprits to blame for acute kidney injury emerging in healthy rats during general anesthesia. *Nephrology* (2012) 17:591–602. doi: 10.1111/j.1440-1797.2012.01638.x
21. Ishihara M. Acute hyperglycemia in patients with acute myocardial infarction. *Circ J* (2012) 76:563–71. doi: 10.1253/circj.cj-11-1376
22. Long YS, Zheng S, Kralik PM, Benz FW, Epstein PN. Impaired Albumin Uptake and Processing Promote Albuminuria in OVE26 Diabetic Mice. *J Diabetes Res* (2016) 2016:1–8. doi: 10.1155/2016/8749417
23. Gilbert RE. Proximal Tubulopathy: Prime Mover and Key Therapeutic Target in Diabetic Kidney Disease. *Diabetes* (2017) 66:791–800. doi: 10.2337/db16-0796
24. Zeni L, Norden AGW, Cancarini G, Unwin RJ. A more tubulocentric view of diabetic kidney disease. *J Nephrol* (2017) 30:701–17. doi: 10.1007/s40620-017-0423-9
25. Tang SC, Lai KN. The pathogenic role of the renal proximal tubular cell in diabetic nephropathy. *Nephrol Dial Transplant* (2012) 27:3049–56. doi: 10.1093/ndt/gfs260

26. Sprenkle P, Russo P. Molecular markers for ischemia, do we have something better then creatinine and glomerular filtration rate? *Arch Esp Urol* (2013) 66:99–114.
27. Vallon V, Komers R. Pathophysiology of the diabetic kidney. *Compr Physiol* (2011) 1:1175–232. doi: 10.1002/cphy.c100049
28. Russell RD, Hu D, Greenaway T, Sharman JE, Rattigan S, Richards SM, et al. Oral glucose challenge impairs skeletal muscle microvascular blood flow in healthy people. *Am J Physiol Endocrinol Metab* (2018) 315:E307–15. doi: 10.1152/ajpendo.00448.2017
29. Varsamis P, Walther G, Share B, Taylor F, Stewart S, Lorenzen C, et al. Transient endothelial dysfunction induced by sugar-sweetened beverage consumption may be attenuated by a single bout of aerobic exercise. *Microvasc Res* (2018) 115:8–11. doi: 10.1016/j.mvr.2017.07.003
30. Wu N, Shen H, Liu H, Wang Y, Bai Y, Han P. Acute blood glucose fluctuation enhances rat aorta endothelial cell apoptosis, oxidative stress and pro-inflammatory cytokine expression in vivo. *Cardiovasc Diabetol* (2016) 15:109. doi: 10.1186/s12933-016-0427-0
31. Shilpasree AS, Patil VS, Patil VP, Ingleshwar DG. Urine albumin excretion as a marker of acute glycemic changes in isolated postprandial hyperglycemia. *J Lab Physicians* (2017) 9:36–41. doi: 10.4103/0974-2727.187925
32. Chowdhury S, Ghosh S, Das AK, Sil PC. Ferulic Acid Protects Hyperglycemia-Induced Kidney Damage by Regulating Oxidative Insult, Inflammation and Autophagy. *Front Pharmacol* (2019) 10:27. doi: 10.3389/fphar.2019.00027
33. Lemasters JJ. Selective mitochondrial autophagy, or mitophagy, as a targeted defense against oxidative stress, mitochondrial dysfunction, and aging. *Rejuvenation Res* (2005) 8:3–5. doi: 10.1089/rej.2005.8.3
34. Zhang J, Ney PA. NIX induces mitochondrial autophagy in reticulocytes. *Autophagy* (2008) 4:354–6. doi: 10.4161/auto.5552
35. Ding W-X, Ni H-M, Li M, Liao Y, Chen X, Stolz DB, et al. Nix is critical to two distinct phases of mitophagy, reactive oxygen species-mediated autophagy induction and Parkin-ubiquitin-p62-mediated mitochondrial priming. *J Biol Chem* (2010) 285:27879–90. doi: 10.1074/jbc.M110.119537
36. Vallon V, Rose M, Gerasimova M, Satriano J, Platt KA, Koepsell H, et al. Knockout of Na-glucose transporter SGLT2 attenuates hyperglycemia and glomerular hyperfiltration but not kidney growth or injury in diabetes mellitus. *Am J Physiol Renal Physiol* (2013) 304:F156–67. doi: 10.1152/ajprenal.00409.2012
37. Ha J, Kim J. Novel pharmacological modulators of autophagy: an updated patent review (2012-2015). *Expert Opin Ther Pat.* (2016) 26:1273–89. doi: 10.1080/13543776.2016.1217996
38. Koya D, Kitada M, Kume S, Kanasaki K. Interventions against nutrient-sensing pathways represent an emerging new therapeutic approach for diabetic nephropathy. *Clin Exp Nephrol* (2014) 18:210–3. doi: 10.1007/s10157-013-0908-3
39. Thorwald M, Rodriguez R, Lee A, Martinez B, Peti-Peterdi J, Nakano D, et al. Angiotensin receptor blockade improves cardiac mitochondrial activity in response to an acute glucose load in obese insulin resistant rats. *Redox Biol* (2018) 14:371–8. doi: 10.1016/j.redox.2017.10.005
40. Hei C, Liu P, Yang X, Niu J, Li PA. Inhibition of mTOR signaling Confers Protection against Cerebral Ischemic Injury in Acute Hyperglycemic Rats. *Int J Biol Sci* (2017) 13:878–87. doi: 10.7150/ijbs.18976

Conflict of Interest: The authors declare that the research was conducted in the absence of any commercial or financial relationships that could be construed as a potential conflict of interest.

frontiers in Endocrinology

ORIGINAL RESEARCH
published: 18 February 2021
doi: 10.3389/fendo.2021.626390

Ferroptosis Enhanced Diabetic Renal Tubular Injury *via* HIF-1α/HO-1 Pathway in db/db Mice

Xiaomeng Feng[1], Shuo Wang[2], Zhencheng Sun[3], Hengbei Dong[4], Haitian Yu[5], Mengxiu Huang[6] and Xia Gao[1]**

[1] Department of Endocrinology, Beijing Chao-Yang Hospital, Capital Medical University, Beijing, China, [2] Department of Infectious Diseases, Beijing Traditional Chinese Medical Hospital, Capital Medical University, Beijing, China, [3] Department of Osteology, Beijing Chao-Yang Hospital, Capital Medical University, Beijing, China, [4] Department of Reproductive Medicine, Beijing Obstetrics and Gynecology Hospital, Capital Medical University, Beijing, China, [5] Education Division, Beijing Chao-Yang Hospital, Capital Medical University, Beijing, China, [6] Department of Hepatobiliary, Beijing Chao-Yang Hospital, Capital Medical University, Beijing, China

OPEN ACCESS

Edited by:
Anca Dana Dobrian, Eastern Virginia Medical School, United States

Reviewed by:
Subhashini Bolisetty, University of Alabama at Birmingham, United States
Elina Akalestou, Imperial College London, United Kingdom

***Correspondence:**
Xiaomeng Feng
goalmesy@qq.com
Xia Gao
elngao@163.com

Specialty section:
This article was submitted to Diabetes: Molecular Mechanisms, a section of the journal Frontiers in Endocrinology

Received: *05 November 2020*
Accepted: *06 January 2021*
Published: *18 February 2021*

Citation:
Feng X, Wang S, Sun Z, Dong H, Yu H, Huang M and Gao X (2021) Ferroptosis Enhanced Diabetic Renal Tubular Injury via HIF-1α/HO-1 Pathway in db/db Mice. Front. Endocrinol. 12:626390. doi: 10.3389/fendo.2021.626390

Background: Ferroptosis is a recently identified iron-dependent form of cell death as a result of increased reactive oxygen species (ROS) and lipid peroxidation. In this study, we investigated whether ferroptosis aggravated diabetic nephropathy (DN) and damaged renal tubules through hypoxia-inducible factor (HIF)-1α/heme oxygenase (HO)-1 pathway in db/db mice.

Methods: Db/db mice were administered with or without ferroptosis inhibitor Ferrostatin-1 treatment, and were compared with db/m mice.

Results: Db/db mice showed higher urinary albumin-to-creatinine ratio (UACR) than db/m mice, and Ferrostatin-1 reduced UACR in db/db mice. Db/db mice presented higher kidney injury molecular-1 and neutrophil gelatinase-associated lipocalin in kidneys and urine compared to db/m mice, with renal tubular basement membranes folding and faulting. However, these changes were ameliorated in db/db mice after Ferrostatin-1 treatment. Fibrosis area and collagen I were promoted in db/db mouse kidneys as compared to db/m mouse kidneys, which was alleviated by Ferrostatin-1 in db/db mouse kidneys. HIF-1α and HO-1 were increased in db/db mouse kidneys compared with db/m mouse kidneys, and Ferrostatin-1 decreased HIF-1α and HO-1 in db/db mouse kidneys. Iron content was elevated in db/db mouse renal tubules compared with db/m mouse renal tubules, and was relieved in renal tubules of db/db mice after Ferrostatin-1 treatment. Ferritin was increased in db/db mouse kidneys compared with db/m mouse kidneys, but Ferrostatin-1 reduced ferritin in kidneys of db/db mice. Diabetes accelerated nicotinamide adenine dinucleotide phosphate (NADPH) oxidase-derived ROS formation in mouse kidneys, but Ferrostatin-1 prevented ROS formation derived by NADPH oxidases in db/db mouse kidneys. The increased malondialdehyde (MDA) and the decreased superoxide dismutase (SOD), catalase (CAT), glutathione peroxidases (GSH-Px) were detected in db/db mouse kidneys compared to db/m mouse kidneys, whereas Ferrostatin-1 suppressed MDA and elevated SOD, CAT, and GSH-Px in db/db mouse kidneys. Glutathione

peroxidase 4 was lower in db/db mouse kidneys than db/m mouse kidneys, and was exacerbated by Ferrostatin-1 in kidneys of db/db mice.

Conclusions: Our study indicated that ferroptosis might enhance DN and damage renal tubules in diabetic models through HIF-1α/HO-1 pathway.

Keywords: ferroptosis, diabetic nephropathy, renal tubular injury, heme oxygenase-1, hypoxia-inducible factor-1α

INTRODUCTION

Ferroptosis is a recently identified iron-dependent cell death, which is characterized by the increase of reactive oxygen species (ROS) to lethal levels (1). Iron is required for various vital processes such as heme synthesis, iron-sulfur cluster synthesis, and deoxyribonucleic acid synthesis (2). Iron also plays a critical role in the active sites of numerous enzymes which participate in the formation of nicotinamide adenine dinucleotide phosphate (NADPH) oxidases, xanthine oxidase, lysyl oxidase, and mitochondrial complex I and III (3).

However, the excess of iron in the cell damages cellular functions by producing ROS and ultimately leads to cell death (4). The formation of intracellular ROS is mainly through NADPH oxidases (5), which is regulated by iron (3). Lipid peroxidation is the damage by ROS on polyunsaturated fatty acids in cellular membranes or organelle membranes (6). Ferroptosis has been documented to be induced by lipid peroxidation which is caused by iron overloading (1). Iron-dependent lipid peroxidation is the oxidative process which is regulated by enzymatic antioxidants, such as superoxide dismutase (SOD), catalase (CAT), and glutathione peroxidases (GSH-Px) (6). GSH-Px includes multiple isoenzymes with different subcellular locations presenting distinct tissue-specific expression patterns (7). Glutathione peroxidase 4 (GPX4) is a specific and important regulator of ferroptotic cell death, since GPX4 can inhibit ferroptosis by repression of phospholipid peroxidation (8).

Heme is a main source of iron that synthesized (9). Heme oxygenase (HO)-1 is a phase II enzyme that metabolizes heme into biliverdin/bilirubin, carbon monoxide, and ferrous iron (10). HO-1 can be induced by a wide spectrum of cues, including inflammatory mediators, oxidants, and physical or chemical stimuli (10). Recent studies have suggested that HO-1 has a dual role in ferroptosis. The increasing studies have demonstrated that HO-1 acts as a key mediator in the cause of ferroptosis and plays a causative role for the development of several diseases (11–13), although there have been some researches indicating that HO-1 has protective effects against oxidative stress-related disorders (14). Hypoxia-inducible factor (HIF) is a heterodimer composed of a constitutive β-subunit and one of at least two different oxygen-dependent α-subunits (HIF-1α and -2α). The activity of HIF is mainly regulated by oxygen-dependent proteolysis of the α-subunits (15). HO-1 is one of the HIF target genes (15). Therefore, HIF-1α also regulates ferroptosis and is associated with the expression of GPX4 (16).

Diabetic nephropathy (DN) is the leading cause of end-stage renal disease. The previous studies of DN have mainly focused on glomeruli. However, recent data have shown that defects in tubules also result in albuminuria or proteinuria (17). Clinical observations in patients with type 1 diabetes highlighted the early involvement of the tubules in generating albuminuria (18). Subsequently, diabetic rats showed the decreased reabsorption of albumin in proximal tubules compared with the controls, despite of no promotion in glomerular filtration rate in diabetic rats (19). Additionally, no significant difference in glomerular sieving coefficient between diabetic rats and the controls was observed, while albuminuria presented in the diabetic rats (20). A good correlation has been found between urinary albumin excretion and the markers of tubular dysfunction. All these researches suggested that albuminuria might origin from renal tubules in DN (21). Thus, the causative factor of renal tubular injury in DN is supported by diabetic patients and experimental models, as well as credible pathogenetic mechanisms (22).

Intra-renal oxidative stress plays a critical role in the initiation and development of DN. There is considerable evidence that hyperglycemia causes oxidative stress through the increased generation of ROS, which plays a key role in DN (23). The increased MDA, the main aldehyde product of lipid peroxidation (24), and the decreased SOD, CAT, and GSH-Px were also noted in kidneys of diabetic animals (25, 26). For the sensitivity of renal tubules to oxidative stress and lipid peroxidation (27), ferroptosis often occurs in tubules during the development of renal diseases (28, 29). However, the researches of relation between ferroptosis and DN have been few in number. A recently published study reported that ferroptosis involved in renal tubular cell death in diabetic nephropathy (30). While clearly of great importance, there were still some limitations in that study. In vitro part of the research, renal tubular cells were not cultured under high glucose condition; in vivo study, the injury of renal tubules was not detected, and diabetic models were not treated with ferroptosis inhibitor to verify the role of ferroptosis in DN. Thus, it is necessary to further investigate whether ferroptosis enhanced renal tubular injury caused by diabetes (30).

It has been demonstrated that ferroptosis plays a crucial role in renal ischemia injury (1). DN is one of the diabetic microvascular complications. Renal ischemia has been considered as one of the major causes of DN (31). The high energy requirements and dependence on aerobic metabolism render renal tubules especially susceptible to hypoxia (17). Chronic hypoxia due to renal ischemia induces the increase of HIF-1α in renal tubules of diabetic models, with the elevated HO-1 level (32). Degradation of heme by the excessive HO-1

leads to iron overloading which causes oxidative stress and lipid peroxidation. Recent studies have documented the great effects of iron accumulation in kidneys on the progression of DN (33, 34). These studies suggested that the process of ferroptosis might affect the development of DN, diabetic renal tubular injury in particular, through HIF-1α/HO-1 pathway. However, few studies have explored it.

Furthermore, diabetic renal tubular injury contributes to renal fibrosis (35), and ferroptosis is regarded as the cause of fibrosis (36, 37). It has been proven that tubular epithelial cells under high glucose condition exhibited higher activation of pro-inflammatory and pro-fibrotic signal pathways, which led to progressive fibrosis (38). Given that the degree of renal tubular dysfunction associates well with the extent of renal fibrosis, diabetic tubular injury might be recognized as the reason of renal fibrosis (39). Moreover, our previous study showed that endothelial-specific prolyl hydroxylase domain protein-2 knockout (PHD2ECKO) mice, with the upregulated expression of HIF-α due to the deficient PHD2 which degrades HIF, presented significant renal fibrosis (40). However, whether ferroptosis-induced-renal fibrosis is regulated by HIF-1α/HO-1 pathway has been unclear.

Therefore, in this study, we aimed to investigate whether ferroptosis involved in tubular injury and fibrosis through HIF-1α/HO-1 pathway in kidneys of diabetic mouse models.

MATERIALS AND METHODS

The animal experiments were approved by the Animal Ethics Committee of Beijing Chao-Yang Hospital, Capital Medical University and were performed in accordance with animal care guidelines of Beijing Chao-Yang Hospital, Capital Medical University.

Experimental Animal Models and Treatment

Eight-week-old male C57BLKs/J db/m and db/db mice were purchased from Nanjing Biomedical Research Institute of Nanjing University, Nanjing, China. Mice were divided into 3 groups (n = 9 for each group): (1) db/m group, (2) db/db group, and (3) db/db+Fer1 group. Db/db mice were given daily intraperitoneal injections of either 0.1% DMSO (diluted in 0.9% NaCl with 20% SBE-β-CD) for db/db group or 1 mg/kg Ferrostatin-1 (MCE, NJ, USA) for db/db+Fer1 group for 10 weeks starting at 10 weeks of age. Ferrostatin-1 was dissolved in DMSO first, and was diluted in 0.9% NaCl with 20% SBE-β-CD. The final concentrations of Ferrostatin-1 and DMSO were 0.2 mg/ml and 0.1%, respectively.

The mice were housed in clear plastic cages (n = 3/cage) at 22°C on a 12:12 h light-dark cycle (lights on 08:00–20:00 h), with free access to standard rodent chow and tap water. After 10-week administration, all mice were placed in metabolic cages separately to take 24 h urine. After 10 weeks, all mice were anesthetized by intraperitoneal injection of a mixture of Rompun 10 mg/kg (Bayer Korea, Ansan, Gyeonggi-Do, Korea) and Zoletil 30 mg/kg (Virbac, Carros, France). The kidneys were rapidly dissected for subsequent analyses. Blood was collected from the left ventricle and centrifuged, stored at -80°C.

Measurements of Blood and Urinary Parameters

Fasting blood glucose concentration was measured using HemoCue B-Glucose kit (HemoCue AB, Angelholm, Sweden). Fasting insulin concentration was measured using radioimmunoassay kit (Linco Reasearch, St Charles, MO, USA). Serum and urine creatinine values were measured using HPLC (Beckman Instruments, Fullerton, CA, USA). Urinary albumin value was measured by an immunoassay (Bayer, Elkhart, IN, USA). Urinary albumin-to-creatinine ratio (UACR) was calculated as urine albumin/urine creatinine (μg/mg). Urinary kidney injury molecular-1 (KIM-1) and neutrophil gelatinase-associated lipocalin (NGAL) concentrations of mice were measured with ELISA (R&D systems, MN, USA). Serum iron ion, ferritin, and transferrin were determined with ELISA (Lai Er Bio-Tech, Hefei, China). All assays were performed according to the manufacturer's protocol.

Light Microscopic Study

The renal tissues fixed in neutral-buffered 10% formalin solution (SF93-20; Fisher Scientific, Pittsburgh, PA, USA). Paraffin sections were prepared in 8 μm. Apoptosis in kidneys was detected by TUNEL (Boster, Wuhan, China). Hexamine silver staining was performed to detect the injury of renal tubules. Masson's trichrome staining and Sirius red staining were performed to measure the degree of renal fibrosis. Then, slices were washed with distilled water, and were dipped in Lillie staining solution (Solarbio Life Sciences, Beijing, China) for 30 min. Subsequently, slices were immersed in nucleus staining solution (Solarbio Life Sciences, Beijing, China) for 5 min, after washed by distilled water. Finally, dehydrated slices were used for measuring iron content after washed with distilled water again. The renal samples were also embedded in frozen optimal cutting temperature compound (4585; Fisher Health Care, Houston, TX, USA). Frozen sections were also prepared in 8 μm. ROS (frozen sections) was measured by dihydroethidium staining in fresh frozen sections. All analyses were performed by image-analysis software (Image J, NIH, Bethesda, MD, USA).

Western Blot Analyses

Mouse renal tissues were collected and homogenized in lysis buffer. The homogenates were centrifuged at 16,000×g at 4°C for 15 min. A bicinchoninic acid protein assay kit (Pierce Co, Rockford, IL, USA) was used to analyze the protein concentrations. Equal amounts (20 μg) of the protein were separated by 10% sodium dodecyl sulfate polyacrylamide gel electrophoresis geland transferred to a polyvinylidene difluoride membrane. The membranes were blocked with 5% nonfat dry milk in Tris-buffered saline and incubated with the following primary antibodies overnight: cleaved caspase-3 (1:1000; Abcam, Cambridge, MA, USA), KIM-1 (1:1,000; Abcam, Cambridge, MA, USA), NGAL (1:1,000; Abcam, Cambridge, MA, USA), collagen I (1:1,000; Abcam, Cambridge, MA, USA), HIF-1α (1:1,000; Novus Bio, Littleton, CO, USA), HO-1 (1:1,000; BD transduction, San Jose, CA, USA), ferritin heavy chain (1:1000; Abcam, Cambridge, MA, USA), gp91 phox (1:1,000; BD transduction, San Jose, CA, USA), GPX4 (1:1,000; Abcam, Cambridge, MA, USA), and β-actin (1:1,000; Cell Signaling, Danvers, MA, USA). After washed, the

membranes were incubated for 2 h with a secondary antibody coupled to horseradish peroxidase (1:5,000; Santa Cruz, CA, USA). Densitometric analyses were carried out with image acquisition and analysis software (Bio-Rad).

SAssessment of Oxidative Stress Parameters in Mouse Renal Tissues

MDA was measured by thiobarbituric acid method, SOD was measured by xanthine oxidase method, GSH-Px was measured by NADPH method, and CAT was determined by coloration method in the renal tissue sample homogenates using commercial kits (Beyotime Institute of Biotechnology, Shanghai, China), according to the manufacturer's protocols.

Statistical Analyses

All analyses were performed using Statistical Package for Social Sciences version 20.0 (SPSS, Inc., Chicago, IL, USA). Data are expressed as means ± S.E.M. The significance of differences in the means of corresponding values among groups was determined by using the one-way ANOVA. The significance of differences between two values was determined using LSD test. In all statistical tests, all tests were two-sided, and P values <0.05 were considered significant.

RESULTS

Assessment of Physical and Biochemical Characteristics

As shown in **Figure 1**, body weight, kidney weight, blood glucose, and insulin were significantly higher for db/db mice than db/m mice, and there was no difference in body weight, kidney weight, blood glucose, and insulin in db/db mice between with and without Ferrostatin-1 treatment (**Figures 1A–D**). All mice in three groups were similar in serum creatinine (SCR) (**Figure 1E**). In addition, db/db mice presented higher UACR than db/m mice, and db/db+Fer1 group had the significantly decreased level of UACR compared with db/db group (**Figure 1F**), suggesting that ferroptosis was involved in DN.

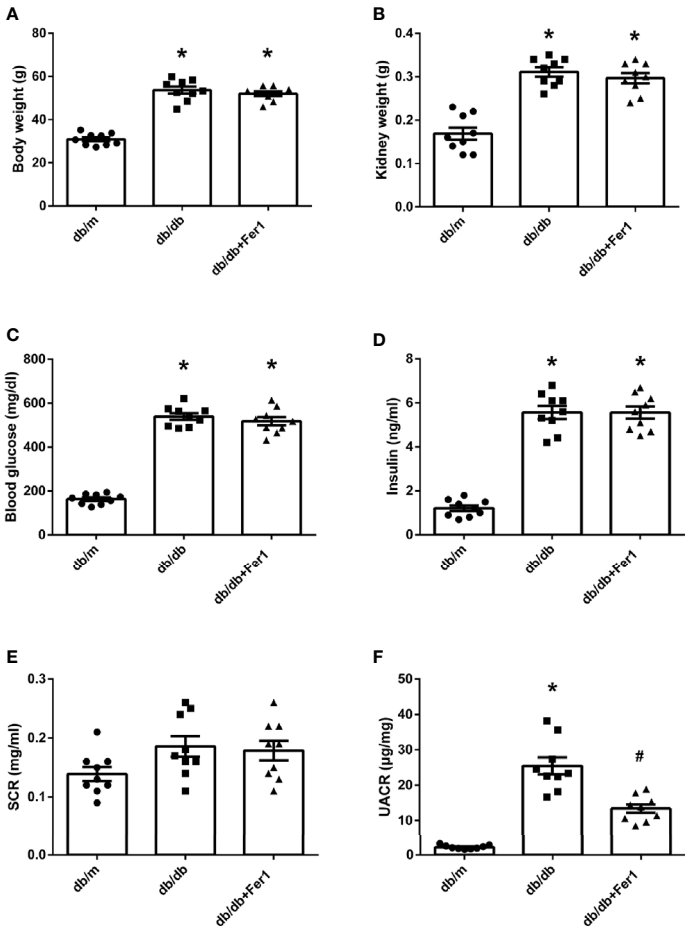

FIGURE 1 | Physical and biochemical characteristics in db/m, db/db, and db/db+Fer1 groups. **(A)**. Body weight. **(B)**. Kidney weight. **(C)**. Blood glucose. **(D)**. Insulin. **(E)**. Serum creatinine (SCR). **(F)**. Urinary albumin-to-creatinine ratio (UACR). Male mice, n = 9/group. *P < 0.05, vs db/m group; #P < 0.05, vs db/db group. Db/m, db/m mice; db/db, db/db mice without Ferrostatin-1 treatment; db/db+Fer1, db/db mice with Ferrostatin-1 treatment. Data are means ± S.E.M.

Assessment of Renal Tubular Injury

Since the renal tubules are vulnerable to metabolic disorders and ischemia, defects in tubules might be the primary cause of albuminuria in DN (17). To determine if there was ferroptosis-related renal tubular injury in diabetic mice, we detected the levels of KIM-1 and NGAL, the markers of renal tubular damage. Western blot showed that diabetes promoted the expression of KIM-1 and NGAL in the mouse kidneys, but ferroptosis inhibitor Ferrostatin-1 reduced the expression of KIM-1 and NGAL in db/db mouse kidneys (**Figures 2A, B**). Consistent with these changes, urinary KIM-1 and NGAL were increased in db/db group compared with db/m group, and were decreased after Ferrostatin-1 treatment in db/db mice (**Figures 2C, D**). Furthermore, hexamine silver staining showed that diabetes led to fold and fault of renal tubular basement membranes (**Figure 2E**). However, Ferrostatin-1 treatment improved the injury of renal tubular basement membranes in db/db mice. These results indicated that ferroptosis enhanced diabetic renal tubular injury.

Assessment of Renal Fibrosis

The previous researches have provided a strong evidence of ferroptosis to accelerate fibrosis (36, 37). Thus, we examined renal fibrosis. As shown in **Figure 3**, Masson's staining and Sirius red staining showed that diabetes significantly enhanced mouse renal fibrosis, and Ferrostatin-1 treatment reduced renal fibrosis in diabetic mice (**Figures 3A–C**). Western blot analysis further showed that diabetes promoted the expression of fibrosis associated protein-collagen I in mouse kidneys, and Ferrostatin-1 treatment depressed the expression of collagen I in kidneys of db/db mice (**Figure 3D**). These results indicated that ferroptosis accelerated renal fibrosis in diabetic mice.

Assessment of HIF-1α and HO-1 in Mouse Kidneys

Subsequently, we measured the expression of HIF-1α and HO-1 in mouse kidneys, since HO-1 has been suggested to act as a critical role in ferroptosis (10), and HIF-1α adjusts the expression of HO-1 (15).

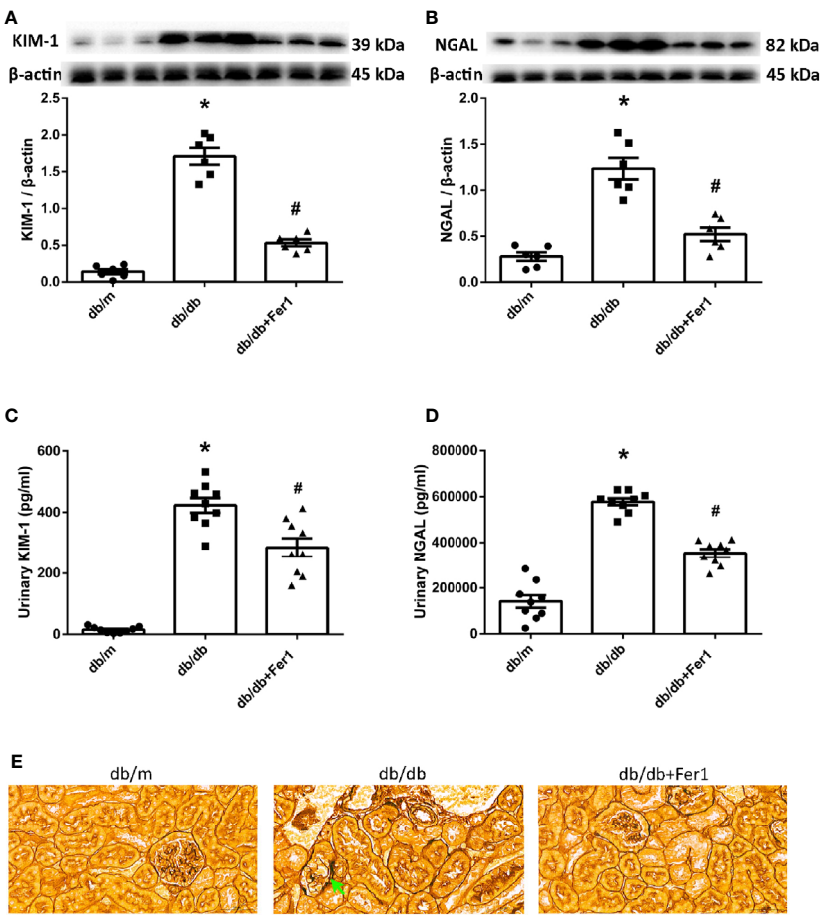

FIGURE 2 | Renal tubular injury in db/m, db/db, and db/db+Fer1 groups. **(A, B)**. Representative photographs and quantification of kidney injury molecular-1 (KIM-1) **(A)** and neutrophil gelatinase-associated lipocalin (NGAL) **(B)** in mouse kidneys measured by western blot. **(C, D)**. Quantification of urinary KIM-1 **(C)** and NGAL **(D)** levels measured by ELISA. **(E)** Representative photographs of mouse kidneys by hexamine silver staining staining. Male mice, n = 6-9/group. $^{*}P < 0.05$, vs db/m group; $^{\#}P < 0.05$, vs db/db group. Db/m, db/m mice; db/db, db/db mice without Ferrostatin-1 treatment; db/db+Fer1, db/db mice with Ferrostatin-1 treatment. Data are means ± S.E.M.

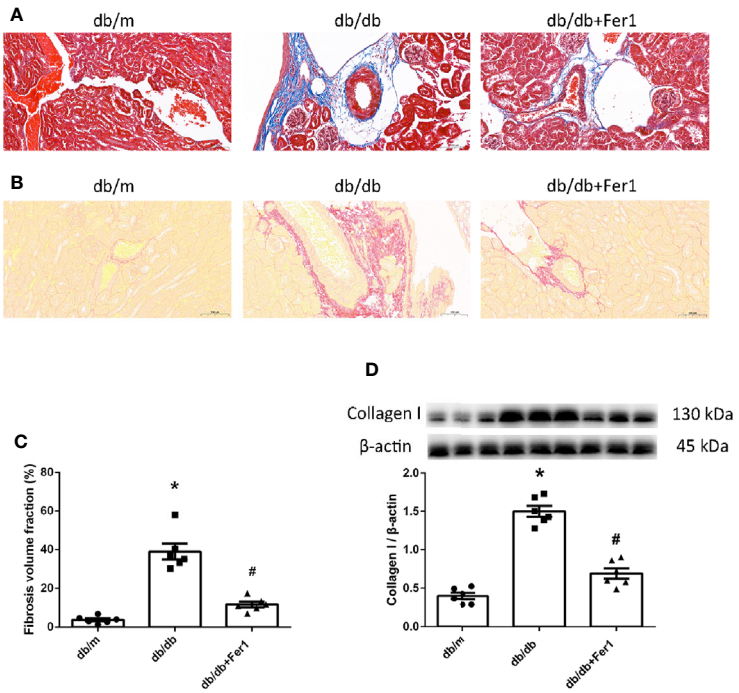

FIGURE 3 | Renal fibrosis in db/m, db/db, and db/db+Fer1 groups. **(A–C)**. Representative photographs and quantification of renal fibrosis by Masson's staining (blue) **(A)** and Sirius red staining (red) **(B)** (six sections per mouse were analyzed). **(D)**. Representative photographs and quantification of collagen I in mouse kidneys measured by western blot. Male mice, n = 6/group. *$P < 0.05$, vs db/m group; #$P < 0.05$, vs db/db group. Db/m, db/m mice; db/db, db/db mice without Ferrostatin-1 treatment; db/db+Fer1, db/db mice with Ferrostatin-1 treatment. Data are means ± S.E.M.

As exhibited in **Figure 4**, western blot showed that the levels of HIF-1α and HO-1 were increased in db/db mouse kidneys compared with db/m mouse kidneys, while Ferrostatin-1 treatment decreased the levels of HIF-1α and HO-1 in kidneys of db/db mice (**Figures 4A, B**). These results suggested that HIF-1α/HO-1 pathway might involve in ferroptosis-induced DN.

Assessment of Iron Content

Iron overloading is a risk factor for many disorders, because iron regulates considerable enzymes which are involved in lipid peroxidation and oxidative stress (2, 3). Ferroptosis is a form of regulated cell death resulting from iron overloading (1). Therefore, we measured the iron content in mouse kidneys and blood. As shown in **Figure 5**, Lillie staining showed that diabetes increased the iron content in mouse renal tubules, which was relieved in diabetic mouse renal tubules after Ferrostatin-1 treatment (**Figures 5A, B**). Western blot showed that the expression of ferritin heavy chain was increased in db/db mouse kidneys compared with db/m mouse kidneys, but Ferrostatin-1 reduced the expression of ferritin heavy chain in

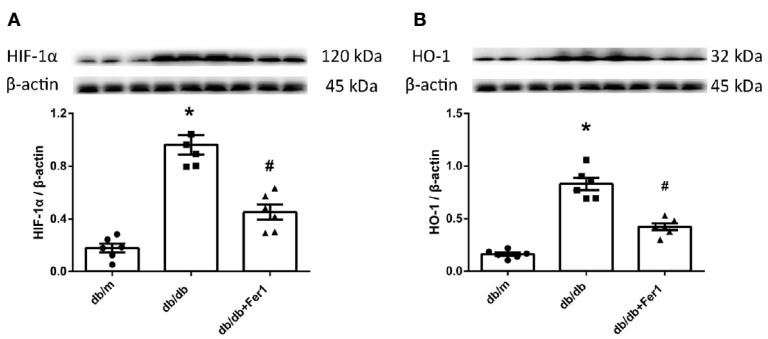

FIGURE 4 | The expression of hypoxia-inducible factor (HIF) -1α and heme oxygenase (HO) -1 in mouse renal tissues. **(A, B)**. Representative photographs and quantification of HIF-1α **(A)** and HO -1 **(B)** in mouse kidneys measured by western blot. Male mice, n = 6/group. *$P < 0.05$, vs db/m group; #$P < 0.05$, vs db/db group. Db/m, db/m mice; db/db, db/db mice without Ferrostatin-1 treatment; db/db+Fer1, db/db mice with Ferrostatin-1 treatment. Data are means ± S.E.M.

kidneys of db/db mice (**Figure 5C**). Additionally, db/db group had higher serum iron ion, ferritin, and transferrin in comparison to db/m group, but Ferrostatin-1 treatment inhibited these parameters in db/db mice (**Figures 5D–F**). These results showed that diabetes contributed to iron overloading in mouse renal tubules, but ferroptosis inhibitor alleviated iron overloading in renal tubules of db/db mice.

Assessment of ROS Formation in Mouse Kidneys

Next, we detected ROS formation in mouse renal tissues. As presented in **Figure 6**, dihydroethidium staining showed that diabetes exacerbated ROS formation in mouse kidneys, while Ferrostatin-1 treatment depressed ROS formation in db/db mouse kidneys (**Figures 6A, B**). Moreover, diabetes resulted in a similar increased expression of NADPH oxidase subunit-gp91 phox in mouse kidneys, whereas Ferrostatin-1 treatment lessoned gp91 phox in db/db mouse kidneys (**Figure 6C**). These findings documented that diabetes promoted NADPH oxidase-derived ROS formation in mouse kidneys, which was suppressed by ferroptosis inhibitor Ferrostatin-1 treatment in diabetic mouse kidneys.

Assessment of Lipid Peroxidation and GPX4 in Mouse Kidneys

Then, we assessed oxidative stress and lipid peroxidation in mouse renal tissues. As exhibited in **Figure 7**, compared with db/m group, the enhanced MDA and the reduced SOD, CAT and GSH-Px in mouse kidneys were noted in db/db group. In contrast, Ferrostatin-1 treatment resulted in the reduction on MDA and the enhancement on SOD, CAT and GSH-Px in kidneys of db/db mice (**Figures 7A–D**). Importantly, we measured the expression of GPX4 in mouse kidneys. Western blot showed that diabetes caused the decreased expression of GPX4 in mouse kidneys, but Ferrostatin-1 treatment increased the expression of GPX4 in kidneys of db/db mice (**Figure 7E**). These findings further indicated that lipid peroxidation induced-ferroptosis was involved in DN, which was improved by ferroptosis inhibitor Ferrostatin-1.

Assessment of Renal Apoptosis

Apoptosis has been found to play a role in renal injury and fibrosis induced by diabetes (41). Therefore, we detected mouse renal apoptosis. As shown in **Figure 8**, TUNEL assay showed that diabetes significantly promoted mouse renal apoptosis, but

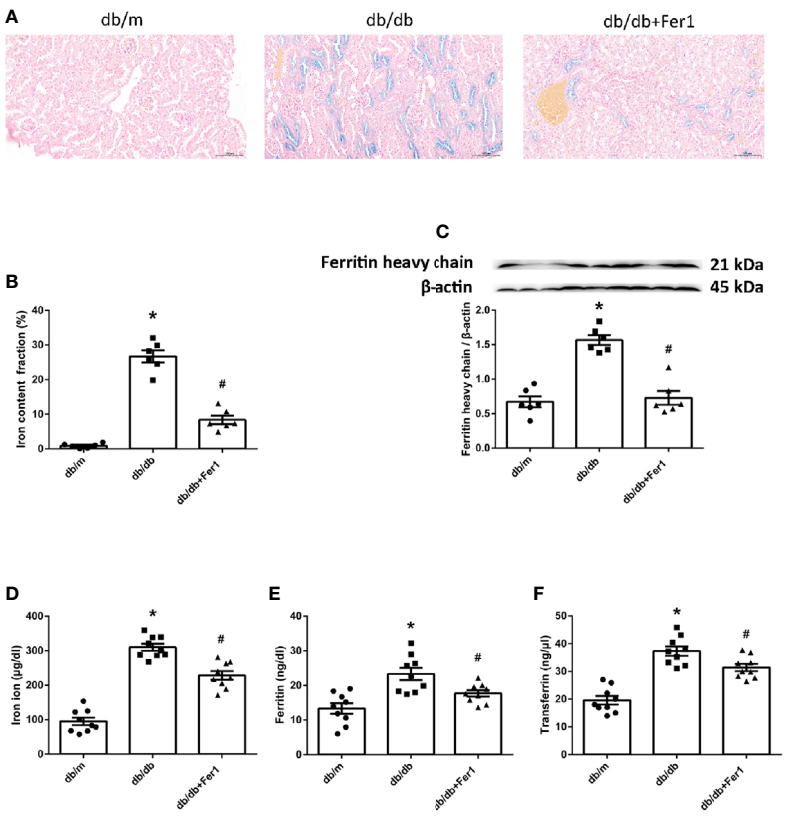

FIGURE 5 | Iron content in db/m, db/db, and db/db+Fer1 groups. **(A, B)**. Representative photographs and quantification of iron content (blue) in kidneys by Lillie staining (six sections per mouse were analyzed). **(C)**. Representative photographs and quantification of ferritin heavy chain in mouse kidneys measured by western blot. **(D–F)**. Quantification of serum iron ion **(D)**, ferritin **(E)**, and transferrin **(F)** measured by ELISA. Male mice, n = 6–9/group. *$P < 0.05$, vs db/m group; #$P < 0.05$, vs db/db group. Db/m, db/m mice; db/db, db/db mice without Ferrostatin-1 treatment; db/db+Fer1, db/db mice with Ferrostatin-1 treatment. Data are means ± S.E.M.

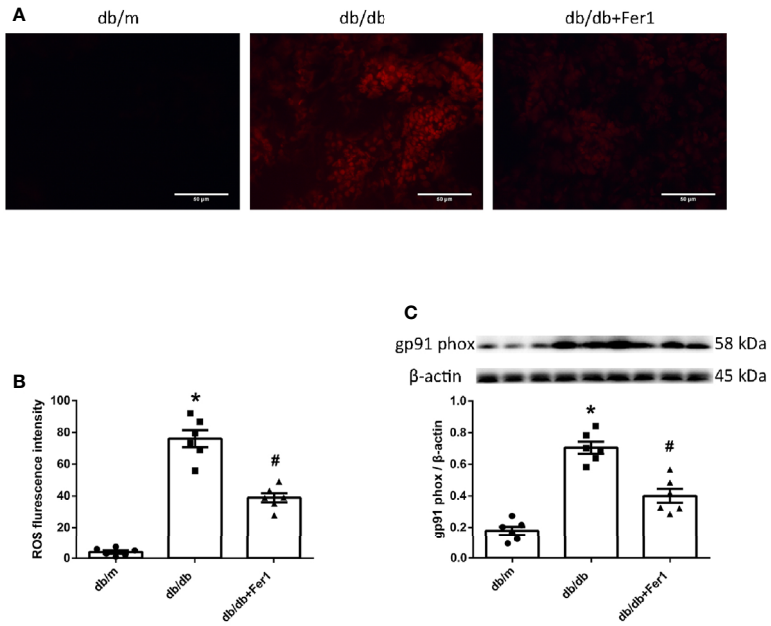

FIGURE 6 | ROS formation in mouse renal tissues. **(A, B)**. Representative photographs and quantification of ROS formation (red) in mouse kidneys by dihydroethidium staining (six sections per mouse were analyzed). **(C)**. Representative photographs and quantification of gp91 phox in mouse kidneys measured by western blot. Male mice, n = 6/group. $^{*}P < 0.05$, vs db/m group; $^{\#}P < 0.05$, vs db/db group. Db/m, db/m mice; db/db, db/db mice without Ferrostatin-1 treatment; db/db+Fer1, db/db mice with Ferrostatin-1 treatment. Data are means ± S.E.M.

Ferrostatin-1 treatment did not relieve renal apoptosis in diabetic mice (**Figures 8A, B**). Moreover, western blot analysis showed that diabetes enhanced the expression of apoptosis associated protein-cleaved caspase-3 in mouse kidneys, while Ferrostatin-1 treatment did not suppress the expression of cleaved caspase-3 in kidneys of diabetic mice (**Figure 8C**). These results showed that diabetes accelerated apoptosis in mouse kidneys, but ferroptosis inhibitor Ferrostatin-1 treatment could not improve apoptosis in mouse kidneys.

DISCUSSION

In present study, we found that diabetes increased UACR level in mice, and diabetic state enhanced tubular injury, promoted fibrosis, elevated the levels of HIF-1α and HO-1, accelerated tubular iron overloading, and exacerbated ROS formation, oxidative stress, and lipid peroxidation in mouse kidneys. On the contrary, ferroptosis inhibitor Ferrostatin-1 decreased the level of UACR in diabetic mice, and Ferrostatin-1 improved tubular injury, reduced fibrosis, repressed the expression of HIF-1α and HO-1, suppressed tubular iron overloading, and inhibited ROS formation, oxidative stress, and lipid peroxidation in diabetic mouse kidneys.

Ferroptosis is a kind of regulated cell death characterized by iron-dependent accumulation of lipid peroxides. Ferroptosis associates well with renal ischemia injury (1) that is one of the major causes of DN (31). Our present research showed that diabetic mice presented higher UACR than control mice, but ferroptosis inhibitor Ferrostatin-1 reduced the level of UACR in diabetic mice, suggesting that ferroptosis was involved in the pathogenesis of DN, and inhibition of ferroptosis can protect against DN.

Initially, the underlying mechanism of albuminuria in DN has been attributed to the increased glomerular leakage. While great importance, changes in glomeruli may not be the main determinant in the prognosis of DN. As renal tubular injury participates in the development of DN, interest in the mechanism of DN has transferred to the renal tubules (35). As a result of emerging evidence supporting a role for ferroptosis in damaging renal tubules (28–30), we detected the damage of renal tubules in diabetic mice. In current study, diabetic mice presented higher KIM-1 and NGAL, the markers of renal tubular damage, both in kidneys and in urine, as compared to non-diabetic mice, with renal tubular basement membranes folding and faulting by hexamine silver staining. However, these changes about renal tubular injury were ameliorated in diabetic mice after ferroptosis inhibitor Ferrostatin-1 treatment. These results provided a strong evidence of ferroptosis to participate in renal tubular injury in diabetic mice.

Ferroptosis has been considered as a trigger of many diseases, and it is also associated with fibrosis (36, 37). Because renal tubular dysfunction is correlated with the extent of renal fibrosis, tubular injury induced by diabetes is identified as the cause of renal fibrosis (39). In current study, both Masson's staining and Sirius red staining showed that there was a significant increase in the renal fibrosis area in diabetic mice as compared to non-diabetic mice. Consistent with the changes of renal fibrosis

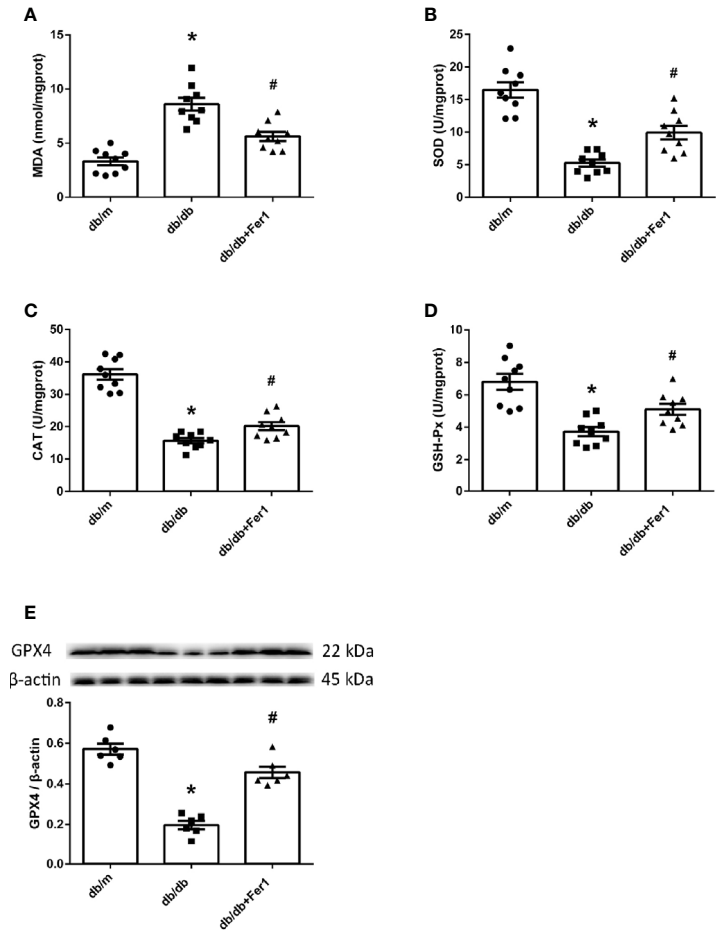

FIGURE 7 | Lipid peroxidation and GPX4 in mouse renal tissues. **(A–D)**. Quantification of malondialdehyde (MDA) **(A)**, superoxide dismutase (SOD) **(B)**, catalase (CAT) **(C)** and glutathione peroxidases (GSH-Px) **(D)** in mouse kidneys. **(E)**. Representative photographs and quantification of glutathione peroxidase 4 (GPX4) in mouse kidneys measured by western blot. Male mice, n = 6–9/group. $^{*}P < 0.05$, vs db/m group; $^{\#}P < 0.05$, vs db/db group. Db/m, db/m mice; db/db, db/db mice without Ferrostatin-1 treatment; db/db+Fer1, db/db mice with Ferrostatin-1 treatment. Data are means ± S.E.M.

fractional area, the expression of fibrosis-associated protein-collagen I was significantly increased in diabetic mouse kidneys as compared to non-diabetic mouse kidneys. However, all changes of renal fibrosis were alleviated by ferroptosis inhibitor Ferrostatin-1 treatment in diabetic mice, which suggested that ferroptosis induced renal fibrosis in diabetic mice.

Previous studies have demonstrated intra-renal hypoxia in clinical patients and experimental models with diabetes (32, 42). The renal tubules are susceptible to the damage from metabolic disorders and hypoxia that are the pathogenesis of diabetes influencing the kidneys (39). The adaptation of hypoxia is mainly conferred through HIF-1α, which induces the expression of HO-1 (15) and regulates ferroptosis (10). HIF-1α and HO-1 have been demonstrated to serve the dual roles in multiple models of kidney injury, including DN. There have been some studies about the significant protective role of HIF-1α/HO-1 pathway (43). However, several recent studies have validated the promoted HIF-1α and HO-1 levels in kidneys of diabetic models (32). Furthermore, in contrast to the protective role in kidneys, our previous studies exhibited that the upregulated expression of HIF-α caused significant renal fibrosis (40), and that the increased HO-1 and iron overloading were presented in kidneys of hypertensive mice (44). Morover, genetic knockdown and pharmacological inhibition of HO-1 validated that activation of HO-1 triggers ferroptosis through iron overloading and subsequently excessive production of ROS and lipid peroxidation (11, 13). It is possible that these conflicting results are due to the poly-pharmacotherapy or other confounding variables of the experimental models, such as species, strains, gender, age and the diseases of models. These discrepancies might also be caused by differences in assays used in different researches. In current study, the increased levels of HIF-1α and HO-1 were observed in diabetic mouse kidneys compared with non-diabetic mouse kidneys. By contrast, ferroptosis inhibitor Ferrostatin-1 treatment reduced the levels of HIF-1α and HO-1 in kidneys of diabetic mice. These findings suggested that ferroptosis might enhanced DN through HIF-1α/HO-1 pathway.

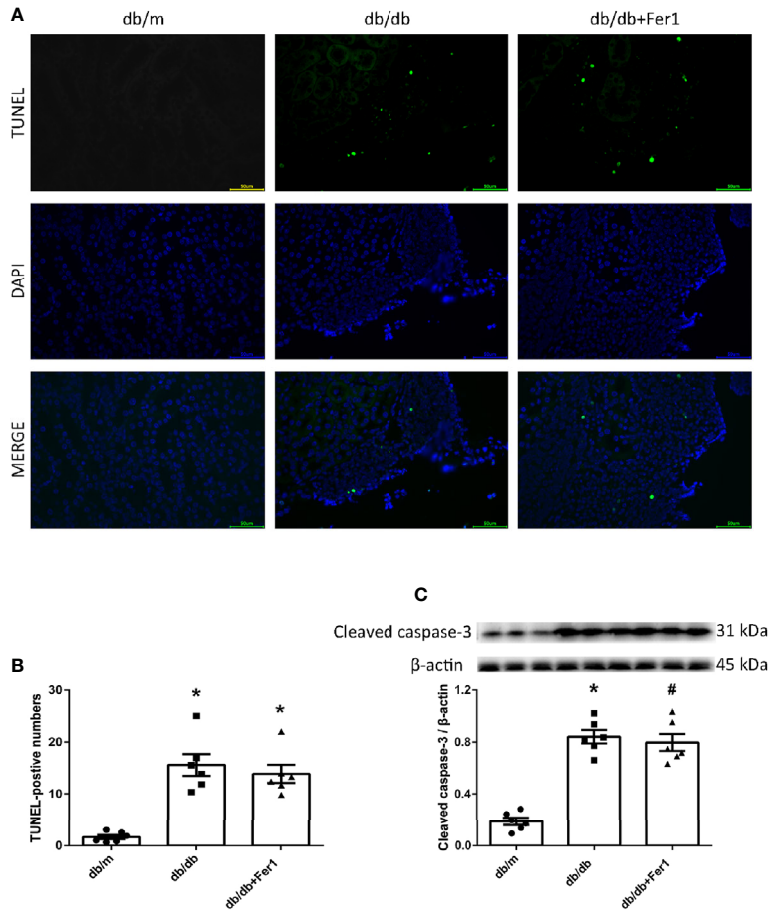

FIGURE 8 | Renal apoptosis in db/m, db/db, and db/db+Fer1 groups. **(A, B)**. Representative photographs and quantification of renal apoptosis by TUNEL assay (six sections per mouse were analyzed). **(C)**. Representative photographs and quantification of cleaved caspase-3 in mouse kidneys measured by western blot. Male mice, n = 6/group. $^{*}P < 0.05$, vs db/m group; $^{\#}P < 0.05$, vs db/db group. Db/m, db/m mice; db/db, db/db mice without Ferrostatin-1 treatment; db/db+Fer1, db/db mice with Ferrostatin-1 treatment. Data are means ± S.E.M.

The increased HO-1 contributes to more iron accumulation by accelerating degradation of heme. Iron is essential for cell survival. Iron overloading is a known risk factor for various disorders. Ferroptosis is a form of regulated cell death that is induced by iron overloading (1). Renal iron accumulation has been proposed to promote the progression of DN (33, 34). However, Ferrostatin-1 can form a complex compounded with iron (45). Previous studies have found that ferroptosis inhibitor Ferrostatin-1 alleviated atherosclerosis lesion and inhibited the iron accumulation in HFD-fed ApoE$^{-/-}$ mice (46), protected against early brain injury and decreased the iron content in subarachnoid hemorrhage rats (47), and inhibited death of microglia and alleviated iron overloading induced by nitrogen-doped graphene quantum dots (48). In current research, Lillie staining showed that there was more iron accumulation in diabetic mouse renal tubules compared with non-diabetic mouse renal tubules, but iron overloading was relieved in renal tubules of diabetic mice after Ferrostatin-1 treatment. Ferritin and transferrin are regulated by HO-1, and the elevated HO-1 increases the levels of ferritin and transferrin (49). Western blot showed that ferritin heavy chain was promoted in diabetic mouse kidneys compared with non-diabetic mouse kidneys, while Ferrostatin-1 treatment decreased ferritin heavy chain in kidneys of diabetic mice. Additionally, diabetic mice had higher serum iron ion, ferritin, and transferrin than non-diabetic mice, but Ferrostatin-1 treatment inhibited these parameters in diabetic mice. These results showed that diabetes contributed to iron overloading in mouse renal tubules, but inhibition of ferroptosis alleviated iron accumulation in diabetic mouse renal tubules.

Ferroptosis occurs as a result of elevated ROS levels due to the increased intracellular iron concentration (1). Renal ROS generation in diabetes is predominantly mediated by NADPH oxidases (50). The excess of ROS caused by hyperglycemia plays a dominant role in DN (23). The current study showed that diabetes resulted in a significant elevation of ROS formation in mouse kidneys, and ferroptosis inhibitor Ferrostatin-1 induced the reduction of ROS formation in diabetic mouse kidneys.

This was accompanied by a significant increased expression of NADPH oxidase subunit-gp91 phox in diabetic mouse kidneys compared with non-diabetic mouse kidneys, and ferroptosis inhibitor Ferrostatin-1 treatment suppressed gp91 phox in diabetic mouse kidneys. These findings indicated that diabetes accelerated NADPH oxidase-derived ROS formation in mouse kidneys, but inhibition of ferroptosis prevented ROS formation derived by NADPH oxidases in diabetic mouse kidneys.

Iron overloading results in the overproduction of ROS, which contributes to an excess of oxidative stress and lipid peroxidation owing to insufficient antioxidant pathways (6). MDA is the main aldehyde product of lipid peroxidation (24). The enzymatic antioxidants consist of SOD, CAT, GSH-Px, etc (6). Recent researches have verified the increased MDA and the decreased SOD, CAT and GSH-Px in kidneys of diabetic animals compared with kidneys of the controls (25, 26). GPX4 has been identified to specifically prevent ferroptosis by suppression of phospholipid peroxidation. Ferrostatin-1 is an antioxidant and generates the same anti-ferroptotic effect as GPX4 proven by previous researches (45). Our current findings presented the increased MDA and the decreased SOD, CAT, and GSH-Px in diabetic mouse kidneys compared to non-diabetic mouse kidneys. However, ferroptosis inhibitor Ferrostatin-1 treatment repressed MDA, and promoted SOD, CAT, and GSH-Px in diabetic mouse kidneys. Moreover, GPX4 was lower in diabetic mouse kidneys than non-diabetic mouse kidneys, whereas GPX4 was increased by ferroptosis inhibitor Ferrostatin-1 treatment in kidneys of diabetic mice. These data supported that lipid peroxidation induced-ferroptosis deteriorated DN in db/db mice.

In addition, previous researches have documented that apoptosis has involved in diabetic renal injury (41). Our current results showed that apoptosis damaged diabetic mouse kidneys, but inhibition of ferroptosis could not reverse the diabetic damages in mouse kidneys, indicating that Ferrostatin-1 protected against DN through another mechanism instead of apoptosis, and ferroptosis might play a critical role in pathogenesis of DN.

CONCLUSIONS

In summary, diabetes led to the increased UACR in mice, and diabetes further resulted in a significant mouse renal tubular injury and mouse renal fibrosis, a promotion of HIF-1α and HO-1 levels in mouse kidneys, an elevation of iron accumulation in mouse renal tubules, and an increase of lipid peroxidation due to the enhanced ROS generation in kidneys of mice; however, inhibition of ferroptosis decreased the UACR in diabetic mice, and inhibition of ferroptosis alleviated renal tubular injury and renal fibrosis in diabetic mice, repressed the levels of HIF-1α and HO-1 in diabetic mouse kidneys, reduced iron accumulation in renal tubules of diabetic mice, and prevented lipid peroxidation by decreasing ROS generation in kidneys of diabetic mouse models. Our study indicated that the process of ferroptosis might aggravate albuminuria, damage renal tubules, and enhance renal fibrosis in diabetic models through HIF-1α/HO-1 pathway, which may contribute to the further study on the pathogenesis of DN and provide a therapeutic target for DN.

DATA AVAILABILITY STATEMENT

The raw data supporting the conclusions of this article will be made available by the authors, without undue reservation.

ETHICS STATEMENT

The animal study was reviewed and approved by the Animal Ethics Committee of Beijing Chao-Yang Hospital, Capital Medical University.

AUTHOR CONTRIBUTIONS

XF: design, experimentation, statistics, article revision. SW: experimentation. ZS: experimentation. HD: experimentation. HY: experimentation. MH: experimentation. XG: design, experimentation, statistics, article revision. All authors contributed to the article and approved the submitted version.

FUNDING

This work was supported by grants from the Chinese National Natural Science Foundation (No. 81700713) to XF.

REFERENCES

1. Lei P, Bai T, Sun Y. Mechanisms of ferroptosis and relations with regulated cell death: A review. *Front Physiol* (2019) 10:139. doi: 10.3389/fphys.2019.00139
2. Yien YY, Shi J, Chen C, Cheung JTM, Grillo AS, Shrestha R, et al. FAM210B is an erythropoietin target and regulates erythroid heme synthesis by controlling mitochondrial iron import and ferrochelatase activity. *J Biol Chem* (2018) 293:19797–811. doi: 10.1074/jbc.RA118.002742
3. Stehling O, Sheftel AD, Lill R. Chapter 12 twelve controlled expression of iron-sulfur cluster assembly components for respiratory chain complexes in mammalian cells. *Methods Enzymol* (2009) 456:209–31. doi: 10.1016/S0076-6879(08)04412-1
4. Stoyanovsky DA, Tyurina YY, Shrivastava I, Bahar I, Tyurin VA, Protchenko O, et al. Iron catalysis of lipid peroxidation in ferroptosis: Regulated enzymatic or random free radical reaction? *Free Radic Biol Med* (2019) 133:153–614. doi: 10.1016/j.freeradbiomed.2018.09.008
5. Sakellariou GK, Jackson MJ, Vasilaki A. Redefining the major contributors to superoxide production in contracting skeletal muscle. The role of NAD(P)H oxidases. *Free Radic Res* (2014) 48:12–29. doi: 10.3109/10715762.2013.830718
6. Su LJ, Zhang JH, Gomez H, Murugan R, Hong X, Xu D, et al. Reactive oxygen species-induced lipid peroxidation in apoptosis, autophagy, and ferroptosis. *Oxid Med Cell Longev* (2019) 2019:1–3. doi: 10.1155/2019/5080843
7. Bela K, Horváth E, Gallé Á, Szabados L, Tari I, Csiszár J. Plant glutathione peroxidases: Emerging role of the antioxidant enzymes in plant development and stress responses. *J Plant Physiol* (2015) 176:192–201. doi: 10.1016/j.jplph.2014.12.014
8. Seibt TM, Proneth B, Conrad M. Role of GPX4 in ferroptosis and its pharmacological implication. *Free Radic Biol Med* (2019) 133:144–52. doi: 10.1016/j.freeradbiomed.2018.09.014

9. Lawen A, Lane DJR. Mammalian iron homeostasis in health and disease: Uptake, storage, transport, and molecular mechanisms of action. *Antioxid Redox Signal* (2013) 18:2473–507. doi: 10.1089/ars.2011.4271
10. Chiang SK, Chen SE, Chang LC. A dual role of heme oxygenase-1 in cancer cells. *Int J Mol Sci* (2019) 20:39. doi: 10.3390/ijms20010039
11. Chang LC, Chiang SK, Chen SE, Yu YL, Chou RH, Chang WC. Heme oxygenase-1 mediates BAY 11–7085 induced ferroptosis. *Cancer Lett* (2018) 416:124–37. doi: 10.1016/j.canlet.2017.12.025
12. Khan ZA, Barbin YP, Cukiernik M, Adams PC, Chakrabarti S. Heme-oxygenase-mediated iron accumulation in the liver. *Can J Physiol Pharmacol* (2004) 82:448–56. doi: 10.1139/y04-052
13. Hassannia B, Wiernicki B, Ingold I, Qu F, Van Herck S, Tyurina YY, et al. Nano-targeted induction of dual ferroptotic mechanisms eradicates high-risk neuroblastoma. *J Clin Invest* (2018) 128:3341–55. doi: 10.1172/JCI99032
14. Adedoyin O, Boddu R, Traylor A, Lever JM, Bolisetty S, George JF, et al. Heme oxygenase-1 mitigates ferroptosis in renal proximal tubule cells. *Am J Physiol - Ren Physiol* (2018) 314:F702–14. doi: 10.1152/ajprenal.00044.2017
15. Otterbein LE, Soares MP, Yamashita K, Bach FH. Heme oxygenase-1: Unleashing the protective properties of heme. *Trends Immunol* (2003) 24:449–55. doi: 10.1016/S1471-4906(03)00181-9
16. Zou Y, Palte MJ, Deik AA, Li H, Eaton JK, Wang W, et al. A GPX4-dependent cancer cell state underlies the clear-cell morphology and confers sensitivity to ferroptosis. *Nat Commun* (2019) 10:1617. doi: 10.1038/s41467-019-09277-9
17. Tang SCW, Leung JCK, Lai KN. Diabetic tubulopathy: An emerging entity. *Contrib Nephrol* (2011) 170:124–34. doi: 10.1159/000325647
18. Gibb DM, Tomlinson PA, Dalton NR, Turner C, Shah V, Barratt TM. Renal tubular proteinuria and microalbuminuria in diabetic patients. *Arch Dis Child* (1989) 64:129–34. doi: 10.1136/adc.64.1.129
19. Tojo A, Onozato M, Ha H, Kurihara H, Sakai T, Goto A, et al. Reduced albumin reabsorption in the proximal tubule of early-stage diabetic rats. *Histochem Cell Biol* (2001) 116:269–76. doi: 10.1007/s004180100317
20. Russo LM, Sandoval RM, Campos SB, Molitoris BA, Comper WD, Brown D. Impaired tubular uptake explains albuminuria in early diabetic nephropathy. *J Am Soc Nephrol* (2009) 20:489–94. doi: 10.1681/ASN.2008050503
21. Comper WD, Deen WM, Haraldsson B. Resolved: Normal glomeruli filter nephrotic levels of albumin. *J Am Soc Nephrol* (2008) 19:427–32. doi: 10.1681/ASN.2007090997
22. Dickson LE, Wagner MC, Sandoval RM, Molitoris BA. The proximal tubule and albuminuria: Really! *J Am Soc Nephrol* (2014) 25:443–53. doi: 10.1681/ASN.2013090950
23. Davì G, Falco A, Patrono C. Lipid peroxidation in diabetes mellitus. *Antioxid Redox Signal* (2005) 7:256–68. doi: 10.1089/ars.2005.7.256
24. Ayala A, Muñoz MF, Argüelles S. Lipid peroxidation: Production, metabolism, and signaling mechanisms of malondialdehyde and 4-hydroxy-2-nonenal. *Oxid Med Cell Longev* (2014) 2014:1–31. doi: 10.1155/2014/360438
25. Kędziora-Kornatowska K, Szram S, Kornatowski T, Szadujkis-Szadurski L, Kędziora J, Bartosz G. Effect of vitamin E and vitamin C supplementation on antioxidative state and renal glomerular basement membrane thickness in diabetic kidney. *Nephron* (2003) 95:e134–43. doi: 10.1159/000074840
26. Ulas M, Cay M. 17β-estradiol and vitamin e modulates oxidative stress-induced kidney toxicity in diabetic ovariectomized rat. *Biol Trace Elem Res* (2011) 144821–31. doi: 10.1007/s12011-011-9025-x
27. Ratliff BB, Abdulmahdi W, Pawar R, Wolin MS. Oxidant mechanisms in renal injury and disease. *Antioxid Redox Signal* (2016) 25:119–46. doi: 10.1089/ars.2016.6665
28. Friedmann Angeli JP, Schneider M, Proneth B, Tyurina YY, Tyurin VA, Hammond VJ, et al. Inactivation of the ferroptosis regulator Gpx4 triggers acute renal failure in mice. *Nat Cell Biol* (2014) 16:1180–91. doi: 10.1038/ncb3064
29. Deng F, Sharma I, Dai Y, Yang M, Kanwar YS. Myo-inositol oxygenase expression profile modulates pathogenic ferroptosis in the renal proximal tubule. *J Clin Invest* (2019) 129:5033–49. doi: 10.1172/JCI129903
30. Wang Y, Bi R, Quan F, Cao Q, Lin Y, Yue C, et al. Ferroptosis involves in renal tubular cell death in diabetic nephropathy. *Eur J Pharmacol* (2020) 888:173574. doi: 10.1016/j.ejphar.2020.173574
31. Alpers CE, Hudkins KL. Mouse models of diabetic nephropathy. *Curr Opin Nephrol Hypertens* (2011) 20:278–84. doi: 10.1097/MNH.0b013e3283451901
32. Sun HK, Lee YM, Han KH, Kim HS, Ahn SH, Han SY. Phosphodiesterase inhibitor improves renal tubulointerstitial hypoxia of the diabetic rat kidney. *Korean J Intern Med* (2012) 27:163–70. doi: 10.3904/kjim.2012.27.2.163
33. Chaudhary K, Chilakala A, Ananth S, Mandala A, Veeranan-Karmegam R, Powell FL, et al. Renal iron accelerates the progression of diabetic nephropathy in the HFE gene knockout mouse model of iron overload. *Am J Physiol - Ren Physiol* (2019) 317:F512–7. doi: 10.1152/ajprenal.00184.2019
34. Dominguez JH, Liu Y, Kelly KJ. Renal iron overload in rats with diabetic nephropathy. *Physiol Rep* (2015) 3:e12654. doi: 10.14814/phy2.12654
35. Zeni L, Norden AGW, Cancarini G, Unwin RJ. A more tubulocentric view of diabetic kidney disease. *J Nephrol* (2017) 30:701–17. doi: 10.1007/s40620-017-0423-9
36. Kong Z, Liu R, Cheng Y. Artesunate alleviates liver fibrosis by regulating ferroptosis signaling pathway. *BioMed Pharmacother* (2019) 109:2043–53. doi: 10.1016/j.biopha.2018.11.030
37. Li X, Duan L, Yuan S, Zhuang X, Qiao T, He J. Ferroptosis inhibitor alleviates Radiation-induced lung fibrosis (RILF) via down-regulation of TGF-β1. *J Inflammation (United Kingdom)* (2019) 16:11. doi: 10.1186/s12950-019-0216-0
38. Nath KA. Tubulointerstitial changes as a major determinant in the progression of renal damage. *Am J Kidney Dis* (1992) 20:1–17. doi: 10.1016/S0272-6386(12)80312-X
39. Gilbert RE. Proximal tubulopathy: Prime mover and key therapeutic target in diabetic kidney disease. *Diabetes* (2017) 66:791–800. doi: 10.2337/db16-0796
40. Wang S, Zeng H, Chen ST, Zhou L, Xie XJ, He X, et al. Ablation of endothelial prolyl hydroxylase domain protein-2 promotes renal vascular remodelling and fibrosis in mice. *J Cell Mol Med* (2017) 21:1967–78. doi: 10.1111/jcmm.13117
41. Sifuentes-Franco S, Padilla-Tejeda DE, Carrillo-Ibarra S, Miranda-Díaz AG. Oxidative stress, apoptosis, and mitochondrial function in diabetic nephropathy. *Int J Endocrinol* (2018) 2018:1–13. doi: 10.1155/2018/1875870
42. Bessho R, Takiyama Y, Takiyama T, Kitsunai H, Takeda Y, Sakagami H, et al. Hypoxia-inducible factor-1α is the therapeutic target of the SGLT2 inhibitor for diabetic nephropathy. *Sci Rep* (2019) 9:14754. doi: 10.1038/s41598-019-51343-1
43. Jiang N, Zhao H, Han Y, Li L, Xiong S, Zeng L, et al. HIF-1α ameliorates tubular injury in diabetic nephropathy via HO-1–mediated control of mitochondrial dynamics. *Cell Prolif* (2020) 53:e12909. doi: 10.1111/cpr.12909
44. Feng X, Su H, He X, Chen JX, Zeng H. SIRT3 Deficiency sensitizes angiotensin-II-Induced renal fibrosis. *Cells* (2020) 9:2510. doi: 10.3390/cells9112510
45. Miotto G, Rossetto M, Di Paolo ML, Orian L, Venerando R, Roveri A, et al. Insight into the mechanism of ferroptosis inhibition by ferrostatin-1. *Redox Biol* (2020) 28:101328. doi: 10.1016/j.redox.2019.101328
46. Bai T, Li M, Liu Y, Qiao Z, Wang Z. Inhibition of ferroptosis alleviates atherosclerosis through attenuating lipid peroxidation and endothelial dysfunction in mouse aortic endothelial cell. *Free Radic Biol Med* (2020) 160:92–102. doi: 10.1016/j.freeradbiomed.2020.07.026
47. Li Y, Liu Y, Wu P, Tian Y, Liu B, Wang J, et al. Inhibition of ferroptosis alleviates early brain injury after subarachnoid hemorrhage in vitro and in vivo via reduction of lipid peroxidation. *Cell Mol Neurobiol* (2020). doi: 10.1007/s10571-020-00850-1
48. Wu T, Liang X, Liu X, Li Y, Wang Y, Kong L, et al. Induction of ferroptosis in response to graphene quantum dots through mitochondrial oxidative stress in microglia. *Part Fibre Toxicol* (2020) 17:30. doi: 10.1186/s12989-020-00363-1
49. Ewing JF. Distribution of constitutive (HO-2) and heat-inducible (HO-1) heme oxygenase isozymes in rat testes: HO-2 displays stage-specific expression in germ cells. *Endocrinology* (1995) 136:2294–302. doi: 10.1210/en.136.5.2294
50. Jha JC, Banal C, Chow BSM, Cooper ME, Jandeleit-Dahm K. Diabetes and Kidney Disease: Role of Oxidative Stress. *Antioxid Redox Signal* (2016) 25:657–84. doi: 10.1089/ars.2016.6664

Conflict of Interest: The authors declare that the research was conducted in the absence of any commercial or financial relationships that could be construed as a potential conflict of interest.

frontiers in Endocrinology

ORIGINAL RESEARCH
published: 27 August 2021
doi: 10.3389/fendo.2021.690784

Sp1-Induced lncRNA Rmrp Promotes Mesangial Cell Proliferation and Fibrosis in Diabetic Nephropathy by Modulating the miR-1a-3p/JunD Pathway

Hansen Yang[1†], Jia Wang[1†], Zheng Zhang[1†], Rui Peng[2], Dan Lv[1], Handeng Liu[1] and Yan Sun[1]*

[1] Department of Cell Biology and Genetics, Chongqing Medical University, Chongqing, China, [2] Department of Bioinformatics, Chongqing Medical University, Chongqing, China

OPEN ACCESS

Edited by:
Katsumi Iizuka,
Gifu University Hospital, Japan

Reviewed by:
Yusuke Seino,
Fujita Health University, Japan
Yanyan Liu,
Gifu University, Japan

***Correspondence:**
Yan Sun
yansun@cqmu.edu.cn

[†]These authors have contributed equally to this work

Specialty section:
This article was submitted to Diabetes: Molecular Mechanisms, a section of the journal Frontiers in Endocrinology

Received: 04 April 2021
Accepted: 06 August 2021
Published: 27 August 2021

Citation:
Yang H, Wang J, Zhang Z, Peng R, Lv D, Liu H and Sun Y (2021) Sp1-Induced lncRNA Rmrp Promotes Mesangial Cell Proliferation and Fibrosis in Diabetic Nephropathy by Modulating the miR-1a-3p/JunD Pathway. Front. Endocrinol. 12:690784. doi: 10.3389/fendo.2021.690784

Diabetic nephropathy (DN) is a serious complication of diabetes mellitus. Long non-coding RNAs (lncRNAs) are regulators in DN progression. However, the regulatory mechanisms of multiple lncRNAs in DN remain to be determined. Our aim was to investigate the function and molecular mechanism of lncRNA RNA component of mitochondrial RNAase P (Rmrp) in DN. Here, we observed that the expression of Rmrp was up-regulated in the kidney of db/db DN mice and high glucose induced glomerular mesangial cells (MC). More importantly, the abnormal transcription of Rmrp was induced by nuclear transcription factor Sp1, which promotes the proliferation and production of fibrotic markers in MC. Subsequently, we screened the miRNAs related to Rmrp and found that Rmrp and miR-1a-3p are co-localized at the subcellular level of MC, and Rmrp could directly binds to miR-1a-3p. Further mechanism research demonstrated that the elevated miR-1a-3p significantly attenuated the proliferation and fibrosis-promoting effects induced by up-regulation of Rmrp. At the same time, we also investigated that miR-1a-3p can directly bind to Jun D proto-oncogene (JunD), thereby regulating the protein level of JunD. Rmrp-induced proliferation and fibrogenesis were reversed by co-transfection with JunD siRNA. In summary, Sp1 induced lncRNA Rmrp could drive the expression of JunD *via* sponging miR-1a-3p in DN progression.

Keywords: diabetic nephropathy, Rmrp, mesangial cells, miR-1a-3p, JunD

INTRODUCTION

The increasing global prevalence of diabetic nephropathy (DN) is closely associated with end-stage renal disease (1, 2). Glomerular mesangial enlargement is the basic pathophysiological mechanisms of DN and a recognized feature in the early of DN process. This lesion in mesangial tissue is initially due to the mesangial cells (MC) proliferation and extracellular matrix (ECM) accumulation (3, 4). Although hyperglycemia is the main determinant in the mesangial change of DN, the current

interventions and medication are not ideal (5). Therefore, it is an urgent need to illustrate the mechanisms of DN.

Long non-coding RNAs (lncRNAs) are identified as RNAs>200 nucleotides and play important regulatory roles in many diseases (6, 7). In the past decade, researchers demonstrate lncRNAs that play key modulators in DN pathogenesis. For instance, LRNA9884 could promote renal inflammation by regulating MCP-1 transcriptional level in DN mice (8). In addition, a recent study also found that glomerular ECM and hypertrophy are regulated by lncRNA lncMGC, which is provoked by endoplasmic reticulum stress (9). Nevertheless, the potential roles, biogenesis process and molecular functions of lncRNAs in DN are still largely unclear.

MicroRNAs (miRNAs) as small non-coding RNAs are demonstrated to play an important agent in cellular processes and molecular mechanism of the disease state, including DN (10, 11). Many miRNAs have been exhibited to a negative effect on gene expression and function at the transcriptional and post-transcriptional regulation. One classic hypothesis of miRNA function is the competitive endogenous RNA (ceRNA) hypothesis that RNA transcripts can band to miRNA-complementary sequence and regulate each other by competing specifically for shared miRNAs (12). Mounting evidence shows that lncRNAs could act as ceRNAs to bind with miRNA and free its target genes for translation in DN (13). It has been reported that lncRNA-NR_033515 could promote MC proliferation and trigger fibrogenesis-related proteins by targeting miR-743b-5p in DN (14). Our previous study also showed lncRNA H2k2 could serve as ceRNA activates Trim11/Mek pathway *via* binding the miR-449a/b and promotes mesangial cell proliferation in DN (15).

By using high-throughput RNA-seq, we recently reported the involvement of lncRNAs in the kidney of DN mice and identified lncRNAs associated with DN (16, 17). In the current study, we found that lncRNA RNA component of mitochondrial RNAase P (Rmrp) is the high expressed lncRNAs in the DN mice and high glucose induced-MC. Rmrp as a non-coding RNA (ncRNA), is located on mouse chromosome 4 (Chr4: 43492785-43493059) and having a length of 275 bp, and is a part of the RNase MRP complex functioning in mitochondrial and ribosomal RNA processing (18). The full-length Rmrp is highly conserved between human and mouse (84% homology) (19). However, there is no report about Rmrp in DN up to now. More importantly, we found that transcription factor Sp-1 might mediate the transcription of Rmrp. We further proved that Rmrp up-regulated JunD expression through sponge miR-1a-3p, which may contribute to MC proliferation and fibrosis in DN. Collectively, Our results provide novel insight into the functions of RMRP in DN.

MATERIALS AND METHODS

Animal Tissue Specimens

The kidney tissue stripped from C57BL/BKS background db/db male mice ($Lepr^{db}$/+$Lepr^{db}$) or age-matched male genetic control db/m mice (m+/+ $Lepr^{db}$), that were purchased from Nanjing Biomedical Research Institute (Nanjing, China). As we previously published (16), the levels of blood glucose, albuminuria and creatinine were detected in db/db mice and db/m mice, and the 8 weeks of age of db/db mice were regarded as the early stage of DN. The tissue specimens were stored in liquid nitrogen until further use. All procedures follow Chongqing Medical University's facility guidelines for animal experiments and management. The study was approved by the Ethics Committee of Chongqing Medical University.

Cell Culture

Mouse glomerular endothelial cell (MGEC), glomerular mesangial cells (MC), glomerular podocyte cells (MPC5) and renal tubular epithelial cells (TCMK-1) were preserved in our laboratory. MPC5 were cultured in RPMI 1640 medium (Invitrogen, CA, USA). MGEC, MC and TCMK-1were cultured in DMEM medium (Gibco, CA, USA). As previously reported (17), these cells were stimulated with glucose at 5.5 mmol/L glucose and 19.5 mmol/L mannitol (low glucose MC, LMC) or at 25 mmol/L glucose (high glucose MC, HMC).

Vector Construction, Small Interfering RNA, and Cell Transfection

The full length of Rmrp was amplified in MCs and was cloned into the lentivirus vector LV5 (GenePharma, Shanghai, China). The full length of Sp1 was amplified from cDNA and was cloned into pcDNA3.1 (Genecreate Biotech, Wuhan, China). Vectors were identified by enzyme digestion identification (Rmrp over-expression lentivirus digested by BamHI and NotI; Sp-1 over-expression plasmid digested by BamHI and EcoRV). The empty sequence (NC) of LV5 and pcDNA3.1 vector was used as controls, respectively. Small interfering RNAs (siRNAs) targeting Rmrp were designed and purchased by Ribo Biotech (Guangzhou, China); JunD siRNAs, Ap-1siRNAs and negative control (siNC) were designed and purchased by Sangon Biotech (Shanghai, China). MiR-1a-3p mimic, inhibitor and matched negative controls were provided by GenePharma. Lentivirus containing Rmrp were generated in 293T cells. MCs were infected with the lentivirus and selected with puromycin (Gibco). The transfections were performed with Lipofectamine 3000 (Invitrogen) according to the manufacturer's instructions. The sequences of siRNA, mimics, inhibitor and negative control in this study were listed in **Supplementary Table 1**.

RNA Extraction, Nuclear-Cytoplasmic Fractionation, and qRT-PCR Assays

All the processes were executed with the manufacturer's instructions. Cytoplasmic and nuclear RNA were isolated by PARIS™ Kit (Invitrogen). TRIzol® Reagent (Invitrogen) was used to extract total RNA from tissues or cell. The PrimeScript RT kit (Takara, Dalian, China) was applied to the reverse transcription of RNA. The TB Green Premix Ex Taq (Takara) and CFX Connect™ Real-Time PCR Detection System (Bio-Rad, CA, USA) were used to perform the quantitative real-time PCR (qRT-PCR). Relative expression changes of genes were calculated

by the $2^{-\Delta\Delta Ct}$ method. All the primer sequences were displayed in **Supplementary Table 2**.

Fluorescence *In Situ* Hybridization

Cy3-labeled Rmrp and FITC-labeled miR-1a-3p fluorescence probe were synthesized by GenePharma (Shanghai, China). FISH analysis was performed using a FISH kit (GenePharma, Shanghai, China) according to the manufacturer's instructions. The images were observed with the fluorescence microscope (Leica, Wetzlar, Germany) and analyzed with Image-Pro Plus (Media Cybernetics, Bethesda, MD, USA).

Immunohistochemistry

The detailed method was performed as previously reported (20). Briefly, Paraffin-embedded renal tissues were sectioned at 4 μm thickness. Antigen retrieval was used with citrate buffer for 15 min in a microwave oven at 95–98°C. Endogenous peroxidase of renal tissues was occluded by 3% H_2O_2 for 20 min at room temperature. Next, the sections were blocked with 0.5% Triton and 10% normal goat for 30 min at room temperature and then incubated with anti-JunD (1:100, Abcam) at 4°C for 12 h. Subsequently, the sections were washed with PBS three times and carried out with biotinylated secondary antibody at room temperature for 30 min. The diaminobenzidine (Zhongshan Biosciences, Beijing, China) was applied to the chromogenic reaction and hematoxylin was used to stain the nuclei for the sections. The immunohistological images were observed by light microscopy (Leica).

Cell Proliferation and Flow Cytometric Analysis

Cell proliferation rate was measured by 5-ethynyl-2'-deoxyuridine (EdU) assays according to the manufacturer's instructions. Flow cytometric analysis was performed as previously reported (15).

Western Blot Analysis

The proteins were extracted by cold RIPA lysis buffer, quantified and electrophoresed by SDS-PAGE (8, 10, or 12%). Next, the target protein transferred onto PVDF membranes (Millipore, Massachusetts, USA). The membranes were blocked with 5% skimmed milk at room temperature, and then incubated with primary antibodies overnight at 4°C. Antibodies against Cyclin D1 (1:1000, Abcam), CDK4 (1:1000, Abcam), Fibronectin (1:1000, Abcam), Collagen IV (1:400, Abcam), JunD (1:1000, Abcam), Sp1 (1:1000, Millipore), β-actin (1:5000, Abcam). The second day, the membranes were incubated with goat anti-rabbit HRP-IgG secondary antibodies (1: 5000, Beyotime, Shanghai, China) for 90 min. The immune response bands were detected by an enhanced chemiluminescence (ECL) system (Millipore). The semi-quantified data of bands were using ImageJ software.

Dual-Luciferase Reporter Assay

Based on the experimental design for Sp1 binding sites, the 100bp sequence before and after the P1, P2, or P3 sites of Rmrp promoter was synthesized and constructed into pGL3-basic luciferase reporter vector (WT). Meanwhile, the binding sites of P1, P2, or P3 sequence were mutant and constructed into pGL3-basic vector (Mut). According to the manufacturer's protocol, the above vectors were co-transfected with pcDNA3.1-Sp1 vector, respectively. To verify the seed-sequence complementation between miR-1a-3p and Rmrp, the wild-type (wt) or seed-sequence mutant (mut) of full-length Rmrp was constructed by Ribo Biotech (Guangzhou, China), and co-transfected with mimics NC or miR-1a-3p or in MC, respectively. Meanwhile, MC and the over-expressed Rmrp of MC were co-transfected with the wt-JunD 3' UTR reporter plasmid or mut-JunD 3' UTR and mimics NC or miR-1a-3p (Ribo Biotech, Guangzhou, China). After 48 h transfection, the activities of firefly and Renilla luciferase were measured by the Dual-Glo Luciferase Assay System (Promega, WI, USA).

Chromatin Immunoprecipitation Assay

The detailed method was performed as previously reported (20). In brief, according to the protocol of Millipore EZ-ChIP kit (Millipore), the protein-DNA complex were combined with anti-Sp1 antibody (Millipore) overnight at 4°CC. 1% the protein-DNA complex was reserved as input control. Normal rabbit IgG (Millipore) was used as the negative control of anti-Sp1 antibody. Immunoprecipitate complexes were collected with protein G Sepharose. After washing and extracting, the purified genomic DNA fragments were analyzed by qRT-PCR. All the primer sequences were displayed in **Supplementary Table 2**.

RNA Immunoprecipitation Assay

The detailed method was performed as previously reported (21). In brief, EZ-Magna RIP kit (Millipore) was performed to the RIP assays. The Ago2 antibody (Abcam) was used to combine the Ago2-dependent complex and normal rabbit IgG (Millipore) was used as negative control. One tenth of the lysate was reserved as input control. The enrichment levels of miR-1A-3p and Rmrp were analyzed by qRT-PCR.

Statistical Analysis

All statistical analyses were conducted by GraphPad Prism 7.0 (GraphPad Software, San Diego, CA). The data are presented as mean ± standard deviation (SD). Student's t-test or one-way ANOVA were used for statistical comparisons as indicated. $p< 0.05$ was considered as statistically significant.

RESULTS

LncRNA Rmrp Is Significantly Up-regulated in DN

In order to further explore the expressions of Rmrp in DN progression, qRT-PCR was applied to determine the expression level of Rmrp in 8W and 12W DN mice and the age-matched normal mice, which were conserved in our laboratory (16). The results demonstrated that Rmrp was significantly up-regulated in the kidney of DN mice (**Figure 1A**). To observe the effect of glucose on the expression of Rmrp in glomerular endothelial cell (MGEC), glomerular mesangial cells (MC), glomerular podocyte cells (MPC5) and renal tubular epithelial cells (TCMK-1), we

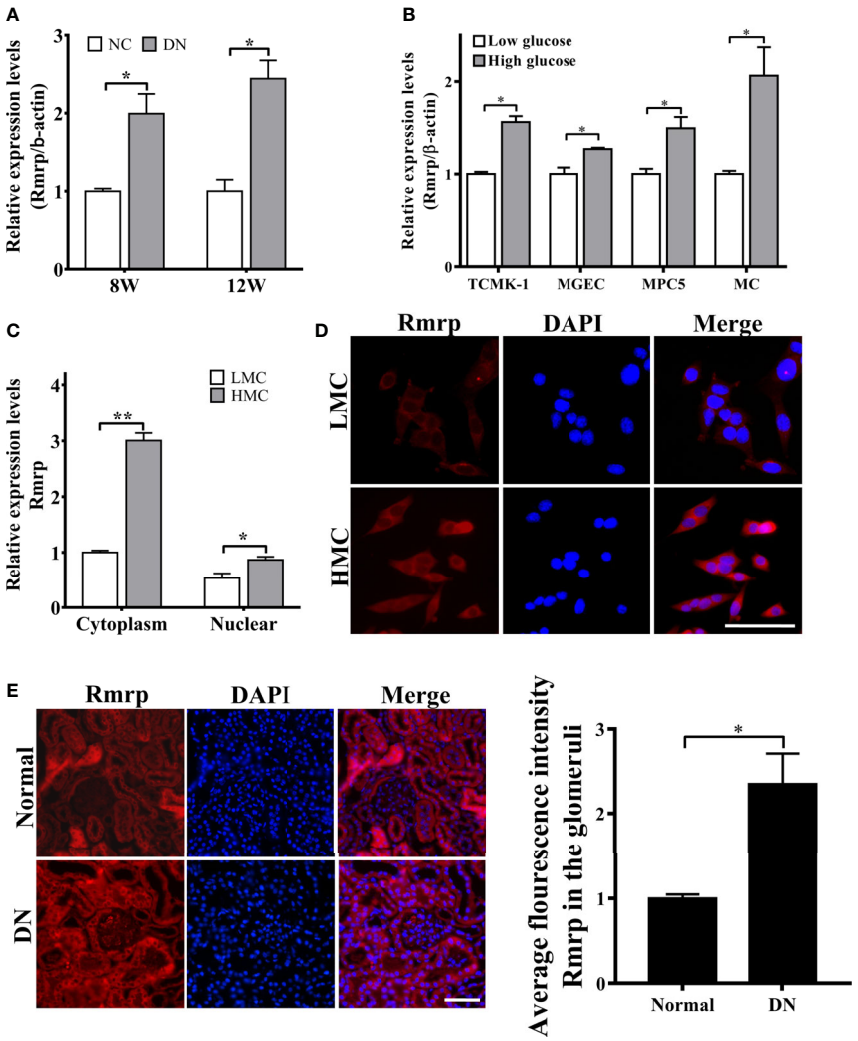

FIGURE 1 | Rmrp is up-regulated in DN. **(A)** Relative expression of Rmrp was identified by quantitative real-time PCR (qRT-PCR) in the renal tissues of db/db DN mice and normal mice at 8 or 12 weeks of age (n=5/group). **(B)** Relative expression of Rmrp was determined by qRT-PCR in four types of renal cells cultured under low (5.5 mmol/L glucose) or high glucose (25 mmol/L glucose) conditions. **(C)** Nuclear-cytoplasmic fractionation assay showed that Rmrp was mainly observed in the cytoplasm of H-MCs by qRT-PCR; β-actin was the cytoplasm control and U6 was the nucleus control. **(D)** FISH was performed to observe the cellular location of Rmrp (red) in LMC and HMC (Scale bar: 50 μm); the nuclei were stained with DAPI. The nuclei were stained with DAPI. **(E)** The localization of Rmrp (red) was observed by FISH and quantitative analysis in the renal tissue of db/db DN mice and the normal group (Scale bar: 50 μm). Data were represented as the mean ± SD of three independent experiments; $^{*}p < 0.05$, $^{**}p < 0.01$.

cultured four types of cells in low glucose levels (5.5 mM glucose and 19.5 mM mannitol) or high glucose levels (25 mM) medium for 48 hr. In high glucose levels, the expression of Rmrp was the most up-regulated in MC (**Figure 1B**). Subsequently, RT-PCR and FISH assays were used to detect the subcellular localization of Rmrp. The qRT-PCR results showed that Rmrp was markedly higher in the cytoplasm of high glucose-induced MC (HMC) than in the cytoplasm of low glucose induced MC (LMC) (**Figure 1C**). Similarly, FISH assays revealed that Rmrp was mainly localized in the cytoplasm of MC and in the glomerulus of DN mice (**Figures 1D, E**). These data suggested that lncRNA Rmrp might participate in the mesangial cell dysfunction of DN.

Rmrp Promotes Proliferation and Fibrosis in MC

To explore the biological effects of Rmrp in DN, we constructed the overexpression lentivirus of Rmrp and designed three Rmrp siRNAs (siRmrp-1, siRmrp-2, and siRmrp-3). The results of qRT-PCR showed that the expression of Rmrp in LMC transfected with Rmrp lentivirus was significantly up-regulated (**Supplementary Figure 1A**). Meanwhile, the knockdown effect of siRmrp-1 and siRmrp-2 were better to that of siRmrp-3 in HMC (**Supplementary Figure 2B**). Thus, siRmrp-1 and siRmrp-2 were selected for further study.

In our previous studies, we found that high glucose possess MC proliferation and fibrosis (21). Thus, we wondered to know

the role of Rmrp in these findings. The EdU assays, cell cycle analysis and western blot were used to detect cell growth predominance. Through EdU assay and quantitative analysis, the proportion of cell proliferation was increased after overexpression of Rmrp in LMC, and was attenuated in HMC which knock down of Rmrp (**Figure 2A**). The flow cytometry analysis displayed that the percentage of G1 phase was declined and S phase ratio was raised after overexpression of Rmrp in LMC, while the percentage of cells were arrested in G1 phase and less cells were progressed through to the S phase after silencing Rmrp in HMC (**Figure 2B**). Furthermore, western blot assay demonstrated that overexpression of Rmrp increased the expression of G1 phase-related proteins Cyclin-dependent kinase 4 (CDK4) and Cyclin D1 in LMC, while the protein levels of CDK4 and Cyclin D1 was reversed once Rmrp was restrained in HMC (**Figure 2C**). Similarly, we found that

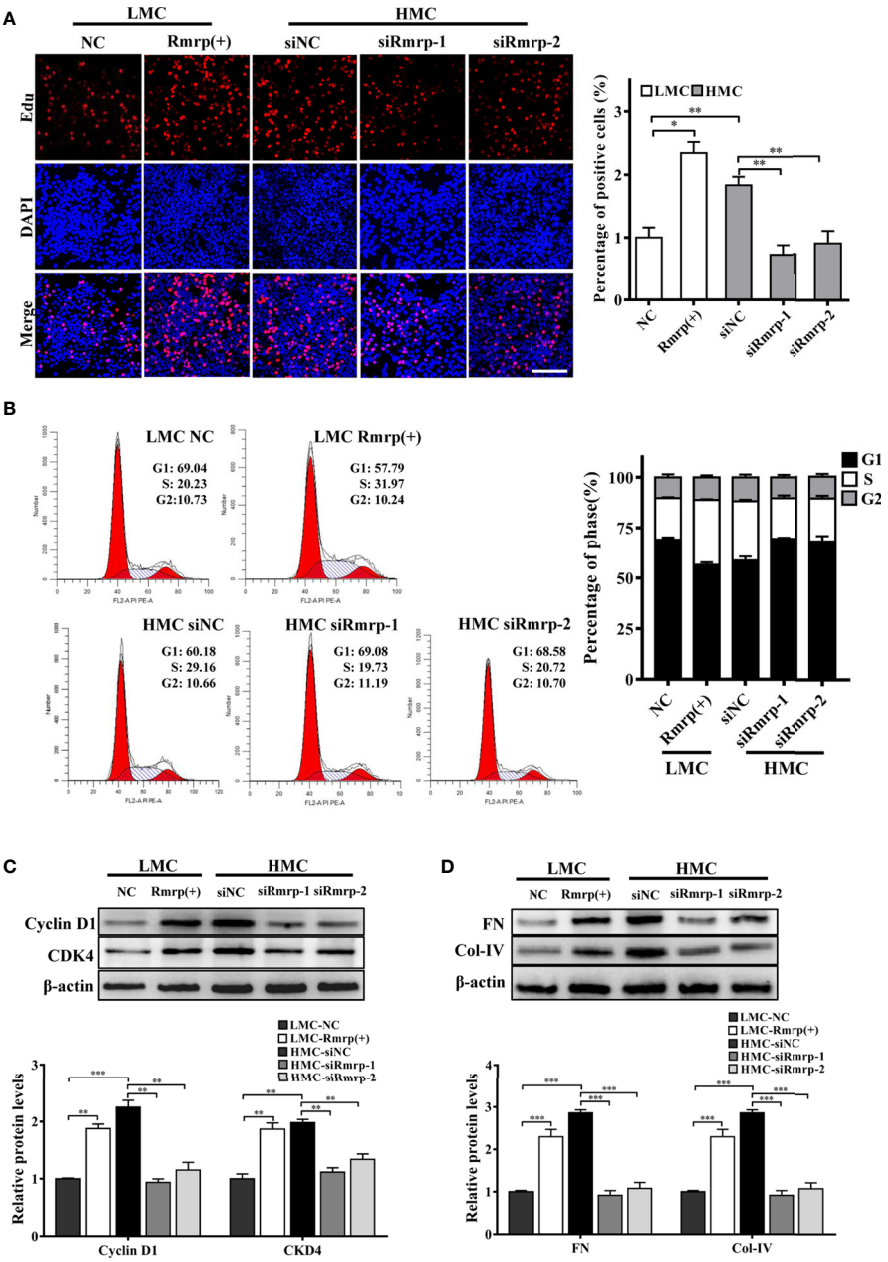

FIGURE 2 | Rmrp regulated cell proliferation and fibrosis in MC. **(A)** cells proliferating were performed by EdU after transfection of Rmrp siRNA in HMC, or over-expression Rmrp in LMC (Scale bar, 100 μm). **(B)** Cell cycle analysis was performed using flow cytometry in MC transfected with si-Rmrp and Rmrp (+). **(C)** The expressions of cell-cycle-related proteins Cyclin D1 and Cyclin-dependent kinase 4 (CDK4) regulated by Rmrp were analyzed by western blot. **(D)** The fibrosis-related protein expression of Collagen IV (Col-IV) and Fibronectin (FN) in LMCs transfected with Rmrp (+) and in HMC transfected with siRmrp was analyzed by western blot. Data were represented as the mean ± SD of three independent experiments; $^{*}p < 0.05$, $^{**}p < 0.01$, and $^{***}p < 0.001$.

Collagen IV (Col-IV) and Fibronectin (FN) as the renal fibrosis biomarkers, were significantly enhanced after overexpression of Rmrp in LMC and were declined in HMC transfected with Rmrp siRNA (**Figure 2D**). Collectively, our results showed that high Rmrp expression drove cell proliferation and fibrosis in MCs, whereas inhibition of Rmrp alleviated cell proliferation and fibrosis.

Transcription Factor Sp1 Activated Expression of lncRNA Rmrp in MC

As a preceding study of the whole transcriptome analysis in DN mice, we find some transcription factors are abnormal expression in the progression of DN (16). The study indicates that transcription factors play an important role in lncRNA dysfunction (22). To explore the potential transcriptional regulators of Rmrp promoter in MC, the binding sites of potential transcription factors were scanned by online bioinformatics tool (http://jaspar.genereg.net). After analyzing the potential transcription factors of Rmrp promoter and the aberrant transcription factors in our previous RNA-seq data of DN mice (16), the Specificity protein 1 (Sp1) was found 8 putative binding sites on Rmrp promoter. To explore the effects of Sp1, the expression of Sp1 were evaluated in the kidney of DN mice and HMC by western blot. The results showed that Sp1 protein was significantly up-regulated in the kidney of DN mice and HMC (**Figures 3A, B**). Therefore, we hypothesized that elevated Sp1 might regulated the expression level of Rmrp in the transcription, and selected 3 binding sites with scores > 9 for further study. Sp1 expressing plasmids or siRNA were constructed respectively, and qRT-PCR showed that the expression level of Sp1 was changed accordingly (**Supplementary Figure 2**). Correspondingly, the results

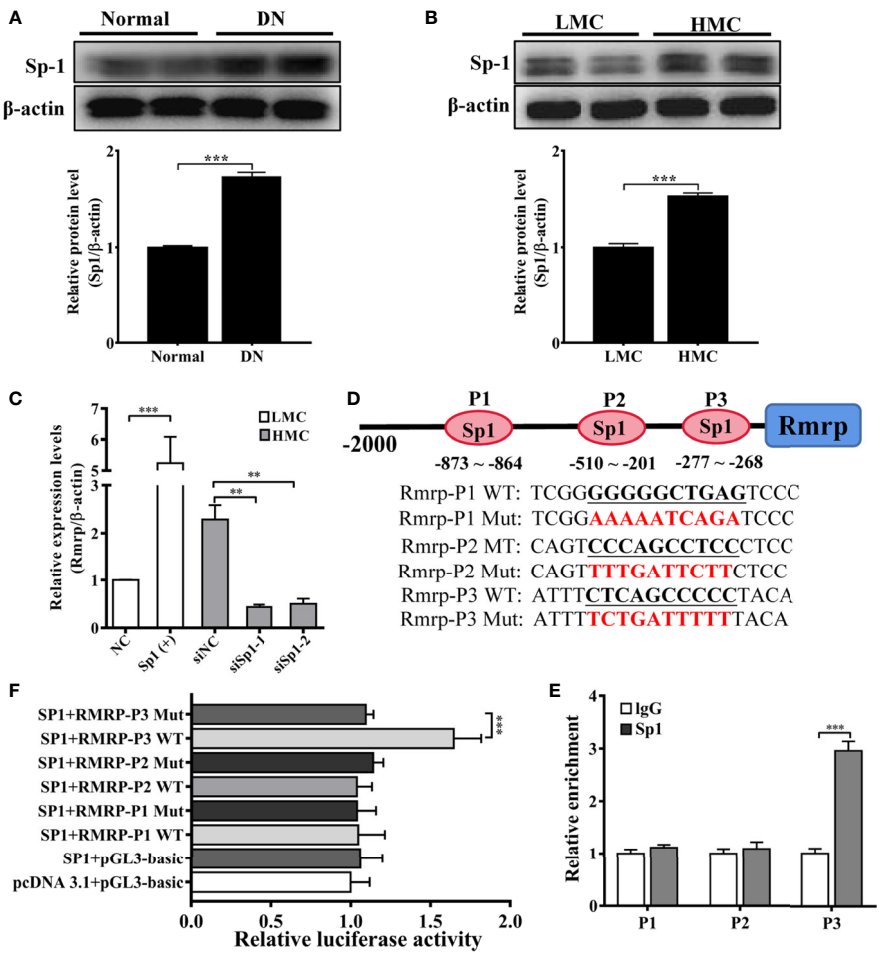

FIGURE 3 | Sp1 enhance the Rmrp expression in the transcription. **(A)** Western blot and quantitative analysis of Sp1 in the kidneys of DN mice and normal mice. **(B)** Western blot and quantitative analysis of Sp1 levels in HMC and LMC. **(C)** The expression of Rmrp was detected by qRT-PCR in HMC with transfection of Sp1 siRNA or in LMC with Sp1 overexpression plasmids. **(D)** Schematic illustration revealed the three predicted positions of SP1 and the wild type (WT) and mutant (Mut) sequences in -2000bp Rmrp promoter. **(E)** The relative luciferase activities were detected in cells co-transfected with Sp1 overexpression plasmids and luciferase reporter plasmids containing wild type or mutant Rmrp promoter sequence. **(F)** ChIP-qPCR assays were performed to determine the potential Sp1 binding site to the promoter of Rmrp in MC; IgG was used as a negative control. Data were represented as the mean ± SD of three independent experiments; $^{*}p < 0.05$, $^{**}p < 0.01$, and $^{***}p < 0.001$.

revealed that Sp1 overexpression vectors significantly increased the expression level of Rmrp in MC (**Figure 3C**), whereas the Sp1 siRNA annihilated the level of Rmrp (**Figure 3D**). Furthermore, we want to explore whether the Sp1 could bind on the potential sites to accelerate the transcription activity of Rmrp, thus the 3 binding sites of the wild type (WT) or mutant (Mut) Rmrp sequence were integrated into luciferase reporter plasmids, respectively (**Figure 3B**). The results revealed that the luciferase activity of the P3 sites but not mutant P3 sites was promoted by Sp1 in Rmrp promoter (**Figure 3E**). Similarly, the results of ChIP-qPCR further confirmed that Sp1 could bind to the P3 sites in the promoter of Rmrp (**Figure 3F**). These data demonstrated that transcription activity of Rmrp was mediated by transcription factor Sp1.

LncRNA Rmrp Acts as a Sponge for miR-1a-3p

LncRNAs can function as miRNA sponges to regulate target gene expressions. In order to explore the potential molecular mechanism of Rmrp, the miRcode database (http://mircode.org/index.php), miRanda database (http://www.microrna.org) and RNAhybrid (http://bibiserv.techfak.uni-bielefeld.de/rnahybrid) were applied for bioinformatics analysis, and the possibility of Rmrp and miRNA was determined binding site. The data suggested that miR-1a-3p and miR-206 are potential downstream targets of Rmrp. Based on the prediction, the expression of miR-1a-3p and miR-206 were evaluated in the renal tissue and MC by qRT-PCR. Strikingly, results revealed that the expression level of miR-1a-3p was decreased in the kidney of DN mice and HMC (**Figures 4A, B**). Therefore, we supposed that miR-1a-3p could be sponged by Rmrp. Next, miR-1a-3p mimics or inhibitor changed the down-regulation or up-regulation of miR-1a-3p in MC, respectively (**Figure 4C**). Correspondingly, the expression levels of Rmrp was improved or restrained with miR-1a-3p mimics or inhibitor (**Figure 4D**). In addition, miR-1a-3p was silenced after overexpression of Rmrp in LMC, and was enhanced in HMC which knock down of Rmrp (**Figure 4E**). Therefore, the expression of Rmrp and miR-1a-3p should act as a bidirectional repression.

To explore the exact binding site, the dual-luciferase reporter assays were applied to evaluate the interaction between Rmrp and miR-1a-3p. The WT or Mut Rmrp sequence which was complementary to miR-1-3p was integrated into dual luciferase reporter plasmids, respectively (**Figure 4F**). The data showed that miR-1a-3p mimics significantly suppressed the luciferase intensity of WT Rmrp sequence, but did not reduce the luciferase intensity of Mut Rmrp (**Figure 4G**). This indicates that Rmrp may directly bind to miR-1a-3p. Moreover, miRNAs could bind their target gene to regulate RNA expression through RNA-induced silencing complex (RISC) in an Ago2-dependent manner (21). To further identify the interactive binding of Rmrp with miR-1a-3p, the antibody against Ago2 was used to conduct RIP assay, and IgG as a negative control. Results revealed that both Rmrp and miR-1a-3p were abundantly pulled down by Ago2 antibody rather than IgG control (**Figure 4H**). Furthermore, FISH assay proved that miR-1a-3p was co-localized with Rmrp in the glomerulus of DN mice and in the cytoplasm of MC (**Figures 4I, J**). These data confirmed that Rmrp interacted with miR-1a-3p by directly targeting way in an Ago2-dependent manner. To summarize, Rmrp might play a sponge of miR-1a-3p in MC.

MiR-1a-3p Reverses the Effects of lncRNA Rmrp in MC

In order to prove the interaction between Rmrp and miR-1a-3p in MC, Rescue experiments were performed by co-transfecting miR-1a-3p mimic or miR-1a-3p inhibitor with Rmrp vector or si-Rmrp. The EdU assay showed that the up-regulated Rmrp increased the proliferation rate of LMC, while these effects were blocked by miR-1a-3p mimics (**Figure 5A**). Meanwhile, reduced HMC proliferation by knockdown of Rmrp was regained with miR-1a-3p inhibitors. The flow cytometry analysis displayed that the percentage of S phase was raised after overexpression of Rmrp in LMC, while these phenomenon were repressed by miR-1a-3p mimics. Although t the percentage of S phase were down-regulate by silence of Rmrp, these changes were blocked by miR-1a-3p inhibitor (**Figure 5B**). Additionally, western blot results showed that the miR-1a-3p mimics significantly reduced the expression Cyclin D1, CKD4, FN and Col-IV promotion caused by the up-regulation of Rmrp in LMC, while miR-1a-3p inhibitors could offset the inhibiting effect of siRmrp in the expression Cyclin D1, CKD4, FN and Col-IV of HMC (**Figure 5C**). Therefore, these experiments demonstrated that Rmrp regulated the proliferation and fibrosis of MC by acting as a ceRNA to sponge miR-1a-3p.

JunD Is a Direct Target of miR-1a-3p and Promotes Proliferation and Fibrosis Through Rmrp/miR-1a-3p/JunD Axis in DN

According to the TargetScan (http://www.targetscan.org/vert_72/), TarBase V.8 (http://carolina.imis.athena-innovation.gr/diana_tools/web/index.php?r=tarbasev8%2Findex), and our previous RNA-seq data of DN mice (16), Jun D proto-oncogene (JunD) contains conserved target sites of miR-1a-3p. As known, JunD plays a crucial regulator of cell proliferation (23) and fibrogenesis (23) in the progression of disease. Therefore, the qRT-PCR and western blot analysis exhibited that miR-1a-3p inhibitor could enhanced the RNA and protein level of JunD in LMC, while miR-1a-3p mimics significantly reduce the RNA and protein level of JunD in HMC (**Figures 6A, B**). Next, we constructed dual-luciferase reporter plasmids embedding the wild and mutant JunD 3' -untranslated regions (UTRs), respectively (**Figure 6C**). Using dual-luciferase assay, miR-1a-3p mimics strongly reduced the fluorescent intensity of JunD 3'-UTR WT luciferase reporter but not that of mutants (**Figure 6D**). Interestingly, we found that the fluorescent activity of JunD 3'-UTR WT reporter plasmids was not influenced by miR-1a-3p mimics in MC when Rmrp was up-regulated. These data suggest that miR-1a-3p directly regulated the expression of JunD.

To clarify whether the effect of Rmrp on proliferation and fibrosis was the interaction with JunD, the JunD expression was detected by evaluated with immunohistochemistry (IHC) and

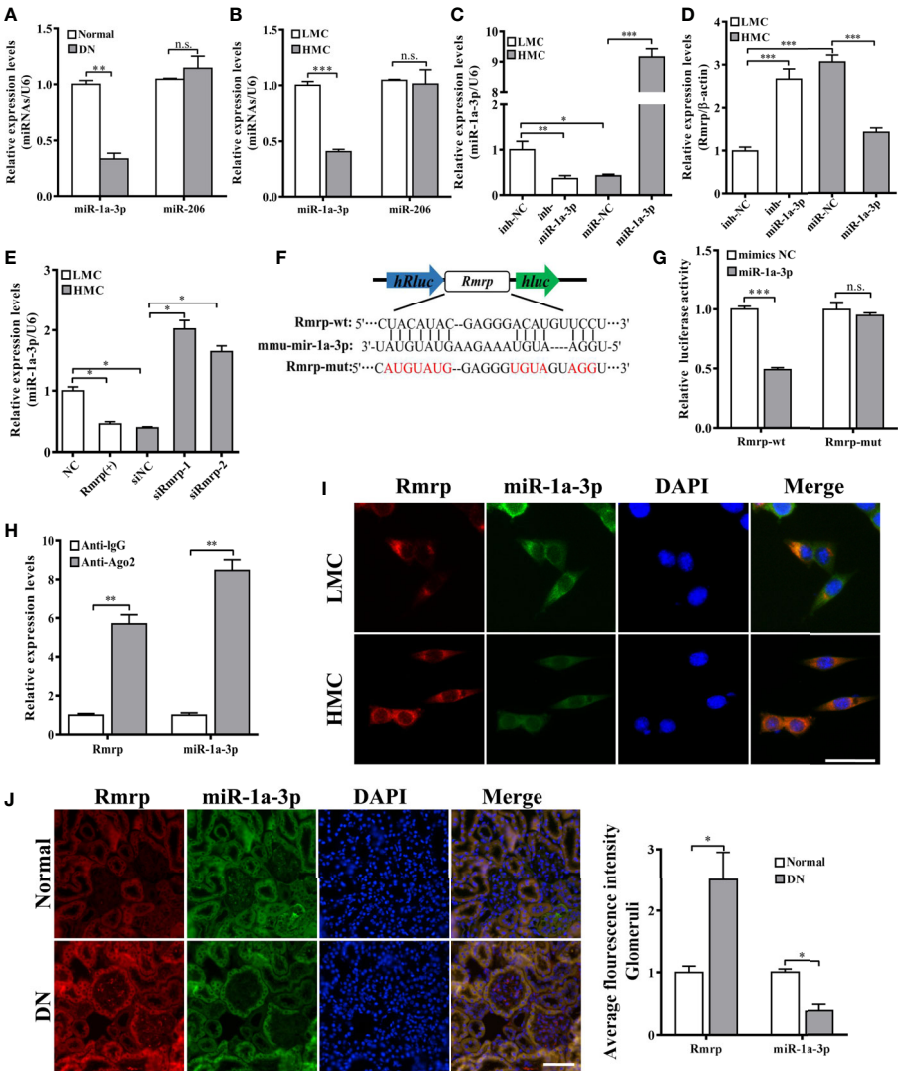

FIGURE 4 | Rmrp functioned as a ceRNA by sponging miR-1a-3p. **(A)** The expression of miR-1a-3p and miR-206 were detected by qRT-PCR in the renal tissues of db/db DN mice and normal mice (n = 5/group). **(B)** The expression of miR-1a-3p and miR-206 were detected by qRT-PCR in LMC and HMC. **(C)** The expression levels of miR-1a-3p were detected by qRT-PCR after transfection with miR-1a-3p mimics and inhibitor in MCs. **(D)** The expression of Rmrp regulated by miR-1a-3p mimics and inhibitor were detected by qRT-PCR. **(E)** The expression of miR-1a-3p were detected in LMCs transfected with Rmrp (+) and in HMC transfected with siRmrp. **(F)** Schematic illustration revealed the base complementation of miR-1a-3p with Rmrp and mutant (Mut) sequences. **(G)** Luciferase assay was used to test relative luciferase activities of Rmrp in MC co-transfected with the indicated miR-1a-3p or control vector. **(H)** Anti-AGO2 RIP was performed in HMC and the RNA levels of Rmrp and miR-1a-3p were determined by qRT-PCR. **(I)** The co-localization of Rmrp and miR-1a-3p was observed in LMC and HMC (Scale bar, 50 μm) by FISH assay. **(J)** The co-localization of Rmrp and miR-1a-3p was observed in the renal tissues of db/db DN mice and normal mice by FISH assay and quantitative analysis (Scale bar, 50 μm). Data were represented as the mean ± SD of three independent experiments; $^{*}p < 0.05$, $^{**}p < 0.01$, and $^{***}p < 0.001$. ns, no significant.

western blot in DN mice. The results revealed JunD was increased in the kidney of DN mice compared with matched the normal tissues (**Figures 6E, F**). Meanwhile, the qRT-PCR data showed that the enhancive effect of Rmrp overexpression on JunD mRNA level was rescued by miR-1a-3p mimics. The results showed that Rmrp and miR-1a-3p could be working together to regulate the expression of JunD (**Figures 6G**). Additionally, we designed three JunD siRNAs (siJunD-1, siJunD-2, and siJunD-3). The qRT-PCR and results showed the knockdown effect of siJunD-1 was the best in HMC (**Supplementary Figure 3**). Thus, siJunD-1 was selected for further study. Next, the EdU assay revealed that overexpression of Rmrp was beneficial to MC proliferation, while these effects were suppressed by JunD siRNA (**Figure 6H**). Similarly, the results of Western blot showed that overexpression of Rmrp increased the expression Cyclin D1, CKD4, FN and Col-IV, whereas knockdown of JunD could abolish the effects, respectively (**Figure 6I**). These results indicated that Rmrp can act as a sponge for miR-1a-3p by regulating JunD, thereby promoting proliferation and fibrosis in MC. As shown in **Figure 6J**, we found that Rmrp was

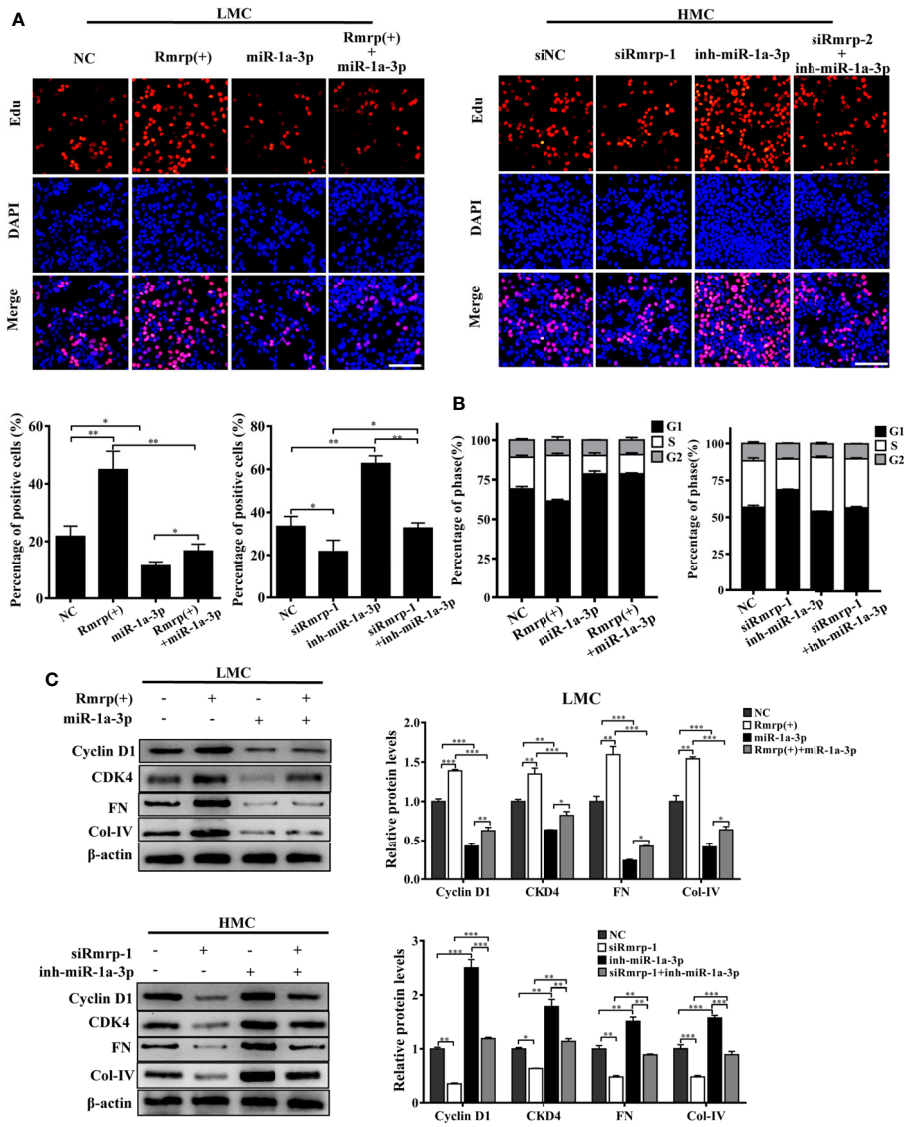

FIGURE 5 | miR-1a-3p reversed the proliferation and fibrosis of MC induced by Rmrp. **(A, B)** The cells proliferating and cell cycle analysis were performed to detect the competition effects of Rpph1 and miR-1a-3p by EdU(Scale bar, 100 μm) and flow cytometry, respectively. **(C)** The expressions level of Cyclin D1, CKD4, Col-IV and FN was analyzed after regulation the level of Rmrp, miR-1a-3p or both of them by western blot. Data were represented as the mean ± SD of three independent experiments; $^{*}p < 0.05$, $^{**}p < 0.01$, and $^{***}p < 0.001$.

significantly upregulated by Sp1 and Rmrp functioned as amiR-1a-3p sponge to positively regulate JunD expression, thereby leading to mesangial cell proliferation and fibrosis in DN.

DISCUSSION

It is well known that MC organizes the extracellular matrix production and degradation to regulate glomerular structure and function in DN (24). However, the complex mechanisms of MC activation and the underlying effects have yet to be explored in DN. In recent years, more and more evidence has demonstrated that the abnormal lncRNAs could participate in the expression and/or function of genes, and modulate the progression of DN. However, the potential roles of lncRNAs in the progression of DN are still unknown.

It was previously shown RMRP was important for mitochondrial DNA replication as the RNA primer and essential for enzymatic activity (25), but how Rmrp work in the cross regulation between nucleus and mitochondria remain largely unclear. Interestingly, in the generation of human disease, Rmrp was initially identified to be essential for cartilage-hair hypoplasia (26). Since RMRP was translocated to the cytoplasm for mitochondrial RNA processing activity (27), it was reported that the elevation in the expression of RMRP could promote the progression of diseases, such as lung Cancer (28), atherosclerosis

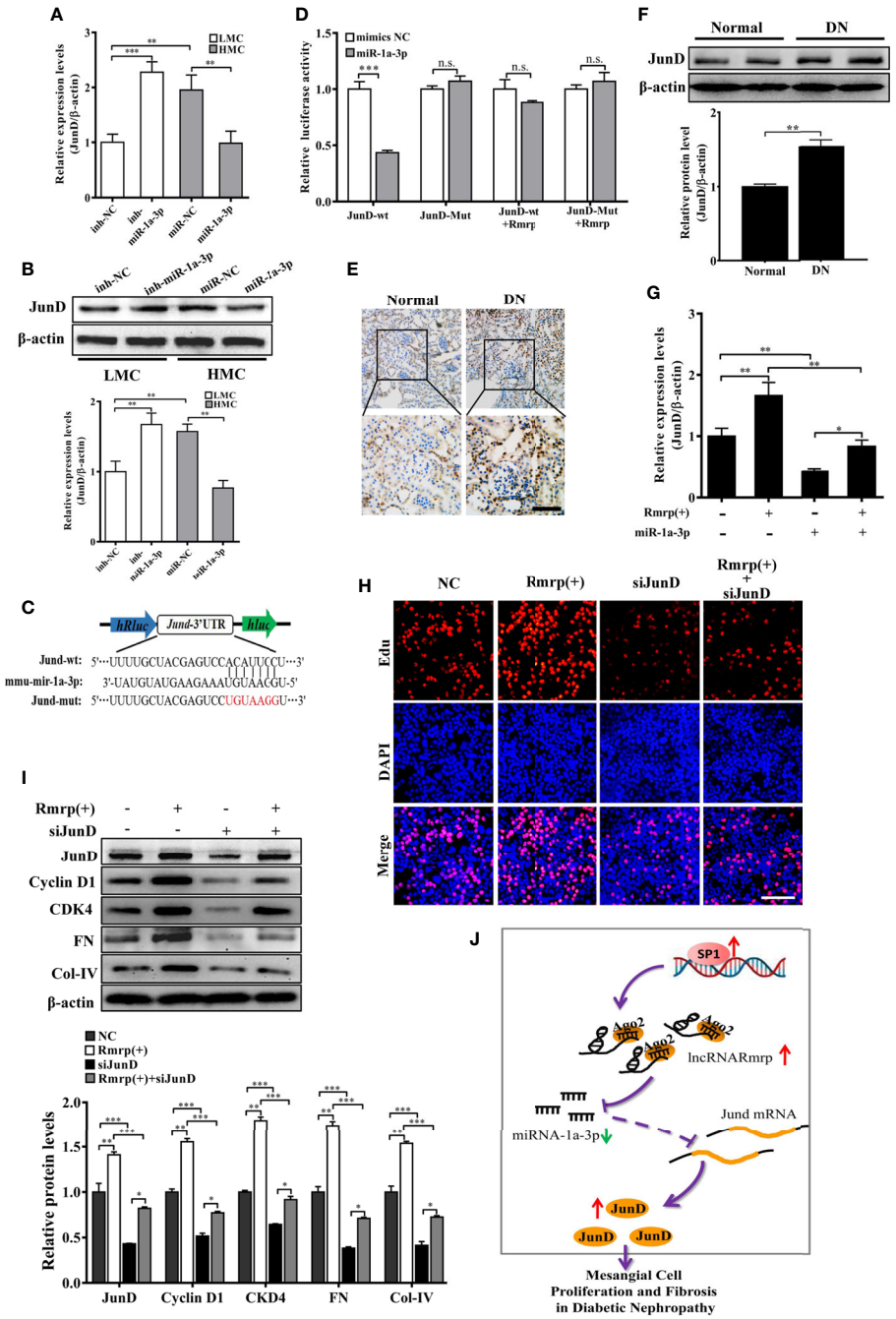

FIGURE 6 | Rmrp regulated the proliferation and fibrosis of MC *via* miR-1a-3p/JunD signaling. **(A, B)** The relative expression of JunD was detected after transfection with miR-1a-3p mimics and inhibitor by qRT-PCR and western blot. **(C)** The schematic model revealed the JunD 3' -UTR wide type (WT) and mutant (Mut) luciferase reporter vectors. **(D)** The luciferase reporter assays showed that miR-1a-3p directly inhibited the luciferase activity of JunD 3' -UTR WT, but lost efficacy when the Rmrp was up-regulated. **(E, F)** IHC analysis and western blot assessed JunD expression in the renal tissues of DN and normal mice (Scale bar, 50 μm). **(G)** The relative expression of JunD in MC after transfection with Rmrp expression vector or/and miR-1a-3p mimics by qRT-PCR. **(H)** The cells proliferating were performed to detect the competition effects of Rmrp and JunD siRNA by EdU (Scale bar, 50 μm). **(I)** The protein expression of JunD, Cyclin D1, CKD4, Col-IV and FN was analyzed after regulation the level of Rmrp expression vector, JunD siRNA or both of them by western blot. **(J)** The schematic diagram illustrates the mechanism of Rmrp mediated by Sp1 to mesangial cell proliferation and fibrosis through Rmrp/miR-1a-3p/JunD axis in DN. Data were represented as the mean ± SD of three independent experiments; $^{*}p < 0.05$, $^{**}p < 0.01$, and $^{***}p < 0.001$. ns, no significant.

(29) and coronary heart disease (30). Moreover, the functions of RMRP activated the abundant signaling pathways, which included PI3K/AKT/mTOR (30), NF-κB (31), TACR1/Erk1/2 (32) and other. It was suggested RMRP should play an important role/part in the distinct mechanisms of tumor and other diseases. By using high-throughput RNA-seq, we had found the up-regulated expression of lncRNAs Rmrp in the kidney of DN mice (16, 17). Nevertheless, the function of abnormal RMRP in the progression of DN is poorly known. In this report, we demonstrated that the lncRNA RMRP was significantly upregulated in the renal tissues of DN mice and in high glucose-induced MC damage *in vitro*. Rmrp promoted the proliferation of MC as well as the expression of CKD4 and Cyclin D1, and also fortified the overproduction of Collagen IV and Fibronectin, which were both critical for ECM components. Inhibition of Rmrp significantly reversed these above impacts, implying that the Rmrp could contribute to the progression of DN.

To further explore the regulatory mechanism of the abnormal Rmrp expression in DN, we focused on transcription factors which were contributed to lncRNAs dysregulation. By bioinformatics analyses, Sp1 was found to possess potential binding sites in the Rmrp promoter. Sp1 is one such ubiquitous and multifunctional transcription factor from the Sp/Kruppel-like family (KLF) (33), and interact with GC-rich motifs of promoter regions to execute transcriptional activation function. Sp1 was involved in the dysregulation of multiple lncRNAs. For instance, Chen et al. reported that lncRNA ZFAS1 expression was increased in colorectal cancer and was activated by Sp1 (34). Our result supported that the expression level of Sp1 had been activated by glucose and in the DN. Subsequently, the overexpression of Sp1 increased the level of Rmrp and Sp1 siRNA inhibited the expression of Rmrp. Furthermore, we used bioinformatics assay, Luciferase reporter assays and ChIP assay to confirm that Sp1 could bind to the Rmrp promoter region. These data clearly verified that Rmrp was transcriptionally activated by Sp1 in the progression of DN.

Accumulating data indicates that lncRNAs are emerging as important regulators in gene expression networks by regulate mRNA stability *via* associated miRNAs (35). LncRNAs perform ceRNAs function as miRNA sponges to derepressing miRNA target gene binding (36). For example, it was reported that LINC01619 was downregulated in human DN renal biopsy tissues, and exerted its biological function by binding to miR-27a to act the FOXO1-mediated ER stress and podocyte injury in DN (37). In addition, RMRP might promote cell proliferation, migration, and invasion in non-small-cell lung cancer *via* sponging miR-1a-3p (38). To explore the mechanism of Rmrp in DN, the target miRNAs were analyzed by online databases and qRT-PCR assay. The results revealed that miR-1a-3p was the opposite expression compared with Rmrp expression in DN and there was a bidirectional repression between miR-1a-3p and Rmrp. FISH assay indicated co-localization of Rmrp and miR-1a-3p in the sub cellular level of MC. Furthermore, the direct relationship between Rmrp and miR-1a-3p was further identified by Dual-luciferase reporter assay and RIP assay. It is well known that a single lncRNA can bind on multiple miRNAs to regulate gene expression. Whether Rmrp sponges other miRNAs involved in DN still needs to be explored. Here, in the present study, the results showed that Rmrp should function interact with miR-1a-3p by both directly targeting and Ago2-dependent ways in DN.

Based on the ceRNA hypothesis, miRNAs exert their function by blocking the translation of target genes or inducing mRNA degradation (39). MiR-1a-3pa-5p have been reported be decreased levels as a tumor suppressor and suppresses tumor progression in colorectal cancer (40), glioblastoma (41) and lung cancer (42). In diabetic complications, only a few studies have been reported miR-1a-3p is downregulated in retinal and renal tissues of STZ-induced diabetic mice (43). However, detailed mechanisms in the regulatory process of miR-1a-3p need further elucidation. In this study, we foundmiR-1a-3p was also downregulated in DN mice and glucose-induced MC, and loss of miR-1a-3p in mouse MC improved cell proliferation and fibrosis. Moreover, bioinformatics analysis showed that JunD is a latent target of miR-1a-3p. Subsequently, we confirmed that miR-1a-3p might directly bind to the 3' -UTR JunD by dual-luciferase assay. Besides, JunD could be modulated by the miR-1a-3p mimics and inhibitor at the mRNA and protein levels. Other studies reported JunD expression was increased in hearts from diet-induced obese mice, and regulated PPARc signaling leading to cardiac damage (44). miR-548d-3p directly targets JunD and loss of miR-548d-3p enhances JunD/RSK3 signaling in the chemotherapy resistant of breast cancer (45). JunD as a member of the transcription factors Activated Protein-1 (AP-1) family, is essential as a major gatekeeper in cell proliferation and fibrogenesis. Studies showed that JunD as a transcription factor could bind to the TRE site of Cyclin D1 promoter to influence Cyclin D1 transcription (46). Meanwhile, JunD could up-regulate the expression of CDK4 through inducing c-MYC (23). In other studies, the data demonstrated that JunD is implicated in the transcriptional regulation of fibrosis (47) and JunD is a mediator of the profibrotic effects of TGF-β (48). The detailed mechanisms in the regulatory process need further elucidation. Herein, our results showed JunD was up-regulated in DN mice and glucose-induced MC. At the same time, we revealed that the upregulation of JunD mRNA and protein could be regulated by overexpression of Rmrp. Subsequently, Rmrp-induced proliferation and fibrogenesis were reversed by co-transfection with JunD siRNA. In sum, our results further suggested that Rmrp serves as a ceRNA formiR-1a-3p to enhance JunD expression and activate proliferation and fibrogenesis in DN through miR-1a-3p/JunD axis.

In summary, Rmrp expression was found to be increased in DN and high glucose induced-MC, and the abnormal re-activation of Rmrp was mediated by transcription factor SP1.Furthermore, we found that Rmrp might sponge miR-1a-3p to release JunD expression and activate cell proliferation and fibrosis during DN. Finally, we hoped that these data would provide a new glimpse of the underlying mechanism and a new prospective therapeutic target for DN.

DATA AVAILABILITY STATEMENT

The original contributions presented in the study are included in the article/**Supplementary Material**. Further inquiries can be directed to the corresponding author.

ETHICS STATEMENT

The animal study was reviewed and approved by the Ethics Committee of Chongqing Medical University.

AUTHOR CONTRIBUTIONS

YS designed the research and supervised the project. HY and JW executed all experiments. HSY and ZZ performed statistical analysis of data. RP was responsible for bioinformatics analysis. DL and HL provided support experimental technical support. YS and ZZ wrote the manuscript. All authors contributed to the article and approved the submitted version.

FUNDING

This study was supported by the National Natural Science Foundation of China (No. 81700639, 81770811 and 81970702); the Top-notch Talents Program for graduate students of Chongqing Medical University (BJRC201916 and BJRC201919).

SUPPLEMENTARY MATERIAL

The Supplementary Material for this article can be found online at: https://www.frontiersin.org/articles/10.3389/fendo.2021.690784/full#supplementary-material

REFERENCES

1. Akhtar M, Taha NM, Nauman A, Mujeeb IB, Al-Nabet ADMH. Diabetic Kidney Disease: Past and Present. *Adv Anat Pathol* (2020) 27(2):87–97. doi: 10.1097/Pap.0000000000000257
2. Zheng Y, Ley SH, Hu FB. Global Aetiology and Epidemiology of Type 2 Diabetes Mellitus and Its Complications. *Nat Rev Endocrinol* (2018) 14(2):88–98. doi: 10.1038/nrendo.2017.151
3. Anders HJ, Huber TB, Isermann B, Schiffer M. CKD in Diabetes: Diabetic Kidney Disease *Versus* Nondiabetic Kidney Disease. *Nat Rev Nephrol* (2018) 14(6):361–77. doi: 10.1038/s41581-018-0001-y
4. Zhao H, Ma SX, Shang YQ, Zhang HQ, Su W. microRNAs in Chronic Kidney Disease. *Clinica Chimica Acta; Int J Clin Chem* (2019) 491:59–65. doi: 10.1016/j.cca.2019.01.008
5. de Zeeuw D. The Future of Diabetic Kidney Disease Management: Reducing the Unmet Need. *J Nephrol* (2020) 33(6):1163–9. doi: 10.1007/s40620-020-00820-2
6. Goodall GJ, Wickramasinghe VO. RNA in Cancer. *Nat Rev Cancer* (2020) 21(1):22–36. doi: 10.1038/s41568-020-00306-0
7. Marchese FP, Raimondi I, Huarte M. The Multidimensional Mechanisms of Long Noncoding RNA Function. *Genome Biol* (2017) 18(1):206. doi: 10.1186/s13059-017-1348-2
8. Zhang YY, Tang PM, Tang PC, Xiao J, Huang XR, Yu C, et al. LRNA9884, a Novel Smad3-Dependent Long Noncoding RNA, Promotes Diabetic Kidney Injury in Db/Db Mice *via* Enhancing MCP-1-Dependent Renal Inflammation. *Diabetes* (2019) 68(7):1485–98. doi: 10.2337/db18-1075
9. Kato M, Wang M, Chen Z, Bhatt K, Oh HJ, Lanting L, et al. An Endoplasmic Reticulum Stress-Regulated lncRNA Hosting a microRNA Megacluster Induces Early Features of Diabetic Nephropathy. *Nat Commun* (2016) 7:12864. doi: 10.1038/ncomms12864
10. Zhang Y, Sun X, Icli B, Feinberg MW. Emerging Roles for MicroRNAs in Diabetic Microvascular Disease: Novel Targets for Therapy. *Endocrine Rev* (2017) 38(2):145–68. doi: 10.1210/er.2016-1122
11. Slack FJ, Chinnaiyan AM. The Role of Non-Coding RNAs in Oncology. *Cell* (2019) 179(5):1033–55. doi: 10.1016/j.cell.2019.10.017
12. Tay Y, Rinn J, Pandolfi PP. The Multilayered Complexity of ceRNA Crosstalk and Competition. *Nature* (2014) 505(7483):344–52. doi: 10.1038/nature12986
13. Lv J, Wu Y, Mai Y, Bu S. Noncoding RNAs in Diabetic Nephropathy: Pathogenesis, Biomarkers, and Therapy. *J Diabetes Res* (2020) 2020:3960857. doi: 10.1155/2020/3960857
14. Gao J, Wang W, Wang F, Guo C. LncRNA-NR_033515 Promotes Proliferation, Fibrogenesis and Epithelial-to-Mesenchymal Transition by Targeting miR-743b-5p in Diabetic Nephropathy. *BioMed Pharmacother* (2018) 106:543–52. doi: 10.1016/j.biopha.2018.06.104
15. Chen W, Peng R, Sun Y, Liu H, Zhang L, Peng H, et al. The Topological Key lncRNA H2k2 From the ceRNA Network Promotes Mesangial Cell Proliferation in Diabetic Nephropathy *via* the miR-449a/B/Trim11/Mek Signaling Pathway. *FASEB J* (2019) 33(10):11492–506. doi: 10.1096/fj.201900522R
16. Wen L, Zhang Z, Peng R, Zhang L, Liu H, Peng H, et al. Whole Transcriptome Analysis of Diabetic Nephropathy in the Db/Db Mouse Model of Type 2 Diabetes. *J Cell Biochem* (2019) 120(10):17520–33. doi: 10.1002/jcb.29016
17. Zhang P, Sun Y, Peng R, Chen W, Fu X, Zhang L, et al. Long non-Coding RNA Rpph1 Promotes Inflammation and Proliferation of Mesangial Cells in Diabetic Nephropathy *via* an Interaction With Gal-3. *Cell Death Dis* (2019) 10(7):526. doi: 10.1038/s41419-019-1765-0
18. Park J, Jeong S. Wnt Activated Beta-Catenin and YAP Proteins Enhance the Expression of Non-Coding RNA Component of RNase MRP in Colon Cancer Cells. *Oncotarget* (2015) 6(33):34658–68. doi: 10.18632/oncotarget.5778
19. Hsieh CL, Donlon TA, Darras BT, Chang DD, Topper JN, Clayton DA, et al. The Gene for the RNA Component of the Mitochondrial RNA-Processing Endoribonuclease Is Located on Human Chromosome 9p and on Mouse Chromosome 4. *Genomics* (1990) 6(3):540–4. doi: 10.1016/0888-7543(90)90483-b
20. Sun Y, Peng R, Peng H, Liu H, Wen L, Wu T, et al. miR-451 Suppresses the NF-KappaB-Mediated Proinflammatory Molecules Expression Through Inhibiting LMP7 in Diabetic Nephropathy. *Mol Cell Endocrinol* (2016) 433:75–86. doi: 10.1016/j.mce.2016.06.004
21. Li A, Peng R, Sun Y, Liu H, Peng H, Zhang Z. LincRNA 1700020I14Rik Alleviates Cell Proliferation and Fibrosis in Diabetic Nephropathy *via* miR-34a-5p/Sirt1/HIF-1alpha Signaling. *Cell Death Dis* (2018) 9(5):461. doi: 10.1038/s41419-018-0527-8
22. Wang H, Huo X, Yang XR, He J, Cheng L, Wang N, et al. STAT3-Mediated Upregulation of lncRNA HOXD-AS1 as a ceRNA Facilitates Liver Cancer Metastasis by Regulating SOX4. *Mol Cancer* (2017) 16(1):136. doi: 10.1186/s12943-017-0680-1
23. Elliott B, Millena AC, Matyunina L, Zhang M, Zou J, Wang G, et al. Essential Role of JunD in Cell Proliferation Is Mediated *via* MYC Signaling in Prostate Cancer Cells. *Cancer Lett* (2019) 448:155–67. doi: 10.1016/j.canlet.2019.02.005
24. Beck KF, Pfeilschifter J. Gasotransmitter Synthesis and Signalling in the Renal Glomerulus. Implications for Glomerular Diseases. *Cell Signal* (2020) 77:109823. doi: 10.1016/j.cellsig.2020.109823
25. Dong YR, Yoshitomi T, Hu JF, Cui JZ. Long Noncoding RNAs Coordinate Functions Between Mitochondria and the Nucleus. *Epigenet Chromatin* (2017) 10(1):41. doi: 10.1186/s13072-017-0149-x
26. Ridanpaa M, van Eenennaam H, Pelin K, Chadwick R, Johnson C, Yuan B, et al. Mutations in the RNA Component of RNase MRP Cause a Pleiotropic Human Disease, Cartilage-Hair Hypoplasia. *Cell* (2001) 104(2):195–203. doi: 10.1016/s0092-8674(01)00205-7

27. Mattijssen S, Welting TJ, Pruijn GJ. RNase MRP and Disease. *Wiley Interdiscip Rev RNA* (2010) 1(1):102–16. doi: 10.1002/wrna.9
28. Yang M, Ke H, Zhou W. LncRNA RMRP Promotes Cell Proliferation and Invasion Through miR-613/NFAT5 Axis in Non-Small Cell Lung Cancer. *OncoTargets Ther* (2020) 13:8941–50. doi: 10.2147/OTT.S255126
29. An JH, Chen ZY, Ma QL, Li YB, Shi FW. Liraglutide Improves Atherosclerosis by Regulating Long Non-Coding RNA RMRP/miR-128-1-5p/Gadd45g Axis. *Eur Rev Med Pharmacol Sci* (2020) 24(5):2725–37. doi: 10.26355/eurrev_202003_20545
30. Kong F, Jin J, Lv X, Han Y, Liang X, Gao Y, et al. Long Noncoding RNA RMRP Upregulation Aggravates Myocardial Ischemia-Reperfusion Injury by Sponging miR-206 to Target ATG3 Expression. *BioMed Pharmacother* (2019) 109:716–25. doi: 10.1016/j.biopha.2018.10.079
31. Han Y, Cai YX, Lai XQ, Wang ZL, Wei SQ, Tan K, et al. lncRNA RMRP Prevents Mitochondrial Dysfunction and Cardiomyocyte Apoptosis *via* the miR-1-5p/Hsp70 Axis in LPS-Induced Sepsis Mice. *Inflammation* (2020) 43 (2):605–18. doi: 10.1007/s10753-019-01141-8
32. Zhao HF, Ju AD, Sun LW, Bi MP, Yang XW, Li MY, et al. lncRNA RMRP Knockdown Suppress Hepatocellular Carcinoma Biological Activities *via* Regulation miRNA-206/Tacr1. *J Cell Biochem* (2019) 121(2):1690–702. doi: 10.1002/jcb.29404
33. Briggs MR, Kadonaga JT, Bell SP, Tjian R. Purification and Biochemical Characterization of the Promoter-Specific Transcription Factor, Sp1. *Science* (1986) 234(4772):47–52. doi: 10.1126/science.3529394
34. Chen XX, Zeng KX, Xu M, Hu XX, Lui XX, Xu T, et al. SP1-Induced lncRNA-ZFAS1 Contributes to Colorectal Cancer Progression *via* the miR-150-5p/VEGFA Axis. *Cell Death Dis* (2018) 9(10):982. doi: 10.1038/S41419-018-0962-6
35. Yao RW, Wang Y, Chen LL. Cellular Functions of Long Noncoding RNAs. *Nat Cell Biol* (2019) 21(5):542–51. doi: 10.1038/s41556-019-0311-8
36. Kopp F, Mendell JT. Functional Classification and Experimental Dissection of Long Noncoding RNAs. *Cell* (2018) 172(3):393–407. doi: 10.1016/j.cell.2018.01.011
37. Bai XY, Geng J, Li X, Wan J, Liu JX, Zhou ZM, et al. Long Noncoding RNA LINC01619 Regulates MicroRNA-27a/Forkhead Box Protein O1 and Endoplasmic Reticulum Stress-Mediated Podocyte Injury in Diabetic Nephropathy. *Antioxid Redox Sign* (2018) 29(4):355–76. doi: 10.1089/ars.2017.7278
38. Wang Y, Luo XG, Liu Y, Han GY, Sun DP. Long Noncoding RNA RMRP Promotes Proliferation and Invasion *via* Targeting miR-1-3p in Non-Small-Cell Lung Cancer. *J Cell Biochem* (2019) 120(9):15170–81. doi: 10.1002/jcb.28779
39. Bartel DP. MicroRNAs: Target Recognition and Regulatory Functions. *Cell* (2009) 136(2):215–33. doi: 10.1016/j.cell.2009.01.002
40. Xu W, Zhang Z, Zou K, Cheng Y, Yang M, Chen H, et al. MiR-1 Suppresses Tumor Cell Proliferation in Colorectal Cancer by Inhibition of Smad3-Mediated Tumor Glycolysis. *Cell Death Dis* (2017) 8(5):e2761. doi: 10.1038/cddis.2017.60
41. Yang CH, Wang Y, Sims M, Cai C, Pfeffer LM. MicroRNA-1 Suppresses Glioblastoma in Preclinical Models by Targeting Fibronectin. *Cancer Lett* (2019) 465:59–67. doi: 10.1016/j.canlet.2019.08.021
42. Korde A, Jin L, Zhang JG, Ramaswamy A, Hu B, Kolahian S, et al. Lung Endothelial MicroRNA-1 Regulates Tumor Growth and Angiogenesis. *Am J Respir Crit Care Med* (2017) 196(11):1443–55. doi: 10.1164/rccm.201610-2157OC
43. Feng B, Cao Y, Chen S, Ruiz M, Chakrabarti S. miRNA-1 Regulates Endothelin-1 in Diabetes. *Life Sci* (2014) 98(1):18–23. doi: 10.1016/j.lfs.2013.12.199
44. Costantino S, Akhmedov A, Melina G, Mohammed SA, Othman A, Ambrosini S, et al. Obesity-Induced Activation of JunD Promotes Myocardial Lipid Accumulation and Metabolic Cardiomyopathy. *Eur Heart J* (2019) 40(12):997–1008. doi: 10.1093/eurheartj/ehy903
45. Tai F, Gong KX, Song K, He YL, Shi J. Enhanced JunD/RSK3 Signalling Due to Loss of BRD4/FOXD3/miR-548d-3p Axis Determines BET Inhibition Resistance. *Nat Commun* (2020) 11(1):258. doi: 10.1038/s41467-019-14083-4
46. Meixner A, Karreth F, Kenner L, Penninger JM, Wagner EF. Jun and JunD-Dependent Functions in Cell Proliferation and Stress Response. *Cell Death Differentiation* (2010) 17(9):1409–19. doi: 10.1038/cdd.2010.22
47. Smart DE, Green K, Oakley F, Weitzman JB, Yaniv M, Reynolds G, et al. JunD Is a Profibrogenic Transcription Factor Regulated by Jun N-Terminal Kinase-Independent Phosphorylation. *Hepatology* (2006) 44(6):1432–40. doi: 10.1002/hep.21436
48. Palumbo K, Zerr P, Tomcik M, Vollath S, Dees C, Akhmetshina A, et al. The Transcription Factor JunD Mediates Transforming Growth Factor Beta-Induced Fibroblast Activation and Fibrosis in Systemic Sclerosis. *Ann Rheumatic Dis* (2011) 70(7):1320–6. doi: 10.1136/ard.2010.148296

Conflict of Interest: The authors declare that the research was conducted in the absence of any commercial or financial relationships that could be construed as a potential conflict of interest.

frontiers in Endocrinology

ORIGINAL RESEARCH
published: 14 January 2022
doi: 10.3389/fendo.2021.797025

PFKP Activation Ameliorates Foot Process Fusion in Podocytes in Diabetic Kidney Disease

Zongwei Zhang[1,2†], Wei Liang[1,2†], Qiang Luo[1,2], Hongtu Hu[1,2], Keju Yang[1,2,3], Jijia Hu[1,2], Zhaowei Chen[1,2], Jili Zhu[1,2], Jun Feng[1,2], Zijing Zhu[1,2], Qingjia Chi[4] and Guohua Ding[1,2*]*

[1] Division of Nephrology, Renmin Hospital of Wuhan University, Wuhan, China, [2] Nephrology and Urology Research Institute of Wuhan University, Wuhan, China, [3] The First College of Clinical Medical Science, China Three Gorges University, Yichang, China, [4] Department of Mechanics and Engineering Structure, Wuhan University of Technology, Wuhan, China

OPEN ACCESS

Edited by:
Jehad Ahmed Abubaker,
Dasman Diabetes Institute, Kuwait

Reviewed by:
Petra Simic,
Massachusetts Institute of Technology, United States
Xiao Cui,
Tianjin Medical University, China
Baocheng Chang,
Tianjin Medical University, China

***Correspondence:**
Wei Liang
dr.liangwei@whu.edu.cn
Guohua Ding
ghxding@whu.edu.cn

[†]These authors have contributed equally to this work

Specialty section:
This article was submitted to Diabetes: Molecular Mechanisms, a section of the journal Frontiers in Endocrinology

Received: 02 November 2021
Accepted: 20 December 2021
Published: 14 January 2022

Citation:
Zhang Z, Liang W, Luo Q, Hu H, Yang K, Hu J, Chen Z, Zhu J, Feng J, Zhu Z, Chi Q and Ding G (2022) PFKP Activation Ameliorates Foot Process Fusion in Podocytes in Diabetic Kidney Disease. Front. Endocrinol. 12:797025. doi: 10.3389/fendo.2021.797025

Background: Glycolysis dysfunction is an important pathogenesis of podocyte injury in diabetic kidney disease (DKD). Foot process fusion of podocytes and increased albuminuria are markers of early DKD. Moreover, cytoskeletal remodeling has been found to be involved in the foot process fusion of podocytes. However, the connections between cytoskeletal remodeling and alterations of glycolysis in podocytes in DKD have not been clarified.

Methods: mRNA sequencing of glomeruli obtained from db/db and db/m mice with albuminuria was performed to analyze the expression profiling of genes in glucose metabolism. Expressions of phosphofructokinase platelet type (PFKP) in the glomeruli of DKD patients were detected. Clotrimazole (CTZ) was used to explore the renal effects of PFKP inhibition in diabetic mice. Using *Pfkp* siRNA or recombinant plasmid to manipulate PFKP expression, the effects of PFKP on high glucose (HG) induced podocyte damage were assessed *in vitro*. The levels of fructose-1,6-bisphosphate (FBP) were measured. Targeted metabolomics was performed to observe the alterations of the metabolites in glucose metabolism after HG stimulation. Furthermore, aldolase type b *(Aldob)* siRNA or recombinant plasmid were applied to evaluate the influence of FBP level alteration on podocytes. FBP was directly added to podocyte culture media. Db/db mice were treated with FBP to investigate its effects on their kidney.

Results: mRNA sequencing showed that glycolysis enzyme genes were altered, characterized by upregulation of upstream genes (*Hk1, and Pfkp*) and down-regulation of downstream genes of glycolysis (*Pkm, and Ldha*). Moreover, the expression of PFKP was increased in glomeruli of DKD patients. The CTZ group presented more severe renal damage. *In vitro*, the *Pfkp* siRNA group and ALDOB overexpression group showed much more induced cytoskeletal remodeling in podocytes, while overexpression of PFKP and suppression of ALDOB *in vitro* rescued podocytes from cytoskeletal remodeling through regulation of FBP levels and inhibition of the RhoA/ROCK1 pathway. Furthermore, targeted metabolomics showed FBP level was significantly increased in HG group

compared with the control group. Exogenous FBP addition reduced podocyte cytoskeletal remodeling and renal damage of db/db mice.

Conclusions: These findings provide evidence that PFKP may be a potential target for podocyte injury in DN and provide a rationale for applying podocyte glycolysis enhancing agents in patients with DKD.

Keywords: PFKP, diabetic kidney diseases, glycolysis, podocyte injury, cytoskeletal remodeling, FBP

INTRODUCTION

Diabetic kidney disease (DKD) is one of the most common and severe microvascular complications of diabetes. It is the leading risk factor for progression to end-stage renal disease (ESRD) in patients with renal failure. DKD is the primary cause of death in people with diabetes. A total of 3-40% of patients with type 1 diabetes (T1DM) or type 2 diabetes (T2DM) develop DKD, accounting for 30-47% of ESRD (1, 2). However, existing treatments for DKD are extremely limited once proteinuria occurs at the early stage (3). Thus, the identification of treatment targets for DKD is urgently needed.

The presence of microalbuminuria is marked by a urinary albumin creatinine ratio (ACR) greater than 30 mg/g, and it is a marker of early renal damage in diabetic patients (4). Podocytes have a close relationship with proteinuria because they are located outside the glomerular basement membrane (GBM) (5). Hyperglycemia is the most prominent and essential feature of diabetes, and it can lead to podocyte damage through various mechanisms, including affecting podocyte metabolism and cytoskeletal structures (6).

One study suggested that both anaerobic glycolysis and aerobic glycolysis are crucial energy resources for podocytes (7). Besides, previous studies indicated that both glycolysis processes were altered in DKD (8, 9). Notably, one study determined that pyruvate kinase muscle type 2 (PKM2) deletion in podocytes accelerated DKD progression (10), proving that glycolysis plays a critical role in podocytes.

Podocytes exhibit the unique cytoskeletal architecture that is fundamentally linked to their function in maintaining the kidney filtration barrier. In addition, cytoskeletal architecture can regulate the podocyte shape, adhesion, stability, structure, slit diaphragm insertion, plasticity, and dynamic response to environmental stimulations (5). Therefore, even slight impairment of the podocyte cytoskeletal apparatus can result in foot process fusion in podocytes and proteinuria, finally leading to glomerular disease, including DKD (6, 11). Hence, it is vital to maintain the normal structure and function of the podocyte cytoskeleton.

Many glycolytic enzymes anchor to the cytoskeleton, thus, enzymes and the cytoskeleton are closely related (12). Movement of the cytoskeleton can affect the activity of glycolytic enzymes (13), and glycolytic enzymes can also affect the podocyte cytoskeleton by regulating glucose metabolism (12). However, the interactions between glycolytic enzyme and podocyte cytoskeleton have not been reported. Here, we found that the glycolytic enzyme PFKP can protect the normal cytoskeletal structure of podocytes through its catalyzed metabolite fructose-1,6-bisphosphate (FBP).

MATERIALS AND METHODS

Animal Studies

Db/db and db/m male mice (8-9 weeks, 20-40 g) were obtained (CAWENS, Changzhou, China) and housed in specific pathogen-free conditions with unrestricted access to food and water at the Center for Animal Experiments of Wuhan University. All protocols were approved by the Animal Ethics Review Board of Wuhan University and performed in accordance with the guidelines of the National Health and Medical Research Council of China (No.20200306). For the mRNA sequencing samples, db/db and db/m male mice (n=30 each) were raised from 8 weeks to 24 weeks, and kidney samples were harvested at 16 weeks and 24 weeks. The mice were randomly divided into four groups (n=6 each), db/m+0.1% DMSO (D2650, Sigma-Aldrich, USA), db/db+0.1% DMSO, db/m + Clotrimazole (CTZ) (HY-10882, MCE, China), and db/db + CTZ group. The dosage of CTZ is 100 mg/kg/day for two weeks by intraperitoneal injection in db/m + CTZ and db/db + CTZ group since 24 weeks (14). Besides, the mice were divided into another six groups randomly (n=6 each), db/m+ saline (Baxter, China), db/db+ saline, db/m + FBP (500 or 1000 mg/kg/day) (SC-214805, Santa cruz), and db/db + FBP (500 or 1000 mg/kg/day) group. The dosage of FBP is 500 or 1000 mg/kg/day for two weeks by intraperitoneal injection in db/m + FBP and db/db + FBP group beginning at 24 weeks (15, 16). 24-hour urine samples were collected in metabolic cages, and the urine ACR was measured every two weeks. The animals were sacrificed, and their kidneys were perfused with physiological saline before isolation and storage at -80°C for biochemical and renal pathological analysis.

Glomerular Isolation, mRNA Sequencing and Data Analysis

Renal cortices from 24-week-old db/m and db/db mice were minced and digested with collagenase. Glomeruli were isolated by successive sieving through 100-, 70-, and 40- μm mesh sieves. The glomeruli-rich preparation retained on the 40- μm strainer was rinsed into a cell culture dish, and then glomeruli were collected into 15ml centrifuge tubes. After centrifugation, glomeruli were collected into cryopreservation tubes and stored at -80°C. Total RNA extraction from glomeruli was

performed with Trizol reagent (Invitrogen, USA), according to the manufacturer's instructions. The RNA concentration was calculated by a NanoDrop spectrophotometer. mRNA sequencing analysis was performed by Myhalic Biotechnoligical Co., Ltd. (Wuhan, China). RNA-seq raw data and processed data were uploaded to the GEO database (GSE184836). Differentially expressed genes were determined using DESeq2 (adjusted $P < 0.05$). Heatmaps of differentially expressed genes identified in our study were generated by TBtools (17).

Targeted Metabolomics

The harvested podocytes were stored in the refrigerator at -80°C, and the samples were taken out. 1mL methanol acetonitrile aqueous solution (2:2:1, V/V) was added, followed by 60s vortex and low-temperature ultrasound for 30min, twice, at -20°C. The precipitated protein was placed for 1h, and 14000RCF was centrifuged at 4°C for 20min. The supernatant was freeze-dried, and the samples were stored at -80°C. The samples were separated by Agilent 1290 Infinity LC ULTRA performance liquid chromatography system. Mobile phase: Liquid A was 10 mM ammonium acetate aqueous solution, and liquid B was acetonitrile. The samples were placed in an automatic sampler at 4°C, the column temperature was 45°C, the flow rate was 300 μL/min, and the injection volume was 2 μL. A 5500 QTRAP mass spectrometer (AB SCIEX) was used for mass spectrometry analysis in negative ion mode. 5500 QTRAP ESI source conditions are as follows: Source Temperature 450°C, Ion Source Gas1(Gas1):45, Ion Source Gas2(Gas2):45, Curtain Gas (CUR):30, ionSapary Voltage Floating(ISVF)-4500 V; MRM mode was adopted to detect the ion pairs to be measured, and the ion pairs information of all energy metabolites was shown in **Supplementary Data Set 1**. The peak area and retention time were extracted by Multiquant software. The energy metabolite standard was used to correct the retention time and identify metabolites.

Human Renal Samples

Renal biopsy samples from patients diagnosed with DKD according to the ADA and KDOQI guideline (18, 19) (3 males and 3 females; age, 45–55 years; mean age, 49.17 ± 3.43 years) were obtained from the Division of Nephrology, Renmin Hospital of Wuhan University, Wuhan, China. The control samples (3 from males and 3 from females; age, 37–56 years; mean age, 46.17 ± 6.49 years) were para-carcinoma tissues from individuals without other renal diseases who had tumor nephrectomies, and were obtained from the Division of Pathology, Renmin Hospital of Wuhan University, Wuhan, China. The detail clinical information of these patients was shown in **Table S1**. This investigation was performed in accordance with the principles of the Declaration of Helsinki. The experiment was performed in accordance with the approved guidelines of Wuhan University and was approved by the Research Ethics Committee of Renmin Hospital of Wuhan University. Informed consent was received from the patients.

Reagents and Antibodies

NaCl solution (0.9%) was purchased from Baxter China. Anti-PFKP antibody (GTX35238, 1:100-1:1000), PKM2 (CST, 4053, 1:1,000), HK1(CST, 2024,1:800) and LDHA(Sigma Aldrich, QC52376, 1:1000) were used for Western blotting, immunofluorescence (IF) staining and immunohistochemical (IHC) staining. The primary antibodies for Western blotting against PFKM (ab154804, 1:1000), and PFKL (ab45688, 1:1000) were all from Abcam (Cambridge, MA). The primary antibodies for Western blotting against ROCK1 (21850-1-AP, 1:1000), RhoA (10749-1-AP, 1:1000), α-tubulin (11224-1-AP, 1:1000), ALDOB (18065-1-AP,1:1000), and alpha-tubulin(11224-1-AP,1:1000) were purchased from proteintech (Wuhan, China). Anti-GAPDH (sc-365062, 1:1000) was purchased from Santa Cruz (Santa Cruz, CA). DAPI and secondary antibodies against rabbit IgG-HRP(ANT020), IgG-HRP (ANT019), Alexa Fluor 488, 594 conjugated anti-mouse IgG, and anti-rabbit IgG were obtained from Antgene (Wuhan, China).

Histological and Immunohistochemistry Examination

Kidney tissues were systemically perfused with cold PBS and 4% paraformaldehyde (pH 7.4). Harvested kidneys were processed by a standard protocol for histological examination. Briefly, the tissues were embedded in paraffin, sectioned at 5 μm, stained with periodic acid-Schiff stain (PAS), and observed and photographed under a microscope (Olympus, Tokyo, Japan). For IHC staining, sections were incubated with the indicated primary antibodies. Five visual fields from individual groups were randomly selected to determine the percentage of positive staining area using ImageJ analysis software.

Cell Culture and Transfection

Conditionally immortalized human podocytes kindly provided by Dr. Moin A. Saleem (Academic Renal Unit, Southmead Hospital, Bristol, UK) were cultured under standard conditions. The medium consisted of RPMI 1640 (HyClone, USA) containing 10% heat-inactivated fetal bovine serum (FBS; Gibco, USA), 100 U/mL penicillin G, 100 μg/mL streptomycin (Invitrogen, USA) and 1× insulin-transferrin-selenium (ITS; Invitrogen, USA) at 33°C. To induce differentiation, podocytes were cultured at 37°C for 10-14 days without ITS, and differentiated podocytes were used in all experiments. Differentiated podocytes were stimulated with 30 mM high glucose (HG) for 24 h. For siRNA transfection, we performed HiPerFect transfection (Qiagen, Germany) according to the manufacturer's protocol with *Pfkp*, and *Aldob* siRNA and control siRNA (Qiagen). Briefly, cells were liberated, seeded into 6-well plates and transfected with serum-free medium containing 100 nM Pfkp siRNA or control siRNA for 6-8 hours until reaching 70% confluence, after which the cells were recovered in complete medium and 30 mM HG when necessary. The sequence of human *Pfkp* siRNA oligonucleotides in this study was 5′-GCAACGTAGCTGTCATCAA-3′. The sequence of human *Aldob* siRNA oligonucleotides in this study was 5′-CCAGAGCATTGTTGCCAAT-3′. To overexpress PFKP, transfection of the *Pfkp* plasmid (GeneChem, Wuhan, China) was conducted with X-tremeGENE HP DNA Transfection Reagent (Roche) according to the manufacturer's instructions. A density of 2×10^5 cells was first seeded into each well of a 6-well plate and then transfected with complexes containing 2 μg of Pfkp plasmid or a negative control with pcDNA3.1 and 2 μl of

the X-tremeGENE transfection reagent. Then, the cells were incubated under normal conditions for 24 h at 37°C, recovered in complete medium and stimulated with 30 mM glucose (HG) as necessary. Similarly, the *Aldob* plasmid (GeneChem, Wuhan, China) was used to overexpress ALDOB. FBP (SC-214805, Santa Cruz) was added to complete medium at 5 mM or 10 mM. Each experimental result was confirmed in three independent podocyte clones.

ATP Production

After treatment, the intracellular ATP content was assessed using a luciferase ATP detection assay kit (Beyotime, China) according to the manufacturer's protocol. Briefly, the cells were harvested and lysed. Then, the protein content of the supernatant was determined with a BCA protein kit (Beyotime, China), and the protein supernatant was mixed with ATP detection solution. Finally, the luminescence of each sample was measured by a fluorescence microplate reader.

PFK Enzymatic Activity

The enzymatic activity of PFK was determined using a kit (BC0530, Solarbio, China) according to the manufacturer's protocol. Since PFK catalyzes the conversion of fructose-6-phosphate and ATP to FBP and ADP, and Pyruvate kinase and lactate dehydrogenase further catalyze the oxidation of NADH to NAD^+, the decrease rate of NADH was measured at 340 nm to detect PFK activity and the absorbance of each sample was analyzed by a fluorescence microplate reader.

FBP Level

The level of FBP was measured using a kit (BC2240, Solarbio, China) according to the manufacturer's protocol. The reaction of fructose 1,6-diphosphate with 2,4-dinitrophenylhydrazine catalyzed by aldolase in acidic medium produces 2,4-dinitrophenylhydrazone, which is reddish brown in alkaline solution, has a characteristic absorption peak at 540 nm, and could indicate the level of FBP. A fluorescence microplate reader analyzed the absorbance of each sample.

Wound-Healing Assay

Podocytes were seeded into 12-well plates to reach 80% confluence. Then, a wound was created by scratching with a pipette tip, and the cultures were washed with PBS to remove cell debris. Cells stimulated with HG were visualized by light microscopy at 0 h, 24 h, and 48 h (3 separate fields/well). Covered surface areas were measured by ImageJ.

Cytoskeleton Staining

Phalloidin (ab176753, Abcam, Cambridge, MA) stained the cell cytoskeleton. After treatment as described above, the cells were washed with PBS, fixed in 4% paraformaldehyde, and blocked with 5% bovine serum albumin (BSA). Then, the cells were stained with phalloidin for 60 min. After three washes, the nuclei were stained with DAPI. Finally, the results were observed *via* fluorescence microscopy. A normal podocyte cytoskeleton structure contains F-actin distributed as obvious homogenous bundles that traverse the cell along the axis of the podocyte. Cytoskeletal remodeling signs include F-actin assembly in cortical regions, agminated F-actin along the podocyte periphery, and a slight diffuse F-actin cytoplasmic distribution (20).

Western Blotting

After treatment, cells or kidney tissue were homogenized in RIPA lysis buffer with PMSF and protease inhibitor cocktail (Roche) for 30 min at 4°C. Total proteins were separated in an 8-10% SDS-PAGE gel and transferred onto PVDF membranes. Then, the membranes were blocked with 5% milk for 1h. After blocking with milk, the membranes were incubated with primary antibodies (PFKP, PFKM, PFKL, PKM2, ALDOB, ROCK1, RhoA, α-tubulin and GAPDH) overnight at 4°C. The next day, the membranes were incubated with a secondary antibody (Antgene, China). After washing the membranes three times, bands were revealed by an ECL chemiluminescent kit (Biosharp, China). Finally, the bands were analyzed using a ChemiDocTM MP Imaging system (Bio-Rad, USA).

Immunofluorescence Staining

After the indicated treatment, cells and tissues were fixed with 4% paraformaldehyde and blocked with 5% BSA. Specific primary antibodies (PFKP) were then applied overnight at 4°C. Next, the samples were incubated with fluorescent secondary antibodies for 1 h. After washing, the nuclei of the samples were counterstained with DAPI. Fluorescence results were analyzed using a confocal laser microscope (Olympus, Japan).

Real-Time PCR

Total RNA from cells and kidney tissue was prepared using TRIzol reagent (Invitrogen, USA). The concentration was measured by a NanoDrop spectrophotometer. Then, 1 μg RNA was retrotranscribed to cDNA using the PrimeScript RT Reagent Kit. PCR amplification was performed using a SYBR Green Kit (Takara, Japan) with the following conditions: 95°C for 30 s; followed by 40 cycles of application at 95°C for 5 s and 60°C for 30 s; and annealing at 60°C for 34 s. All primer sequences are shown in **Table S2**. The relative gene expression was quantified by the $2^{-\Delta\Delta CT}$ method, and GAPDH was used as an endogenous control.

Statistical Analyses

All experiments were repeated at least 3 times. Quantitative data were presented as the mean ± SD, and statistical analyses were performed using SPSS v22.0. Statistical comparisons of groups were performed using one-way ANOVA, and the least-significant difference (LSD) test was used for multiple comparisons. Differences for which $P<0.05$ were considered statistically significant.

RESULTS

Renal Phenotype Alteration of db/db Mice and Profiling of Genes Involved in Glucose Catabolism in Glomeruli From db/db and db/m Mice by mRNA Sequencing

To profile the altered genes in db/db mice compared with db/m mice, the renal phenotype changes of db/db mice were observed

by PAS staining (**Figure 1A**) and transmission electron microscopy (**Figure 1B**), blood sugar test results (**Figure 1C**), body weights (**Figure 1D**), and ACR values (**Figure 1E**) were systemically evaluated. PAS staining indicated dilated mesangial matrix in the glomeruli of db/db mice. Electron microscopy showed that podocyte foot processes were fused, and the glomerular basement membrane was thickened in db/db mice compared with db/m mice. Additionally, db/db mice presented higher blood sugar levels, body weights, ACR values, and mortality rates (**Figure 1F**). Subsequently, the isolated glomeruli were subjected to mRNA sequencing. Glucose metabolism-related genes were systemically evaluated between db/db mice and db/m mice. Intriguingly, several upstream glycolysis genes were upregulated, including *Pfkp* and *Hk1*. Conversely, downstream glycolysis genes were downregulated, including *Pkm*, *Ldha*, *Pdh*, etc. (**Figures 1G, H**). To further confirm the pattern of glycolysis in DKD, the mRNA expression of *Hk1*, *Pfkp*, *Pkm*, and *Ldha* in mouse glomeruli was evaluated by qPCR. Consistent with the sequencing results, *Hk1* and *Pfkp* gene expression was elevated in the glomeruli of db/db mice compared with db/m mice, while *Pkm* and *Ldha* expression was decreased, as shown in **Figure 1I**. Additionally, the protein expression pattern was confirmed by immunohistochemical staining in the glomerular area (**Figure 1J**).

PFK Expressions in db/m and db/db Mice

The sequencing data suggests that the compromise of downstream glycolysis could promote the accumulation of intermediates in upstream glycolysis. As shown in **Figure 1H**, *Pfkp* connects the upstream and downstream portions of the glycolysis cascade. Hence, exploring *Pfkp* alteration in db/db mice was of importance. Since three subtypes of PFK1 have been reported in rodents, all three subtypes were evaluated in the glomeruli. Interestingly, PFKP showed elevated expressions in db/db glomeruli, while the expression of PFKL and PFKM remained comparable according to IHC staining (**Figures 2A, B**). The protein (**Figures 2C, D**) and mRNA (**Figure 2E**) levels of PFKP in the glomeruli of db/db mice and db/m mice were verified by western blotting and q-PCR, respectively. Double staining of glomeruli indicated that PFKP was highly enriched in podocytes from db/db mice (**Figure 2F**).

PFKP Expression in Podocytes From Patients With Biopsy-Proved DKD

Based on the above results, PFKP was activated in db/db mice. The expression profile of PFKP was tested in patients with biopsy-proved DKD. Clinical characteristics of DKD patients including age, serum creatinine (SCr), ACR, and total proteinuria (UTP) were presented in **Figures 3A–D**. Then, PAS stain showed the mesangial expansion and segmental glomerulosclerosis in glomeruli in patients with DKD (**Figure 3E**). PFKP staining in podocyte was enhanced in glomeruli from patients with DKD compared with that in control subjects. The above pattern was tested by IHC (**Figure 3F**) and double immunofluorescent staining approaches (**Figure 3G**) respectively.

Suppression of PFKP Overactivation Aggravated Renal Damage in Diabetic Mice

To further investigate the function of PFKP in podocytes, db/db and db/m mice at 24 weeks of age were administrated intraperitoneally with CTZ for two weeks to inhibit the activity of PFKP (21) (**Figure 4A**). The same volume of solvent with 0.1% DMSO was injected as the control group. No significant changes in body weight and blood sugar were found in CTZ-administrated mice compared with solvent-treated animals. (**Figures S1**, **S2**). However, ACR was significantly higher in CTZ–administrated db/db mice when compared with solvent-treated db/db mice (**Figure 4C**). The pathologic glomerular sclerosis (**Figure 4B**) and foot process fusion by TEM (**Figure 4D**) were worsened in CTZ–administrated db/db mice compared with vehicle-treated db/db mice. Moreover, the mortality of db/db mice with proteinuria at 24-26week age was deteriorated by CTZ administration (**Figure 4E**). To a certain degree, CTZ administration promoted mild proteinuria (**Figure 4C**) and modest pathologic changes, including glomerular sclerosis (**Figure 4B**) and foot process fusion (**Figure 4D**) in db/m mice at comparable age with proteinuria-onset db/db mice. Conversely, the mortality rate was not impacted by CTZ administration in db/m mice. In order to identify the inhibition ability of CTZ on PFKP, IHC and immunofluorescence double staining were used to evaluate the expression of PFKP in glomeruli (**Figure 4G**) and podocyte (**Figure 4F**) respectively. In addition, western blotting analyses indicated that the innate and enhanced protein levels of PFKP were suppressed by CTZ administration in glomeruli from both db/m and db/db mice respectively (**Figure 4H**). Overall, CTZ accelerated podocyte damage under diabetic conditions, which indicates that PFKP may play a protective role in podocytes in DKD.

High Glucose Promoted PFKP Expression and Cytoskeletal Remodeling in Podocytes *In Vitro*

The above CTZ administration indicated that PFKP potentially plays a protective role in podocytes in physical and stress conditions *in vivo*. However, the mechanisms remain to be elucidated. In subsequent experiments, the expression of PFKP was analyzed in podocytes exposed to HG *in vitro*. The three subtypes of PFK were evaluated in culturing podocytes *in vitro* (**Figures S3**, **S4**), and it was found that PFKP was the dominant subtype in podocytes in consist with *in vivo* studies. The expression of PFKP was markedly increased in a dose-dependent manner in the cultured podocytes (0, 10, 15, 20, 25 and 30mM HG) (**Figure 5B**) over 24h exposure. Similarly, a time-dependent increase of the PFKP protein level was exhibited in podocytes under HG (30mM) conditions (0, 6, 12, 18, and 24 h) (**Figure 5A**). In addition, HG-treated podocytes exhibited a dramatic increase in PFKP in the cytoplasm, as shown by immunofluorescence assays (**Figure 5C**). Furthermore, mannitol (MA) hypertonic control had no impact on PFKP

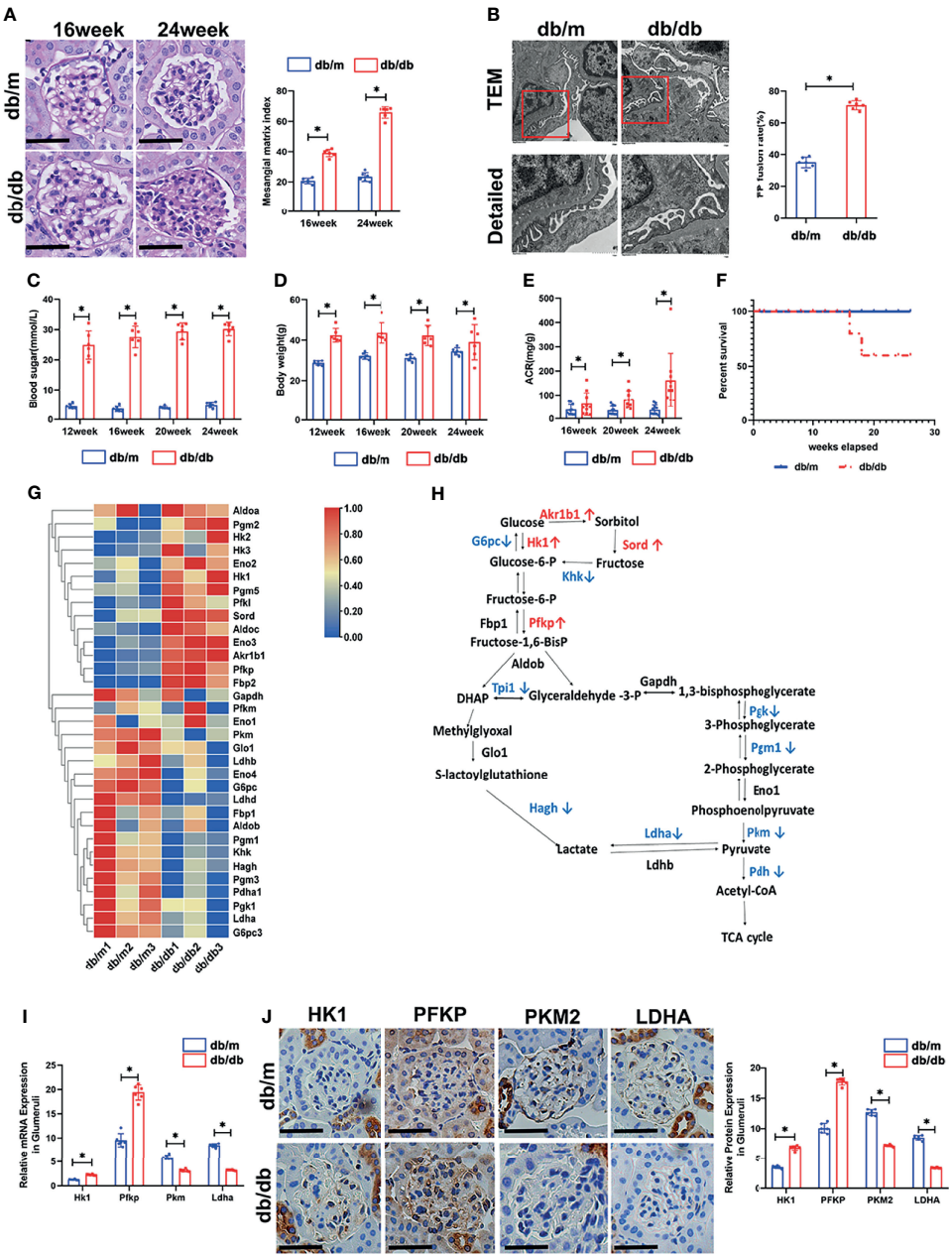

FIGURE 1 | Renal phenotype alteration of db/db mice and profiling of genes involved in glucose catabolism in glomeruli from db/db and db/m mice by mRNA sequencing. **(A)** Representative microscopy images and quantification of PAS staining of kidney sections from db/m and db/db mice at 16 and 24 weeks of age (original magnification ×400). **(B)** Representative findings of the ultrastructure of capillary loops collected from db/m and db/db mice at different timepoints, as examined by transmission electron microscopy (original magnification×8,000, ×12,000). **(C)** Blood sugar of db/m and db/db mice. **(D)** Body weight of db/m and db/db mice. **(E)** Quantitative analysis of ACR (albumin-to-creatinine ratio) in db/m and db/db mice. **(F)** Survival curve of db/m and db/db mice over time. **(G)** Gene expression profiles were compared between glomeruli of db/m and db/db mice, and heat maps were generated based on significantly differential expression of genes related to glucose metabolism. **(H)** Schematic flow illustrating the representative genes in the glycolysis cascade. Red text represents upregulated genes, and blue text represents downregulated genes in the glomeruli of db/db mice in comparison to db/m mice. Akr1b1, aldo-keto reductase family 1, member B1 (aldose reductase); Hk, hexokinase; G6pc, glucose-6-phosphatase, catalytic subunit; Sord, sorbitol dehydrogenase; Pfk, phosphofructokinase; Fbp2, fructose-1,6-diphosphatase 2; Gapdh, glyceraldehyde 3-phosphate dehydrogenase; Tpi1, triosephosphate isomerase 1; Pgk, phosphoglycerate kinase; Pgm1, phosphoglucomutase-1; Eno1, enolase 1; Pkm, pyruvate kinase isoenzyme; Pdh, pyruvate dehydrogenase; Ldh, lactate dehydrogenase; Hagh, hydroxyacyl glutathione hydrolase; Glo1, glyoxalase 1. **(I)** Relative mRNA expression of Hk1, Pfkp, Pkm and Ldha in the glomeruli of db/m and db/db mice determined by real-time PCR. **(J)** Representative immunohistochemistry staining of glomerular HK1, PFKP, PKM2, and LDHA in db/m and db/db mice. For all figures, n=6 independent experiments/group. In all statistical plots, $^*P < 0.05$. Scale bars: 20 μm, HK1, hexokinase 1; PFKP, phosphofructokinase 1 platelet type; PKM2, pyruvate kinase isoenzyme 2; LDHA, lactate dehydrogenase A.

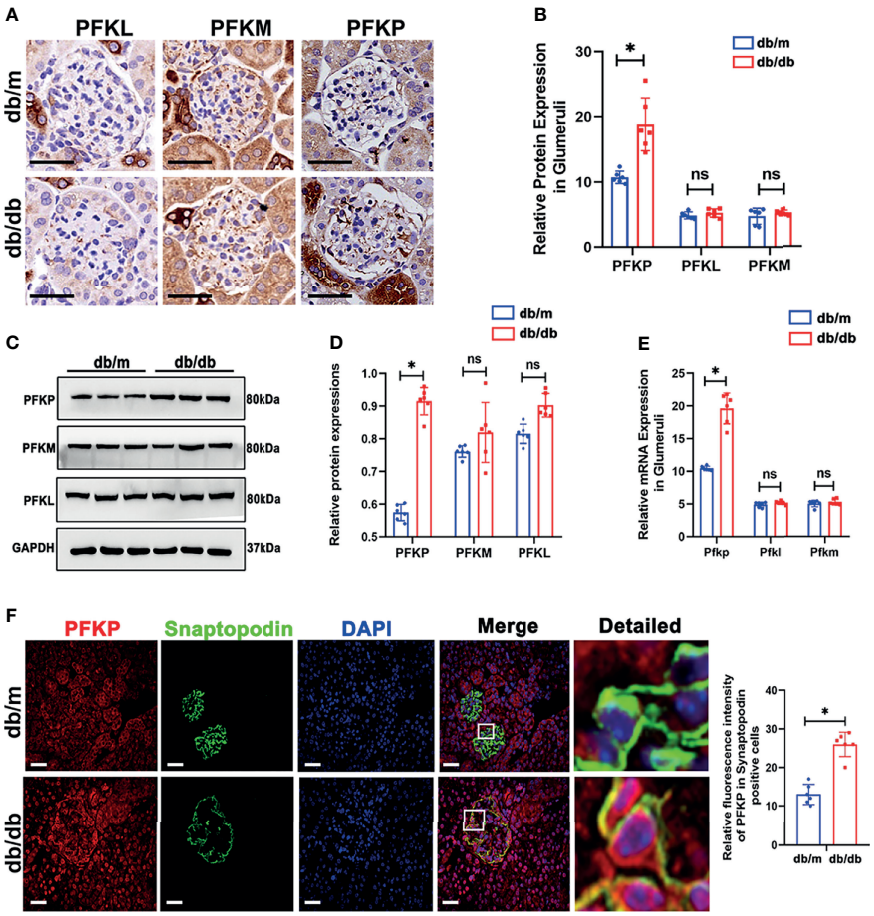

FIGURE 2 | PFK expressions in db/m and db/db mice. **(A, B)** Representative immunohistochemistry staining of glomerular PFKP, PFKM and PFKL in db/m and db/db mice. **(C, D)** Western blotting analysis of the expression of PFKP, PFKM and PFKL in glomeruli of db/m and db/db mice. GAPDH was used as the loading control. **(E)** Relative mRNA expression of *Pfkp, Pfkm* and *Pfkl* in glomeruli of db/m and db/db mice determined by real-time PCR. **(F)** Representative immunofluorescent staining of PFKP in podocyte of glomeruli from db/m and db/db mice. Synaptopodin was used as podocyte markers. For all figures, n=6 independent experiments/group. In all statistical plots, $^*P < 0.05$, ns, No significance. Scale bars: 20 μm, PFKP, phosphofructokinase 1 platelet type; PFKM, phosphofructokinase 1 muscle type; PFKL, phosphofructokinase 1 liver type.

expression and distribution in podocytes compared with normal glucose conditions (**Figure 5C**). In addition, PFK enzymatic activity and FBP levels were increased in HG-exposed podocytes (**Figures 5D, E**), while ATP production was decreased under HG exposure (**Figure 5F**). As PFKP was reported as a cytoskeleton binding protein, the cytoskeleton assembling pattern was evaluated in HG-exposed podocytes. Phalloidin labeling technique was performed to assess F-actin assembling in podocytes. Interestingly, F-actin rearrangement occurred over HG exposure in cultured podocytes. F-actin assembling model switched from being uniformly parallel with long axis of cell body in control group to being aggregating along cell edge in HG-exposed podocyte (**Figure 5H**). Moreover, the wound healing test indicated that HG exposure promoted podocyte migration than normal glucose (**Figure 5I**). RhoA/ROCK1 pathway was reported to be crucial in regulating cytoskeleton in podocytes (22). In line with F-actin remodeling over HG exposure, it was found that RhoA/ROCK1 pathway was activated in HG-exposed podocytes (**Figure 5G**).

Deletion of PFKP Aggravated HG-Induced Cytoskeletal Remodeling in Podocytes *In Vitro*

To further investigate the impact of PFKP suppression on cytoskeletal assembling *in vitro*, siRNA interference was performed to silence *Pfkp* gene, and the efficiency of si*Pfkp* interference was confirmed by western blot analysis (**Figure 6A**). Accordingly, PFK enzymatic activity was suppressed and FBP level, the converted product of PFKP, was lower in *Pfkp*-downregulated podocytes (**Figure 6B**). In addition, suppressing PFKP by siRNA activated RhoA/ROCK1 signaling, magnified by HG exposure (**Figure 6D**). Morphologically, F-actin assemble remodeling was induced by suppression of PFKP in podocyte which was worsened by HG exposure (**Figure 6C**). Moreover, the migration ability of

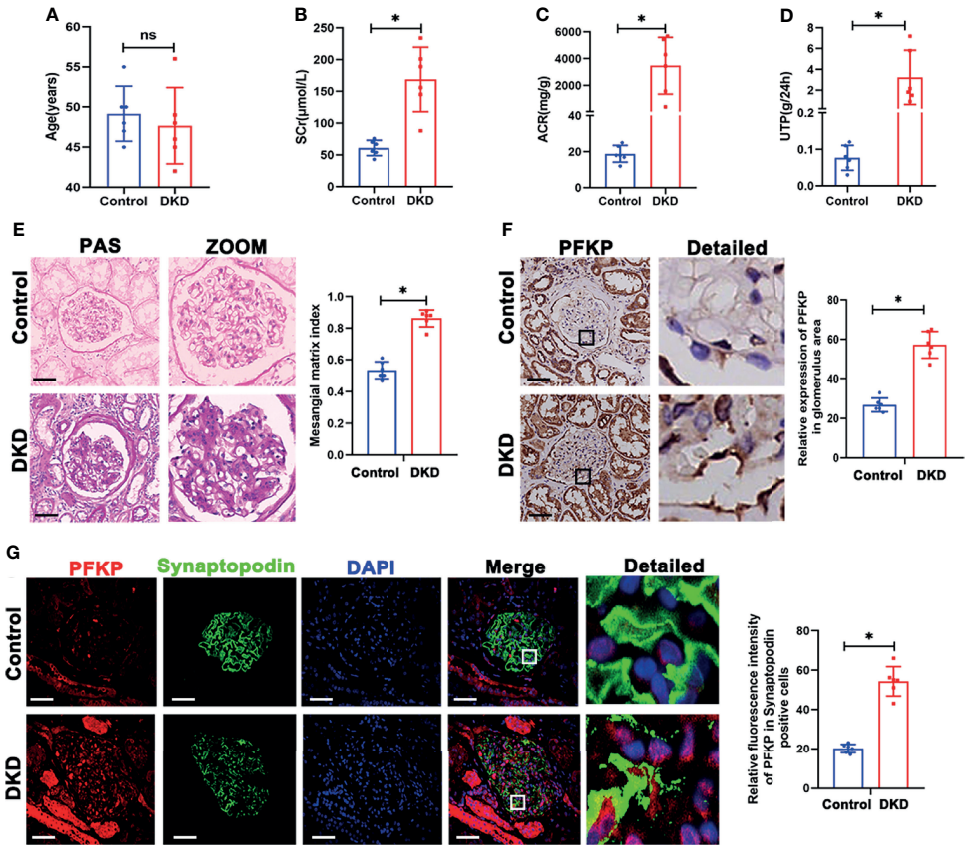

FIGURE 3 | PFKP expression in podocytes from patients with biopsy proved DKD. **(A)** Age of subjects in each group. **(B)** SCr values of subjects in each group. **(C)** ACR values of subjects in each group. **(D)** UTP values of subjects in each group. **(E)** Representative microscopy images and quantification of PAS staining of kidney sections in each group (original magnification ×200). **(F)** Representative immunohistochemistry staining of glomerular PFKP in each group. (Original magnification ×200). **(G)** Representative immunofluorescence staining of PFKP in podocytes in each group. Synaptopodin was used as podocyte markers. For all figures, n=6 independent experiments/group. In all statistical plots, *$P < 0.05$, ns, No significance. Scale bars: 20 μm, DKD, diabetic kidney disease; PFKP, Phosphofructokinase 1 platelet type; SCr, Serum creatinine; UTP, Total proteinuria; ACR, urine albumin/creatinine ratio.

podocytes was enhanced by *Pfkp* interference and accelerated under HG conditions (**Figure 6E**).

Overexpression of PFKP Ameliorated HG-Induced Cytoskeletal Remodeling in Podocytes *In Vitro*

As described above, PFKP deletion aggravated podocyte migration under HG conditions. To further confirm the effect of PFKP on podocyte migration, a recombinant plasmid (pcDNA3.1-*Pfkp*) was transfected into podocytes to overexpress PFKP *in vitro*. The efficiency of plasmid transfection was confirmed by western blot analysis (**Figures 7A, B**). Accordingly, PFK enzymatic activity and FBP levels were increased in *Pfkp*-overexpressed cells (**Figures 7C, D**). Moreover, overexpression of PFKP prevented activation of RhoA/ROCK1 signaling and remodeling of F-actin assemble even in the presence of HG exposures (**Figures 7E, F**). In addition, the wound healing test showed that with pcDNA3.1-*Pfkp* transfection, podocyte migration and movement slowed (**Figure 7G**).

Exogenous FBP Ameliorated HG-Induced Cytoskeletal Remodeling in Podocytes *In Vitro*

PFKP is the glycolytic enzyme that catalyzes the phosphorylation of fructose-6-phosphate (Fructose-6-P) to FBP(Fructose-1,6-P). The dynamic changes in PFKP and FBP levels suggest that PFKP may participate in cytoskeletal regulation by regulating FBP levels. To confirm that, targeted metabolomics was performed to observe the alterations of the metabolites of glucose metabolism. It showed that the level of isocitrate, fructose 6-phosphate, FBP, etc. were significantly increased, while the level of flavin mononucleotide and lactate decreased (**Figure 8A**). To further investigate the role of FBP in podocytes, we used aldolase (ALDO), which is the enzyme that catalyzes the breakdown of FBP, to control FBP levels in podocytes. First, the relative mRNA expression of the three subtypes of *Aldo* (*Aldoa*, *Aldob*, and *Aldoc*) in cultured podocytes was assessed by real-time PCR (**Figure S5**), which showed that *Aldob* was the dominant subtype in podocytes. With si*Aldob*, the RhoA/ROCK1 pathway declined as the level of FBP increased

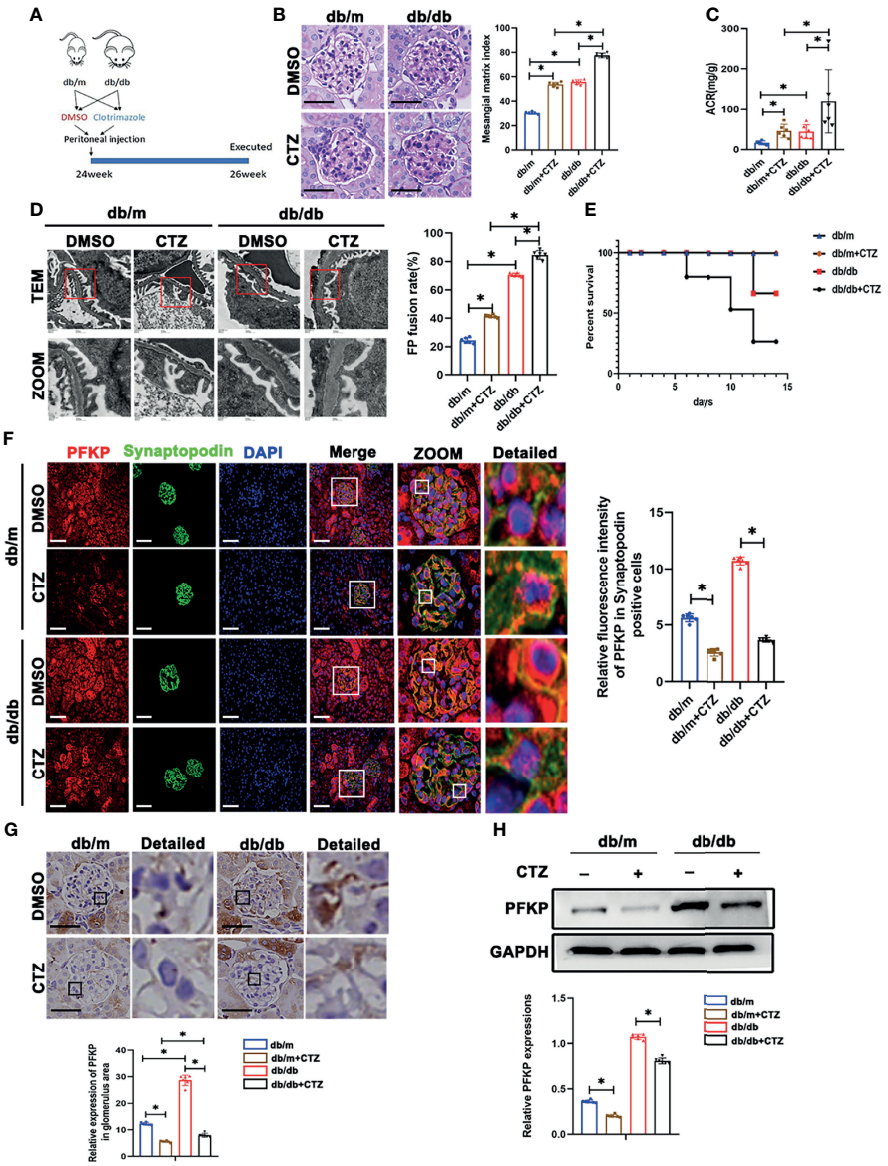

FIGURE 4 | Suppression of PFKP overactivation aggravated renal damage in db/db mice. **(A)** Schematic diagram of Clotrimazole administration in advanced db/db mice. **(B)** Representative microscopy images and quantification of PAS staining of kidney sections in each group (original magnification ×400). **(C)** Quantitative of ACR (albumin-to-creatinine ratio) in each group. **(D)** Representative transmission electron microscopy images of the ultrastructure of capillary loops in each group (original magnification×8,000, ×12,000). **(E)** Survival curve of db/m and db/db mice treated with CTZ over time. **(F)** Representative immunofluorescence staining of podocytes PFKP in each group. Synaptopodin was used as the podocyte marker. **(G)** Representative immunohistochemistry staining of glomerular PFKP in each group. **(H)** Western blotting analysis of PFKP expression in glomeruli of each group. GAPDH was set as loading control. For all figures, n=6 independent experiments/group. *$P < 0.05$. Scale bars: 20 μm, CTZ, Clotrimazole; PFKP, Phosphofructokinase 1 platelet type.

(**Figures 8B, C**). No significant cytoskeletal remodeling occurred in the si*Aldob* group (**Figure 8D**), and the motility of the podocytes was unaffected either (**Figure 8E**). In contrast, when transfected with a recombinant *Aldob* plasmid (pcDNA3.1-*Aldob*), FBP levels were decreased (**Figure 8G**), and the RhoA/ROCK1 pathway was activated (**Figure 8F**). Moreover, cytoskeletal remodeling occurred in the pcDNA3.1-Aldob group (**Figure 8H**), and the podocytes' motility was higher (**Figure 8I**). Finally, to prove the protective role of FBP in podocytes, we treated podocytes with HG and FBP (5 mM and 10 mM). Western blotting showed that HG induced RhoA/ROCK1 activation was inhibited by FBP (**Figure 8J**) and the cytoskeletal remodeling and motility effect in podocytes under HG conditions were ameliorated (**Figures 8K, L**).

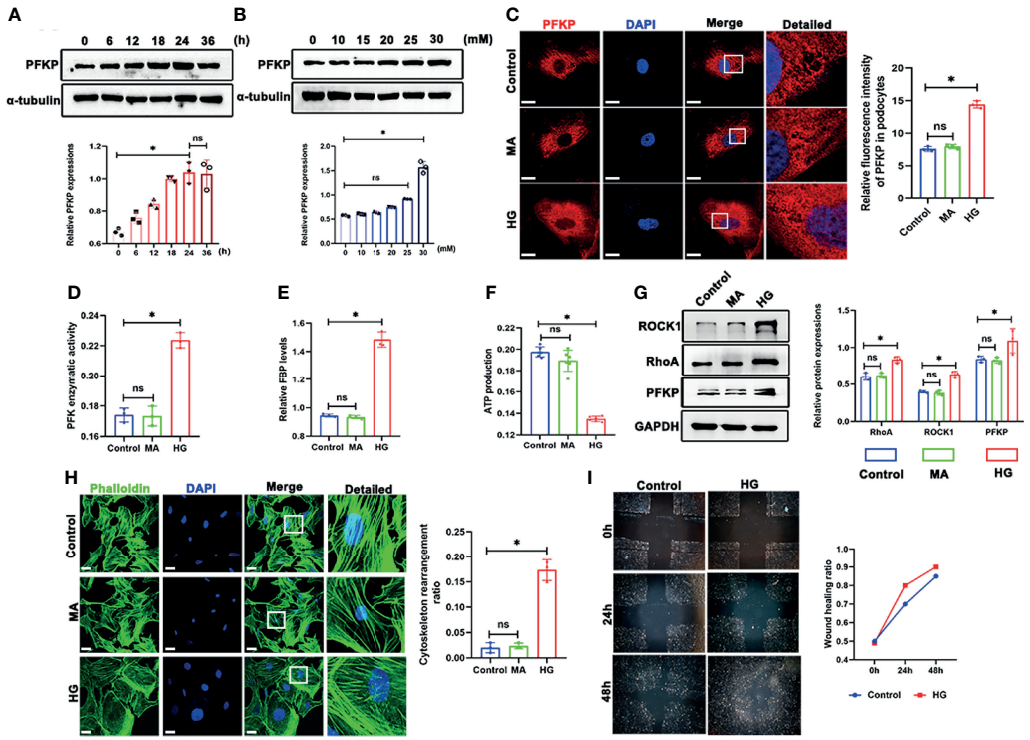

FIGURE 5 | High glucose promoted PFKP expression and cytoskeletal remodeling in podocytes *in vitro*. **(A)** Representative western blots of PFKP expression in 30 mM HG-treated podocytes at various times points and quantification of these results, with α-tubulin as the loading control. **(B)** Representative western blots of PFKP expression in cultured podocytes stimulated with different concentrations of glucose for 24 h and quantification of these results, with α-tubulin set as the loading control. **(C)** Representative immunofluorescence staining of podocytes PFKP in each group. **(D)** PFK enzymatic activity in each group. **(E)** FBP level in each group. **(F)** ATP production in each group. **(G)** Western blotting analyses of the expression of ROCK1, PFKP and RhoA in podocytes in each group. GAPDH was set as the loading control. **(H)** Cytoskeletal structures of podocytes labeled with phalloidin. **(I)** Motility of podocytes quantified by a wound-healing assay using an inverted microscope. For all figures, n=3 independent experiments/group. *$P < 0.05$, ns, No significance. Scale bars: 10 μm. HG, high glucose; MA, mannitol; ROCK1, Rho-associated, coiled-coil containing protein kinase 1; PFKP, phosphofructokinase 1 platelet type; RhoA, RhoA-GTPase.

FBP Administration Protected Diabetic Mice From Foot Process Fusion in Podocytes

To further investigate the role of FBP *in vivo*, we treated db/m and db/db mice with FBP intraperitoneal injection (**Figure 9A**). Surprisingly, we found that in db/db mice treated with a high dose of FBP, glomerular lesions (**Figure 9B**), the fusion of foot processes (**Figure 9C**), urinary ACR (**Figure 9D**) and mortality (**Figure 9G**) were reduced. However, there were no significant changes in blood glucose (**Figure 9F**) and body weight (**Figure 9E**) in mice after FBP treatment. This part of our research indicates that FBP may protect db/db mice from foot process fusion in podocytes and can be potential medications for DKD.

DISCUSSION

In this study, we observed abnormalities in glycolysis and disorder in the cytoskeletal structure of podocytes under HG stimulation. We identified PFKP as playing a novel endogenous protective role against diabetic injury in podocytes through its catalyzed metabolite FBP. *In vivo* studies showed the activation of PFKP in different models and the detrimental effects of the inhibition of PFKP. Mechanistically, our *in vitro* studies showed that FBP could ameliorate HG-induced cytoskeletal remodeling in podocytes.

In the past few decades, molecular targets for DKD treatment have been intensively investigated (3). However, there are no specific agents for the prevention and treatment of early DKD. Hyperglycemia, which is known to be a crucial part of the pathogenesis of DKD, can damage podocyte function and structure in many ways, thus leading to the occurrence of proteinuria (5, 6), but the underlying mechanisms remain unclarified.

Alteration of glucose metabolism in podocytes under diabetic conditions has received much attention in recent years. Altered glycolytic flux has been postulated to induce a series of transcriptional and translational changes that lead to DKD (23). Moreover, the activation of glycolysis has been proven to have positive effects in DKD patients (8, 10). A study focused on PKM2, which is another key enzyme in the glycolysis process, found that PKM2 activation could protect podocytes from HG-induced injury by protecting mitochondria (10). In our mRNA array, we

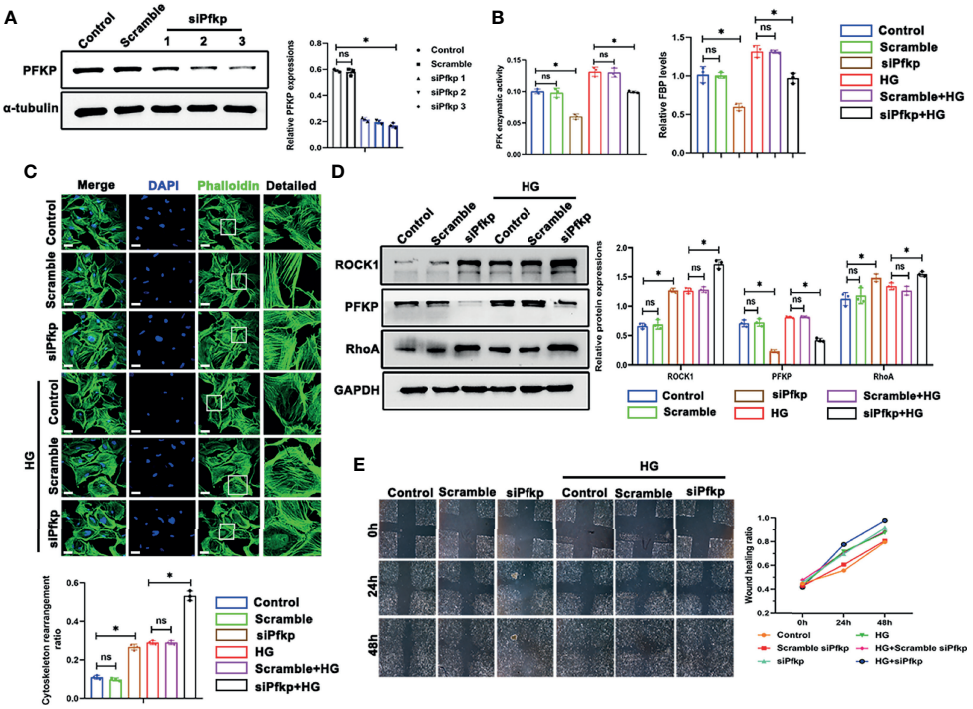

FIGURE 6 | Deletion of PFKP aggravated HG-induced cytoskeletal remodeling in podocytes *in vitro*. **(A)** Western blots of PFKP expression after transfection with various *siPfkps*, with GAPDH set as the loading control. **(B)** PFK enzymatic activity and FBP level in each group. **(C)** Cytoskeletal structures of podocytes labeled with phalloidin and the cytoskeletal rearrangement ratio in each group (original magnification ×600). **(D)** Western blotting analyses of the expression of ROCK1, PFKP, and RhoA in podocytes of each group. GAPDH was set as the loading control. **(E)** Motility of podocytes measured by a wound-healing assay using an inverted microscope. For all figures, n=3 independent experiments/group. *$P < 0.05$, ns, No significance. Scale bars: 10 μm. HG, high glucose; ROCK1, Rho-associated, coiled-coil containing protein kinase 1; PFKP, phosphofructokinase 1 platelet type; RhoA, RhoA-GTPase.

detected changes of glycolysis enzyme mRNA levels, including the increased level of *Pfkp* and *Hk1*, and decreased in *Pkm* and *Ldha*, indicating the dysfunction of glomeruli glycolysis in db/db mice and the accumulation of glycolysis intermediates. PFK1 is one of the key glycolytic enzymes that catalyzes the conversion of F-1-P to FBP. To date, three subtypes of PFK1 have been identified in vertebrate genomes, termed PFKM (muscle type), PFKL (liver type) and PFKP (platelet type), according to the site of discovery, among which PFKP plays the leading role in the kidney (24). As a major isoform of PFK-1 in cancer glycolysis, PFKP has become an emerging anticancer target (25). Here we found that PFKP showed the highest expression level and was significantly upregulated in the glomeruli of db/db mice. Consistently, PFKP was upregulated in DKD patients compared with control renal tissues obtained from cancer patients, the result was surprising because PFKP was previously reported to be upregulated in cancer (25). In addition, we detected increased ACR level, mortality, and more severe foot process fusion in db/db mice when treated with CTZ, which is an inhibitor of PFKP (21). Besides, the use of FBP, a catalysate of PFKP, improved proteinuria and renal injury in db/db mice. These results indicate that PFKP may play the role of endogenous protective factors.

In the last few decades, studies have shown that the actin cytoskeleton directly binds to many metabolic enzymes, including PFK-1, ALDO and glycerol triphosphate dehydrogenase (GAPDH), and recent studies have shown that remodeling and assembly of the actin cytoskeleton is a major energy-consuming process, accounting for approximately 50% of ATP consumption (12). It was reported that on the soft extracellular matrix, the active E3 ubiquitin ligase TRIM21 binds and ubiquitinates PFK-1 in the cytoplasm, resulting in targeted degradation of PFK-1 and thereby maintaining glycolysis at a relatively low level. When cells move to the hard extracellular matrix, the contraction force is increased, F-actin and Talin binding of bound integrins is also increased, thereby stimulating actin-binding and TRIM21 chelation. Inactivation of this process results in PFK-1 accumulation in the cytoplasm and increases glycolysis (13). Furthermore, FBP is a high-energy glycolytic intermediate that exerts protective action against many harmful conditions in various cell types and tissues through its anti-inflammatory, immunomodulatory and neuroprotective properties (26). Moreover, it can regulate the activation of Ras, which is a major regulator of cell proliferation (27). Additionally, FBP mediates glucose sensing by AMPK (28), and AMPK signaling can increase the phosphorylation of vinculin at Y822, which triggers the activation of the RhoA–ROCK–MLCK–MLC pathway, culminating in the reinforcement of the actin cytoskeleton (12). AMPK is also the energy sensor in cells and is activated when cells are starved of nutrients. Local activation of AMPK increased ATP

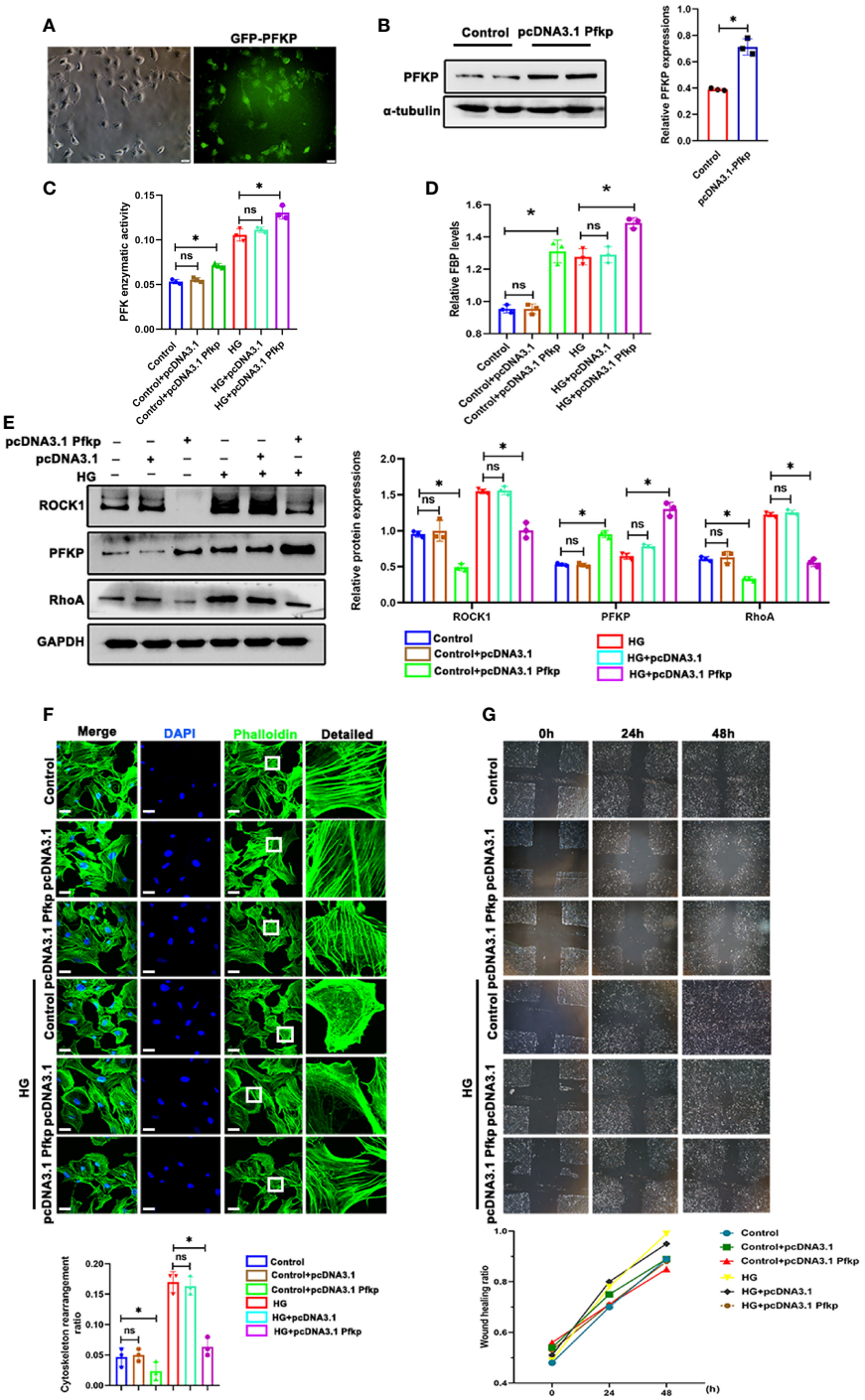

FIGURE 7 | Overexpression of PFKP ameliorated HG-induced cytoskeletal remodeling in podocytes *in vitro*. **(A)** After recombinant plasmid (pcDNA3.1-Pfkp) transfection into podocytes, the expression of EGFP was observed by fluorescence microscopy. **(B)** Western blots of PFKP expression after transfection with pcDNA3.1-Pfkp, with GAPDH set as the loading control. **(C)** PFK enzymatic activity in each group. **(D)** FBP level in each group. **(E)** Western blotting analyses of the expression of ROCK1, PFKP, and RhoA in podocytes in each group. GAPDH was set as the loading control. **(F)** Cytoskeletal structures of podocytes labeled with phalloidin. **(G)** Motility of podocytes measured by a wound-healing assay using an inverted microscope. For all figures, n=3 independent experiments/group. *$P < 0.05$, ns, No significance. Scale bars: 10 μm. HG, high glucose; ROCK1, Rho-associated, coiled-coil containing protein kinase 1; PFKP, phosphofructokinase 1 platelet type; RhoA, RhoA-GTPase.

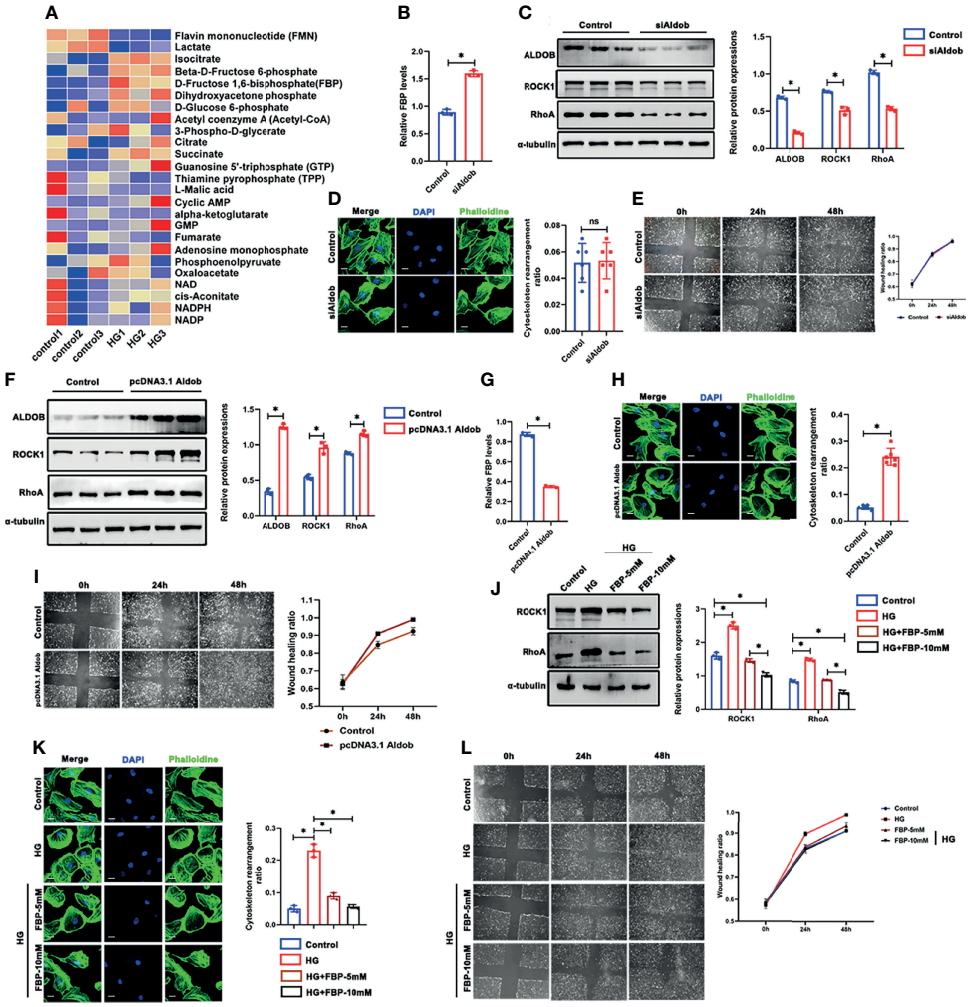

FIGURE 8 | FBP ameliorated HG-induced cytoskeletal remodeling in podocytes *in vitro*. **(A)** Targeted metabolomics was performed between control and HG group of cultured podocytes, and heat maps were generated based on levels of the metabolites related to glucose metabolism. **(B)** Western blots of ALDOB, ROCK1, PFKP, and RhoA after transfected with siAldob, GAPDH was set as the loading control. **(C)** FBP level in control and siAldob group. **(D)** Cytoskeletal structure of podocytes labeled with phalloidin in control and siAldob group. **(E)** Motility ability of podocytes were measured by wound-healing assay using an inverted microscope in control and siAldob group. **(F)** Western blotting analyses the expression of ALDOB, ROCK1, PFKP, and RhoA in podocytes after transfected with pcDNA3.1-Aldob. GAPDH was set as loading control. **(G)** FBP level in control and pcDNA3.1-Aldob group. **(H)** Cytoskeleton structure of podocytes labeled with phalloidin in control and pcDNA3.1-Aldob group. **(I)** Motility ability of podocytes were measured by wound-healing assay using an inverted microscope in control and pcDNA3.1-Aldob group. **(J)** Western blotting analyses the expression of ALDOB, ROCK1, PFKP, and RhoA in podocytes after FBP treatment. GAPDH was set as loading control. **(K)** Cytoskeleton structure of podocytes labeled with phalloidin in each group. **(L)** Motility ability of podocytes were measured by wound-healing assay using an inverted microscope in each group. For all figures, n=3 independent experiments/group. *$P < 0.05$, ns, No significance. Scale bars: 10 μm. HG, high glucose; FBP, fructose-1,6-bisphosphate; ROCK1, Rho-associated, coiled-coil containing protein kinase 1; PFKP, Phosphofructokinase 1 platelet type; RhoA, RhoA-GTPase.

production, mitochondrial flux, and cytoskeletal dynamics, and excessive energy may promote actin cytoskeletal remodeling (29). In addition, FBP can promote a feedback loop between PFK1, phosphatidylinositol-3-kinase/protein kinase B (PI3K/Akt), and PFK2/PFKFB3 in T cells (30), and the PI3K/Akt signaling pathway is closely related to the podocyte cytoskeleton (31). Hence, FBP is involved in the regulation of cytoskeletal structure.

Cytoskeletal architecture in podocytes is pivotal to its function (5, 11). Cytoskeletal remodeling in podocytes contributes to the progression of DKD (32, 33), as the assembly of F-actin is associated with the formation and migration of podocyte foot processes. Treatment targeted toward the cytoskeletal architecture has been proven effective in glomerular diseases (34). Small GTPases that belong to the Ras homology (Rho) family play essential roles in regulating cell migration by controlling cytoskeletal system (35). RhoA is the most important member of the Rho family, and its major downstream effector is Rho-associated kinase (ROCK), which is a serine/threonine kinase, is highly involved in the biological processes of cell movement, cell migration, gene transcription,

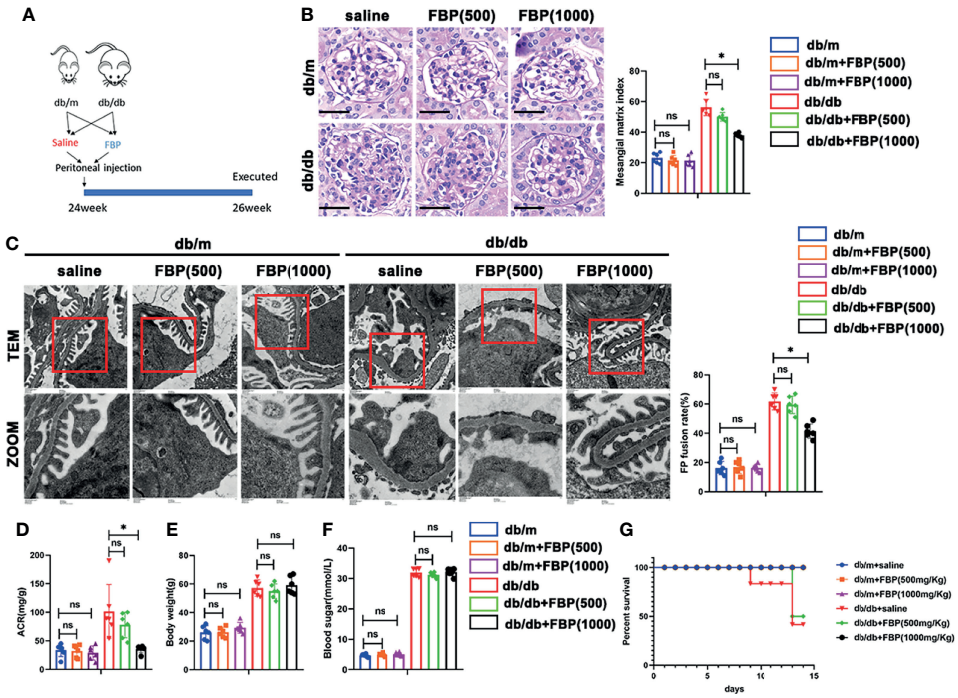

FIGURE 9 | FBP protected db/db mice from foot process fusion in podocytes. **(A)** Schematic diagram of FBP administration in advanced db/db mice. **(B)** Representative microscopy images and quantification of PAS staining of kidney sections from individual group (original magnification ×400). **(C)** Representative transmission electron microscopy images of the ultrastructure of capillary loops in each group (original magnification×8,000, ×12,000). **(D)** Quantitative of ACR (albumin-to-creatinine ratio) in each group. **(E)** Body weight of mice in each group. **(F)** Blood sugar of mice in each group. **(G)** Survival curve of db/m and db/db mice treated with FBP over time. For all figures, n=6 independent experiments/group. *$P < 0.05$, ns, No significance. Scale bars: 20 μm, FBP, fructose-1,6-bisphosphate; 500, 500mg/kg/d; 1000, 1000mg/kg/d.

nerve regeneration, and apoptosis (36). ROCK1 is localized to the plasma membrane and plays an important role in cell movement, and RhoA is critical for the recruitment of ROCK1 to the plasma membrane (37). It has also been found that RhoA/ROCK1 pathway contributes to the development of DKD (22). Moreover, inhibition of RhoA/ROCK1 pathway prevents the occurrence of pathologic changes in DKD *in vivo* (38). We found that the suppression of PFKP with siRNA resulted in lower FBP levels and more severe cytoskeletal remodeling in podocytes *in vitro*. Conversely, overexpression of PFKP in the HG environment relieved cytoskeletal remodeling and increased FBP production. Furthermore, inhibition of ALDOB can ameliorate podocyte damage by elevating FBP levels. In contrast, the activation of ALDOB reduced FBP production and led to increased cytoskeletal remodeling. More importantly, FBP addition rescued podocytes from cytoskeletal remodeling under HG conditions and could alleviate the renal injury of db/db mice *in vivo*.

To our knowledge, the present study demonstrates for the first time that glucose metabolism is associated with the cytoskeletal remodeling in podocytes through ROCK1/RhoA signaling pathway. Suppression of PFKP in podocytes exacerbates diabetic kidney injury and cytoskeletal remodeling in podocytes. PFKP, the key regulator of glucose metabolism, affected cytoskeletal structure by regulating FBP levels. These findings provide evidence that PFKP may be a potential target for podocyte injury in DKD and provide a rationale for applying glycolysis enhancing agents in patients with DKD.

Limitations of Study

The protective role of PFKP against DKD is revealed here only in male mice. Whether PFKP has the same function in female mice has not been investigated. We did not use *Pfkp* gene overexpression or knockout mice to perform our experiments. While we demonstrate that FBP directly affects the RhoA/ROCK1 pathway, how FBP influences it deserves to be further investigated. Lastly, whether PFKP and FBP protect against DKD in clinical situations, or at least in nonhuman primates, remains to be further investigated.

DATA AVAILABILITY STATEMENT

The datasets presented in this study can be found in online repositories. The names of the repository/repositories and accession number(s) can be found below: Gene Expression Omnibus GSE184836, https://www.ncbi.nlm.nih.gov/geo/query/acc.cgi?acc=GSE184836.

ETHICS STATEMENT

The studies involving human participants were reviewed and approved by the Research Ethics Committee of Renmin Hospital of Wuhan University. The patients/participants provided their written informed consent to participate in this study.

AUTHOR CONTRIBUTIONS

ZWZ, WL, and GD participated in research design. ZWZ, QL, HH, KY, ZJZ, and JH performed experiments. ZWZ, QL, ZC, JZ, JF, QC, and WL performed data analysis and interpretation; ZWZ and WL drafted the paper. ZWZ, JH, and GD designed and supervised the studies. All authors contributed to the article and approved the submitted version.

FUNDING

This work was supported by grants from the National Natural Science Foundation of China (81970631 to WL and 82070713 to GD).

SUPPLEMENTARY MATERIAL

The Supplementary Material for this article can be found online at: https://www.frontiersin.org/articles/10.3389/fendo.2021.797025/full#supplementary-material

REFERENCES

1. Zhang L, Long J, Jiang W. Trends in Chronic Kidney Disease in China. *N Engl J Med* (2016) 375(9):905–6. doi: 10.1056/NEJMc1602469
2. Duan J, Wang C, Liu D. Prevalence and Risk Factors of Chronic Kidney Disease and Diabetic Kidney Disease in Chinese Rural Residents: A Cross-Sectional Survey. *Sci Rep* (2019) 9(1):10408. doi: 10.1038/s41598-019-46857-7
3. Samsu N. Diabetic Nephropathy: Challenges in Pathogenesis, Diagnosis, and Treatment. *Biomed Res Int* (2021) 2021:1497449. doi: 10.1155/2021/1497449
4. Lee SY, Choi ME. Urinary Biomarkers for Early Diabetic Nephropathy: Beyond Albuminuria. *Pediatr Nephrol* (2015) 30(7):1063–75. doi: 10.1007/s00467-014-2888-2
5. Garg P. A Review of Podocyte Biology. *Am J Nephrol* (2018) 47 Suppl 1:3–13. doi: 10.1159/000481633
6. Zhang L, Wen Z, Han L. Research Progress on the Pathological Mechanisms of Podocytes in Diabetic Nephropathy. *J Diabetes Res* (2020) 2020:7504798. doi: 10.1155/2020/7504798
7. Brinkkoetter PT, Bork T, Salou S. Anaerobic Glycolysis Maintains the Glomerular Filtration Barrier Independent of Mitochondrial Metabolism and Dynamics. *Cell Rep* (2019) 30;27(5):1551–66.e5. doi: 10.1016/j.celrep.2019.04.012
8. Imasawa T, Obre E, Bellance N, Lavie J, Imasawa T, Rigothier C, et al. High Glucose Repatterns Human Podocyte Energy Metabolism During Differentiation and Diabetic Nephropathy. *FASEB J* (2017) 31(1):294–307. doi: 10.1096/fj.201600293r
9. Sharma K, Karl B, Mathew AV, Gangoiti JA, Wassel CL, Saito R, et al. Metabolomics Reveals Signature of Mitochondrial Dysfunction in Diabetic Kidney Disease. *J Am Soc Nephrol* (2013) 24(11):1901–12. doi: 10.1681/ASN.2013020126
10. Qi W, Keenan HA, Li Q, Ishikado A, Kannt A, Sadowski T, et al. Pyruvate Kinase M2 Activation may Protect Against the Progression of Diabetic Glomerular Pathology and Mitochondrial Dysfunction. *Nat Med* (2017) 23(6):753–62. doi: 10.1038/nm.4328
11. Schell C, Huber TB. The Evolving Complexity of the Podocyte Cytoskeleton. *J Am Soc Nephrol* (2017) 28(11):3166–74. doi: 10.1681/ASN.2017020143
12. DeWane G, Salvi AM, DeMali KA. Fueling the Cytoskeleton - Links Between Cell Metabolism and Actin Remodeling. *J Cell Sci* (2021) 134(3):jcs248385. doi: 10.1242/jcs.248385
13. Park JS, Burckhardt CJ, Lazcano R, Solis LM, Isogai T, Li L, et al. Mechanical Regulation of Glycolysis *via* Cytoskeleton Architecture. *Nature* (2020) 578(7796):621–6. doi: 10.1038/s41586-020-1998-1
14. Wang J, Jia L, Kuang Z. The *In Vitro* and *In Vivo* Antitumor Effects of Clotrimazole on Oral Squamous Cell Carcinoma. *PLoS One* (2014) 9(6):e98885. doi: 10.1371/journal.pone.0098885
15. Janicot R, Stafstrom CE, Shao LR. The Efficacy of Fructose-1,6-Bisphosphate in Suppressing Status Epilepticus in Developing Rats. *Epilepsy Res* (2020) 168:106500. doi: 10.1016/j.eplepsyres.2020.106500
16. Dias HB, de Oliveira JR, Donadio MVF, Kimura S. Fructose-1,6-Bisphosphate Prevents Pulmonary Fibrosis by Regulating Extracellular Matrix Deposition and Inducing Phenotype Reversal of Lung Myofibroblasts. *PLoS One* (2019) 14(9):e0222202. doi: 10.1371/journal.pone.0222202
17. Chen C, Chen H, Zhang Y, Thomas HR, Frank MH, He Y, et al. TBtools: An Integrative Toolkit Developed for Interactive Analyses of Big Biological Data. *Mol Plant* (2020) 13(8):1194–202. doi: 10.1016/j.molp.2020.06.009
18. American Diabetes Association. Microvascular Complications and Foot Care: Standards of Medical Care in Diabetes-2019. *Diabetes Care* (2019) 42(Suppl 1):S124–38. doi: 10.2337/dc19-S011
19. KDOQI. KDOQI Clinical Practice Guidelines and Clinical Practice Recommendations for Diabetes and Chronic Kidney Disease. *Am J Kidney Dis* (2007) 49(2 Suppl 2):S12–154. doi: 10.1053/j.ajkd.2006.12.005
20. Lv Z, Hu M, Ren X, Fan M, Zhen J, Chen L, et al. Fyn Mediates High Glucose-Induced Actin Cytoskeleton Reorganization of Podocytes *via* Promoting ROCK Activation *In Vitro*. J. *Diabetes Res* (2016) 2016:5671803. doi: 10.1155/2016/5671803
21. Meira DD, Marinho-Carvalho MM, Teixeira CA. Clotrimazole Decreases Human Breast Cancer Cells Viability Through Alterations in Cytoskeleton-Associated Glycolytic Enzymes. *Mol Genet Metab* (2004) 84(4):354–62. doi: 10.1016/j.ymgme.2004.11.012
22. Kolavennu V, Zeng L, Peng H, Wang Y, Danesh FR. Targeting of RhoA/ROCK Signaling Ameliorates Progression of Diabetic Nephropathy Independent of Glucose Control. *Diabetes* (2008) 57(3):714–23. doi: 10.2337/db07-1241
23. Nakamichi R, Hayashi K, Itoh H. Effects of High Glucose and Lipotoxicity on Diabetic Podocytes. *Nutrients* (2021) 13(1):241. doi: 10.3390/nu13010241
24. Fernandes PM, Kinkead J, McNae I, Michels PAM, Walkinshaw MD. Biochemical and Transcript Level Differences Between the Three Human Phosphofructokinases Show Optimisation of Each Isoform for Specific Metabolic Niches. *Biochem J* (2020) 477(22):4425–41. doi: 10.1042/BCJ20200656
25. Lang L, Chemmalakuzhy R, Shay C, Teng Y. PFKP Signaling at a Glance: An Emerging Mediator of Cancer Cell Metabolism. *Adv Exp Med Biol* (2019) 1134:243–58. doi: 10.1007/978-3-030-12668-1_13
26. Alva N, Alva R, Carbonell T. Fructose 1,6-Bisphosphate: A Summary of Its Cytoprotective Mechanism. *Curr Med Chem* (2016) 23(39):4396–417. doi: 10.2174/0929867323666161014144250
27. Peeters K, Van Leemputte F, Fischer B, Bonini BM, Quezada H, Tsytlonok M, et al. Fructose-1,6-Bisphosphate Couples Glycolytic Flux to Activation of Ras. *Nat Commun* (2017) 8(1):922. doi: 10.1038/s41467-017-01019-z
28. Zhang CS, Hawley SA, Zong Y, Li M, Wang Z, Gray A, et al. Fructose-1,6-Bisphosphate and Aldolase Mediate Glucose Sensing by AMPK. *Nature* (2017) 548(7665):112–6. doi: 10.1038/nature23275
29. Cunniff B, McKenzie AJ, Heintz NH, Howe AK. AMPK Activity Regulates Trafficking of Mitochondria to the Leading Edge During Cell Migration and Matrix Invasion. *Mol Biol Cell* (2016) 27(17):2662–74. doi: 10.1091/mbc.e16-05-0286

30. Icard P, Alifano M, Donnadieu E, Simula L. Fructose-1,6-Bisphosphate Promotes PI3K and Glycolysis in T Cells? *Trends Endocrinol Metab* (2021) 32(8):540–3. doi: 10.1016/j.tem.2021.04.013
31. Zhu J, Sun N, Aoudjit L, Li H, Kawachi H, Lemay S, et al. Nephrin Mediates Actin Reorganization *via* Phosphoinositide 3-Kinase in Podocytes. *Kidney Int* (2008) 73(5):556–66. doi: 10.1038/sj.ki.5002691
32. Perico L, Conti S, Benigni A, Remuzzi G. Podocyte-Actin Dynamics in Health and Disease. *Nat Rev Nephrol* (2016) 12(11):692–710. doi: 10.1038/nrneph.2016.127
33. Sever S, Schiffer M. Actin Dynamics at Focal Adhesions: A Common Endpoint and Putative Therapeutic Target for Proteinuric Kidney Diseases. *Kidney Int* (2018) 93(6):1298–307. doi: 10.1016/j.kint.2017.12.028
34. Schiffer M, Teng B, Gu C. Pharmacological Targeting of Actin-Dependent Dynamin Oligomerization Ameliorates Chronic Kidney Disease in Diverse Animal Models. *Nat Med* (2015) 21(6):601–9. doi: 10.1038/nm.3843
35. Etienne-Manneville S, Hall A. Rho GTPases in Cell Biology. *Nature* (2002) 420(6916):629–35. doi: 10.1038/nature01148
36. Shimokawa H, Sunamura S, Satoh K. RhoA/Rho-Kinase in the Cardiovascular System. *Circ Res* (2016) 118(2):352–66. doi: 10.1161/CIRCRESAHA.115.306532
37. Miyazaki K, Komatsu S, Ikebe M. Dynamics of RhoA and Rokα Translocation in Single Living Cells. *Cell Biochem Biophys* (2006) 45:243–54. doi: 10.1385/CBB:45:3:243
38. Peng F, Wu D, Gao B. RhoA/Rho-Kinase Contribute to the Pathogenesis of Diabetic Renal Disease. *Diabetes* (2008) 57(6):1683–92. doi: 10.2337/db07-1149

Conflict of Interest: The authors declare that the research was conducted in the absence of any commercial or financial relationships that could be construed as a potential conflict of interest.

Publisher's Note: All claims expressed in this article are solely those of the authors and do not necessarily represent those of their affiliated organizations, or those of the publisher, the editors and the reviewers. Any product that may be evaluated in this article, or claim that may be made by its manufacturer, is not guaranteed or endorsed by the publisher.

frontiers in Endocrinology

ORIGINAL RESEARCH
published: 24 March 2022
doi: 10.3389/fendo.2022.862545

Increased Serum VEGF-B Level Is Associated With Renal Function Impairment in Patients With Type 2 Diabetes

*Yaping Wei[1,3], Shiyu Han[2,3], Ruonan Zhou[2,3], Pingyuan Xu[2,3], Lingyan Zhou[2,3], Ziwei Zhu[2,3], Yue Kan[2,3], Xiaoying Yang[2,3], Yingying Xiang[2,3], Yue Cao[2,3], Yu Jin[3], Jing Yan[3], Xizhong Yu[3], Xin Wang[2] and Wenbin Shang[2,3]**

[1] Department of Endocrinology, Changzhou Traditional Chinese Medicine Hospital Affiliated to Nanjing University of Chinese Medicine, Changzhou, China, [2] Department of Endocrinology, Jiangsu Province Hospital of Chinese Medicine, The Affiliated Hospital of Nanjing University of Chinese Medicine, Nanjing, China, [3] Key Laboratory for Metabolic Diseases in Chinese Medicine, First College of Clinical Medicine, Nanjing University of Chinese Medicine, Nanjing, China

OPEN ACCESS

Edited by:
Jehad Ahmed Abubaker, Dasman Diabetes Institute, Kuwait

Reviewed by:
Junfeng Han, Shanghai Jiao Tong University, China
Mohamed El-Sherbiny, Almaarefa University, Saudi Arabia

***Correspondence:**
Wenbin Shang
wbshang@njucm.edu.cn

Specialty section:
This article was submitted to Diabetes: Molecular Mechanisms, a section of the journal Frontiers in Endocrinology

Received: *26 January 2022*
Accepted: *02 March 2022*
Published: *24 March 2022*

Citation:
Wei Y, Han S, Zhou R, Xu P, Zhou L, Zhu Z, Kan Y, Yang X, Xiang Y, Cao Y, Jin Y, Yan J, Yu X, Wang X and Shang W (2022) Increased Serum VEGF-B Level Is Associated With Renal Function Impairment in Patients With Type 2 Diabetes. Front. Endocrinol. 13:862545. doi: 10.3389/fendo.2022.862545

Aims/Introduction: Renal function impairment related to type 2 diabetes (T2DM) presents serious threat to public health. Previous studies suggest that vascular endothelial growth factor-B (VEGF-B) might contribute to renal injury. Therefore, this study investigated the association of serum VEGF-B level with the risk of renal function impairment in T2DM patients.

Materials and Methods: Serum VEGF-B levels were measured in 213 patients with type 2 diabetes and 31 healthy participants. Participants with type 2 diabetes were further divided into a group of 112 participants with eGFR<90 mL/min/1.73m^2 and 101 participants with eGFR≥ 90 mL/min/1.73m^2. Clinical data were collected, and a binary logistic regression model was employed to test the association between potential predictors and eGFR.

Results: Serum VEGF-B levels evaluated in type 2 diabetes patients compared with healthy controls. In patients with type 2 diabetes, serum VEGF-B level was positively correlated with triglyceride, serum creatinine and cystatin C while negatively correlated with HDL-C and eGFR. Binary logistic regression showed that serum VEGF-B level was an independent risk factor of eGFR<90 mL/min/1.73m^2.

Conclusions: Serum VEGF-B level is associated with renal function impairment in patients with type 2 diabetes and may be a potential drug target for diabetic kidney disease.

Keywords: vascular endothelial growth factor B, type 2 diabetes mellitus, diabetic kidney disease, glomerular filtration rate, cystatin C

INTRODUCTION

With the global prevalence of type 2 diabetes mellitus (T2DM), diabetic kidney disease (DKD) has become the leading cause of end stage renal disease (ESRD), and poses a great burden to diabetes patients and the health care system (1). Progressing renal function impairment characterized by declining glomerular filtration rate (GFR) runs through the course of T2DM, and eventually results in DKD. Multifactorial pathological processes have been proven to be contributors of diabetes-related renal function impairment, including advanced glycation end products (AGEs), ectopic lipid deposition, hemodynamic perturbations and inflammation (2, 3). However, further study is still required to explore the exact mechanisms underlying renal function impairment in T2DM patients.

Vascular endothelial growth factor-B (VEGF-B) is a member of the vascular endothelial growth factor (VEGF) family expressing in multiple organs, such as heart, adipose, muscle, brain, and kidney (4). Different with other members from VEGF family, VEGF-B shows faint angiogenic effect *in vivo*, which triggers a widespread speculation of VEGF-B playing its angiogenic role mainly through its recruitment of other VEGFs (5, 6). However, VEGF-B was reported to regulate fatty acid transport proteins (FATPs) in endothelial cells *via* membrane receptors neuropilin-1(NRP-1) or vascular endothelial growth factor receptor-1 (VEGFR-1), and an improvement of insulin sensitivity along with blood lipid profiles was observed in VEGF-B deficient mice fed with high-fat diet (4, 7). Moreover, the activation of VEGFR-1, one of the VEGF-B receptors, was demonstrated to promote the generation of pro-inflammatory and pro-angiogenic cytokines in macrophages and accelerate the process of inflammatory diseases, for instance, rheumatoid arthritis and retinal injury (8, 9). Seeing the coincidences between VEGF-B biological functions and diabetes-related renal function impairment, several studies reported that VEGF-B could directly impair podocyte insulin sensitivity by promoting ectopic lipid accumulation in podocytes and cause the occurrence of DKD in various diabetic mouse models (10, 11). Furthermore, a newly produced anti-VEGFB/IL22 fusion protein was found to be capable to ameliorate renal dysfunction in db/db mice recently (11).

Although evidences from animal experiments suggest the vital role of VEGF-B in DKD occurrence, the relationship between circulating VEGF-B level and renal function impairment in T2DM patients still remains unclear. In this study, we tested the serum VEGF-B levels of 213 T2DM patients as well as 31 healthy participants, and analyzed the potential link between serum VEGF-B levels and renal function of patients with T2DM. Our results would provide a better insight into the role of VEGF-B in the pathogenesis of diabetic renal impairment as well as the intervention of diabetic kidney disease.

METHODS

Subjects

31 healthy participants were recruited from the health examination center of the affiliated hospital of Nanjing university of Chinese medicine. None of the healthy participants had known metabolic disorders, kidney injury or other kind of diseases. 213 T2DM patients were recruited from the department of endocrinology of the affiliated hospital of Nanjing university of Chinese medicine. All participants with T2DM satisfied the world health organization 1999 criteria when diagnosed (12). This study was approved by the medical research ethics committee of the affiliated hospital of Nanjing university of Chinese medicine and carried out under the principles of the Declaration of Helsinki. Written informed consents were obtained from all participants.

Clinical Data Collection

All participants were admitted to the department of endocrinology. Detailed medical history and physical examination data, including gender, age, medicine usage, resting blood pressure, weight and height were obtained upon admission. Venous blood and midstream urine samples were collected at 6:00 a.m. from participants after 12 hours of fasting. The examination of total cholesterol (TC), triglyceride (TG), low density lipoprotein (LDL-C), high density lipoprotein (HDL-C), fasting blood-glucose (FBG), fasting C peptide (FCP), glycosylated hemoglobin (HbA1c), serum creatinine (SCr), blood urea nitrogen (BUN), Cystatin C (CysC), urine albumin-to-creatinine ratio (UACR) and 24-hour urine total protein (UTP) were performed at laboratory center of the affiliated hospital of Nanjing university of Chinese medicine. Body mass index (BMI) = body weight (kg)/the square of body height (m^2). Homeostasis model of assessment for insulin resistance (HOMA-IR) = fasting glucose (mmol/L)$\times$fasting insulin (mU/L)/22.5. Estimated glomerular filtration rate (eGFR) was calculated according to CKD-EPI2012scr-cys.

Serum VEGF-B Measurement

Fresh blood samples were stood at room temperature (22°C) for 30min and then centrifuged at 3000rpm for 10 min. The supernatant were collected as serum samples and stored at -80°C. Serum VEGF-B values were determined by human enzyme-linked immunosorbent assay (ELISA) kits (CB5521, Biorbyt, UK).

Statistical Analysis

Statistical analyses were performed using SPSS 25.0. All data were represented as mean ± standard deviation (SD), median with interquartile range (IQR) or percentage, as appropriate. Data that were not normally distributed, including Diabetes duration, FBG, HbA1c, HOMA-IR, Triglyceride, Total cholesterol, HDL-C, LDL-C, Serum creatinine, Blood urea nitrogen, Cystatin C, UACR, UTP, eGFR, Serum VEGF-B were logarithmically transformed before analysis. ANOVA and Mann-Whitney U tests were used for continuous variables distributed normally and asymmetrically, respectively. Chisquared test (χ^2) was employed for comparisons of categorical variables. The relationships between clinical indicators were examined using *Pearson* correlation, *Spearman* correlation or partial correlation. Binary logistic regression analysis was used to test the association between potential

predictors and eGFR. A p-value of <0.05 was indicated statistically significant.

RESULTS

Serum VEGF-B Level Elevates in T2DM Patients

The study recruited 244 eligible participants, including 213 patients explicitly diagnosed with T2DM at baseline and 31 healthy subjects seeking for routine examination. Fasting blood samples were collected from all participants and serum VEGF-B levels were tested. As shown in **Figure 1**, compared to the healthy controls, a significantly elevated level of serum VEGF-B was observed in T2DM patients (p<0.001).

Baseline Characteristics of Participants With T2DM

Based on the accepted eGFR cutoff value (90 mL/min/1.73m^2), we further divided the enrolled T2DM patients into a group of 112 participants with eGFR<90 mL/min/1.73m^2 and 101 participants with eGFR≥ 90 mL/min/1.73m^2 (13). Gender distribution, drinking history, smoking history, BMI, SBP, HbA1c, FPG, HOMA-IR, TC, TG, HDL-C, LDL-C, UCR and UTP were similar between the groups (all p>0.05). However, the eGFR<90 mL/min/1.73m^2 group had older age (p<0.001), longer diabetes duration (p=0.004), lower DBP (p=0.003), as well as worse renal dysfunction characterized by higher levels of SCr (p<0.001), BUN (p<0.001), CysC (p<0.001) and UACR (p=0.005). Most importantly, eGFR<90 mL/min/1.73m^2 group also showed a significantly increased level of serum VEGF-B (p=0.002) (**Table 1**). Upon the usage of medications, no significant difference was observed between 2 groups on the usage of metformin, sulfonylureas, pioglitazone, glucosidase inhibitors, GLP1rA (glucagon-like peptide 1 receptor agonists), DPP4 inhibitors, SGLT2 inhibitors, statins, insulin and ACEI/ARB (all p>0.05). But, a higher percentage of patients using beta-blockers (p=0.007) and Calcium channel blockers (p=0.039) in eGFR<90 mL/min/1.73m^2 group was showed by Chisquared test (**Table 2**).

Serum VEGF-B Level Significantly Associates With Renal Function Indicators in T2DM Patients

As shown in **Table 3**, in T2DM patients, serum VEGF-B level was positively correlated with triglyceride (r=0.172, p=0.013), serum creatinine (r=0.150, p=0.031) and cystatin C (r=0.245, p<0.001) while inversely correlated with HDL-C (r=-0.138, p=0.047) and eGFR (r=-0.205, p=0.003) after adjusting gender, age, smoking history, drinking history, diabetes duration and BMI. However, although partial correlation confirmed that VEGF-B level significantly associates with several renal function indicators (**Figures 2A–C**), no significant correlation was observed between serum VEGF-B and UACR nor UTP (both p>0.05).

Regression Model of eGFR in T2DM Patients

We further employed binary logistic regression analysis to analyze the associations between serum VEGF-B and the risk of eGFR<90 mL/min/1.73m^2. We found that serum VEGF-B level (p=0.002) was significant in predicting eGFR<90 mL/min/1.73m^2, even after controlling age, UACR, diabetes duration and diastolic pressure (based on the results from **Table 1**). Of the risk factors above, age (p<0.001) showed a significant, positive relationship with eGFR<90 mL/min/1.73m^2 as well (**Table 4** and **Figure 3**).

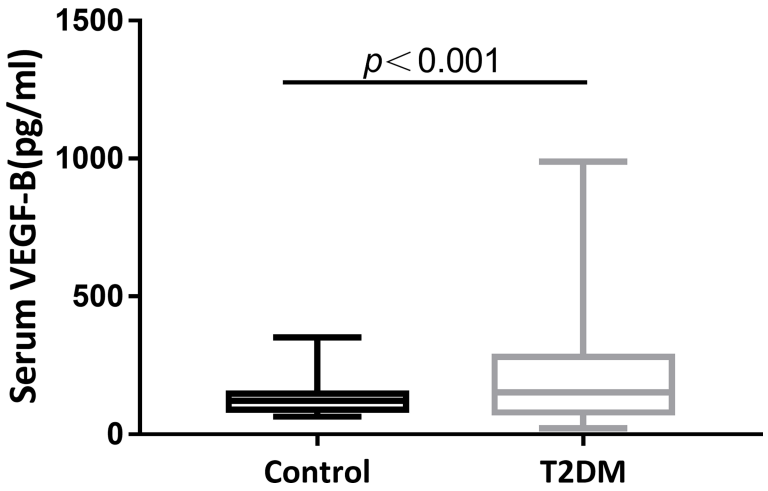

FIGURE 1 | Serum VEGF-B level elevates in T2DM patients. A significantly increase of serum VEGF-B levels in T2DM patients compared to healthy control subjects was observed (p < 0.001).

TABLE 1 | Anthropometric characteristics, clinical characteristics and VEGF-B levels.

Characteristic	eGFR<90 mL/min/1.73m^2(n = 112)	eGFR≥ 90 mL/min/1.73m^2(n = 101)	*p*-value
Female, n (%)	39 (34.82)	36 (35.64)	0.090[c]
Age (years)	66.00 (57.25, 72.00)	53.00 (46.00, 58.50)	<0.001[b]*
Smoking, n (%)	25 (22.32)	22 (21.78)	0.925[c]
Drinking, n (%)	12 (10.71)	20 (19.80)	0.064[c]
△Diabetes duration (years)	0.99 ± 2.06	1.77 ± 1.86	0.004[a]*
BMI (kg/m^2)	25.16 ± 3.23	25.42 ± 3.71	0.590[a]
△Systolic pressure (mmHg)	4.88 ± 0.13	4.91 ± 0.14	0.236[a]
Diastolic pressure (mmHg)	75.46 ± 10.35	79.96 ± 11.60	0.003[a]*
△FBG (mmol/L)	1.93 ± 0.35	1.91 ± 0.37	0.692[a]
△HbA1c (%)	2.17 ± 0.25	2.16 ± 0.26	0.670[a]
△HOMA-IR	1.11 ± 0.80	1.20 ± 0.86	0.424[a]
△Triglyceride (mmol/L)	0.55 ± 0.64	0.57 ± 0.61	0.281[a]
△Total cholesterol (mmol/L)	1.50 ± 0.24	1.47 ± 0.26	0.916[a]
△HDL-C (mmol/L)	0.16 ± 0.24	0.13 ± 0.27	0.262[a]
△LDL-C (mmol/L)	1.02 ± 0.32	1.00 ± 0.37	0.544[a]
△Serum creatinine (umol/L)	4.03 ± 0.21	4.33 ± 0.33	<0.001[a]*
△Blood urea nitrogen (mmol/L)	1.68 ± 0.27	1.88 ± 0.33	<0.001[a]*
△Cystatin C (mg/L)	-0.21 ± 0.13	0.20 ± 0.25	<0.001[a]*
△UACR (mg/g)	2.36 ± 1.22	2.94 ± 1.88	0.005[a]*
△UTP (mg/24h)	4.21 ± 0.98	4.43 ± 1.44	0.465[a]
△eGFR (mL/min/1.73m^2)	4.66 ± 0.10	4.22 ± 0.34	<0.001[a]*
△Serum VEGF-B (pg/mL)	4.80 ± 0.77	5.16 ± 0.84	0.002[a]*

BMI, body mass index; FBG, fasting blood-glucose; HDL-C, high density lipoprotein; LDL-C, low density lipoprotein; UACR, urine albumin-to-creatinine ratio; UTP, 24-hour urine total protein; eGFR, estimated glomerular filtration rate.
△Log-transformed before analysis.
**Significance, p < 0.05.*
[a]Student's t-test.
[b]Mann-Whitney U test.
[c]Chisquared test.

TABLE 2 | Medicine usage of T2DM patients recruited.

Use of medications	eGFR<90 mL/min/1.73m^2 (n = 112)	eGFR≥ 90 mL/min/1.73m^2 (n = 101)	*p*-value
Metformin, %	46.08%	44.55%	0.296
Sulfonylureas, %	27.45%	27.72%	0.167
Pioglitazone, %	5.88%	5.94%	0.551
Glucosidase inhibitors, %	24.51%	24.75%	0.440
GLP1rA, %	2.94%	2.97%	0.898
DPP4 inhibitors, %	25.49%	24.75%	0.115
SGLT2i, %	11.76%	11.88%	0.741
Statins, %	23.53%	23.76%	0.077
Insulin, %	65.69%	65.35%	0.911
ACEI/ARB, %	27.45%	27.72%	0.129
Beta-blockers, %	36.61%	19.80%	0.007*
CCB, %	35.71%	22.77%	0.039*
Diuretics, %	3.92%	3.96%	0.095

GLP1rA, glucagon-like peptide 1 receptor agonists; SGLT2i, sodium-glucose co-transporter 2 inhibitors; CCB, Calcium Channel Blockers.
**Significance, p < 0.05.*

DISCUSSION

Diabetic kidney disease is one of the leading complications of type 2 diabetes. Currently, the mechanisms underlying T2DM-related renal function impairment remains unclear, and the strategies of DKD prediction are still limited (14). In this study, we assessed whether serum VEGF-B, a biomarker from vascular endothelial growth factor family, was associated with progression of diabetes-related renal function impairment in 213 patients with established T2DM. Our results showed that elevated level of VEGF-B in T2DM patients was significantly correlated with markers of lipid metabolism and glomerular function. Regression model also indicated that serum VEGF-B was one of the independent risk factors of eGFR<90 mL/min/1.73m^2 in T2DM patients.

Previously, several studies have observed increased VEGF-B levels in DKD patients compared to healthy controls (10, 11). Our study further proved that, not only in DKD patients, just in T2DM population (only 28 of 213 T2DM patients fit the diagnostic criteria of DKD), a significantly rising level of serum

TABLE 3 | The correlation of serum VEGF-B (log-transformed) with clinical indicators in T2DM patients.

	Serum VEGF-B level	
	r	***p*-value**
Gender	0.013	0.853[a]
Age	0.070	0.308[b]
Smoking	-0.080	0.248[a]
Drinking	-0.003	0.962[a]
△Diabetes duration	0.130	0.059[a]
BMI	0.000	0.994[a]
△Systolic pressure	0.019	0.790[c]
Diastolic pressure	0.056	0.422[c]
△FBG	0.098	0.160[c]
△HbA1c	0.056	0.420[c]
△HOMA-IR	0.050	0.472[c]
△Triglyceride	0.172	0.013[c*]
△Total cholesterol	0.062	0.371[c]
△HDL-C	-0.138	0.047[c*]
△LDL-C	0.121	0.083[c]
△Serum creatinine	0.150	0.031[c*]
△Blood urea nitrogen	0.026	0.713[c]
△Cystatin C	0.245	<0.001[c*]
△UACR	0.025	0.721[c]
△UTP	-0.030	0.668[c]
△eGFR	-0.205	0.003[c*]

BMI, body mass index; FBG, fasting blood-glucose; HDL-C, high density lipoprotein; LDL-C, low density lipoprotein; UACR, urine albumin-to-creatinine ratio; UTP, 24-hour urine total protein; eGFR, estimated glomerular filtration rate.

△Log-transformed before analysis.

**Significance, $p < 0.05$.*

[a]Pearson correlation.

[b]Spearman correlation.

[c]Partial correlation analysis adjusted for gender, age, smoking history, drinking history, diabetes duration and BMI.

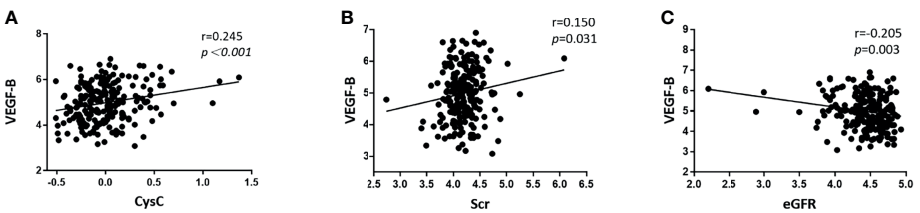

FIGURE 2 | Scatter diagrams showing the significant partial correlations between serum VEGF-B levels and renal function indicators in T2DM patients after adjusting for gender, age, smoking history, drinking history, diabetes duration and BMI. **(A)** The serum VEGF-B level was positively correlated with Cystatin C (r=0.245, $p < 0.001$); **(B)** The serum VEGF-B level was positively correlated with Scr (r=0.150, p=0.031); **(C)** The serum VEGF-B level was negatively correlated with eGFR (r=-0.205, p=0.003). All data was log-transformed before analysis.

VEGF-B could be marked. This may provide evidence for the hypothesis that VEGF-B might be a cause for T2DM-related renal function impairment rather than a result. A genome-wide association study demonstrated that the up-regulation of *vegf-b* is related to chronic kidney disease, T2DM, hypertension and hyperlipidemia (15). In animal models of diabetes, VEGF-B increment was found in various type of cells, such as choroidal cells and podocytes (10, 16). Furthermore, *vegf-b* overexpression impaired whereas *vegf-b* knockout rescued the insulin sensitivity and blood lipid profile of gene-edited mouse models (7, 17). Hence, we can assume that VEGF-B may be a future drug target of T2DM and the complications related with huge potential. In addition, a cross-sectional study involving 45 patients with newly diagnosed T2DM also showed an elevation of circulating VEGF-B level in newly diagnosed T2DM patients compared with healthy subjects, and the study exhibited a significantly correlation between circulating VEGF-B and markers of glucose metabolism as well (18). However, in our study, no significant correlation between serum VEGF-B and FBP nor HOMA-IR was observed, which may on account of the anti-diabetic drug usage. We will further expand the sample size and refine the groups to see if more evidence could be provided.

By correlation analysis, we also demonstrated that serum VEGF-B in T2DM patients was correlated with triglyceride and HDL-C, besides renal function markers. Consistent with our findings, Ye etc. found that circulating VEGF-B level was

TABLE 4 | Risk factors of eGFR<90 mL/min/1.73m^2 (Binary logistic regression).

Variables	B	SE	Wald	*p*-value	OR	95% CI	
△VEGF-B	0.619	0.202	9.376	0.002*	1.858	1.250	2.762
Age	0.121	0.021	32.468	<0.001*	1.129	1.083	1.177
Diabetes duration	-0.025	0.181	0.019	0.891	0.975	0.684	1.392
△UACR	0.188	0.119	2.499	0.114	1.207	0.956	1.524
△Diastolic pressure	-0.015	0.016	0.837	0.360	0.985	0.954	1.017

Reference category: IC negative.
OR, odds ratio; CI, confidence interval for the odds ratio.
△Log-transformed before analysis.

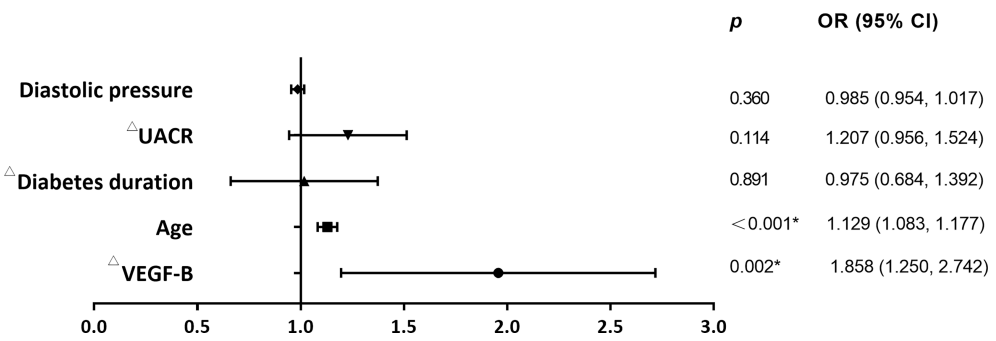

FIGURE 3 | Serum VEGF-B level is an independent risk factor for eGFR<90 mL/min/1.73m^2. As shown in the forest plots, binary logistic regression demonstrated that serum VEGF-B level and age are independent risk factors for eGFR<90 mL/min/1.73m^2. *Significance, p<0.05. △Log-transformed before analysis.

positively correlated with HDL-C and negatively correlated with eGFR in patients with non-alcoholic fatty liver disease (19). Disorder of lipid metabolism is an acknowledged contributor of diabetes-related renal function impairment (20). It has been proven that VEGF-B could destroy glomerular filtration barrier by inducing ectopic lipid deposition in podocyte, and VEGF-B antibody injection prevented renal lipotoxicity and further improved the renal function of db/db mice (10). Our results confirmed that serum VEGF-B is positively correlated with triglyceride and HDL-C while negatively correlated with eGFR, which supports the point that VEGF-B affects renal function of T2DM patients at least partially *via* regulating lipid metabolism.

It is well known that the classic characteristics of DKD are descending GFR and progressing albuminuria. However, epidemiological investigation exhibits a gradually increasing incidence rate of chronic kidney disease with normoalbuminuria in diabetic patients, especially type 2 diabetes, and the disease was recently referred to as normoalbuminuric diabetic kidney disease (NADKD) (21). Our data also showed that after grouping T2DM patients by eGFR, no difference could be seen in UTP between eGFR≥ 90 mL/min/1.73m^2 group and eGFR<90 mL/min/1.73m^2 group (the slight decline of UACR in eGFR<90 mL/min/1.73m^2 group may depend on the increase of creatinine). This could be partially explained by the limited sample size, but also, the phenomenon was consistent with the epidemic of NADKD in T2DM. Moreover, traditionally, albuminuria and diabetic retinopathy are important components of early DKD prediction and diagnosis. But increasing studies point out that substantial numbers of T2DM patients with DKD do not have retinopathy nor abnormal albuminuria, and normoalbuminuria T2DM patients with low GFR (<60 mL/min/1.73m^2) are more likely to show diffuse lesions, nodular lesions, tubulointerstitial lesions or vascular lesions compared to those with preserved GFR (≥60 mL/min/1.73m^2) (22, 23). And as such, more sensitive indicators are urgently needed for early diagnosis and intervention of DKD. In our research, we found that serum VEGF-B level in T2DM patients was positively correlated with SCr and CysC, while negatively correlated with eGFR and is an independent predictor of eGFR<90 mL/min/1.73m^2. Interestingly, no significant correlation between serum VEGF-B and UTP nor UACR was observed, which suggested that the relationship between serum VEGF-B level and renal function impairment in T2DM patients was independent of albuminuria, and the VEGF-B up regulation is likely to be a new mechanism underlying NADKD in T2DM patients.

Overall, in this study, we demonstrated that T2DM patients exhibited an elevated serum VEGF-B level, which was associated with renal function impairment. The increased serum VEGF-B level was an independent risk factor of eGFR<90 mL/min/1.73m^2 in patients with type 2 diabetes and it was irrelevant to albuminuria. However, certain limitations of this study should be noted. Firstly, owing to the difficulty in obtaining renal samples from T2DM patients, VEGF-B levels in serum were tested only, thus we are unable to trace the accurate source of the increasing VEGF-B. Secondly, the persuasion as well as the reproducibility of our findings might be blunted by the limited

sample size. Current chronic kidney disease nomenclature used by KDIGO is based on eGFR (G1-G5) along with albuminuria (A1-A3), but most of our cases were restricted at G1 and G2 stage, which made it far too difficult to further stage the patients by KDIGO standard. 90 mL/min/1.73m^2 is an eGFR cutoff value widely accepted by guidelines (13, 24). eGFR<90 mL/min/1.73m^2 usually indicates renal function impairment. By dividing T2DM patients into eGFR≥ 90 mL/min/1.73m^2 group and eGFR<90 mL/min/1.73m^2 group, we found a strong link between serum VEGF-B level and renal function impairment in T2DM patients. However, we will further expand the sample size in the future to explore the role of serum VEGF-B level in different stages of DKD. Lastly, as a cross-sectional research, this study was constrained in inferring causal relationships, and usage of medications was unavoidable in patients recruited. Although Chisquared test showed no significant differences in the usage of RAS inhibitors, SGLT2 inhibitors and statins between eGFR≥ 90 mL/min/1.73m^2 group and eGFR<90 mL/min/1.73m^2 group, which sharpens our observations, future studies designed in cohorts are still required to confirm the findings and to determine the role of VEGF-B in DKD pathology as well as whether serum VEGF-B level could be used for early prediction of DKD or NADKD.

DATA AVAILABILITY STATEMENT

The raw data supporting the conclusions of this article will be made available by the authors, without undue reservation.

ETHICS STATEMENT

The studies involving human participants were reviewed and approved by the medical research ethics committee of the affiliated hospital of Nanjing university of Chinese medicine. The patients/participants provided their written informed consent to participate in this study.

AUTHOR CONTRIBUTIONS

In this study, YW and WS designed the project, analyzed the data and wrote portions of the manuscript. SH, RZ, PX, LZ, ZZ, YK, XYY, YX, YC, and XW performed the collection of samples and data. YJ, JY and XZY performed the measurement of serum VGEF-B. WS guided the project and wrote portions of the manuscript. All authors are in agreement with the content of the manuscript, and the authors declare no conflict of interest. All authors contributed to the article and approved the submitted version.

FUNDING

The present study was supported by the open projects of the discipline of Chinese Medicine of Nanjing University of Chinese Medicine supported by the subject of academic priority discipline of Jiangsu higher education institutions (ZYX03KF058).

REFERENCES

1. Khan NU, Lin J, Liu X, Li H, Lu W, Zhong Z, et al. Insights Into Predicting Diabetic Nephropathy Using Urinary Biomarkers. *Biochim Biophys Acta Proteins Proteom* (2020) 1868(10):140475. doi: 10.1016/j.bbapap.2020.140475
2. Chen X, Yin Q, Ma L, Fu P. The Role of Cholesterol Homeostasis in Diabetic Kidney Disease. *Curr Med Chem* (2021) 28(36):7413–26. doi: 10.2174/0929867328666210419132807
3. Ricciardi CA, Gnudi L. Kidney Disease in Diabetes: From Mechanisms to Clinical Presentation and Treatment Strategies. *Metab Clin Exp* (2021) 124:154890. doi: 10.1016/j.metabol.2021.154890
4. Hagberg CE, Falkevall A, Wang X, Larsson E, Huusko J, Nilsson I, et al. Vascular Endothelial Growth Factor B Controls Endothelial Fatty Acid Uptake. *Nature* (2010) 464(7290):917–21. doi: 10.1038/nature08945
5. Uemura A, Fruttiger M, D'Amore PA, De Falco S, Joussen AM, Sennlaub F, et al. VEGFR1 Signaling in Retinal Angiogenesis and Microinflammation. *Prog Retin Eye Res* (2021) 84:100954. doi: 10.1016/j.preteyeres.2021.100954
6. Bry M, Kivelä R, Leppänen V-M, Alitalo K. Vascular Endothelial Growth Factor-B in Physiology and Disease. *Physiol Rev* (2014) 94(3):779–94. doi: 10.1152/physrev.00028.2013
7. Hagberg CE, Mehlem A, Falkevall A, Muhl L, Fam BC, Ortsäter H, et al. Targeting VEGF-B as a Novel Treatment for Insulin Resistance and Type 2 Diabetes. *Nature* (2012) 490(7420):426–30. doi: 10.1038/nature11464
8. Murakami M, Iwai S, Hiratsuka S, Yamauchi M, Nakamura K, Iwakura Y, et al. Signaling of Vascular Endothelial Growth Factor Receptor-1 Tyrosine Kinase Promotes Rheumatoid Arthritis Through Activation of Monocytes/Macrophages. *Blood* (2006) 108(6):1849–56. doi: 10.1182/blood-2006-04-016030
9. Ogura S, Kurata K, Hattori Y, Takase H, Ishiguro-Oonuma T, Hwang Y, et al. Sustained Inflammation After Pericyte Depletion Induces Irreversible Blood-Retina Barrier Breakdown. *JCI Insight* (2017) 2(3):e90905. doi: 10.1172/jci.insight.90905
10. Falkevall A, Mehlem A, Palombo I, Heller Sahlgren B, Ebarasi L, He L, et al. Reducing VEGF-B Signaling Ameliorates Renal Lipotoxicity and Protects Against Diabetic Kidney Disease. *Cell Metab* (2017) 25(3):713–26. doi: 10.1016/j.cmet.2017.01.004
11. Shen Y, Chen W, Han L, Bian Q, Fan J, Cao Z, et al. VEGF-B Antibody and Interleukin-22 Fusion Protein Ameliorates Diabetic Nephropathy Through Inhibiting Lipid Accumulation and Inflammatory Responses. *Acta Pharm Sin B* (2021) 11(1):127–42. doi: 10.1016/j.apsb.2020.07.002
12. Alberti KG, Zimmet PZ. Definition, Diagnosis and Classification of Diabetes Mellitus and Its Complications. Part 1: Diagnosis and Classification of Diabetes Mellitus Provisional Report of a WHO Consultation. *Diabet Med* (1998) 15(7):539–53. doi: 10.1002/(SICI)1096-9136(199807)15:7<539::AID-DIA668>3.0.CO;2-S
13. Levin A, Stevens PE, Bilous RW, Coresh J, De Francisco ALM, De Jong PE, et al. Kidney Disease: Improving Global Outcomes (KDIGO) CKD Work Group. KDIGO 2012 Clinical Practice Guideline for the Evaluation and Management of Chronic Kidney Disease. *Kidney Int Suppl* (2013) 3:1–150. doi: 10.1038/kisup.2012.73
14. Sugahara M, Pak WLW, Tanaka T, Tang SCW, Nangaku M. Update on Diagnosis, Pathophysiology, and Management of Diabetic Kidney Disease. *Nephrol (Carlton)* (2021) 26(6):491–500. doi: 10.1111/nep.13860
15. Shungin D, Winkler TW, Croteau-Chonka DC, Ferreira T, Locke AE, Mägi R, et al. New Genetic Loci Link Adipose and Insulin Biology to Body Fat Distribution. *Nature* (2015) 518(7538):187–96. doi: 10.1038/nature14132
16. Huang D, Zhao C, Ju R, Kumar A, Tian G, Huang L, et al. VEGF-B Inhibits Hyperglycemia- and Macugen-Induced Retinal Apoptosis. *Sci Rep* (2016) 6:26059. doi: 10.1038/srep26059
17. Karpanen T, Bry M, Ollila HM, Seppänen-Laakso T, Liimatta E, Leskinen H, et al. Overexpression of Vascular Endothelial Growth Factor-B in Mouse

Heart Alters Cardiac Lipid Metabolism and Induces Myocardial Hypertrophy. *Circ Res* (2008) 103(9):1018–26. doi: 10.1161/CIRCRESAHA.108.178459
18. Wu J, Wei H, Qu H, Feng Z, Long J, Ge Q, et al. Plasma Vascular Endothelial Growth Factor B Levels Are Increased in Patients With Newly Diagnosed Type 2 Diabetes Mellitus and Associated With the First Phase of Glucose-Stimulated Insulin Secretion Function of β-Cell. *J Endocrinol Invest* (2017) 40 (11):1219–26. doi: 10.1007/s40618-017-0677-z
19. Ye X, Kong W, Zafar MI, Zeng J, Yang R, Chen L-L. Plasma Vascular Endothelial Growth Factor B Is Elevated in Non-Alcoholic Fatty Liver Disease Patients and Associated With Blood Pressure and Renal Dysfunction. *EXCLI J* (2020) 19:1186–95. doi: 10.17179/excli2020-2647
20. Tuttle KR, Bakris GL, Bilous RW, Chiang JL, de Boer IH, Goldstein-Fuchs J, et al. Diabetic Kidney Disease: A Report From an ADA Consensus Conference. *Am J Kidney Dis* (2014) 64(4):510–33. doi: 10.1053/j.ajkd.2014.08.001
21. Chen C, Wang C, Hu C, Han Y, Zhao L, Zhu X, et al. Normoalbuminuric Diabetic Kidney Disease. *Front Med* (2017) 11(3):310–8. doi: 10.1007/s11684-017-0542-7
22. Shimizu M, Furuichi K, Toyama T, Kitajima S, Hara A, Kitagawa K, et al. Long-Term Outcomes of Japanese Type 2 Diabetic Patients With Biopsy-Proven Diabetic Nephropathy. *Diabetes Care* (2013) 36(11):3655–62. doi: 10.2337/dc13-0298
23. Shimizu M, Furuichi K, Yokoyama H, Toyama T, Iwata Y, Sakai N, et al. Kidney Lesions in Diabetic Patients With Normoalbuminuric Renal Insufficiency. *Clin Exp Nephrol* (2014) 18(2):305–12. doi: 10.1007/s10157-013-0870-0
24. Tomson CRV, Cheung AK, Mann JFE, Chang TI, Cushman WC, Furth SL, et al. Management of Blood Pressure in Patients With Chronic Kidney Disease Not Receiving Dialysis: Synopsis of the 2021 KDIGO Clinical Practice Guideline. *Ann Intern Med* (2021) 174(9):1270–81. doi: 10.7326/M21-0834

Conflict of Interest: The authors declare that the research was conducted in the absence of any commercial or financial relationships that could be construed as a potential conflict of interest.

frontiers | Frontiers in Endocrinology

ORIGINAL RESEARCH
published: 11 May 2022
doi: 10.3389/fendo.2022.824279

Serum Cystatin C Trajectory Is a Marker Associated With Diabetic Kidney Disease

Nana Wang[1], Zhenyu Lu[2], Wei Zhang[1], Yu Bai[1], Dongmei Pei[2†] and Ling Li[1*†]*

[1] Endocrinology Department, Shengjing Hospital of China Medical University, Shenyang, China, [2] Department of Health Management, Shengjing Hospital of China Medical University, Shenyang, China

Objective: To explore the association of the trajectory of serum Cystatin C (Cysc) with diabetic kidney disease (DKD), a retrospective cohort study of Chinese subjects was carried out.

Method: A review of 2,928 diabetes mellitus (DM) patients admitted to the clinic and ward of the Endocrinology Department, Shengjing Hospital of China Medical University from January 1, 2014 to December 31, 2014 was performed. Subsequent visits to the hospital were followed until December 31, 2020. The primary endpoint was the incidence of DKD as diagnosed by urinary albumin/creatinine ratio ≥30 mg/g and/or estimated glomerular filtration rate <60 ml/min per 1.73 m^2. Healthy control subjects were identified from a health checkup database in Shengjing Hospital from 2016 to 2019. The latent class growth mixed modeling (LCGMM) method was used to analyze latent classes of serum Cysc in healthy and DM subjects. Finally, the hazard ratios (HRs) of latent classes of Cysc in DM subjects were analyzed by Cox regression analysis.

Results: A total of 805 type 2 diabetes mellitus (T2DM) and 349 healthy subjects were included in the trial. The HRs of quartiles of baseline Cysc in T2DM subjects were 7.15 [95% confidence interval (CI), 2.79 to 25.57], 2.30 (95% CI, 1.25 to 4.24), and 2.05 (95% CI, 1.14 to 3.70), respectively, for quartile 4 (Q4), Q3, and Q2 when compared with Q1. Through LCGMM, a 1-class linear model was selected for the Cysc latent class in healthy subjects. In contrast, a 3-class linear model was selected for that in DM subjects. The slopes of the three latent classes in T2DM subjects were larger than the slope in healthy subjects. The HRs of incident DKD were 3.43 (95% CI, 1.93 to 6.11) for the high-increasing class and 1.80 (95% CI, 1.17 to 2.77) for the middle-increasing class after adjusting for confounding variables.

Conclusions: Patients with T2DM had a higher velocity of increase in Cysc than healthy subjects. Patients with high baseline Cysc values and high latent increasing velocity of Cysc had a higher risk of developing DKD in later life. More attention should be paid to patients with these high-risk factors.

Keywords: cystatin C, diabetic kidney disease, latent class growth mixed modeling, trajectory, velocity

OPEN ACCESS

Edited by:
Katsumi Iizuka,
Fujita Health University, Japan

Reviewed by:
Jingyu Wang,
Tianjin Medical University, China
Mehmet Zahid Kocak,
Meram Faculty of Medicine, Turkey
Rajesh Kathrotia,
All India Institute of Medical Sciences, Rajkot, India

***Correspondence:**
Dongmei Pei
peidm@sj-hospital.org
Ling Li
liling@sj-hospital.org

[†]These authors have contributed equally to this work

Specialty section:
This article was submitted to Diabetes: Molecular Mechanisms, a section of the journal Frontiers in Endocrinology

Received: *29 November 2021*
Accepted: *04 April 2022*
Published: *11 May 2022*

Citation:
Wang N, Lu Z, Zhang W, Bai Y, Pei D and Li L (2022) Serum Cystatin C Trajectory Is a Marker Associated With Diabetic Kidney Disease. Front. Endocrinol. 13:824279. doi: 10.3389/fendo.2022.824279

INTRODUCTION

Diabetic kidney disease (DKD) is one of the major chronic microvascular complications in diabetes mellitus (DM) and a main cause of end-stage renal disease (ESRD). It accounts for almost half of all incident cases of ESRD in DKD patients (1). Chronic kidney disease caused by DM is defined by a persistent estimated glomerular filtration rate (eGFR) of <60 ml/min per 1.73 m^2 or a urinary albumin/creatinine ratio (UACR) of >30 mg/g for more than 3 months (2). Repeated assessment of UACR in two to three samples together with the eGFR is regarded as the best standard screening for DKD (3). However, recent studies show that DKD can occur without increased albuminuria. The Diabetes Control and Complications Trial (DCCT)/Epidemiology of Diabetes Interventions and Complications (EDIC) study demonstrated that 24% of new-onset DKD patients with type 1 diabetes mellitus (T1DM) progressed to eGFR < 60 ml/min per 1.73 m^2 but had albumin excretion rates < 30 mg/24 h at all prior evaluations (4). This indicates that the current standard screening of albuminuria may miss some DKD patients. Moreover, in most cases, decreased eGFR is not an earlier biomarker than proteinuria in the early diagnosis of DKD. Therefore, neither albuminuria nor eGFR is an early sensitive marker of DKD. Because of the severity and heavy burden of DKD, early diagnosis is a crucial topic in the prevention and treatment of DM. Therefore, a new biomarker for early diagnosis of DKD is necessary.

Cystatin C (Cysc) is a low-molecular-weight protein (13 kDa) (5) and is a member of the cystatin superfamily of cysteine proteinase inhibitors. It is produced by all nucleated cells at a constant rate (6). Recently, several studies showed that serum Cysc is a better marker of declining GFR in DM patients than serum creatinine (Scr) (7). Most of the evidence came from cross-sectional studies demonstrating that serum Cysc levels in DKD patients were significantly higher when compared to those in DM cases without DKD (8–10). The elevation of Cysc was correlated with decreased GFR and elevated UACR (11, 12), and serum Cysc performed better compared with Scr and albuminuria in detecting mild diabetic nephropathy (13, 14). In addition, equations using Cysc to calculate eGFR were better than equations using creatinine at predicting the mild stage of chronic kidney disease for DM patients (15–17), indicating that Cysc may be a potential biomarker for early diagnosis of DKD (18). Limited short-term longitudinal analysis demonstrated that Cys-eGFR equations predict GFR changes better in 2 years (19), and serum Cysc correlates with renal function decline in T1DM in 1 year (20). Meanwhile, some investigations held opposite views. A study by Iliadis et al. in 488 type 2 diabetes mellitus (T2DM) patients in Greece showed that eGFRcys did not provide better GFR estimation than eGFRcre (21). Another study by Oddoze et al. showed that serum Cysc is not better than Scr for estimating GFR in patients with steady-state diabetes using ROC curves (22). Nevertheless, Cysc is a promising new biomarker for diagnosis of DKD. Until now, large, long-term longitudinal studies monitoring Cysc in the incidence of DKD have not been performed. In particular, the dynamic changes of Cysc in healthy and DM subjects throughout their lifetime are overlooked.

In this study, we included 805 T2DM subjects without DKD at baseline, and followed them for 6 years, analyzing the trajectory of Cysc increase and its association with the incidence of DKD. We also compared the velocity of increase of Cysc in healthy and T2DM subjects in their lifetime. To our knowledge, this is the first investigation to compare the latent trajectory of serum Cysc in healthy and T2DM subjects by latent class growth mixed modeling (LCGMM) with a long follow-up, and provide a new insight into the association of Cysc trajectory with an incidence of DKD.

MATERIALS AND METHODS

Subjects

We reviewed 2,928 DM patients admitted to the clinic and ward of the Endocrinology Department, Shengjing Hospital of China Medical University from January 1, 2014 to December 31, 2014. Subsequent visits to the clinic and ward in the hospital were followed until December 31, 2020. All the patients came from four provinces of China, including Liaoning, Jilin, Heilongjiang, and Neimenggu.

Subjects with T2DM, aged 18–70 years, were included in the study. The exclusion criteria were as follows: T1DM, baseline UACR ≥30 mg/g, baseline eGFR <60 ml/min per 1.73 m^2, a diagnosis of DKD in the hospital information system (HIS) record at baseline, severe liver dysfunction, history of malignancy, hyperthyroidism, hypothyroidism, pregnancy, missing data for UACR, Cysc or Scr, less than 3 visits, or missing endpoint data in 2019–2020. Subjects' data after diagnosis of DKD were excluded from the analyses.

Healthy subjects were collected from a health checkup database in Shengjing Hospital. In this project, subjects received health checkups every year from 2016 to 2019. We collected Cysc data of subjects from 2016 to 2019 and excluded subjects with diagnosed or new-onset pre-diabetes, DM, hypertension, thyroid disease, malignancy, pregnancy, other diagnosed diseases, or less than 3 visits.

All studies were approved by the Ethical Review Committee of Shengjing Hospital of China Medical University (No. 2019PS089J for health checkup trial and No. 2021PS755K for DKD trial) and conducted in accordance with the guidelines of the Declaration of Helsinki. Written informed consent was obtained from each participant.

Data Collection

Data were collected for age, height, systolic and diastolic blood pressure (SBp and DBp, respectively), and biochemical indices including serum Cysc, UACR, HbA_{1c}, fasting plasma glucose (FPG), serum lipid, liver function, and kidney function. Present history, previous history, personal history, and family history were collected from the HIS.

Serum Cysc was measured by latex-enhanced immunoturbidimetric assay (Beijing Strong Biotechnologies, Inc., Beijing, China). Serum and urine creatinine were determined using an enzymatic method (Kyowa Medex Co., Ltd, Tokyo, Japan). Urea microalbumin was detected by immunoturbidimetric assay (Beckman Coulter, Inc., CA, USA). The eGFR was

calculated according to CKD-EPI under the advice of ADA2021 (23). The following equations were used (24):

	Scr (mg/dl)	Equation (ml/min per 1.73 m^2)
Female	≤0.7	$144 \times (Scr/0.7)^{-0.329} \times 0.993^{age}$
	>0.7	$144 \times (Scr/0.7)^{-1.209} \times 0.993^{age}$
Male	≤0.9	$141 \times (Scr/0.9)^{-0.411} \times 0.993^{age}$
	>0.9	$141 \times (Scr/0.9)^{-1.209} \times 0.993^{age}$

Definitions

In the study, patients with symptoms of diabetes and either a random blood glucose ≥11.1 mmol/L, a fasting blood glucose (FBG) ≥7 mmol/L, or a 2-h blood glucose (BG) ≥11.1 mmol/L following an oral glucose tolerance test (OGTT) (based on 1999 World Health Organization standards for T2DM), or those who were using glucose-lowering drugs were considered to have T2DM.

DKD was diagnosed based on case history, clinical manifestation, and laboratory examinations. Subjects with UACR ≥300 mg/g and/or eGFR <60 ml/min per 1.73 m^2 were diagnosed with DKD. Patients with active urinary sediment, rapid progression of albuminuria or nephrotic syndrome, rapidly decreasing eGFR, or the absence of retinopathy were referred to nephrologists for further diagnosis (23).

Statistical Analysis

Continuous data are presented as mean ± standard deviation (SD) or means with 95% confidence intervals (CIs) and categorical variables as frequencies. Age and DM durations across different groups were assessed using Student's *t*-test for two groups and ANOVA for three groups. Differences between other continuous variables were assessed by covariance analysis adjusting by age and DM duration. The χ^2 test was used for difference of gender between groups. Logistic analysis between groups for other categorical variables was adopted, adjusting for age and DM duration and gender. Time-dependent Cox regression model was used to explore the hazard ratios (HRs) and 95% CIs of quartiles of baseline Cysc and latent trajectory classes for incident DKD, with Model 1 remaining unadjusted; Model 2 adjusted for baseline age, gender, and DM duration; and Model 3 adjusted for baseline age, gender, DM duration, smoker, FPG, HbA1c, total cholesterol (TC), triglycerides (TG), urea, uric acid (UA) and Scr. TG and urea were analyzed as time-dependent variables in Model 3. All statistical analyses were performed using the IBM SPSS Statistics 24 software (IBM Corp., Armonk, NY, USA). $p < 0.05$ was considered statistically significant. Time-dependent Cox regression model was conducted using R software (Version 4.0.3, survival package).

Estimations of latent class models were performed using the lcmm package (version 1.9.2) in R (25). LCGMM consists in assuming that the population is heterogeneous and composed of *G* latent classes of subjects characterized by *G* mean profiles of trajectories. Each subject belongs to one and only one latent class. Cysc trajectories were assumed as functions of age in healthy subjects and assumed as a function of DM duration adjusted for age in T2DM subjects. For computation and interpretation purposes, age and DM duration were replaced by age/100 and duration/100. It made the interpretation of the intercepts easier and reduced numerical problems due to very large ages and DM durations in the models. During the model-fitting process, we tested a series of class numbers from 1 to 5, and a series of linear, quadratic, and cubic curves. LCGMM models with 2 or 5 classes were performed several times with a series of random starting values based on the 1-class model. The optimal numbers of classes and curve shapes were determined using Bayesian information criterion (BIC) and mean posterior probabilities as the following criteria: BIC decreased at least 20, high mean posterior class membership probabilities (>0.65), and high mean posterior probabilities (>0.7) (26–28). Finally, according to LCGMM parameters, a 1-class linear model was selected for healthy subjects and a 3-class linear model was selected as the best fit for T2DM subjects, and the final model was described as:

$$Cysc(\text{healthy})_{ij} = (\upsilon_0 + u_{0i}) + (\upsilon_1 + u_{1i})\text{duration} + \epsilon_{ij}$$

$$Cysc(\text{DM})_{ij} = (\upsilon_{0g} + u_{0ig}) + (\upsilon_{1g} + u_{1ig})\text{duration} + \epsilon_{ij}$$

where Cys_{ij} is the outcome value at occasion *j* that is measured at time t_{ij} of the individual "*i*", $\upsilon = (\upsilon_{0g}, \upsilon_{1g})$ is a vector of fixed-effect parameters in the group "*g*", $u = (\upsilon_{0ig}, u_{1ig})$ is a vector of random-effect parameters of the individual "*i*" in the group "*g*", and ε_{ij} is an unknown error term.

LCGMM computed fixed-effect parameters (for a class) and random-effect parameters (for an individual). In each latent class, the longitudinal Cysc outcome followed a linear mixed model, including continuous time and intercept in the linear model in the study, with class-specific fixed effects and correlated random effects. Fixed effects represented class-specific mean-predicted parameters. The random effect (Gaussian random deviations) represented the differences between the class-specific fixed effect and the observed values for each individual.

RESULTS

Relationship of Serum Cysc With eGFR and UACR

We included 2,924 DM patients between January 1, 2014 and December 31, 2014. At baseline, 1,979 subjects were excluded. Among them, 449 were excluded due to age >70 years, 92 were excluded based on diagnosis of T1DM, 206 were excluded due to UACR ≥30 mg/g, 23 were excluded because of eGFR<60 ml/min per 1.73 m^2, 1,036 patients were excluded due to previously diagnosed DKD, 2 were excluded due to severe liver dysfunction, 92 were excluded due to malignancy, 73 were excluded because of missing indices, and 6 were excluded based on pregnancy. In the follow-ups, 140 subjects were excluded. Among them, 93 subjects with <3 visits were excluded, 2 were excluded because of pregnancy, 9 were excluded due to malignancy, 4 were excluded because of other nephropathies, and 32 with missing endpoint data were excluded. Finally, 805 subjects were included in the trial, with a mean age of 52.1 (± 10.0) years; 459 were men (57.0%).

At the beginning, we computed the latent trajectory of eGFR and UACR by serum Cysc using LCGMM in T2DM subjects, respectively. According to parameters of BIC and mean posterior probabilities, a 1-class quadratic model was selected as the best-fit model for eGFR and a 1-class cubic model for UACR. As shown in **Figure S1**, at 1.1 mg/L of serum Cysc, which is the upper limit of normal reference value (usually, the upper limit of reference is approximately 1.0–1.1 mg/L in different laboratories), the corresponding eGFR and UACR were 98.9 ml/min per 1.73 m^2 and 16.2 mg/g, respectively. It meant that the increase in serum Cysc was earlier than the clinical diagnosis of DKD by eGFR and UACR. Model parameters are presented in **Tables S1–S4** in the **Supplementary Material**.

Baseline and Follow-Up Characteristics of Subjects by DKD Incidence

Then, in order to explore the association of Cysc with DKD prevalence, we divided subjects with T2DM into non-DKD and DKD groups by incidence of DKD in the years 2019–2020. **Table 1** presents the baseline characteristics of the DKD and non-DKD groups. Subjects in the DKD group were older and had longer DM duration. In the statistical analysis, covariance analysis was used, adjusted for age and DM duration. At baseline, subjects in the DKD group had higher levels of Cysc, UACR, HbA1c, FPG, TC, TG, urea, and UA, and had a higher proportion of smokers. In the follow-up analysis by incidence of DKD, subjects in the DKD group had a higher Cysc, Scr, body mass index (BMI), DBp, HbA1c, FPG, urea, and UA; a lower eGFR; and a longer DM duration.

Hazard Ratios of Quartiles of Baseline Serum Cysc

In the study, the subjects were first designated to 4 quartiles according to baseline Cysc levels. Quartile 1 (Q1) ranged from 0.53 to 0.77 mg/L, Q2 ranged from 0.78 to 1.02 mg/L, Q3 ranged from 1.03 to 1.27 mg/L, and Q4 was greater than 1.28 mg/L. Next, the HRs of the quartiles of Cysc were analyzed for incident DKD. As shown in **Table 2**, in Model 1, the HRs were 1.56 (95% CI, 1.01 to 2.40), 2.35 (95% CI, 1.45 to 3.79), and 9.16 (95% CI, 3.70 to 22.65), respectively, for Q2, Q3, and Q4, when unadjusted. After adjusting for baseline age, gender, and DM duration in Model 2, the HRs were 1.44 (95% CI, 0.93 to 2.24), 1.92 (95% CI, 1.15 to 3.21), and 6.69 (95% CI, 2.65 to 16.87) for Q2, Q3, and Q4, respectively. The Q4 quartile maintained an HR of 7.15 (95% CI, 2.79 to 25.57) after adjusting for baseline age, gender, DM duration, smoker, HbA1c, TC, TG, Urea, UA, and AST in Model 3. The HRs for variables in Model 3 are listed in **Table S5**. The analysis identified Cysc, age, DM duration, HbA1c, UA, aspartate transaminase (AST), DBP, smoker, and urea as risk factors for incidence of DKD.

Trajectory of Cysc in Healthy and T2DM Subjects

Healthy subjects from the health checkup database from January 1, 2016 to December 31, 2019 were reviewed. A total of 5,365 subjects had their health checkups for the first time in 2016, and then came back for annual checkups, and were followed for 3 years until 2019. Subjects with diagnosed or new-onset pre-diabetes, DM, hypertension, thyroid disease, malignancy, pregnancy, and other diagnosed diseases and ≤3 visits were excluded. Finally, 349 subjects (142 men, 50.7 ± 3.5 years) were analyzed for trajectory of Cysc. After computing Cysc trajectory by age, testing different classes from 1 to 3, and a series of initial values, according to the parameters of BIC and mean posterior probabilities, a one-class linear model was selected as the best-fit model. As shown in **Figure 1A**, Cysc values increase with age continually. Therefore, in the following analysis, age is considered a confounding variable. Model parameters are presented in **Tables S6, S7** in the **Supplementary Material**. Baseline characteristics of healthy subjects are listed in **Table S8**.

Meanwhile, HCGMM was used to analyze the trajectory of Cysc in DM patients. The trajectory of Cysc was computed by DM durations and adjusted for the covariate of age. After testing different classes from 1 to 5 and different initial values, according to parameters of BIC and mean posterior probabilities, a 3-class linear model was selected as the best-fit model for Cysc trajectory. There were 55 subjects in the high-increasing class, 193 subjects in the middle-increasing class, and 557 subjects in the low-increasing class. As shown in **Figure 1B**, the mean Cysc in the high-increasing class initiated from 0.93 mg/L, with corresponding values of 0.86 mg/L and 0.81 mg/L in the middle- and low-increasing classes, respectively. Cysc in the high-increasing class was increasing at a higher slope at all time points than that in the middle- and low-increasing classes. The slopes of all three classes of DM subjects were higher than that of normal subjects. Model parameters for Cysc in DM subjects are presented in **Tables S9, S10** in the **Supplementary Material**.

Baseline Characteristics of Latent Classes of Cysc

Table 3 presents the baseline characteristics of 3 latent classes of Cysc. Subjects in the high-increasing and middle-increasing classes had a higher proportion of male subjects, increased age, and shorter DM duration. Therefore, in the subsequent statistical analysis, we used covariance analysis, adjusted by gender, age, and DM duration. After analysis, at baseline, subjects in the middle-increasing and high-increasing classes had higher BMI, SBp, UACR, HbA1c, FPG, cholesterol, urea, uric acid, and Cysc, and lower eGFR. In follow-up analysis by incidence of DKD, subjects in the middle-increasing and high-increasing classes had a higher proportion of incidence of DKD. The baseline and follow-up characteristics of sub-classes by incidence of DKD are listed in **Table S11**.

HRs of Latent Classes of Cysc

Finally, we used Cox regression to analyze the HRs for DKD incidence in each latent trajectory class of Cysc. As shown in **Table 4**, in Model 1, the HRs in the high-increasing class and middle-increasing class were 1.45 (95% CI, 0.87 to 2.403) and 1.44 (95% CI, 1.06 to 1.98), respectively, when unadjusted.

TABLE 1 | Baseline and follow-up characteristics by incidence of DKD.

	Non-DKD	DKD	*p*
Baseline			
N (805)	609	196	
Male [% (*n*)]	55.8 (340)	60.7 (119)	0.23
Age (years)	51.6 (10.0)	53.8 (9.7)	0.005
Duration (years)	6.7 (6.0)	9.4 (6.1)	<0.001
BMI (kg/m^2)	25.5 (25.2, 25.8)	25.9 (25.3, 26.4)	0.24
SBP (mmHg)	127.6 (126.3, 129.0)	129.6 (127.2, 132.0)	0.167
DBP (mmHg)	81.6 (80.7, 82.5)	83.2 (81.6, 84.8)	0.101
Family history [Yes, % (*n*)]	41.4 (252)	40.3 (79)	0.791
Smoker [Yes, % (*n*)]	17.4 (106)	28.1 (55)	0.001
Drinker [Yes, % (*n*)]	11.0 (67)	13.3 (26)	0.389
HBP [Yes, % *n*)]	36.5 (222)	41.3 (81)	0.979
CHD [Yes, % (*n*)]	11.3 (69)	15.8 (31)	0.995
INFAR [Yes, % (*n*)]	4.6 (28)	4.6 (9)	0.674
UACR (mg/g)	8.7 (8.1, 9.2)	13.6 (12.6, 14.6)	<0.001
HbA1c (%)	8.1 (7.9, 8.2)	9.1 (8.8, 9.4)	<0.001
FPG (mmol/L)	8.8 (8.5, 9.0)	10.0 (9.6, 10.4)	<0.001
TC (mmol/L)	4.76 (4.69, 4.84)	4.94 (4.80, 5.08)	0.037
TG (mmol/L)	2.53 (2.28, 2.77)	3.21 (2.78, 3.63)	0.007
HDL (mmol/L)	1.07 (1.04, 1.09)	1.04 (1.00, 1.08)	0.281
LDL (mmol/L)	2.95 (2.88, 3.02)	2.95 (2.83, 3.07)	0.981
Urea (mmol/L)	5.3 (5.1, 5.4)	5.7 (5.5, 5.9)	0.001
UA (μmol/L)	304.4 (298.1, 310.8)	323.4 (311.8, 336.0)	0.005
Scr (μmol/L)	60.7 (59.6, 61.7)	62.7 (60.8, 64.5)	0.078
CysC (mg/L)	0.90 (0.89, 0.91)	0.94 (0.92, 0.96)	<0.001
eGFR (ml/min per 1.73 m^2)	105.3 (104.6, 106.0)	104.2 (102.9, 105.4)	0.135
Alb (g/L)	42.7 (42.5, 43.0)	43.6 (43.1, 44.0)	0.004
AST (U/L)	20.0 (18.4, 21.5)	23.3 (20.6, 26.1)	0.04
ALT (U/L)	25.5 (24.2, 26.9)	27.1 (24.7, 29.5)	0.267
Follow-up			
Follow-up time (years)	5.1 (1.4)	4.2 (1.8)	<0.001
Age (years)	56.8 (9.7)	57.2 (10.9)	0.200
Duration (years)	11.8 (6.1)	13.5 (6.3)	0.001
BMI (kg/m^2)	24.7 (24.4, 25.0)	26.6 (26.0, 27.2)	<0.001
SBP (mmHg)	131.8 (130.0, 133.6)	133.7 (130.3, 137.0)	0.336
DBP (mmHg)	77.9 (76.9, 79.0)	82.5 (80.5, 84.4)	<0.001
UACR (mg/g)	10.5 (8.5, 12.4)	51.9 (48.5, 55.3)	<0.001
HbA1c (%)	7.8 (7.7, 8.0)	8.5 (8.2, 8.7)	<0.001
FPG (mmol/L)	8.0 (7.7, 8.2)	9.3 (8.8, 9.8)	<0.001
TC (mmol/L)	4.60 (4.51, 4.68)	4.65 (4.51, 4.80)	0.507
TG (mmol/L)	2.13 (1.98, 2.28)	2.38 (2.11, 2.65)	0.117
HDL (mmol/L)	1.10 (1.07, 1.12)	1.11 (1.07, 1.16)	0.533
LDL (mmol/L)	2.77 (2.71, 2.83)	2.77 (2.66, 2.88)	0.0945
Urea (mmol/L)	5.18 (5.07, 5.29)	5.66 (5.47, 5.85)	<0.001
UA (μmol/L)	320.0 (312.7, 327.2)	350.1 (337.0, 363.3)	<0.001
Scr (μmol/L)	61.7 (60.6, 62.9)	64.5 (62.4, 66.6)	0.026
CysC (mg/L)	0.90 (0.89, 0.91)	0.95 (0.93, 0.97)	<0.001
eGFR (ml/min per 1.73 m^2)	100.7 (99.7, 101.7)	99.2 (97.5, 101.0)	0.040
Alb (g/L)	41.6 (41.4, 41.9)	43.4 (42.9, 43.9)	<0.001
AST (U/L)	19.7 (19.1, 20.4)	19.5 (18.3, 20.6)	0.709
ALT (U/L)	24.0 (22.8, 25.2)	22.5 (20.4, 24.6)	0.235

Variables are presented as means (SD), n (%), or means (95% confidence interval) (after covariate analysis).

DKD, diabetic kidney disease; Non-DKD, non-diabetic kidney disease; BMI, body mass index; SBP, systolic blood pressure; DBP, diastolic blood pressure; HBP, high blood pressure; CHD, coronary heart disease; INFAR, cerebral infarction; UACR, urine albumin/creatinine ratio; HbA1c, glycosylated hemoglobin A-1c; FPG, fasting plasma glucose; TC, total cholesterol; TG, triglyceride; HDL, high-density lipoprotein; LDL, low-density lipoprotein; Scr, serum creatinine; UA, uric acid; Cysc, cystatin C; eGFR, estimated glomerular filtration rate; Alb, albumin; AST, aspartate transaminase; ALT, alanine aminotransferase.

eGFR was calculated as the formula for CKD-EPI 2009.

After adjusting for baseline age, gender, and DM duration in Model 2, the HRs in the high-increasing and low-increasing classes were 2.12 (95% CI, 1.22 to 3.68) and 1.70 (95% CI, 1.18 to 2.44), respectively. In Model 3, the HRs maintained a significance of 3.43 (95% CI, 1.93 to 6.11) for the high-increasing and 1.80 (95% CI, 1.17 to 2.77) for the middle-increasing class after adjusting for baseline age, gender, DM duration, smoker, HbA1c, TC, TG, urea, UA, and AST.

TABLE 2 | Cox regression results of incidence of DKD for quartiles of baseline serum Cysc.

Quartiles of Cysc (mg/L)	Model 1		Model 2		Model 3	
	HR (95% CI)	*p*-value	HR (95% CI)	*p*-value	HR (95% CI)	*p*-value
Q1 (≤0.77)	Reference		Reference		Reference	
Q2 (0.78–1.02)	1.56 (1.01, 2.40)	0.047	1.44 (0.93, 2.24)	0.103	2.05 (1.14, 3.70)	0.017
Q3 (1.03–1.27)	2.35 (1.45, 3.79)	<0.001	1.92 (1.15, 3.21)	0.013	2.30 (1.25, 4.24)	0.008
Q4 (≥1.28)	9.16 (3.70, 22.65)	<0.001	6.69 (2.65, 16.87)	<0.001	7.15 (2.79, 25.57)	<0.001

Model 1, unadjusted by other variables.
Model 2, adjusted for baseline age, gender, and DM duration.
Model 3, adjusted for baseline age, gender, DM duration, smoker, HbA1c, TC, TG, urea, UA and AST. TG and urea are time-dependent covariances.
HR, hazard ratio; 95% CI, 95% confidence interval.

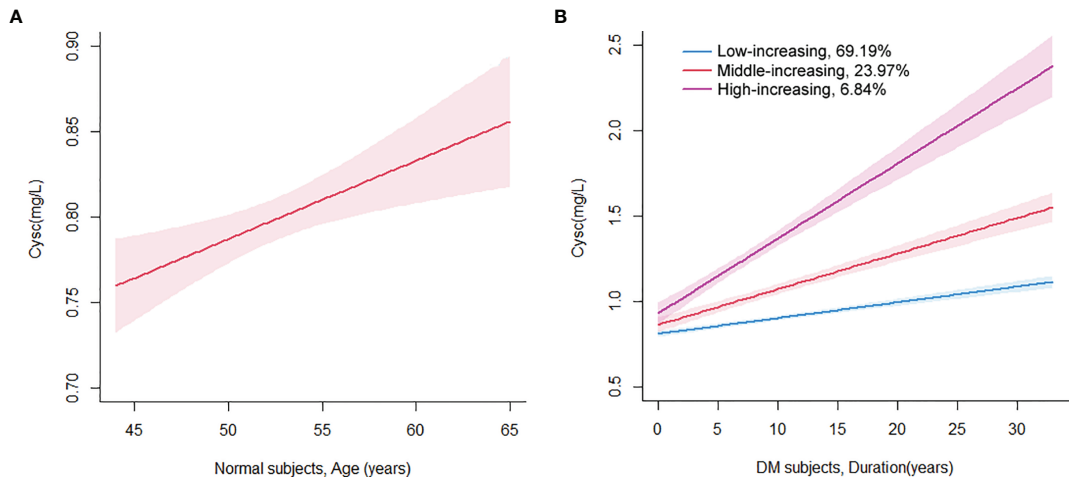

FIGURE 1 | Class-specific mean predicted trajectory of serum cystatin C for healthy subjects **(A)** and T2DM patients **(B)**. A one-class linear model was selected for healthy subjects by age **(A)**, and a three-class linear model was selected for T2DM patients by DM duration as the best-fit models, adjusted for the covariate of age **(B)**.

DISCUSSION

Previous studies have demonstrated that Cysc is an earlier marker than eGFR and UACR associated with a DKD incident. However, a large, longer-duration longitudinal study was needed to further observe the predictive effect of Cysc for DKD. In this study, 805 subjects were included and observed for 5–6 years. The Cysc effect on incidence of DKD was explored from two aspects. At baseline, subjects were segregated into 4 quartiles according to the baseline Cysc values. An HR of 7.15 (95% CI, 2.79 to 25.57) was determined for Q4 when compared with Q1. Subsequently, the Cysc trajectory was analyzed by LCGMM into 3 latent classes. The high-increasing class of Cysc had an HR of 3.43 (95% CI, 1.93 to 6.11) when compared with the low-increasing class. To our knowledge, this is the first large, long-duration longitudinal cohort study on Cysc in DKD, particularly by the latent class analysis of Cysc by LCGMM.

Because of the heavy burden of DKD to patients and society, how to prevent and alleviate DKD is a crucial problem at present. How to discover kidney damage in the early stage is one of the topics. In our study, we computed the dynamic changes of eGFR and UACR with Cysc, and we observed that when the Cysc was already higher than the normal reference, the eGFR and UACR had not met the diagnosis standard of DKD. The following analysis demonstrated that Cysc was associated with the prevalence of DKD. Hence, Cysc is an earlier biomarker than eGFR and UACR associated with future prevalence of DKD. It can help clinical experts to monitor kidney damage in the early stage of DKD to adopt advanced strategies, such as better glucose control, usage of sodium-dependent glucose transporter inhibitors, angiotensin-converting enzyme inhibitors, or administration of uric acid. Cysc offers an alternative to indicate DKD earlier than eGFR and UACR.

In the study, the trajectory of serum Cysc with age was established, and serum Cysc was found to increase with age in normal subjects. There was a slight increase in the velocity of Cysc in normal subjects throughout life (0.46 mg/L per 100 years). This is in accord with previous studies. A study by Norlund et al. found that there were no gender differences for plasma and serum Cysc, whereas an increase in the Cysc levels with age was noted. Reference intervals for serum Cysc in healthy subjects of 0.70–1.21 mg/L for 20–50 years of age and 0.84–1.55 mg/L for over 50 years of age were recommended for practical

TABLE 3 | Baseline characteristics by serum Cysc latent classes.

	Low-increasing	Middle-increasing	High-increasing	*p*
Baseline				
N (805)	557	193	55	
Male [% (*n*)]	54.8 (305)	58.5 (113)	74.5 (41)	0.016
Age (years)	49.6 (10.0)	58.6 (6.4)	55.2 (8.9)	<0.001
Duration (years)	7.8 (6.6)	6.8 (4.8)	4.0 (3.9)	<0.001
BMI (kg/m^2)	25.1 (24.8, 25.5)	26.4 (25.8, 27.0)	26.4 (25.3, 27.4)	0.002
SBp (mmHg)	129.7 (128.2, 131.1)	123.9 (121.2, 126.5)	131.1 (126.3, 135.6)	<0.001
DBp (mmHg)	82.5 (81.5, 83.4)	80.5 (78.7, 82.3)	82.7 (79.6, 85.8)	0.15
DM Family history [Yes, % (*n*)]	41.5 (231)	43.0 (83)	30.9 (17)	0.262
Smoker [Yes, % (*n*)]	17.1 (95)	25.9 (50)	29.1 (16)	0.007
Drinker [Yes, % (*n*)]	10.8 (60)	14.0 (27)	10.9 (6)	0.478
HBP [Yes, % (*n*)]	37.9 (211)	35.2 (68)	43.6 (24)	0.514
CHD [Yes, % (*n*)]	12.4 (69)	11.4 (22)	14.5 (9)	0.615
INFAR [Yes, % (*n*)]	4.3 (24)	6.7 (13)	0 (0)	0.092
UACR (mg/g)	9.6 (9.0, 10.3)	11.5 (10.4, 12.6)	7.7 (5.7, 9.7)	0.001
HbA1c (%)	8.1 (8.0, 8.3)	9.0 (8.6, 9.3)	8.3 (7.7, 8.9)	<0.001
FPG (mmol/L)	8.9 (8.6, 9.1)	9.8 (9.4, 10.3)	8.9 (8.1, 9.7)	0.001
TC (mmol/L)	4.74 (4.66, 4.83)	5.12 (4.96, 5.27)	4.78 (4.50, 5.06)	<0.001
TG (mmol/L)	2.51 (2.25, 2.77)	2.90 (2.43, 3.37)	3.31 (2.45, 4.17)	0.15
HDL (mmol/L)	1.09 (1.06, 1.11)	1.06 (1.01, 1.11)	0.97 (0.88, 1.05)	0.031
LDL (mmol/L)	2.93 (2.96, 3.00)	3.16 (3.03, 3.29)	2.76 (2.52, 3.00)	0.001
Urea (mmol/L)	5.1 (5.0, 5.3)	5.8 (5.6, 6.0)	5.4 (5.0, 5.8)	<0.001
UA (μmol/L)	292.2 (285.9, 298.5)	325.0 (313.9, 336.1)	396.8 (375.4, 418.2)	<0.001
Scr (μmol/L)	57.7 (56.9, 58.6)	63.9 (62.4, 65.4)	70.5 (67.8, 73.2)	<0.001
CysC (mg/L)	0.86 (0.85, 0.87)	0.98 (0.97, 1.00)	1.11 (1.08, 1.14)	<0.001
eGFR (ml/min per 1.73 m^2)	107.0 (106.3, 107.7)	102.0 (100.7, 103.3)	96.4 (94.1, 98.7)	<0.001
Alb (g/L)	42.8 (42.5, 43.1)	43.3 (42.7, 43.8)	42.3 (41.3, 43.2)	0.13
AST (U/L)	19.3 (17.6, 20.9)	24.6 (21.6, 27.6)	26.3 (20.8, 31.7)	0.004
ALT (U/L)	25.0 (23.5, 26.4)	26.0 (23.4, 28.6)	33.5 (28.7, 38.2)	0.004
Follow-up				
Follow-time (years)	4.9 (1.5)	5.0 (1.6)	4.5 (1.9)	0.079
DKD (%, *n*)	21.4 (119)	30.6 (59)	25.5 (14)	0.034

Variables are presented as means (SD), n (%), or means (95% confidence interval) (after covariate analysis).
DKD, diabetic kidney disease; BMI, body mass index; SBp, systolic blood pressure; DBp, diastolic blood pressure; HBP, high blood pressure; CHD, coronary heart disease; INFAR, cerebral infarction; UACR, urine albumin/creatinine ratio; HbA1c, glycosylated hemoglobin A-1c; FPG, fasting plasma glucose; TC, total cholesterol; TG, triglyceride; HDL, high-density lipoprotein; LDL, low-density lipoprotein; Scr, serum creatinine; UA, uric acid; Cysc, cystatin C; eGFR, estimated glomerular filtration rate; Alb, albumin; AST, aspartate transaminase; ALT, alanine aminotransferase.
eGFR was calculated as the formula for CKD-EPI 2009.

TABLE 4 | Cox regression results of incidence of DKD for the latent class of serum Cysc.

	Model 1		Model 2		Model 3	
Latent class	**HR (95% CI)**	***p*-value**	**HR (95% CI)**	***p*-value**	**HR (95% CI)**	***p*-value**
Low-increasing	Reference		Reference		Reference	
Middle-increasing	1.44 (1.06, 1.98)	0.019	1.70 (1.18, 2.44)	0.004	1.80 (1.17, 2.77)	0.007
High-increasing	1.45 (0.87, 2.403)	0.158	2.12 (1.22, 3.68)	0.008	3.43 (1.93, 6.11)	<0.001

Model 1, unadjusted by other variables.
Model 2, adjusted for baseline age, gender, and duration.
Model 3, adjusted for baseline age, gender, DM duration, smoker, HbA1c, TC, TG, urea, UA and AST. TG and urea are time-dependent covariances.

clinical use (29). An investigation by Finney et al. showed that there were slight differences between genders, so a single reference interval was recommended for each gender. An increase in serum Cysc with age was also observed, and the mean 95% reference interval for those under 50 years of age was 0.53–0.92 mg/L, and for those over 50 years of age, it was 0.58–1.02 mg/L (30). In this study, we analyzed computed Cysc trajectory with age by LCGMM and calculated the velocity of serum Cysc increase by modeling. These findings provide novel insights into the understanding of increasing Cysc with age.

Another important finding in the study is that the increasing velocity of serum Cysc in T2DM subjects with age was faster than that in normal subjects. In T2DM subjects, the slope of Cysc was 0.92, 2.08, and 4.39 mg/L per 100 years for the low-increasing, middle-increasing, and high-increasing classes, respectively. The slopes in all three classes for T2DM subjects were higher than the corresponding slope of 0.46 mg/L per 100 years in normal subjects. In previous studies, some cross-sectional investigations showed that serum Cysc was elevated in DM patients over normal controls (31, 32). However, previous

studies did not address the dynamic changes in Cysc in DM patients, especially on the serum Cysc elevation rate, elevation with DM duration, or comparisons with normal controls. To our knowledge, this study is the first investigation on the dynamic changes of Cysc in DM subjects. After analysis, a 2- to 10-fold increasing velocity of serum Cysc was observed in T2DM subjects compared to normal controls. This also indicates a rapid decrease in renal function in DM patients compared to normal subjects.

In the study, subjects were categorized into three latent classes according to serum Cysc increasing velocities. Subjects in the high-increasing class had the highest HR [3.43(95% CI, 1.93 to 6.11)] for incidence of DKD. From the baseline characteristics of the high-increasing class, the data indicate that male subjects with increased age; higher BMI, SBp, urea, UA, Scr, and Cysc; and lower eGFR are more likely to show higher increasing velocity of Cysc. A previous study demonstrated that obesity was associated with increased risk of incidence and progression of DKD (33–35). Weight loss reduced urinary albumin excretion and slowed the decline in GFR (36). Studies on serum UA also demonstrate that higher levels of serum UA are associated with increased risk and progression of DKD in subjects with T1DM and T2DM (37). UA reduction could reduce the rate of GFR loss and decrease the risk of Scr doubling or ESKD in T2DM and other CKD participants (38–40). Combining this and previous studies, attention should be paid to obesity and hyperuricemia, in addition to hyperglycemia and hypertension, to delay DKD incidence in clinical practice.

There are some limitations in our study. Firstly, the endpoint in our study is UACR ≥30 mg/g and/or eGFR<60 ml/min per 1.73 m^2, so only slight or mild DKD was observed, not severe, especially ESRD. A longer follow-up time is needed. Secondly, because of the influence of SARS-CoV-2, some of the subjects in the study missed visits in 2020. Thus, the observation time was defined as 5–6 years in 2019–2020. However, we adjusted for age and DM duration in the statistical analysis when comparing between groups. Additionally, information on socioeconomic status, occupation, income, education, etc. was absent in our study. Finally, new kidney protective medicines, SGLT-2 inhibitors for example, were not included in the study. A longer observational study, with medicines included, is needed. Nevertheless, because of the large size and long duration of the study, it provides a valuable reference for the study of Cysc in DKD, especially for the latent trajectory of serum Cysc.

In conclusion, this investigation demonstrated that higher baseline Cysc was associated with higher incidence of DKD. DM subjects were divided into 3 latent classes by LCGMM, including low-increasing, middle-increasing, and higher-increasing classes. Subjects in the high-increasing and middle-increasing classes had a higher risk of incidence of DKD. Cysc is a sensitive biomarker for the early diagnosis of DKD.

DATA AVAILABILITY STATEMENT

The raw data supporting the conclusions of this article will be made available by the authors, without undue reservation.

ETHICS STATEMENT

The studies involving human participants were reviewed and approved by Shengjing Hospital of China Medical University. The patients/participants provided their written informed consent to participate in this study.

AUTHOR CONTRIBUTIONS

NW collected data, conceived and designed the experiments, analyzed data, and wrote the manuscript. ZL, WZ and YB collected data. DP and LL conceived and designed the experiments, and revised the manuscript. All authors contributed to the article and approved the submitted version.

FUNDING

This work was supported by the Natural Science Foundation of Liaoning Province (No. 2020-MS-149 and No. 2019-ZD-0737), the Science and Technology Talent Program of Shenyang (No. RC200442), and the 345 Talent Project of Shengjing Hospital (No. M0273).

SUPPLEMENTARY MATERIAL

The Supplementary Material for this article can be found online at: https://www.frontiersin.org/articles/10.3389/fendo.2022.824279/full#supplementary-material

REFERENCES

1. Johansen KL, Chertow GM, Foley RN, Gilbertson DT, Herzog CA, Ishani A, et al. US Renal Data System 2020 Annual Data Report: Epidemiology of Kidney Disease in the United States. *Am J Kidney Dis* (2021) 77(4):VII–VIII. doi: 10.1053/ajkd.2021.01.002
2. Tuttle KR, Bakris GL, Bilous RW, Chiang JL, de Boer IH, Goldstein-Fuchs J, et al. Diabetic Kidney Disease: A Report From an ADA Consensus Conference. *Diabetes Care* (2014) 37(10):2864–83. doi: 10.2337/dc14-1296
3. Levin A, Rocco M. KDOQI Clinical Practice Guidelines and Clinical Practice Recommendations for Diabetes and Chronic Kidney Disease. *Am J Kidney Dis* (2007) 49(2):S10–S179. doi: 10.1053/j.ajkd.2006.12.004
4. Molitch ME, Steffes M, Sun W, Rutledge B, Cleary P, de Boer IH, et al. Development and Progression of Renal Insufficiency With and Without Albuminuria in Adults With Type 1 Diabetes in the Diabetes Control and Complications Trial and the Epidemiology of Diabetes Interventions and Complications Study. *Diabetes Care* (2010) 33(7):1536–43. doi: 10.2337/dc09-1098

5. Newman DJ. Cystatin C. *Ann Clin Biochem* (2002) 39:89–104. doi: 10.1258/0004563021901847
6. Abrahamson M, Olafsson I, Palsdottir A, Ulvsback M, Lundwall A, Jensson O, et al. Structure and Expression of the Human Cystatin C Gene. *Biochem J* (1990) 268(2):287–94. doi: 10.1042/bj2680287
7. Zhou B, Zou H, Xu G. Clinical Utility of Serum Cystatin C in Predicting Diabetic Nephropathy Among Patients With Diabetes Mellitus: A Meta-Analysis. *Kidney Blood Pressure Res* (2016) 41(6):919–28. doi: 10.1159/000452593
8. Aksun SA, Ozmen D, Ozmen B, Parildar Z, Mutaf I, Turgan N, et al. Beta 2-Microglobulin and Cystatin C in Type 2 Diabetes: Assessment of Diabetic Nephropathy. *Exp Clin Endocrinol Diabetes* (2004) 112(4):195–200. doi: 10.1055/s-2004-817933
9. Chen HM, Li HB. Clinical Implication of Cystatin C and Beta-Microglobulin in Early Detection of Diabetic Nephropathy. *Clin Lab* (2017) 63(2):241–7. doi: 10.7754/Clin.Lab.2016.160719
10. Xu WH, Tang SH, Xiang MJ, Peng JY. Serum Homocysteine, Cystatin C as Biomarkers for Progression of Diabetic Nephropathy. *Pteridines* (2019) 30 (1):183–8. doi: 10.1515/pteridines-2019-0024
11. La Jeon Y, Kim MH, Lee WI, Kang SY. Cystatin C as an Early Marker of Diabetic Nephropathy in Patients With Type 2 Diabetes. *Clin Lab* (2013) 59 (11-12):1221–9. doi: 10.7754/Clin.Lab.2013.120804
12. Rohani F, Hooman N, Moradi S, Mobarra M, Najafizadeh M. Glomerular Filtration Rate-Based Cystatin C Compared to Microalbuminuria to Detect Early Stage of Diabetic Nephropathy in Children With Type 1 Diabetes Mellitus. *Int J Diabetes Dev Countr* (2015) 35:S342–8. doi: 10.1007/s13410-015-0297-0
13. Christensson AG, Grubb AO, Nilsson JA, Norrgren K, Sterner G, Sundkvist G. Serum Cystatin C Advantageous Compared With Serum Creatinine in the Detection of Mild But Not Severe Diabetic Nephropathy. *J Internal Med* (2004) 256(6):510–8. doi: 10.1111/j.1365-2796.2004.01414.x
14. Rigalleau V, Beauvieux MC, Le Moigne F, Lasseur C, Chauveau P, Raffaitin C, et al. Cystatin C Improves the Diagnosis and Stratification of Chronic Kidney Disease, and the Estimation of Glomerular Filtration Rate in Diabetes. *Diabetes Metab* (2008) 34(5):482–9. doi: 10.1016/j.diabet.2008.03.004
15. Bicik Z, Bahcebasi T, Kulaksizoglu S, Yavuz O. The Efficacy of Cystatin C Assay in the Prediction of Glomerular Filtration Rate. Is it a More Reliable Marker for Renal Failure? *Clin Chem Lab Med* (2005) 43(8):855–61. doi: 10.1515/cclm.2005.144
16. Bevc S, Hojs R, Ekart R, Zavrsnik M, Gorenjak M, Puklavec L. Simple Cystatin C Formula for Estimation of Glomerular Filtration Rate in Overweight Patients With Diabetes Mellitus Type 2 and Chronic Kidney Disease. *Exp Diabetes Res* (2012) 2012:179849. doi: 10.1155/2012/179849
17. Elsayed MS, El Badawy A, Ahmed AE, Omar R, Mohamed A. Serum Cystatin C as an Indicator for Early Detection of Diabetic Nephropathy in Type 2 Diabetes Mellitus. *Diabetes Metab Syndr* (2019) 13(1):374–81. doi: 10.1016/j.dsx.2018.08.017
18. Arceo ES, Dizon GA, Tiongco REG. Serum Cystatin C as an Early Marker of Nephropathy Among Type 2 Diabetics: A Meta-Analysis. *Diabetes Metab Syndr* (2019) 13(6):3093–7. doi: 10.1016/j.dsx.2019.11.007
19. Beauvieux MC, Le Moigne F, Lasseur C, Raffaitin C, Perlemoine C, Barthe N, et al. New Predictive Equations Improve Monitoring of Kidney Function in Patients With Diabetes. *Diabetes Care* (2007) 30(8):1988–94. doi: 10.2337/dc06-2637
20. Papadopoulou-Marketou N, Skevaki C, Kosteria I, Peppa M, Chrousos GP, Papassotiriou I, et al. NGAL and Cystatin C: Two Possible Early Markers of Diabetic Nephropathy in Young Patients With Type 1 Diabetes Mellitus: One Year Follow Up. *Horm-Internat J Endocrinol Metab* (2015) 14(2):232–40. doi: 10.14310/horm.2002.1520
21. Iliadis F, Didangelos T, Ntemka A, Makedou A, Moralidis E, Gotzamani-Psarakou A, et al. Glomerular Filtration Rate Estimation in Patients With Type 2 Diabetes: Creatinine- or Cystatin C-Based Equations? *Diabetologia* (2011) 54(12):2987–94. doi: 10.1007/s00125-011-2307-1
22. Oddoze C, Morange S, Portugal H, Berland Y, Dussol B. Cystatin C is Not More Sensitive Than Creatinine for Detecting Early Renal Impairment in Patients With Diabetes. *Am J Kidney Dis* (2001) 38(2):310–6. doi: 10.1053/ajkd.2001.26096
23. American Diabetes Association. Microvascular Complications and Foot Care: Standards of Medical Care in Diabetes—2021. *Diabetes Care* (2021) 44 (Supplement 1):S151–67. doi: 10.2337/dc21-S011
24. KDIGO. KDIGO 2012 Clinical Practice Guideline for the Evaluation and Management of Chronic Kidney Disease. *Kidney Int Suppl* (2013) 3(1):1–150. doi: 10.1038/kisup.2012.64
25. Proust-Lima C, Philipps V, Liquet B. Estimation of Extended Mixed Models Using Latent Classes and Latent Processes: The R Package Lcmm. *J Stat Softw* (2017) 78(2):1–56. doi: 10.18637/jss.v078.i02
26. Yuan Z, Yang Y, Wang C, Liu J, Sun X, Liu Y, et al. Trajectories of Long-Term Normal Fasting Plasma Glucose and Risk of Coronary Heart Disease: A Prospective Cohort Study. *J Am Heart Assoc* (2018) 7(4):e007607. doi: 10.1161/JAHA.117.007607
27. Fan B, Yang Y, Dayimu A, Zhou G, Liu Y, Li S, et al. Body Mass Index Trajectories During Young Adulthood and Incident Hypertension: A Longitudinal Cohort in Chinese Population. *J Am Heart Assoc* (2019) 8(8): e011937. doi: 10.1161/JAHA.119.011937
28. Lv J, Fan B, Wei M, Zhou G, Dayimu A, Wu Z, et al. Trajectories of Early to Mid-Life Adulthood BMI and Incident Diabetes: The China Health and Nutrition Survey. *BMJ Open Diabetes Res Care* (2020) 8(1):e000972. doi: 10.1136/bmjdrc-2019-000972
29. Norlund L, Fex G, Lanke J, von Schenck H, Nilsson JE, Leksell H, et al. Reference Intervals for the Glomerular Filtration Rate and Cell-Proliferation Markers: Serum Cystatin C and Serum β2-Microglobulin/Cystatin C-Ratio. *Scandinav J Clin Lab Invest* (1997) 57(6):463–70. doi: 10.3109/00365519709084595
30. Finney H, Newman DJ, Price CP. Adult Reference Ranges for Serum Cystatin C, Creatinine and Predicted Creatinine Clearance. *Ann Clin Biochem* (2000) 37:49–59. doi: 10.1258/0004563001901524
31. Liu J, Ma L, Yang J, Ren A, Sun Z, Yan G, et al. Increased Serum Cathepsin S in Patients With Atherosclerosis and Diabetes. *Atherosclerosis* (2006) 186 (2):411–9. doi: 10.1016/j.atherosclerosis.2005.08.001
32. Wang YS, Ye J, Yang X, Zhang GP, Cao YH, Zhang R, et al. Association of Retinol Binding Protein-4, Cystatin C, Homocysteine and High-Sensitivity C-Reactive Protein Levels in Patients With Newly Diagnosed Type 2 Diabetes Mellitus. *Arch Med Sci* (2019) 15(5):1203–16. doi: 10.5114/aoms.2018.79565
33. Araki S, Haneda M, Sugimoto T, Isono M, Isshiki K, Kashiwagi A, et al. Factors Associated With Frequent Remission of Microalbuminuria in Patients With Type 2 Diabetes. *Diabetes* (2005) 54(10):2983–7. doi: 10.2337/diabetes.54.10.2983
34. de Boer IH, Sibley SD, Kestenbaum B, Sampson JN, Young B, Cleary PA, et al. Central Obesity, Incident Microalbuminuria, and Change in Creatinine Clearance in the Epidemiology of Diabetes Interventions and Complications Study. *J Am Soc Nephrol* (2007) 18(1):235–43. doi: 10.1681/asn.2006040394
35. Tziomalos K, Athyros VG. Diabetic Nephropathy: New Risk Factors and Improvements in Diagnosis. *Rev Diabetes Stud* (2015) 12(1-2):110–8. doi: 10.1900/rds.2015.12.110
36. Saiki A, Nagayama D, Ohhira M, Endoh K, Ohtsuka M, Koide N, et al. Effect of Weight Loss Using Formula Diet on Renal Function in Obese Patients With Diabetic Nephropathy. *Int J Obes (Lond)* (2005) 29(9):1115–20. doi: 10.1038/sj.ijo.0803009
37. Mauer M, Doria A. Uric Acid and Diabetic Nephropathy Risk. *Contrib Nephrol* (2018) 192:103–9. doi: 10.1159/000484284
38. Siu YP, Leung KT, Tong MK, Kwan TH. Use of Allopurinol in Slowing the Progression of Renal Disease Through its Ability to Lower Serum Uric Acid Level. *Am J Kidney Dis* (2006) 47(1):51–9. doi: 10.1053/j.ajkd.2005.10.006
39. Goicoechea M, de Vinuesa SG, Verdalles U, Ruiz-Caro C, Ampuero J, Rincón A, et al. Effect of Allopurinol in Chronic Kidney Disease Progression and Cardiovascular Risk. *Clin J Am Soc Nephrol* (2010) 5(8):1388–93. doi: 10.2215/cjn.01580210
40. Miao Y, Ottenbros SA, Laverman GD, Brenner BM, Cooper ME, Parving HH, et al. Effect of a Reduction in Uric Acid on Renal Outcomes During Losartan Treatment: A *Post Hoc* Analysis of the Reduction of Endpoints in non-Insulin-Dependent Diabetes Mellitus With the Angiotensin II Antagonist Losartan Trial. *Hypertension* (2011) 58(1):2–7. doi: 10.1161/hypertensionaha.111.171488

Conflict of Interest: The authors declare that the research was conducted in the absence of any commercial or financial relationships that could be construed as a potential conflict of interest.

this article, or claim that may be made by its manufacturer, is not guaranteed or endorsed by the publisher.

frontiers | Frontiers in Endocrinology

ORIGINAL RESEARCH
published: 31 May 2022
doi: 10.3389/fendo.2022.882700

Potential Role of N-Cadherin in Diagnosis and Prognosis of Diabetic Nephropathy

Hamad Ali[1,2†], Mohamed Abu-Farha[3†], Maha M. Hammad[3], Sriraman Devarajan[4], Yousif Bahbahani[5], Irina Al-Khairi[3], Preethi Cherian[3], Zahra Alsairafi[6], Vidya Vijayan[4], Fahd Al-Mulla[2], Abdulnabi Al Attar[5,7] and Jehad Abubaker[3]*

[1] Department of Medical Laboratory Sciences, Faculty of Allied Health Sciences, Health Sciences Center, Kuwait University, Jabriya, Kuwait, [2] Department of Genetics and Bioinformatics, Dasman Diabetes Institute (DDI), Dasman, Kuwait, [3] Department of Biochemistry and Molecular Biology, Dasman Diabetes Institute (DDI), Dasman, Kuwait, [4] National Dasman Diabetes Biobank, Dasman Diabetes Institute (DDI), Dasman, Kuwait, [5] Medical Division, Dasman Diabetes Institute (DDI), Dasman, Kuwait, [6] Department of Pharmacy Practice, Faculty of Pharmacy, Health Sciences Center, Kuwait University, Jabriya, Kuwait, [7] Diabetology Unit, Amiri Hospital, Ministry of Health, Kuwait City, Kuwait

OPEN ACCESS

Edited by:
Akira Sugawara, Tohoku University, Japan

Reviewed by:
Sungjin Chung, Catholic University of Korea, South Korea
Tatsuo Shimosawa, International University of Health and Welfare (IUHW), Japan
Natalia Jarzebska, Technical University Dresden, Germany

***Correspondence:**
Jehad Abubaker
jehad.abubakr@dasmaninstitute.org

†These authors have contributed equally to this work and share first authorship

Specialty section:
This article was submitted to Diabetes: Molecular Mechanisms, a section of the journal Frontiers in Endocrinology

Received: *24 February 2022*
Accepted: *20 April 2022*
Published: *31 May 2022*

Citation:
Ali H, Abu-Farha M, Hammad MM, Devarajan S, Bahbahani Y, Al-Khairi I, Cherian P, Alsairafi Z, Vijayan V, Al-Mulla F, Attar AA and Abubaker J (2022) Potential Role of N-Cadherin in Diagnosis and Prognosis of Diabetic Nephropathy. Front. Endocrinol. 13:882700. doi: 10.3389/fendo.2022.882700

Diabetic nephropathy (DN) is a serious complication of diabetes affecting about half the people with diabetes and the leading cause of end stage renal disease (ESRD). Albuminuria and creatinine levels are currently the classic markers for the diagnosis of DN. However, many shortcomings are arising from the use of these markers mainly because they are not specific to DN and their levels are altered by multiple non-pathological factors. Therefore, the aim of this study is to identify better markers for the accurate and early diagnosis of DN. The study was performed on 159 subjects including 42 control subjects, 50 T2D without DN and 67 T2D subjects with DN. Our data show that circulating N-cadherin levels are significantly higher in the diabetic patients who are diagnosed with DN (842.6 ± 98.6 mg/l) compared to the diabetic patients who do not have DN (470.8 ± 111.5 mg/l) and the non-diabetic control group (412.6 ± 41.8 mg/l). We also report that this increase occurs early during the developmental stages of the disease since N-cadherin levels are significantly elevated in the microalbuminuric patients when compared to the healthy control group. In addition, we show a significant correlation between N-cadherin levels and renal markers including creatinine (in serum and urine), urea and eGFR in all the diabetic patients. In conclusion, our study presents N-cadherin as a novel marker for diabetic nephropathy that can be used as a valuable prognostic and diagnostic tool to slow down or even inhibit ESRD.

Keywords: N-cadherin, diabetic nephropathy, microalbuminuria, early diagnosis, biomarker, epithelial-mesenchymal transition

INTRODUCTION

Diabetic nephropathy (DN) is a chronic kidney disease that affects around 40% of diabetic patients of both type 1 and type 2 diabetes (1, 2). It is characterized by insistent increased levels of albumin in urine and is associated with high risk of cardiovascular morbidity and mortality (3, 4). DN is a progressive disorder where renal functions are impaired with time leading to end stage renal disease

(ESRD) (5). Despite advances in the management and treatment of diabetes and associated complications, DN continues to be one of the leading causes of ESRD worldwide which highlights the need for more effective diagnostic, prognostic and therapeutic interventions (6, 7).

Clinically DN is divided into five stages; the first stage is characterized by increased glomerular filtration rate (GFR) and hypertrophy. In the second stage, microalbuminuria is noticed as a result of mesangial expansion and thickening of basement membrane leading to glomerular damage. In stage three, albuminuria increases to more than 300 mg/24h and patients do develop hypertension as well. Stage four is characterized by further elevations in albuminuria, blood urea nitrogen (BUN) and creatinine and GFR starts to decrease by approximately 10% every year. The final stage is characterized by insufficient renal functionality and ESRD (5, 8). Despite albuminuria and creatinine being the focal markers in DN diagnostic and prognostic set ups, these two markers showed a number of limitations that could obscure their clinical effectiveness (9). Several studies have shown that levels of microalbuminuria can be significantly influenced by daily physical activity, type of diet, some types of infections and hypertension which could affect its precision as a risk predictor of DN (9–14). Moreover, several diabetic patients have been shown to progress to ESRD with no elevated levels of albuminuria (15). Serum creatinine level which is widely used in monitoring and diagnosis of several chronic kidney diseases including polycystic kidney disease (16, 17) and DN is shown to be significantly influenced by many non-pathological factors including age, gender, muscle mass and hydration levels (18–21). There is a clear need for a sensitive and precise biomarker that can help in detecting DN early and in monitoring treatment outcomes.

In the past decade, efforts have been directed towards the identification of new reliable and sensitive biomarkers for the early diagnosis and monitoring of DN. Our group has identified several potential markers that are specifically elevated in DN patients when compared to diabetic controls and healthy controls. These markers include NGAL and ANGPTL4 (22). Other groups reported a different set of markers that are associated with DN pathology and renal function deterioration including urine Synaptopodin (23), urine Nephrin (23, 24), ANGPTL8 (25) and serum VEGF (26).

The Cadherins, which are a family of transmembrane proteins that are mainly involved in cells adhesion and signaling and are calcium-dependent functionally (27), have been shown to play an integral part in the establishment of renal epithelia polarization *via* their homophilic interaction through the extracellular domains of cadherins between adjacent cells (28). Among the cadherins that are expressed in the human nephron is N-Cadherin which is a 99.7 kDa protein encoded by the *CDH2* gene. This protein which is composed of 906 amino acids is normally expressed in neural tissues and cardiac muscles in addition to renal tissues (29). In acute kidney injury (AKI) due to ischemia, it has been shown that N-Cadherin is depleted from the proximal tubules in the kidney unlike E-cadherin which highlights a potential role of N-Cadherin in kidney functionality (30). From the prospective of DN, there are no solid reports on the role of N-Cadherin in DN or its diagnostic potential. On the other hand, few clinical studies showed serum and urinary elevated levels of E-cadherin in DN patients (31, 32). As N-cadherin expression has been shown to be influenced by pathological impact (AKI) where it is depleted from renal epithelial cells resulting in disruption of cellular functional organization, it might be holding a potential diagnostic benefit for DN.

In this study, we aim to analyze circulatory concentrations of N-cadherin in diabetic nephropathy patients and compare it to the levels in non-diabetic and diabetic controls to determine whether N-cadherin can serve as a biomarker for diabetic nephropathy diagnosis.

MATERIALS AND METHODS

Subjects Recruitments

Our cohort consisting of 67 DN patients, 50 T2D with no DN and 42 healthy controls was clinically identified and recruited in Dasman Diabetes Institute (DDI). Subjects provided written informed consents before their enrollment in the study. The Ethical Review Committee (ERC) of Dasman Diabetes Institute reviewed and approved the study and methodologies in accordance with the ethical declaration of Helsinki. Participants in all groups were age and BMI matched.

Inclusion and Exclusion Criteria

Subjects were enrolled in three groups; healthy subjects with no symptoms or history of T2D or DN; T2D subjects with no DN and DN subjects. DN patients were identified based on elevated Albumin-to-creatinine ratio (ACR) in a spot urine sample in accordance with the American Diabetes Association criteria (33). Patients' exclusion criteria included: 1) Non-diabetic kidney disease, 2) Chronic liver disease, 3) Heart failure, 4) Current/recent infection, 5) Acute/chronic inflammatory disease, 6) Allergic condition, 7) Autoimmune disease, 8) Malignancy, 9) Patients with T1D and 10) ESRD (34).

Sample Collection

Subjects were fasting overnight before the blood and urine samples were collected in the clinics of Dasman Diabetes Institute. Urine first-void samples were collected in 120 ml urine collection containers and blood samples were collected in EDTA tubes. Plasma was isolated from blood samples after centrifugation and then aliquoted and stored at -80°C until analysis.

Anthropometric and Biochemical Measurements

The anthropometric data were obtained and documented. Blood pressure readings were obtained using Omron HEM-907XL Digital sphygmomanometer. Fasting blood Glucose (FBG), triglyceride (TG), total cholesterol (TC), low density

lipoprotein (LDL) and high-density lipoprotein (HDL) were determined using Siemens Dimension RXL chemistry analyzer (Diamond Diagnostics, Holliston, MA). CLINITEK Novus Automated Urine Chemistry Analyzer (Siemens Healthineers, Erlangen, Germany) was utilized to determine levels of urinary albumin "spot" (Alb) and creatinine (Cr) in addition to urinary albumin–to–creatinine ratio (UACR). VITROS 250 automatic analyzer was utilized to perform fully automated Renal Function Test (RFT) and estimated glomerular filtration rate (eGFR) was calculated by the MDRD (Modification of Diet in Renal Disease) Study equation (35).

Determining N-Cadherin Concentration Using BioPlex 200-Luminex Analysis

Thawed plasma samples were utilized to determine N-Cadherin levels in all enrolled subjects. Samples were subject to centrifugation at 10000xg for 5 minutes at 4°C to eliminate any debris. N-Cadherin concentration was determined *via* a customized 11-plex multiplexing analysis kit (R&D systems, Minneapolis, MN, USA. Cat # LXSAHM) following manufacturer protocol. A standard protein mix, provided with the kit, was used to prepare a serial dilution. The results were obtained using the BioPlex 200-Luminex system (Bio-Rad, CA, USA). Analysis of the results were done using the BioPlex manager software. No significant cross reactivity with different proteins was observed. The confidence level between the expected and the observed standard concentration levels for N-Cadherin was between 95-105% as assessed by the system. The concentrations of the N-Cadherin in the study samples were calculated using a 5-Pt standard curve.

Statistical Analysis

Statistical analysis was performed using IBM SPSS Statistics for Windows, Version 25.0. Armonk, NY: IBM Corp. Descriptive statistics were obtained for all variables measured and then presented as (Mean ± SD). Comparisons between the groups (DN, T2D and Heathy subjects) for all the tested variables were performed using one-way analysis of variance (ANOVA). Bonferroni post-hoc was utilized to test pairwise differences. Spearman's correlations were utilized to calculate the univariate association between N-cadherin and the other variables. A P value < 0.05 was considered statistically significant for all tests performed. The ANOVA F score was validated using the F critical table (degrees of freedom; numerator 2; denominator 156). F value above F critical and P value < 0.05 are considered to reject the null hypothesis in our population.

RESULTS

Cohort Demographics

Total of 159 subjects were enrolled in this study including 42 control subjects, 50 T2D without DN and 67 T2D subjects with DN. The demographic data of the study population is shown in **Table 1**. The three groups were age and BMI matched (p-value >0.05).

TABLE 1 | Demographic data of study population.

	Healthy group (n = 42)	T2D group (n = 50)	DN group (n = 67)
Gender n (%)	Males 18 (43%) Females 24 (57%)	Males 22 (44%) Females 28 (56%)	Males 28 (42%) Females 39 (58%)
Age (years) ± S.D	57.74 ± 4.55	58.96 ± 7.22	59.09 ± 5.29
BMI (kg/m^2) ± S.D	33.20 ± 5.47	33.94 ± 6.25	34.23 ± 6.84

Clinical and Biochemical Characteristics of Enrolled Groups

The T2D and DN groups were clinically evaluated and compared to the healthy group. Systolic and diastolic blood pressures between the three groups showed no statistical significance. Fasting glucose levels showed significant differences between the three groups (p<0.001 ANOVA) and the highest values recorded in T2D and DN groups. HbA1C was higher in T2D and DN groups when compared to the healthy group (p<0.05 ANOVA).

To assess renal functions clinical RFT was performed for all subjects. Serum Creatinine and BUN were all elevated in DN group when compared to the healthy and T2D groups (p<0.00005 for all, ANOVA). Consequently, eGFR in DN was the lowest when compared to T2D and healthy groups (p<0.00005 ANOVA). Similarly, urine creatinine was low in DN when compared with the other two groups (p<0.05 ANOVA). ACR and Microalbumin were significantly increased in DN group while the levels in the other two groups were in the normal range (p<0.005, ANOVA, for both). *Post Hoc* Bonferroni indicated significant differences between the DN group and the other two groups for all the RFT markers including the microalbumin and ACR.

N-Cadherin Expression Level and Correlation With Renal Markers

N-cadherin showed significantly elevated levels in the DN group when compared to the other two groups (p<0.01 ANOVA). *Post Hoc* Bonferroni indicated significant differences in N-cadherin between the DN group and the other two groups (**Figure 1A**) and **Table 2**. Reported N-cadherin results have F values greater than F critical. Furthermore, the diabetic nephropathy group was subdivided into two groups according to their Albumin-to-creatinine ratio (ACR) and was compared with the healthy group. Subjects with ACR in the range between 30 to 300 mg/g were considered microalbuminuric and subjects with ACR > 300 mg/g were considered macroalbuminuric. N-cadherin levels were significantly elevated in both groups (i.e. microalbuminuric and macroalbuminuric) when compared to the N-cadherin levels in the healthy group (**Figure 1B**). Furthermore, a trend for increase was detected in the macroalbuminuric when compared to the microalbuminuric but was not statistically significant (p = 0.087) (**Figure 1B**).

Spearman's rank correlation analysis showed significant positive correlation of N-Cadherin in one hand and serum creatinine and BUN on the other hand in DN and T2D groups. Significant negative correlations were also found

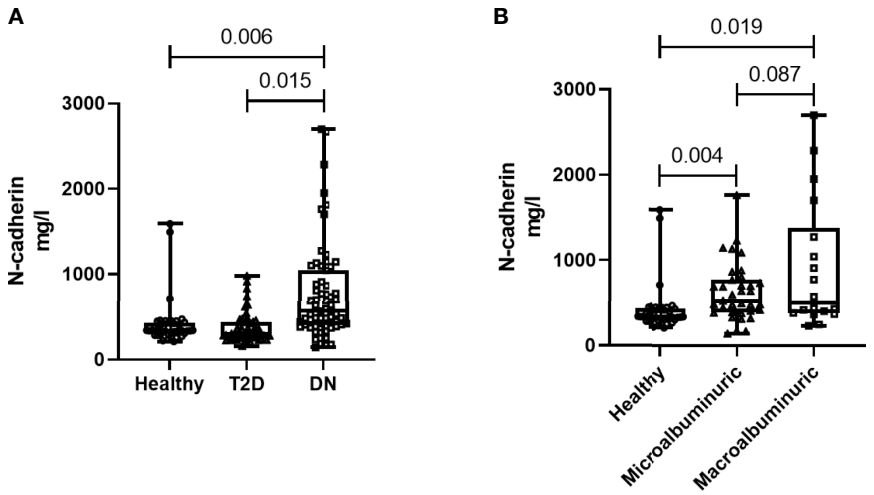

FIGURE 1 | N-cadherin levels in the participants. **(A)** Based on the diabetes status. **(B)** Based on the albuminuria levels.

between N-Cadherin and eGFR in the DN and T2D groups (**Table 3**).

ROC Curve Analysis of N-Cadherin

Receiver Operating Characteristic (ROC) analysis was performed to determine the possible use of N-cadherin as a marker to distinguish between diabetic patients with or without kidney complications, specifically diabetic nephropathy. The area under the curve (AUC) for the analysis was 0.76 (**Figure 2**) reflecting good ability of N-cadherin as a marker. The ROC analysis results were interpreted as follows: AUC <0.70, low diagnostic accuracy; AUC in the range of 0.70–0.90, moderate diagnostic accuracy; and AUC ≥0.90, high diagnostic accuracy.

DISCUSSION

This study analyzed the circulating levels of N-cadherin in diabetic nephropathy in an attempt to find sensitive prognostic and diagnostic markers for this concerning complication. Our findings show that circulating N-cadherin levels are significantly elevated in patients with DN compared to people with T2D and healthy controls. We also report that this increase occurs early during the developmental stages of the disease (second stage) as the increase was significant in microalbuminuric patients. We also show a significant correlation between N-cadherin levels and renal markers including creatinine (in serum and urine), urea and eGFR in all of the diabetic patients.

In the IDF Diabetes Atlas Ninth edition of 2019, the projected prevalence of diabetes was estimated to rise to 700 million by 2045 (36). Diabetic kidney disease (DKD) continues to be one of the major complications of diabetes affecting nearly 40% of all (type I and type II) diabetic patients worldwide (37). Therefore, with such rates, it is expected that DKD will reach epidemic scale by 2045 affecting more than 300 million people. There is currently a need for new predictive and diagnostic markers for DN given that the currently used markers (albuminuria and

TABLE 2 | Clinical and Biochemistry characteristics of study cohort.

Marker	Healthy group (± SEM)	T2D group (± SEM)	DN group (± SEM)	ANOVA (p value)	F value	*Post Hoc* Bonferroni P value adjusted for multiple comparisons with *post hoc* Bonferroni		
						T2D vs. DN	T2D vs. Healthy	DN vs. Healthy
SBP (mmHg)	122.50 ± 2.25	132.98 ± 3.88	132.03 ± 3.41	0.087	2.477	1.000	0.139	0.162
DBP (mmHg)	73.76 ± 1.52	69.72 ± 2.26	68.78 ± 1.98	0.21	1.558	1.000	0.574	0.261
Fasting Glucose (mmol/l)	5.52 ± 0.12	8.27 ± 0.36	9.61 ± 0.48	<0.001	24.763	.050	.000	.000
HbA1C (%)	5.66 ± 0.09	9.53 ± 1.73	8.09 ± 0.22	0.031	3.549	.816	.027	.236
Serum Creatinine (umol/l)	75.69 ± 2.89	79.42 ± 3.54	118.36 ± 6.57	<0.001	21.277	0.0001	1.000	0.0001
BUN (mmol/l)	5.02 ± 0.20	5.10 ± 0.29	7.53 ± 0.52	<0.001	12.338	0.001	1.000	0.0001
eGFR MDRD (mL/min/1.73 m^2)	81.07 ± 2.14	79.22 ± 3.19	59.7 ± 3.00	<0.001	17.422	0.0001	1.000	0.0001
Albumin (g/l)	40.5 ± 0.52	37.94 ± 0.50	37.28 ± 0.42	<0.001	11.771	0.927	0.002	0.0001
Urine Creatinine (mg/l)	14.75 ± 1.22	11.94 ± 0.86	9.08 ± 0.77	0.049	9.415	0.071	0.140	0.001
Microalbumin (mg/l)	14.82 ± 2.0	14.35 ± 1.61	490.72 ± 186.62	<0.001	11.400	0.003	1.000	0.005
ACR (mg/g)	9.77 ± 1.2	11.32 ± 1.07	953.48 ± 327.	0.004	5.658	0.013	1.000	0.02
N-cadherin (mg/l)	412.56 ± 41.78	470.76 ± 111.48	842.57 ± 98.61	<0.01	6.388	0.015	1.000	0.006

creatinine) are not ideal due to sensitivity and specificity issues. The treatment options are also restricted to inhibitors of the renin-angiotensin system as well as maintaining the diabetes under control by managing hyperglycemia, blood pressure and dyslipidemia. Late diagnosis and the lack of treatment options for advanced stages may cause ESRD and eventually a patient would require renal replacement therapy or a kidney transplant. Therefore, our aim from this study was to identify novel markers that could help in early diagnosis of DN. It would be of great benefit for the success of the treatment if DN is detected in the early stages.

Given the established effect of diabetes on kidney function, it is essential to perform a comprehensive evaluation on the kidneys including the different segments of the tubules. While the evaluation of GFR and albuminuria levels is a good indication for the integrity of the filtration membrane and the glomerular function, cadherin levels can more specifically reflect the function of the renal tubules. Therefore, we decided to assess the levels of N-cadherin in patients with diabetic nephropathy.

There have been several previous reports associating E-cadherin with DN (31, 32). Interestingly, serum E-cadherin levels were shown to be reduced in DN in these studies whereas we are demonstrating an increase in N-cadherin levels with DN. This indicates that different cadherin subtypes can have differential expression patterns in disease states. Such variation could be due to their distinct distribution and hence function in the kidneys. Human studies showed that N-cadherin is exclusively expressed in the proximal tubule while E-cadherin is abundant in the distal tubule and collecting duct (38, 39).

Moreover, a recent study confirmed and validated the use of urine E-cadherin as a marker for early detection of kidney injury in diabetic patients in a longitudinal setting (40). Their findings indicated not only that E-cadherin levels are elevated in nephropathy patients, but can also differentiate between the different stages of DN. They even reported that the elevation in urinary E-cadherin levels was detected 20 ± 12.5 months before the onset of microalbuminuria. Studies on E-cadherin showed some discrepancy when the tissue expression levels were measured. In one study, Jiang et al. showed E-cadherin expression in the renal tubular epithelial cells to be downregulated in DN patients compared to the healthy controls (31). In another report, Koziolek et al. analyzed kidney tissues from two biopsy cohorts. They reported a significant upregulation in DN patients in their smaller cohort of 22 samples but no difference in their larger cohort which included 201 biopsies belonging to different diseases groups (40).

To our knowledge, this is the first report to specifically correlate N-cadherin levels with renal markers in diabetic nephropathy patients. By performing Spearman's correlation analysis, we found that there was a significant positive correlation between the levels of N-cadherin and serum creatinine as well as blood urea nitrogen. On the other hand, there was a significant negative correlation between the levels of N-cadherin and urine creatinine and eGFR. It is expected that the renal tubular epithelial cells would undergo ischemia and apoptosis during the progress of renal impairment in DN due to the inflammatory state as well as the high glucose concentrations in diabetes (41). Our correlation data suggest that N-cadherin plays an important role in renal function and its elevation could be a defense mechanism to counteract the damage and apoptosis resulting from renal injury in diabetes. Interestingly, we saw a significant increase in N-cadherin levels in DN patients who showed microalbuminuria compared to the healthy controls. This is a strong evidence that N-cadherin levels start increasing during the early stages of DN and can hence be used as an accurate diagnostic marker. The ROC analysis further supports this conclusion. We also illustrate that N-cadherin levels can be a reflection for the degree of albuminuria in DN since there was a trend of increase in the macroalbuminuric patients compared to their microalbuminuric counterparts. The lack of significance between these two groups in **Figure 1B** (p=0.087) could be attributed to the wide variation of N-cadherin levels in the participants with macroalbuminuria. Surprisingly, N-cadherin levels were reported to be reduced in response to ischemia in acute kidney injury (30), which reflects the differential role for N-cadherin in different renal diseases and that it is a disease-dependent marker.

One of the mechanisms that have been described to contribute to kidney fibrosis after injury is Epithelial-Mesenchymal Transition (EMT) (42). EMT can be defined as the conversion of differentiated epithelial cells to myofibroblasts. EMT was originally associated with cancer metastasis, however, it was later shown to play an important role in renal and tubular interstitial fibrosis. EMT entails the loss of epithelial cell adhesion leading to actin reorganization and disruption of tubular basement membrane. Interestingly, one of the consequences of EMT that was described in cancer is a phenomena called "cadherin switching" where E-cadherin

TABLE 3 | Spearman's rank correlation coefficient between N-cadherin and renal markers.

	HEALTHY		T2D		DN	
	Spearman	**p value**	**Spearman**	**p value**	**Spearman**	**p value**
Serum Creatinine	0.094	0.556	**0.625**	**0.0001**	**0.604**	**0.0001**
BUN (blood urea nitrogen)	0.058	0.714	**0.432**	**0.002**	**0.548**	**0.0001**
eGFR (MDRD)	-0.198	0.208	**-0.647**	**0.0001**	**-0.657**	**0.0001**
Albumin	-0.101	0.525	-0.247	0.084	-0.193	0.127
Urine Creatinine	0.130	0.412	-0.091	0.531	**-0.309**	**0.013**
Microalbumin	0.208	0.187	0.046	0.750	0.019	0.879

BUN, blood urea nitrogen; eGFR, estimated GFR; (calculated using MDRD equation Modification of Diet in Renal Disease).
Bold values indicate significant correlation (P value < 0.05).

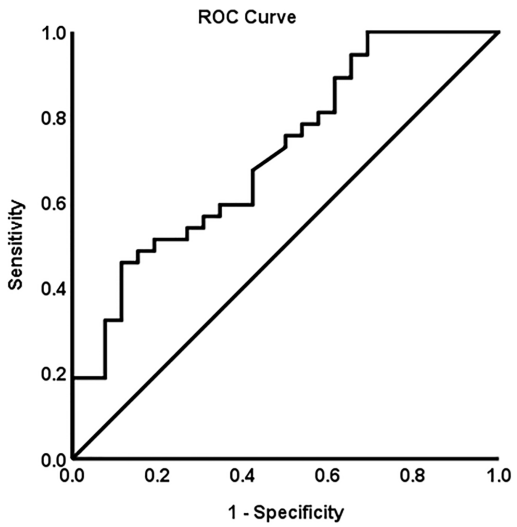

AUC%	Sensitivity	Specificity	P-value
71.4	78.4	57.7	0.004

FIGURE 2 | Receiver Operating Characteristic (ROC) curve analysis for N-cadherin of DN Group compared to the non-diabetic control group.

levels are downregulated and N-cadherin levels are upregulated (43). When E-cadherin levels are reduced, the cell-cell junctions that are mediated by E-cadherin (including tight junctions, gap junctions and adherents junctions) dissociate and this consequently results in the stabilization of the N-cadherin-mediated junctions. Altogether, our results from this study on N-cadherin combined with previous reports on E-cadherin provide evidence that EMT and cadherin switching can occur in diabetic nephropathy and may be mediating the pathophysiological changes associated with it.

One of the main limitations of the study is its cross-sectional design hindering us from concluding causality. Therefore, additional studies are still required looking into the integrity of the tubular segments of the kidney and the components of these segments and how they can influence DN and hence be used as early detection markers. It would be interesting to measure N-cadherin levels in the context of other kidney diseases to determine if it is specific to diabetic nephropathy especially that one of the major shortcomings of serum creatinine is its common use for several kidney diseases. Furthermore, measuring the N-cadherin levels in a larger population would help in determining its clinical value as a DN predictive marker. Validation in a larger cohort using a longitudinal design is the logical next step.

In conclusion, the current study identifies N-cadherin as a novel marker for diabetic nephropathy that can be used to determine the stage of DN. Therefore, assessing N-cadherin levels in diabetic patients could have a valuable impact on slowing down or even inhibiting ESRD.

DATA AVAILABILITY STATEMENT

The original contributions presented in the study are included in the article/supplementary material. Further inquiries can be directed to the corresponding authors.

ETHICS STATEMENT

The studies involving human participants were reviewed and approved by The Ethical Review Committee (ERC) of Dasman Diabetes Institute. The patients/participants provided their written informed consent to participate in this study.

AUTHOR CONTRIBUTIONS

HA: conceptualization and study design, initial manuscript drafting and revision. MA-F: data analysis and interpretation and critical revision of the manuscript. MH: data analysis and manuscript drafting and revision. SD: data analysis, management and statistical analysis. YB: patients' recruitment and data interpretation. IA-K: performed BioPlex assay. PC: performed BioPlex assay. ZA: patient coordination and sample collection. VV: Blood processing, storage and data analysis. FA-M: Data interpretation and critical revision of the manuscript. AA: study design, data interpretation and management. JA: study design, data interpretation, wrote and critically revised the manuscript. All authors have seen and approved the final manuscript. All authors contributed to the article and approved the submitted version.

FUNDING

This work was supported by the Kuwait Foundation for the Advancement of Sciences (KFAS) under projects (RA-2015-012), (PR17-13MM-07) and (RA HM 2019–008).

ACKNOWLEDGMENTS

The authors would like to thank the staff at the Tissue Bank and Clinical Laboratory for their assistance throughout this study.

REFERENCES

1. Gross JL, de Azevedo MJ, Silveiro SP, Canani LH, Caramori ML, Zelmanovitz T. Diabetic Nephropathy: Diagnosis, Prevention, and Treatment. *Diabetes Care* (2005) 28(1):164–76. doi: 10.2337/diacare.28.1.164
2. Rheinberger M, Boger CA. [Diabetic Nephropathy: New Insights Into Diagnosis, Prevention and Treatment]. *Dtsch Med Wochenschr* (2014) 139 (14):704–6. doi: 10.1055/s-0034-1369841
3. Foggensteiner L, Mulroy S, Firth J. Management of Diabetic Nephropathy. *J R Soc Med* (2001) 94(5):210–7. doi: 10.1177/014107680109400504

4. Satirapoj B, Adler SG. Prevalence and Management of Diabetic Nephropathy in Western Countries. *Kidney Dis* (2015) 1(1):61–70. doi: 10.1159/000382028
5. Garud MS, Kulkarni YA. Hyperglycemia to Nephropathy *via* Transforming Growth Factor Beta. *Curr Diabetes Rev* (2014) 10(3):182–9. doi: 10.2174/1573399810666140606103645
6. Rossing P, Persson F, Frimodt-Moller M. Prognosis and Treatment of Diabetic Nephropathy: Recent Advances and Perspectives. *Nephrol Ther* (2018) 14 Suppl 1:S31–S7. doi: 10.1016/j.nephro.2018.02.007
7. Ogurtsova K, da Rocha Fernandes JD, Huang Y, Linnenkamp U, Guariguata L, Cho NH, et al. IDF Diabetes Atlas: Global Estimates for the Prevalence of Diabetes for 2015 and 2040. *Diabetes Res Clin Pract* (2017) 128:40–50. doi: 10.1016/j.diabres.2017.03.024
8. Persson F, Rossing P. Diagnosis of Diabetic Kidney Disease: State of the Art and Future Perspective. *Kidney Int Suppl* (2018) 8(1):2–7. doi: 10.1016/j.kisu.2017.10.003
9. Stevens LA, Greene T, Levey AS. Surrogate End Points for Clinical Trials of Kidney Disease Progression. *Clin J Am Soc Nephrol* (2006) 1(4):874–84. doi: 10.2215/CJN.00600206
10. Fried LF, Lewis J. Rebuttal of the Pro View: Albuminuria Is an Appropriate Therapeutic Target in Patients With CKD. *Clin J Am Soc Nephrol* (2015) 10 (6):1095–8. doi: 10.2215/CJN.01610215
11. Glassock RJ. Is the Presence of Microalbuminuria a Relevant Marker of Kidney Disease? *Curr Hypertension Rep* (2010) 12(5):364–8. doi: 10.1007/s11906-010-0133-3
12. Tuttle KR, Bakris GL, Bilous RW, Chiang JL, de Boer IH, Goldstein-Fuchs J, et al. Diabetic Kidney Disease: A Report From an ADA Consensus Conference. *Am J Kidney Dis* (2014) 64(4):510–33. doi: 10.1053/j.ajkd.2014.08.001
13. Raile K, Galler A, Hofer S, Herbst A, Dunstheimer D, Busch P, et al. Diabetic Nephropathy in 27,805 Children, Adolescents, and Adults With Type 1 Diabetes: Effect of Diabetes Duration, A1C, Hypertension, Dyslipidemia, Diabetes Onset, and Sex. *Diabetes Care* (2007) 30(10):2523–8. doi: 10.2337/dc07-0282
14. Papadopoulou-Marketou N, Chrousos GP, Kanaka-Gantenbein C. Diabetic Nephropathy in Type 1 Diabetes: A Review of Early Natural History, Pathogenesis, and Diagnosis. *Diabetes Metab Res Rev* (2017) 33(2). doi: 10.1002/dmrr.2841
15. Rossi L, Nicoletti MC, Carmosino M, Mastrofrancesco L, Di Franco A, Indrio F, et al. Urinary Excretion of Kidney Aquaporins as Possible Diagnostic Biomarker of Diabetic Nephropathy. *J Diabetes Res* (2017) 2017:4360357. doi: 10.1155/2017/4360357
16. Ali H, Hussain N, Naim M, Zayed M, Al-Mulla F, Kehinde EO, et al. A Novel PKD1 Variant Demonstrates a Disease-Modifying Role in Trans With a Truncating PKD1 Mutation in Patients With Autosomal Dominant Polycystic Kidney Disease. *BMC Nephrol* (2015) 16:26. doi: 10.1186/s12882-015-0015-7
17. Ali H, Al-Mulla F, Hussain N, Naim M, Asbeutah AM, AlSahow A, et al. PKD1 Duplicated Regions Limit Clinical Utility of Whole Exome Sequencing for Genetic Diagnosis of Autosomal Dominant Polycystic Kidney Disease. *Sci Rep* (2019) 9(1):4141. doi: 10.1038/s41598-019-40761-w
18. Delanaye P, Cavalier E, Pottel H. Serum Creatinine: Not So Simple! *Nephron* (2017) 136(4):302–8. doi: 10.1159/000469669
19. Alaini A, Malhotra D, Rondon-Berrios H, Argyropoulos CP, Khitan ZJ, Raj DSC, et al. Establishing the Presence or Absence of Chronic Kidney Disease: Uses and Limitations of Formulas Estimating the Glomerular Filtration Rate. *World J Methodol* (2017) 7(3):73–92. doi: 10.5662/wjm.v7.i3.73
20. Devarajan P. Neutrophil Gelatinase-Associated Lipocalin (NGAL): A New Marker of Kidney Disease. *Scand J Clin Lab Invest Suppl* (2008) 241:89–94. doi: 10.1080/00365510802150158
21. Lin CH, Chang YC, Chuang LM. Early Detection of Diabetic Kidney Disease: Present Limitations and Future Perspectives. *World J Diabetes* (2016) 7 (14):290–301. doi: 10.4239/wjd.v7.i14.290
22. Al Shawaf E, Abu-Farha M, Devarajan S, Alsairafi Z, Al-Khairi I, Cherian P, et al. ANGPTL4: A Predictive Marker for Diabetic Nephropathy. *J Diabetes Res* (2019) 2019:4943191. doi: 10.1155/2019/4943191
23. Hara M, Yamagata K, Tomino Y, Saito A, Hirayama Y, Ogasawara S, et al. Urinary Podocalyxin is an Early Marker for Podocyte Injury in Patients With Diabetes: Establishment of a Highly Sensitive ELISA to Detect Urinary Podocalyxin. *Diabetologia* (2012) 55(11):2913–9. doi: 10.1007/s00125-012-2661-7
24. Tomino Y, Suzuki S, Azushima C, Shou I, Iijima T, Yagame M, et al. Asian Multicenter Trials on Urinary Type IV Collagen in Patients With Diabetic Nephropathy. *J Clin Lab Anal* (2001) 15(4):188–92. doi: 10.1002/jcla.1026
25. Yang L, Song J, Zhang X, Xiao L, Hu X, Pan H, et al. Association of Serum Angiopoietin-Like Protein 8 With Albuminuria in Type 2 Diabetic Patients: Results From the GDMD Study in China. *Front Endocrinol* (2018) 9:414. doi: 10.3389/fendo.2018.00414
26. Kim NH, Kim KB, Kim DL, Kim SG, Choi KM, Baik SH, et al. Plasma and Urinary Vascular Endothelial Growth Factor and Diabetic Nephropathy in Type 2 Diabetes Mellitus. *Diabetic Med* (2004) 21(6):545–51. doi: 10.1111/j.1464-5491.2004.01200.x
27. Hulpiau P, van Roy F. Molecular Evolution of the Cadherin Superfamily. *Int J Biochem Cell Biol* (2009) 41(2):349–69. doi: 10.1016/j.biocel.2008.09.027
28. Hinck L, Nathke IS, Papkoff J, Nelson WJ. Dynamics of Cadherin/Catenin Complex Formation: Novel Protein Interactions and Pathways of Complex Assembly. *J Cell Biol* (1994) 125(6):1327–40. doi: 10.1083/jcb.125.6.1327
29. Prozialeck WC, Lamar PC, Appelt DM. Differential Expression of E-Cadherin, N-Cadherin and Beta-Catenin in Proximal and Distal Segments of the Rat Nephron. *BMC Physiol* (2004) 4:10. doi: 10.1186/1472-6793-4-10
30. Nurnberger J, Feldkamp T, Kavapurackal R, Opazo Saez A, Becker J, Horbelt M, et al. N-Cadherin is Depleted From Proximal Tubules in Experimental and Human Acute Kidney Injury. *Histochem Cell Biol* (2010) 133(6):641–9. doi: 10.1007/s00418-010-0702-1
31. Jiang H, Guan G, Zhang R, Liu G, Cheng J, Hou X, et al. Identification of Urinary Soluble E-Cadherin as a Novel Biomarker for Diabetic Nephropathy. *Diabetes Metab Res Rev* (2009) 25(3):232–41. doi: 10.1002/dmrr.940
32. El-Dawla NMQ, Sallam AM, El-Hefnawy MH, El-Mesallamy HO. E-Cadherin and Periostin in Early Detection and Progression of Diabetic Nephropathy: Epithelial-to-Mesenchymal Transition. *Clin Exp Nephrol* (2019) 23(8):1050–7. doi: 10.1007/s10157-019-01744-3
33. Haneda M, Utsunomiya K, Koya D, Babazono T, Moriya T, Makino H, et al. A New Classification of Diabetic Nephropathy 2014: A Report From Joint Committee on Diabetic Nephropathy. *J Diabetes Invest* (2015) 6(2):242–6. doi: 10.1111/jdi.12319
34. Ali H, Abu-Farha M, Alshawaf E, Devarajan S, Bahbahani Y, Al-Khairi I, et al. Association of Significantly Elevated Plasma Levels of NGAL and IGFBP4 in Patients With Diabetic Nephropathy. *BMC Nephrol* (2022) 23(1):64. doi: 10.1186/s12882-022-02692-z
35. Levey AS, Bosch JP, Lewis JB, Greene T, Rogers N, Roth D. A More Accurate Method to Estimate Glomerular Filtration Rate From Serum Creatinine: A New Prediction Equation. Modification of Diet in Renal Disease Study Group. *Ann Intern Med* (1999) 130(6):461–70. doi: 10.7326/0003-4819-130-6-199903160-00002
36. *IDF Diabetes Atlas*. Brussels, Belgium: International Diabetes Federation (2019). Available at: https://www.diabetesatlas.org.
37. Alicic RZ, Rooney MT, Tuttle KR. Diabetic Kidney Disease: Challenges, Progress, and Possibilities. *Clin J Am Soc Nephrol* (2017) 12(12):2032–45. doi: 10.2215/CJN.11491116
38. Kroening S, Neubauer E, Wullich B, Aten J, Goppelt-Struebe M. Characterization of Connective Tissue Growth Factor Expression in Primary Cultures of Human Tubular Epithelial Cells: Modulation by Hypoxia. *Am J Physiol Renal Physiol* (2010) 298(3):F796–806. doi: 10.1152/ajprenal.00528.2009
39. Nouwen EJ, Dauwe S, van der Biest I, De Broe ME. Stage- and Segment-Specific Expression of Cell-Adhesion Molecules N-CAM, A-CAM, and L-CAM in the Kidney. *Kidney Int* (1993) 44(1):147–58. doi: 10.1038/ki.1993.225
40. Koziolek M, Mueller GA, Dihazi GH, Jung K, Altubar C, Wallbach M, et al. Urine E-Cadherin: A Marker for Early Detection of Kidney Injury in Diabetic Patients. *J Clin Med* (2020) 9(3):639. doi: 10.3390/jcm9030639
41. Lorz C, Benito-Martin A, Boucherot A, Ucero AC, Rastaldi MP, Henger A, et al. The Death Ligand TRAIL in Diabetic Nephropathy. *J Am Soc Nephrol* (2008) 19(5):904–14. doi: 10.1681/ASN.2007050581
42. Liu Y. New Insights Into Epithelial-Mesenchymal Transition in Kidney Fibrosis. *J Am Soc Nephrol* (2010) 21(2):212–22. doi: 10.1681/ASN.2008121226
43. Loh CY, Chai JY, Tang TF, Wong WF, Sethi G, Shanmugam MK, et al. The E-Cadherin and N-Cadherin Switch in Epithelial-to-Mesenchymal Transition:

Signaling, Therapeutic Implications, and Challenges. *Cells* (2019) 8(10):1118. doi: 10.3390/cells8101118

Conflict of Interest: The authors declare that the research was conducted in the absence of any commercial or financial relationships that could be construed as a potential conflict of interest.

Publisher's Note: All claims expressed in this article are solely those of the authors and do not necessarily represent those of their affiliated organizations, or those of the publisher, the editors and the reviewers. Any product that may be evaluated in this article, or claim that may be made by its manufacturer, is not guaranteed or endorsed by the publisher.

frontiers | Frontiers in Endocrinology

TYPE Original Research
PUBLISHED 05 August 2022
DOI 10.3389/fendo.2022.889729

OPEN ACCESS

EDITED BY
Daisuke Yabe,
Gifu University, Japan

REVIEWED BY
Valentina María Parra,
University of Chile, Chile
Xiaoqiang Tang,
Sichuan University, China

*CORRESPONDENCE
Panai Song
spa863@csu.edu.cn

SPECIALTY SECTION
This article was submitted to Renal Endocrinology, a section of the journal Frontiers in Endocrinology

RECEIVED 04 March 2022
ACCEPTED 11 July 2022
PUBLISHED 05 August 2022

CITATION
Tang H, Yang M, Liu Y, Zhu X, Liu S, Liu H, Sun L and Song P (2022) Melatonin alleviates renal injury by activating mitophagy in diabetic nephropathy. *Front. Endocrinol.* 13:889729. doi: 10.3389/fendo.2022.889729

Melatonin alleviates renal injury by activating mitophagy in diabetic nephropathy

Hanfen Tang[1,2], Ming Yang[1,3], Yinghong Liu[1,3], Xuejing Zhu[1,3], Shiping Liu[2], Hong Liu[1,3], Lin Sun[1,3] and Panai Song[1,3]*

[1]Department of Nephrology, Second Xiangya Hospital, Central South University, Changsha, China, [2]Department of Nutrition, Second Xiangya Hospital, Central South University, Changsha, China, [3]Key Laboratory of Kidney Disease & Blood Purification in Hunan Province, Institute of Nephrology, Central South University, Changsha, China

Diabetic nephropathy (DN) causes serious renal tubule and interstitial damage, but effective prevention and treatment measures are lacking. Abnormal mitophagy may be involved in the progression of DN, but its upstream and downstream regulatory mechanisms remain unclear. Melatonin, a pineal hormone associated with circadian rhythms, is involved in regulating mitochondrial homeostasis. Here, we demonstrated abnormal mitophagy in the kidneys of DN mice or high glucose (HG)-treated HK-2 cells, which was accompanied by increased oxidative stress and inflammation. At the same time, the melatonin treatment alleviated kidney damage. After mitochondrial isolation, we found that melatonin promoted AMPK phosphorylation and accelerated the translocation of PINK1 and Parkin to the mitochondria, thereby activating mitophagy, reducing oxidative stress, and inhibiting inflammation. Interestingly, the renal protective effect of melatonin can be partially blocked by downregulation of PINK1 and inhibition of AMPK. Our studies demonstrated for the first time that melatonin plays a protective role in DN through the AMPK-PINK1-mitophagy pathway.

KEYWORDS

melatonin, mitophagy, diabetic nephropathy (DN), p-AMPK, renal tubular injury

Introduction

With the development of the social economy and the improvement of living standards, the incidence of diabetes is increasing. Long-term hyperglycemia can lead to a series of microvascular complications in diabetic patients, such as diabetic nephropathy (DN) (1) and diabetic retinopathy (DR) (2). Approximately 30 to 40% of diabetes mellitus (DM) will develop into DN (3). At present, DN has become an important cause of end-stage renal disease (ESRD). However, the prevention and treatment of DN in clinical practice is very limited, and there is a lack of specific drugs

to treat it. Therefore, a thorough understanding of its pathogenesis is conducive to developing new medicines for DN. Recently, multiple factors have been reported to be involved in the progression of renal injury in DN, such as hypoxia (4, 5) and oxidative stress (6). However, these factors cannot fully reveal the occurrence and progression of DN. Therefore, it is necessary to further explore the molecular mechanism of DN.

As one of the organs with high metabolism, the kidney contains a large number of mitochondria to maintain its physiological function (7). In the state of DN, the kidney needs a large amount of ATP to resist the influence of high glucose (7), and the mitochondria are in a long-term overloaded state. Damaged mitochondria can release many mitochondrial contents, leading to inflammation and apoptosis (7–10). Therefore, timely clearance of damaged mitochondria can help prevent further damage, a process called mitophagy (11). Some studies have revealed the existence of abnormal mitophagy in the kidneys of DN (12) and activation of mitophagy can alleviate tubular injury in DN (13, 14). However, the upstream and downstream regulatory mechanisms of DN have not been clearly described. Melatonin, a pineal hormone associated with circadian rhythms, is involved in mitochondrial homeostasis regulation (15), energy metabolism (16), lipid regulation (17), and reproduction (18). Interestingly, mitochondrial dysfunction (12), abnormalities of energy homeostasis (19) and disorders of lipid metabolism (20) are closely related to the occurrence of DN. Unfortunately, the role of melatonin in DN has been poorly studied.

This study noted abnormal mitophagy in the kidneys of DN mice or high glucose (HG)-treated HK-2 cells, accompanied by increased oxidative stress and inflammation. Melatonin can phosphorylate AMPK, increase mitophagy and alleviate renal injury, while downregulation of PINK1 or inhibition of AMPK can partially block these effects. Our results suggest that melatonin plays a renoprotective role in DN through the AMPK-PINK1-mitophagy pathway.

Materials and methods

Animal models

Eight-week-old C57BL/6 male mice were obtained from Slyke Jingda Biotechnology Company (Hunan, China). All animal models were divided into three groups: the wild type group (WT); DN group; and DN + melatonin group (n = 6). Eight-week-old C57BL/6 male mice were fed a high-fat diet for 1 month and then were subjected to an intraperitoneal injection of STZ (Sigma-Aldrich, 50 mg/kg body weight/day) for 5 consecutive days to induce the diabetic mouse model. Three days after the last injection, the blood glucose level was ≥16.6 mmol/L, and the diabetes mouse model was considered successful. The diabetic mice continued feeding for 12 weeks to induce diabetic kidney damage. For the DN + melatonin group, diabetic mice were treated with melatonin (0.2mg/kg/day) for 12 weeks. The mice were euthanized at 24 weeks, and blood, urine, and kidney samples were collected for subsequent analysis. All animal experiments were approved by the Institutional Committee for Care and Use of Laboratory Animals at Central South University, China.

Renal histology

Hematoxylin and eosin (HE) and Masson staining of paraffin sections of kidney tissue were performed to observe pathological injury of the kidney. Renal tubulointerstitial injury was evaluated by a semiquantitative scoring system as previously described (21). Briefly, a score of 0 means no interstitial fibrosis and tubular atrophy, while scores of 1, 2 and 3 represent interstitial fibrosis and tubular atrophy areas less than 25 percent, less than 50 percent, and more than 50 percent, respectively.

Immunohistofluorescence (IHF) staining

Four-micron-thick renal paraffin sections were used for IHF staining. Briefly, after paraffin section dewaxing, rehydration, antigen repair, permeability, and blocking, the renal tissues were incubated with anti-F4/80 rabbit polyclonal antibody (Servicebio, GB11027, 1:500, Wuhan, China), anti-fibronectin (FN) rabbit polyclonal antibody (Servicebio, GB114057, 1:200, Wuhan, China), anti-α-SMA rabbit polyclonal antibody (Servicebio, GB111364, 1:400, Wuhan, China) and anti-NLRP3 rabbit polyclonal antibody (Servicebio, GB11300, 1:600, Wuhan, China) at 4°C overnight. After rewarming, the kidney tissue was incubated with a secondary antibody at room temperature for 1 hour. After staining the nucleus, the renal paraffin sections were observed and photographed under a fluorescence microscope. For costaining, after dewaxing, rehydration, antigen repair, permeability and blocking, anti-LC3B (Proteintech, 14600-1-AP, 1:200) antibody and anti-COXIV antibody (Abcam, ab33985, 1:500) were incubated in renal tissue simultaneously at 4°C overnight. After rewarming, the kidney tissue was incubated with anti-mouse and anti-rabbit secondary antibodies at room temperature for 1 hour simultaneously. Then the nuclei were stained and photographed.

Dihydroethidium (DHE) staining

6-μm-thick unfixed cryostat sections of renal tissues were stained with the cell-permeable agent dihydroethidium (1 μM,

DHE, Sigma-Aldrich) in the dark for 20 min, followed by fluorescence microscopy to assess ROS production in renal tissue.

Western blotting

The protein concentrations extracted from renal tissue or HK-2 cells were quantified by a BCA Protein Assay Kit (Beyotime Biotechnology, China). Then the samples were mixed with 5× SDS loading buffer and heated it at 95°C for 5 minutes. Equal amounts of proteins were used for western blot analysis.

Cell culture

The renal human proximal tubular epithelial cell line HK-2 was obtained from ATCC, and DMEM/F12 (Gibco, USA) containing 10% fetal bovine serum (Gibco, USA) was used to culture HK-2 cells (the human proximal tubular epithelial cell line) in an incubator with 5% CO2 at 37°C. After overnight culture in serum-free medium, the HK-2 cells were pretreated with 100 μmol/L melatonin (Selleck, USA) for 1 h, followed by high glucose (30 mmol/L) intervention for 24 h. The cells were collected for subsequent experiments.

DCFDA staining

The cells with different interventions were washed with PBS and then incubated with DCFDA (1:1000, Invitrogen) in the dark for 30 min, followed by fluorescence microscopy to assess ROS production in cells.

Confocal

Cells in different groups were stained with MitoTracker (Invitrogen, M22426, 1:1000) for 8 min and then fixed and blocked, followed by LC3B (Proteintech, 14600-1-AP, 1:200) incubation overnight at 4°C. A fluorescence-conjugated secondary antibody was used to incubate cells for 1 h at room temperature. Then, the nucleus was stained and photographed.

Statistical analyses

The experimental data were analyzed by SPSS 13.0 software. The results are presented as the means ± SD. The differences among the groups were compared using one-way ANOVA. Statistical significance was indicated at a P value less than 0.05.

Results

Melatonin ameliorated biochemical indices and pathological damage in diabetic nephropathy mice

Significantly increased blood glucose levels (Figure 1A), and reduced body weight (Figure 1B) were observed in the STZ-induced DN mouse model. In addition, the levels of proteinuria (Figure 1C), serum creatinine (Figure 1D), BUN (Figure 1E), and urinary NAG (Figure 1F) were notably increased in DN mice compared with in the control group, while the intervention of melatonin could mitigate these adverse changes in addition to the blood glucose level and body weight. Furthermore, HE staining showed that an increase in glomerular matrix, dilation of tubules, and exfoliation of nuclei were observed in the kidneys of DN mice compared to the control (Figure 1G), and this pathological renal injury was obviously relieved by melatonin treatment, as indicated by tubular interstitial damage scores (Figure 1H).

Melatonin ameliorated oxidative stress and fibrosis in the kidney of DN mice

DHE staining showed that ROS levels were increased significantly in the kidneys of DN mice compared to the control, while melatonin significantly downregulated oxidative stress levels (Figures 2A, B). The level of renal fibrosis was determined by the expression level of fibrotic proteins (FN and α-SMA) and Masson staining. IHF staining showed increased expression of FN (Figures 2C, D) and α-SMA (Figures 2C, E) in DN mice. Masson staining also revealed increased levels of tubulointerstitial fibrosis in the kidneys of DN mice. Interestingly, these adverse changes were ameliorated by melatonin treatment (Figures 2C–E). To further confirm the above results, the expression levels of FN and α-SMA were detected by WB analysis. Similar results were obtained: the expression levels of FN and α-SMA were upregulated in DN mice, and melatonin downregulated their expression levels (Figures 2F, G).

Melatonin promoted phosphorylation of AMPK and inhibits inflammation in the kidney of DN mice

IHF staining showed that the downregulated p-AMPK expression was observed in the kidneys of DN mice

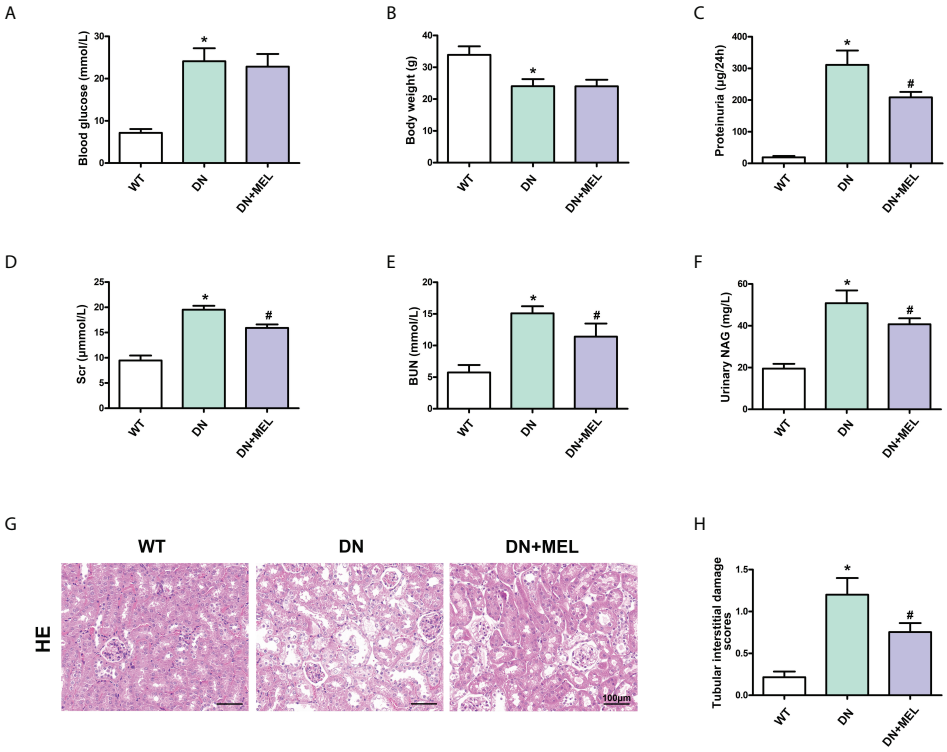

FIGURE 1
The effects of melatonin on biochemical indices and renal pathological changes in the kidneys of DN mice. The blood glucose **(A)**, body weight **(B)**, proteinuria **(C)**, serum creatinine **(D)**, BUN **(E)**, and urinary NAG levels **(F)** in different groups of mice. HE staining of renal paraffin tissue in different groups **(G)**. Tubular injury as assessed by tubular interstitial damage scores **(H)**. The values are the mean ± SD. n = 6/group. *p < 0.05 compared with the control group; #p < 0.05 compared with the DN group.

(Figures 3A, B), which was accompanied by upregulated NLRP3 expression (Figures 3A, C) and increased F4/80 positive cells (infiltration of macrophages) (Figures 3A, D). These changes were reversed by melatonin treatment. Moreover, WB analysis also showed decreased p-AMPK expression in DN mice, and melatonin reversed the downregulation of p-AMPK induced by diabetes (Figures 3E, F). There were no significant changes in total AMPK expression. Similarly, the mRNA levels of the inflammatory cytokines TNF-α (Figure 3G), IL-1β (Figure 3H), and IL-18 (Figure 3I) were increased in the kidneys of DN mice, while melatonin treatment relieved inflammation.

Melatonin restored mitophagy dysfunction in the kidney induced by diabetes

As shown in Figure 4A, mitophagy was observed by costaining mitochondrial protein (COX IV, red) and LC3B (green) in the paraffin section of kidney tissue and the overlapping regions (yellow) represented mitophagy. Compared with the control group, mitophagy activity (yellow area) was significantly reduced in the kidney of the DN group, while it was reactivated after melatonin administration (Figure 4A). Furthermore, to evaluate mitophagy more accurately, we separated the mitochondria and cytoplasm to observe the expression changes of crucial proteins in mitophagy. WB analysis showed that HFD+STZ treatment significantly downregulated PINK1 and Parkin expression levels in both the mitochondria and cytoplasm. Interestingly, melatonin significantly increased the expression of PINK1 and Parkin in mitochondria but did not affect their expression in the cytoplasm (Figures 4B–D). These results indicated that PINK1 and Parkin located in mitochondria are increased in response to melatonin. Moreover, downregulated LC3II expression and upregulated P62 expression (This represents the fluency of autophagy flux) were observed in both the mitochondria and cytoplasm of DN mice, while melatonin reversed these changes (Figures 4B, E, F). This finding indicates that mitophagy is inhibited in DN kidneys and that melatonin can reactivate mitophagy in renal tubular cells.

10.3389/fendo.2022.889729

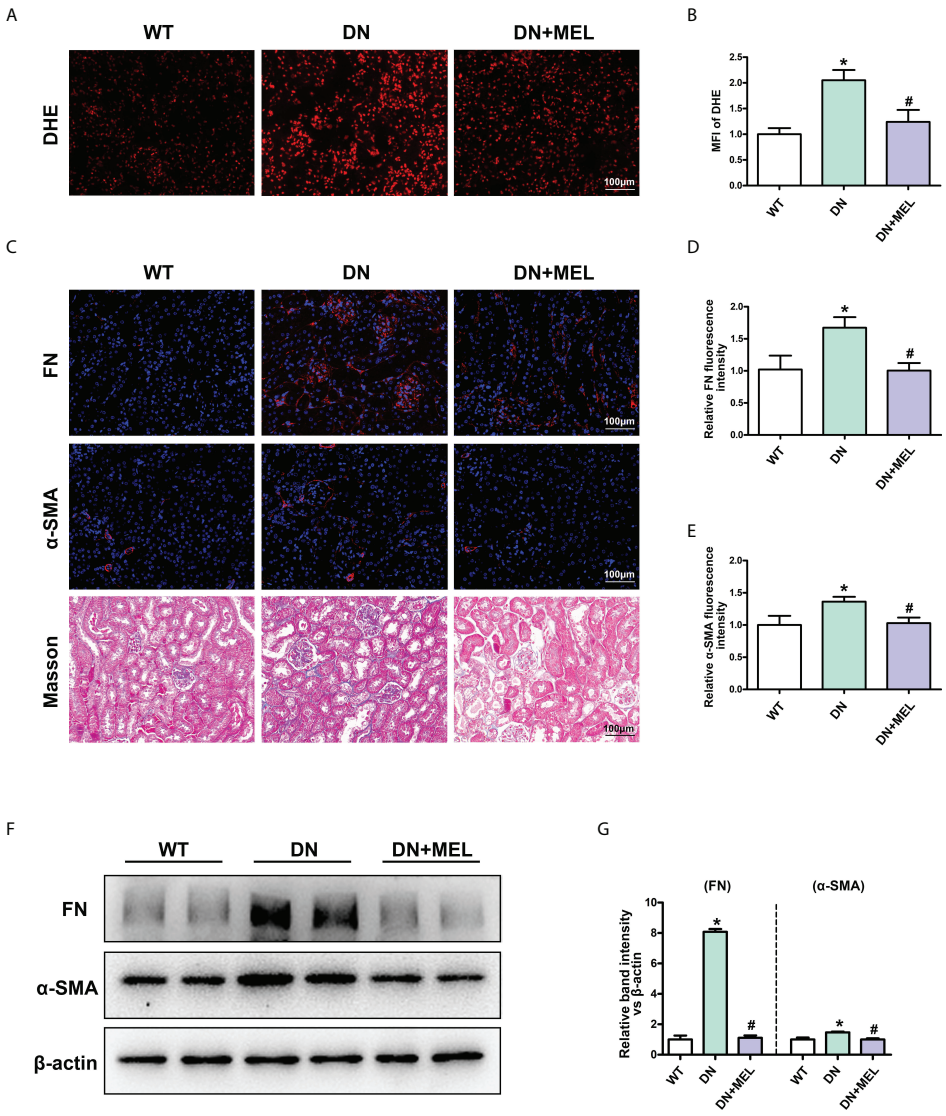

FIGURE 2
The effects of melatonin on oxidative stress and fibrosis in the kidneys of DN mice. DHE staining in the kidneys of different groups **(A, B)**. IHF analysis of FN (upper panel) **(C, D)** and α-SMA (middle panel) **(C. E)** in the kidneys of different groups. Masson staining of renal paraffin tissue in different groups (**C**, lower panel). Western blot analysis revealed the expression of FN and α-SMA **(F, G)**. The values are the mean ± SD. n = 6/group. *p < 0.05 compared with the control group; #p < 0.05 compared with the DN group.

Melatonin restored mitophagy by promoting phosphorylation of AMPK in HK-2 cells

To verify the protective mechanism of melatonin on diabetic kidney injury, we observed changes in mitophagy in HK-2 cells by inhibiting the expression of PINK1 and using the AMPK inhibitor Compound C. Mitophagy was detected by co-staining mitochondria (MitoTracker, red) and LC3B (green) as previously described (22), and the overlapping regions (yellow) represent mitophagy. Compared to the control, mitophagy was obviously inhibited in HK-2 cells treated with HG, while the effect of HG was negated by melatonin. Furthermore, the melatonin-restored mitophagy under HG was abolished by downregulation of PINK1 or inhibition of AMPK phosphorylation (Figure 5A). Moreover, we separated the mitochondria and cytoplasm of HK-2 cells to confirm whether the translocation of PINK1 and Parkin to mitochondria could be inhibited by AMPK inhibition. We observed that the expression levels of PINK1 and Parkin were notably decreased.

In contrast, P62 expression was increased in both the mitochondria and cytoplasm of HK-2 cells under HG conditions,

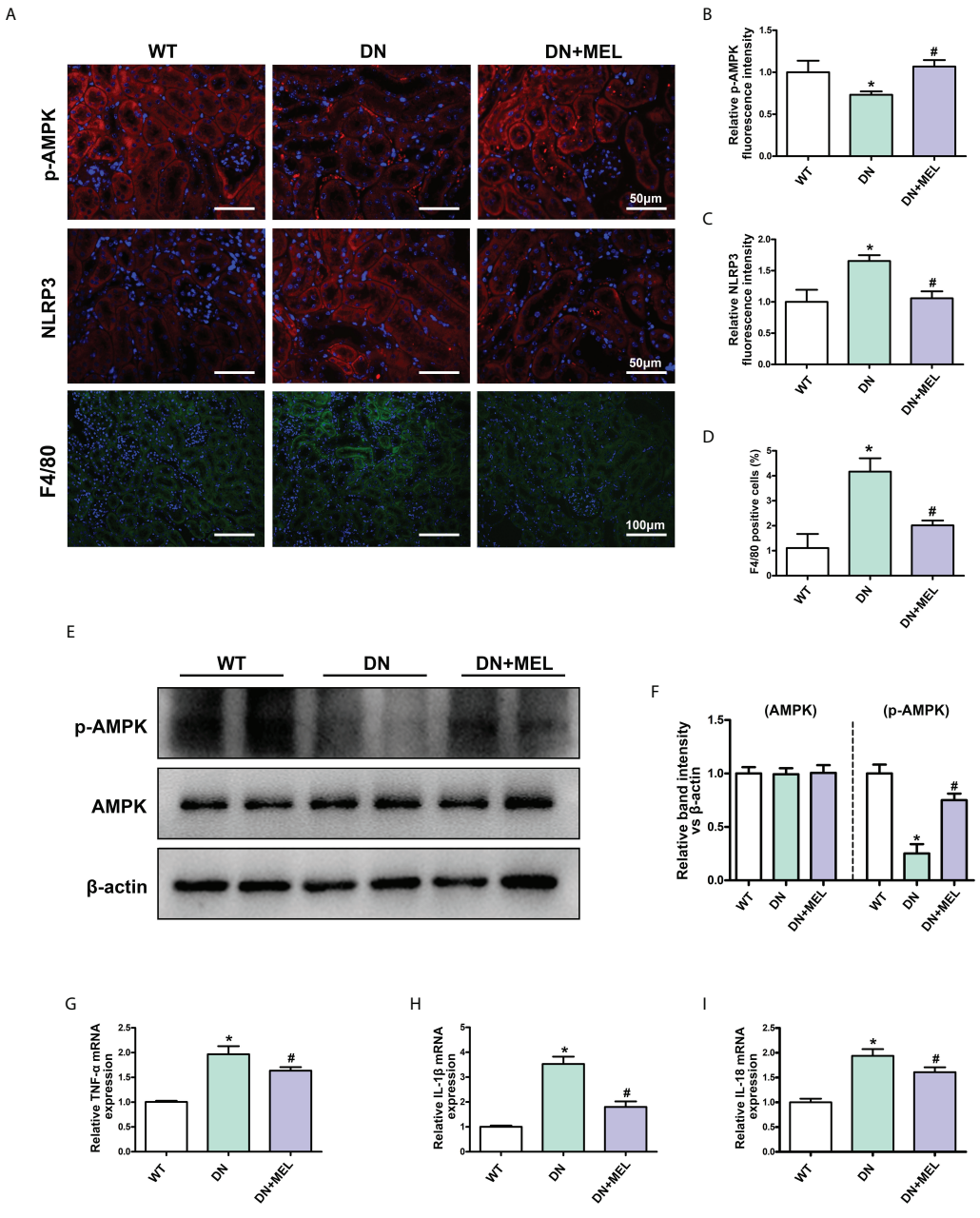

FIGURE 3
The effects of melatonin on the expression of p-AMPK and inflammation in the kidneys of DN mice. IHF analysis of p-AMPK (**A**, upper panel, **B**), NLRP3 (**A**, middle panel, **C**), and F4/80 (**A**, lower panel, **D**) in the kidneys of different groups. Western blot analysis revealed the expression of p-AMPK and AMPK **(E, F)**. The mRNA levels of TNF-α **(G)**, IL-1β **(H)**, and IL-18 **(I)** in the different groups. The values are the mean ± SD. n = 6/group. *$p < 0.05$ compared with the control group; $^{\#}p < 0.05$ compared with the DN group.

and melatonin promoted the translocation of PINK1 and Parkin from the cytoplasm to mitochondria and did not significantly affect their expression levels in the cytoplasm (Figures 5B–D). The protective effects of melatonin on the kidney and the expression changes in LC3II and P62 were partially abolished by treatment with Pink1 siRNA or Compound C (Figures 5B, E, F).

Melatonin relieved inflammation and fibrosis in HK-2 cells treated with HG

Then, we explored the effects of melatonin on inflammation and fibrosis. WB analysis showed decreased p-AMPK expression in HK-2 cells treated with HG treatment, and melatonin restored

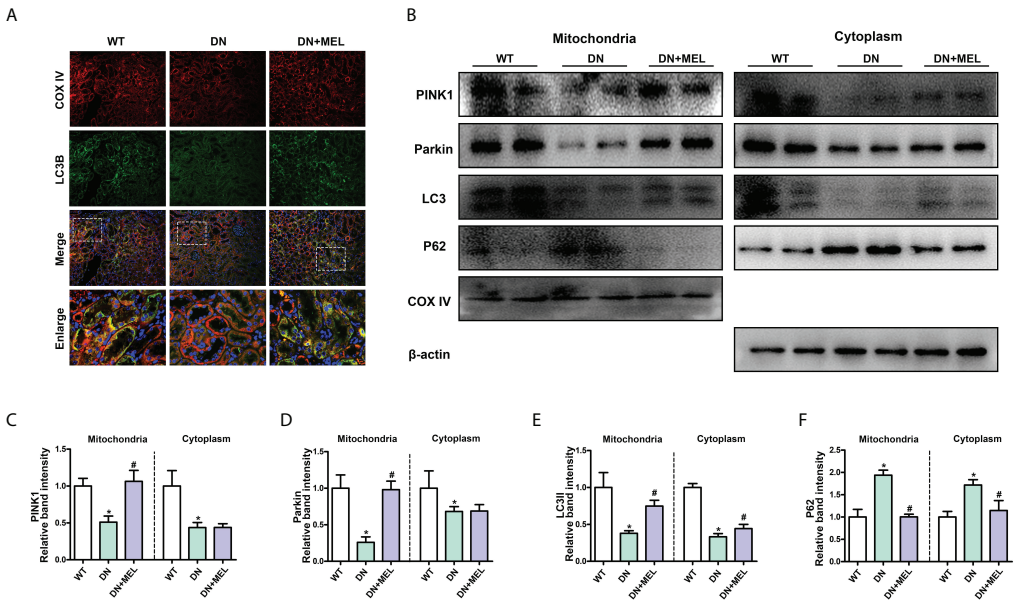

FIGURE 4
The effects of melatonin on mitophagy in the kidneys of DN mice. Costaining for COX IV (A, upper panel) and LC3B (A, second panel) observed the mitophagy changes. Western blot analysis of PINK1, Parkin, Parkin, LC3II, and P62 protein expression in mitochondria (left panels) and cytoplasm (right panels) **(B)**. Quantitative analysis of PINK1 **(C)**, Parkin **(D)**, LC3II **(E)**, and P62 **(F)**. The values are the mean ± SD. n = 6/group. *p < 0.05 compared with the control group; $^{\#}$p < 0.05 compared with the DN group.

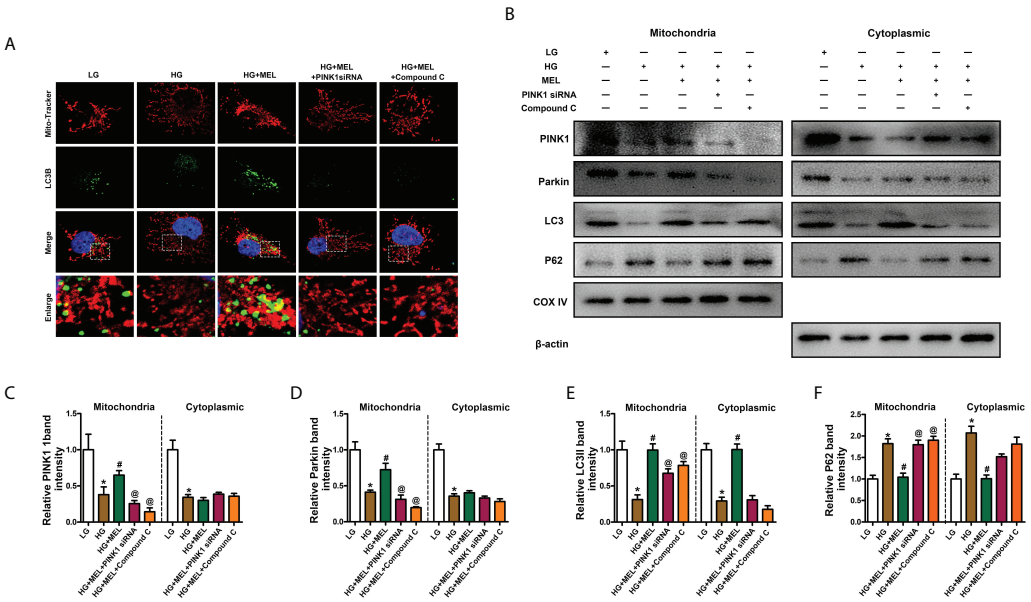

FIGURE 5
Metformin activated mitophagy in HK-2 cells treated with HG through the p-AMPK-PINK1 pathway. Mitophagy was detected by co-staining of MitoTracker and LC3B **(A)**. Western blot analysis of PINK1, Parkin, Parkin, LC3II, and P62 protein expression in mitochondria (left panels) and cytoplasm (right panels) **(B)**. Quantitative analysis of PINK1 **(C)**, Parkin **(D)**, LC3II **(E)**, and P62 **(F)**. The values are the mean ± SD. n = 4/group. *p < 0.05 compared with the control group; $^{\#}$p < 0.05 compared with the HG group. $^{@}$p < 0.05 compared with the HG+MEL group.

p-AMPK expression (Figures 6A, B). There were no apparent changes in total AMPK expression (Figures 6A, C). In addition, the expression levels of NLRP3 and α-SMA were significantly increased in HK-2 cells under HG conditions, and melatonin led to the restoration of HG-induced NLRP3 and α-SMA expression. At the same time, the effect was partially inhibited by PINK1 siRNA or Compound C (Figures 6A, D, E). Similarly, intracellular oxidative stress levels and the mRNA levels of IL-1β and IL-18 were increased under HG conditions, while melatonin reduced the increased expression induced by HG, and PINK1 siRNA or Compound C partially blocked the effects of melatonin (Figures 6F–H).

Discussion

Previous studies have considered that the renal damage caused by diabetes is mainly in the glomerulus, but the latest study shows that renal tubular injury is independent of the glomerulus and even earlier than the glomerulus (7). Multiple factors have been revealed to cause diabetes-induced renal damage, such as reactive oxygen species (23) and advanced glycosylation end products (24), which can lead to tubulointerstitial inflammation and fibrosis, promoting the progression of DN. However, these hypotheses cannot fully explain the pathogenesis of renal injury in DN. This study revealed that melatonin upregulated mitophagy by activating AMPK, alleviating renal inflammation and interstitial fibrosis.

As a highly metabolized organ, tubule cells need a large number of mitochondria to ensure their reabsorption function. Oxidative phosphorylation (OXPHOS) in mitochondria is the primary source of ATP production, and this process involves producing a large number of reactive oxygen species. Damaged mitochondria need to be removed in time; otherwise, the substances in the damaged mitochondria will leak into the cytoplasm, further aggravating cell damage. Zhan et al. demonstrated that there was a large amount of mitochondrial fragmentation accompanied by increased production of ROS and increased apoptosis in the kidneys of DN mice, while the use of drugs to restore mitochondrial function can alleviate kidney damage (25). A similar result was also observed by Ward et al. when db/db mice were treated with Mito. Q, a mitochondria-

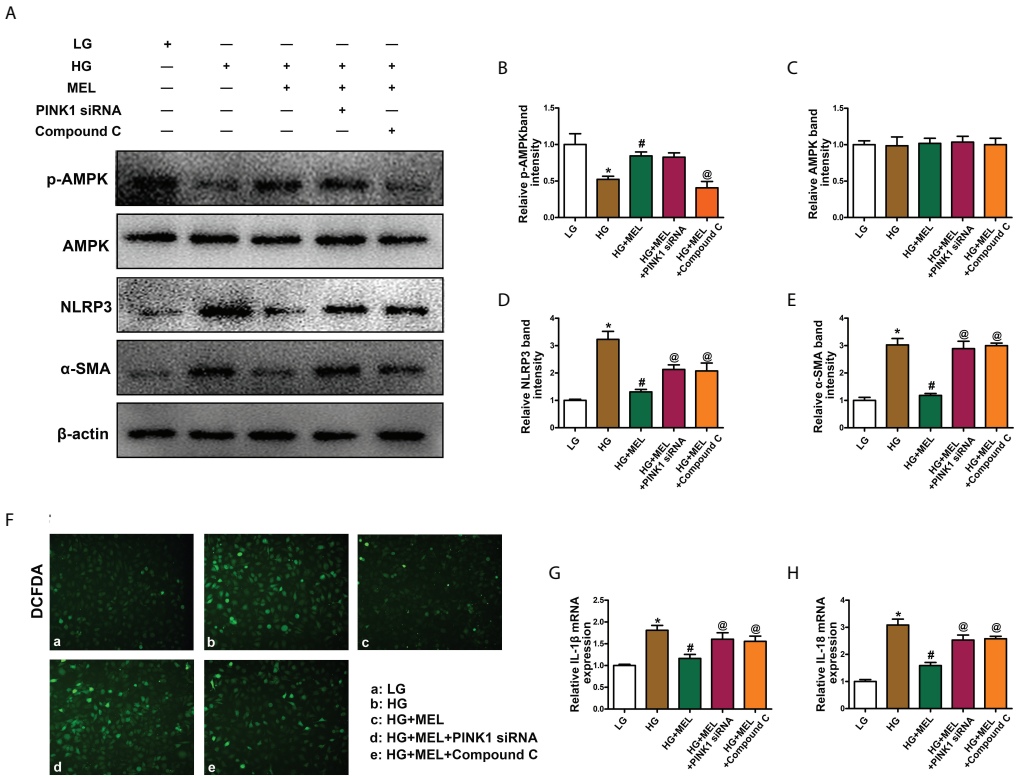

FIGURE 6
The effect of metformin on oxidative stress, inflammation, and fibrosis in HK-2 cells treated with HG. Western blot analysis of p-AMPK **(A, B)**, AMPK **(A, C)**, NLRP3 **(A, D)**, and SMA **(A, E)** expression. DCFDA staining was used to detect intracellular oxidative stress **(F)**. The mRNA levels of IL-1β **(G)** and IL-18 **(H)** in the different groups. The values are the mean ± SD. n = 4/group. *p < 0.05 compared with the control group; #p < 0.05 compared with the HG group. @p < 0.05 compared with the HG+MEL group.

targeted protective agent, and diabetes-induced renal damage was significantly improved compared to the control (26). These evidences suggest that mitochondrial dysfunction plays a vital role in renal injury in DN. Autophagy is the process by which cells remove excess or damaged organelles in time to adapt to changes in the environment (27). Autophagy can be divided into macroautophagy (28), microautophagy (29), and chaperone-mediated autophagy (CMA) (30), according to the occurrence process. Macroautophagy can be divided into mitophagy (31), ER-phagy (32), lipophagy (33), and so on. Mitophagy can temporarily remove damaged mitochondria from cells to prevent them from releasing contents and exacerbating cell damage. Several studies have revealed that disordered mitophagy can promote the progression of DN. There were mitophagy defects, decreased mitochondrial membrane potential, and increased mitochondrial reactive oxygen species (mtROS), accompanied by downregulated PINK and Parkin expression and increased apoptosis in the kidney of db/db mice (34). A similar result was also observed by Lu et al. Mitophagy was destroyed, and apoptosis was increased in HK-2 cells treated with high glucose, while mitophagy was restored with reduced apoptosis and alleviated kidney damage (35). This study noted that the inhibition of mitophagy was accompanied by increased oxidative stress, inflammation, and apoptosis in HFD+STZ induced DN mice and HG-treated HK-2 cells. Moreover, after the isolation of mitochondria, we found that the levels of PINK1 and Parkin (the critical proteins of mitophagy) located in mitochondria were reduced, while their levels in the cytoplasm did not change significantly. This evidence suggests that there is serious mitophagy disorder in renal tubular cells in DN.

Melatonin is a pineal hormone associated with circadian rhythms, and it can also be synthesized in extra-pineal tissues such, as the heart, liver, placenta, skin, kidney, and intestine (36–38). It regulates various life activities, such as energy metabolism, lipid regulation and reproduction, pregnancy, and fetal development (39). Recently, the relationship between melatonin and autophagy has been partially revealed. Stacchiotti et al. have shown that melatonin could alleviate liver metabolism and steatosis, restore autophagy flux and ameliorate mitochondrial damage in the liver of high-fat-fed mice (40). Similarly, Wang et al. demonstrated that melatonin could regulate the interaction between autophagy and apoptosis through SIRT3, thereby alleviating cadmium-induced testicular injury (41). However, in kidney disease, the relationship between melatonin and autophagy, especially mitophagy, has rarely been studied. It has been reported that melatonin could alleviate mitochondrial oxidative damage by promoting AMPK phosphorylation (42). AMPK phosphorylation is inhibited in DN kidneys (43, 44). In addition, studies have confirmed that AMPK was a key molecule regulating mitophagy activity (45, 46). Activation of mitochondrial autophagy can ensure timely clearance of damaged mitochondria, thereby reducing oxidative stress and cellular inflammation (7). Therefore, AMPK and mitophagy may be potential targets of melatonin in DN. Here, we found that melatonin could restore the decreased mitophagy activity caused by diabetes in the kidneys of DN mice or HG-treated HK-2 cells. Mechanistically, melatonin activates mitophagy by promoting AMPK phosphorylation. The expression of PINK1 and Parkin in mitochondria was increased in the kidneys of DN+MEL mice and HG treated HK-2 cells compared to the control. At the same time, their expression did not change significantly in the cytoplasm. This suggests that melatonin can dramatically promote the activation of mitophagy. Interestingly, when PINK1 or AMPK was inhibited, the mitophagy activity restored by melatonin was also inhibited. This evidence further suggests that melatonin activates mitophagy by promoting AMPK phosphorylation. However, what is the molecular mechanism by which melatonin regulates AMPK activity? Rui et al. demonstrated that melatonin could downregulate cAMP levels through melatonin 1A receptor (MT1R), thereby activating AMPK phosphorylation to ameliorate lipid metabolism (47). Thus, the MT1R-cAMP axis is the potential mechanism by which melatonin activates AMPK in the regulation of mitophagy.

Although this study showed that melatonin played a renoprotective role in DN through the AMPK-PINK1-mitophagy pathway, there are still some problems to be solved in the future in this research. What is the molecular mechanism by which melatonin promotes AMPK phosphorylation? Can the simultaneous intervention of melatonin and Compound C (an AMPK inhibitor) in diabetic mice block the protective effect of melatonin in the kidneys of diabetic mice? Although there are some limitations, this study shows a protective effect of melatonin in DN, which is expected to be used to treat DN in the near future.

Data availability statement

The raw data supporting the conclusions of this article will be made available by the authors, without undue reservation.

Ethics statement

The clinical and animal study was reviewed and approved by the Medical Ethics Committee of Central South University.

Author contributions

HT designed the study, analyzed the data, interpreted the results, and drafted the manuscript. MY, YL, XZ, SL, HL, and

LS contributed to the data collection and manuscript revision. PS was the corresponding author and was involved in the study design, data interpretation, and manuscript revision. All authors contributed to the article and approved the submitted version.

Funding

This work was supported by National Natural Science Foundation of China (81800649), Natural Science Foundation of Hunan Province (2022JJ30835,2021JJ30942,2021JJ30986), Changsha Municipal Natural Science Foundation (kq2202401, kq2014235) and General Project of Scientific Research Project of Hunan Provincial Health and Family Planning Commission (20200807).

Conflict of interest

The authors declare that the research was conducted in the absence of any commercial or financial relationships that could be construed as a potential conflict of interest.

Publisher's note

References

1. Tervaert TW, Mooyaart AL, Amann K, Cohen AH, Cook HT, Drachenberg CB, et al. Pathologic classification of diabetic nephropathy. *J Am Soc Nephrol* (2010) 21(4):556–63. doi: 10.1681/ASN.2010010010

2. Lechner J, O'Leary OE, Stitt AW. The pathology associated with diabetic retinopathy. *Vision Res* (2017) 139:7–14. doi: 10.1016/j.visres.2017.04.003

3. Martínez-Castelao A, Navarro-González JF, Górriz JL, de Alvaro F. The concept and the epidemiology of diabetic nephropathy have changed in recent years. *J Clin Med* (2015) 4(6):1207–16. doi: 10.3390/jcm4061207

4. Kang MK, Kim SI, Oh SY, Na W, Kang YH. Tangeretin ameliorates glucose-induced podocyte injury through blocking epithelial to mesenchymal transition caused by oxidative stress and hypoxia. *Int J Mol Sci* (2020) 21(22):8577. doi: 10.3390/ijms21228577

5. Takahashi N, Yoshida H, Kimura H, Kamiyama K, Kurose T, Sugimoto H, et al. Chronic hypoxia exacerbates diabetic glomerulosclerosis through mesangiolysis and podocyte injury in db/db mice. *Nephrology dial Transplant* (2020) 35(10):1678–88. doi: 10.1093/ndt/gfaa074

6. Huang W, Man Y. Short-chain fatty acids ameliorate diabetic nephropathy *via* GPR43-mediated inhibition of oxidative stress and NF-κB signaling. *Oxid Med Cell Longev* (2020) 1(2020):4074832. doi: 10.1155/2020/4074832

7. Yang M, Li C, Yang S, Xiao Y, Chen W, Gao P, et al. Mitophagy: A novel therapeutic target for treating DN. *Curr Med Chem* (2021) 28(14):2717–28. doi: 10.2174/0929867327666201006152656

8. Kolmychkova KI, Zhelankin AV, Karagodin VP, Orekhov AN. Mitochondria and inflammation. *Patol Fiziol Eksp Ter* (2016) 60(4):114–21.

9. Abate M, Festa A, Falco M, Lombardi A, Luce A, Grimaldi A, et al. Mitochondria as playmakers of apoptosis, autophagy and senescence. *Semin Cell Dev Biol* (2020) 98:139–53. doi: 10.1016/j.semcdb.2019.05.022

10. Sinha K, Das J, Pal PB, Sil PC. Oxidative stress: the mitochondria-dependent and mitochondria-independent pathways of apoptosis. *Arch Toxicol* (2013) 87 (7):1157–80. doi: 10.1007/s00204-013-1034-4

11. Yoo SM, Jung YK. A molecular approach to mitophagy and mitochondrial dynamics. *Molecules Cells* (2018) 41(1):18–26. doi: 10.14348/molcells.2018.2277

12. Zhou D, Zhou M, Wang Z, Fu Y, Jia M, Wang X, et al. PGRN acts as a novel regulator of mitochondrial homeostasis by facilitating mitophagy and mitochondrial biogenesis to prevent podocyte injury in diabetic nephropathy. *Cell Death Dis* (2019) 10(7):524. doi: 10.1038/s41419-019-1754-3

13. Guo F, Wang W, Song Y, Wu L, Wang J, Zhao Y, et al. LncRNA SNHG17 knockdown promotes parkin-dependent mitophagy and reduces apoptosis of podocytes through Mst1. *Cell Cycle (Georgetown Tex.)* (2020) 19(16):1997–2006. doi: 10.1080/15384101.2020.1783481

14. Jiang XS, Chen XM, Hua W, He JL, Liu T, Li XJ, et al. PINK1/Parkin mediated mitophagy ameliorates palmitic acid-induced apoptosis through reducing mitochondrial ROS production in podocytes. *Biochem Biophys Res Commun* (2020) 525(4):954–61. doi: 10.1016/j.bbrc.2020.02.170

15. Reiter RJ, Tan DX, Rosales-Corral S, Galano A, Zhou XJ, Xu B. Mitochondria: Central organelles for melatonin's antioxidant and anti-aging actions. *Molecules (Basel Switzerland)* (2018) 23(2):509. doi: 10.3390/molecules23020509

16. Cipolla-Neto J, Amaral FG, Afeche SC, Tan DX, Reiter RJ. Melatonin, energy metabolism, and obesity: a review. *J Pineal Res* (2014) 56(4):371–81. doi: 10.1111/jpi.12137

17. Jin JX, Lee S, Taweechaipaisankul A, Kim GA, Lee BC. Melatonin regulates lipid metabolism in porcine oocytes. *J Pineal Res* (2017) 62(2):. doi: 10.1111/jpi.12388

18. Olcese JM. Melatonin and female reproduction: An expanding universe. *Front Endocrinol* (2020) 11:85. doi: 10.3389/fendo.2020.00085

19. Bhargava P, Schnellmann RG. Mitochondrial energetics in the kidney. *Nat Rev Nephrol* (2017) 13(10):629–46. doi: 10.1038/nrneph.2017.107

20. Herman-Edelstein M, Scherzer P, Tobar A, Levi M, Gafter U. Altered renal lipid metabolism and renal lipid accumulation in human diabetic nephropathy. *J Lipid Res* (2014) 55(3):561–72. doi: 10.1194/jlr.P040501

21. Yang M, Zhao L, Gao P, Zhu X, Han Y, Chen X, et al. DsbA-l ameliorates high glucose induced tubular damage through maintaining MAM integrity. *EBioMedicine* (2019) 43:607–19. doi: 10.1016/j.ebiom.2019.04.044

22. Zhou R, Yazdi AS, Menu P, Tschopp J. A role for mitochondria in NLRP3 inflammasome activation. *Nature* (2011) 469(7329):221–5. doi: 10.1038/nature09663

23. Wu Y, Zhao Y, Yang HZ, Wang YJ, Chen Y. HMGB1 regulates ferroptosis through Nrf2 pathway in mesangial cells in response to high glucose. *Biosci Rep* (2021) 41(2):BSR20202924. doi: 10.1042/BSR20202924

24. Guo J, Zheng HJ. Accelerated kidney aging in diabetes mellitus. *Oxid Med Cell Longev* (2020) 2020:1234059. doi: 10.1155/2020/1234059

25. Zhan M, Usman IM, Sun L, Kanwar YS. Disruption of renal tubular mitochondrial quality control by myo-inositol oxygenase in diabetic kidney disease. *J Am Soc Nephrol* (2015) 26(6):1304–21. doi: 10.1681/ASN.2014050457

26. Ward MS, Flemming NB, Gallo LA. Targeted mitochondrial therapy using MitoQ shows equivalent renoprotection to angiotensin converting enzyme inhibition but no combined synergy in diabetes. *Sci Rep* (2017) 7(1):15190. doi: 10.1038/s41598-017-15589-x

27. Kuma A, Komatsu M, Mizushima N. Autophagy-monitoring and autophagy-deficient mice. *Autophagy* (2017) 13(10):1619–28. doi: 10.1080/15548627.2017.1343770

28. Nieto-Torres JL, Hansen M. Macroautophagy and aging: The impact of cellular recycling on health and longevity. *Mol Aspects Med* (2021) 82:101020. doi: 10.1016/j.mam.2021.101020

29. Li J, Hochstrasser M. Microautophagy regulates proteasome homeostasis. *Curr Genet* (2020) 66(4):683–7. doi: 10.1007/s00294-020-01059-x

30. Xu Y, Zhang Y. Chaperone-mediated autophagy regulates the pluripotency of embryonic stem cells. *Science* (2020) 369(6502):397–403. doi: 10.1126/science.abb4467

31. Pradeepkiran JA, Reddy PH. Defective mitophagy in alzheimer's disease. *Ageing Res Rev* (2020) 64:101191. doi: 10.1016/j.arr.2020.101191

32. Yang M, Luo S, Wang X, Li C, Yang J, Zhu X, et al. ER-phagy: A new regulator of ER homeostasis. *Front Cell Dev Biol* (2021) 9:684526. doi: 10.3389/fcell.2021.684526

33. Cui W, Sathyanarayan A, Lopresti M, Aghajan M, Chen C, Mashek DG. Lipophagy-derived fatty acids undergo extracellular efflux *via* lysosomal exocytosis. *Autophagy* (2021) 17(3):690–705. doi: 10.1080/15548627.2020.1728097

34. Sun J, Zhu H, Wang X, Gao Q, Li Z, Huang H. CoQ10 ameliorates mitochondrial dysfunction in diabetic nephropathy through mitophagy. *J Endocrinol* (2019) 1:JOE–18–0578.R1. doi: 10.1530/JOE-18-0578

35. Lu C, Wu B, Liao Z, Xue M, Zou Z, Feng J, et al. DUSP1 overexpression attenuates renal tubular mitochondrial dysfunction by restoring parkin-mediated mitophagy in diabetic nephropathy. *Biochem Biophys Res Commun* (2021) 559:141–7. doi: 10.1016/j.bbrc.2021.04.032

36. Jiki Z, Lecour S, Nduhirabandi F. Cardiovascular benefits of dietary melatonin: A myth or a reality? *Front Physiol* (2018) 9:528. doi: 10.3389/fphys.2018.00528

37. Venegas C, García JA, Escames G, Ortiz F, López A, Doerrier C, et al. Extrapineal melatonin: analysis of its subcellular distribution and daily fluctuations. *J pineal Res* (2012) 52(2):217–27. doi: 10.1111/j.1600-079X.2011.00931.x

38. Acuña-Castroviejo D, Escames G, Venegas C, Díaz-Casado ME, Lima-Cabello E, López LC, et al. Extrapineal melatonin: sources, regulation, and potential functions. *Cell Mol Life Sci* (2014) 71(16):2997–3025. doi: 10.1007/s00018-014-1579-2

39. Amaral FGD, Cipolla-Neto J. A brief review about melatonin, a pineal hormone. *Arch Endocrinol Metab* (2018) 62(4):472–9. doi: 10.20945/2359-3997000000066

40. Stacchiotti A, Grossi I. Melatonin effects on non-alcoholic fatty liver disease are related to MicroRNA-34a-5p/Sirt1 axis and autophagy. *Cells* (2019) 8(9):1053. doi: 10.3390/cells8091053

41. Wang M, Zhu CQ, Zeng L, Cheng L, Ma L, Zhang M, et al. Melatonin regulates the cross-talk between autophagy and apoptosis by SIRT3 in testicular leydig cells. *Biochem Biophys Res Commun* (2021) 555:182–9. doi: 10.1016/j.bbrc.2021.03.138

42. Liu D, Ma Z, Di S, Yang Y, Yang J, Xu L, et al. AMPK/PGC1α activation by melatonin attenuates acute doxorubicin cardiotoxicity via alleviating mitochondrial oxidative damage and apoptosis. *Free Radical Biol Med* (2018) 129:59–72. doi: 10.1016/j.freeradbiomed.2018.08.032

43. Guo Y, Ran Z, Zhang Y, Song Z, Wang L, Yao L, et al. Marein ameliorates diabetic nephropathy by inhibiting renal sodium glucose transporter 2 and activating the AMPK signaling pathway in db/db mice and high glucose-treated HK-2 cells. *Biomed pharmacother = Biomed pharmacother* (2020) 131:110684. doi: 10.1016/j.biopha.2020.110684

44. Li Z, Guo H, Li J, Ma T, Zhou S, Zhang Z, et al. Sulforaphane prevents type 2 diabetes-induced nephropathy *via* AMPK-mediated activation of lipid metabolic pathways and Nrf2 antioxidative function. *Clin Sci* (2020) 134(18):2469–87. doi: 10.1042/CS20191088

45. Drake JC, Wilson RJ. Mitochondria-localized AMPK responds to local energetics and contributes to exercise and energetic stress-induced mitophagy. *Proc Natl Acad Sci USA* (2021) 118(37):e2025932118. doi: 10.1073/pnas.2025932118

46. Seabright AP, Fine NHF, Barlow JP, Lord SO, Musa I, Gray A, et al. AMPK activation induces mitophagy and promotes mitochondrial fission while activating TBK1 in a PINK1-parkin independent manner. *FASEB J* (2020) 34(5):6284–301. doi: 10.1096/fj.201903051R

47. Rui BB, Chen H, Jang L, Li Z, Yang JM, Xu WP, et al. Melatonin upregulates the activity of AMPK and attenuates lipid accumulation in alcohol-induced rats. *Alcohol Alcoholism* (2016) 51(1):11–9. doi: 10.1093/alcalc/agv126

Frontiers in Endocrinology

Explores the endocrine system to find new therapies for key health issues The second most-cited endocrinology and metabolism journal, which advances our understanding of the endocrine system. It uncovers new therapies for prevalent health issues such as obesity, diabetes, reproduction, and aging.

Discover the latest Research Topics

See more →

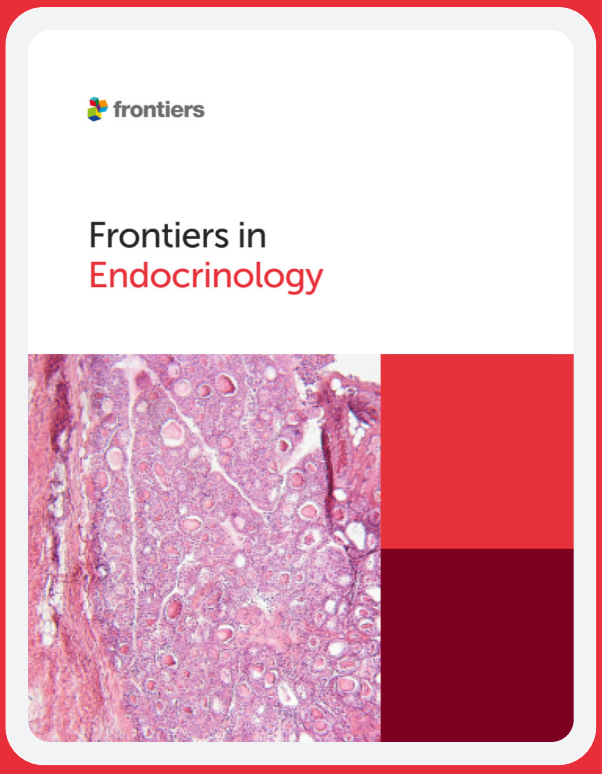

Frontiers

Avenue du Tribunal-Fédéral 34
1005 Lausanne, Switzerland
frontiersin.org

Contact us

+41 (0)21 510 17 00
frontiersin.org/about/contact